Synthesis, structure and reaction studies of diphosphine rhodium complexes

Simon Peter Crabtree

Synthesis, Structure and Reaction Studies of Diphosphine Rhodium Complexes

Simon Peter Crabtree

Submitted for the degree of
Doctor of Philosophy

University of Durham
Department of Chemistry
1996

To All those

lucky enough to read this....

If life seems jolly rotton,

there's something you've forgotten,

and that's to laugh and smile and dance and sing ,

when you're feeling in the dumps,

don't be silly chumps.

just purse your lips and whistle. That's the thing.

And.....

Always look on the bright side of life..... (Eric Idle)

Acknowledgements

I would like to thank the ancillary staff in the chemistry department for their help and assistance; Dr. M. Kilner; for his supervision; the long suffering members of lab 101 past and present especially Nic, Graham, Pete and Emma for surviving this long. Dr. R.L. Tooze, and G. Eastham at ICI Acrylics for their help and support and a CASE award.

The material contained in this thesis has not been submitted for examination for any other degree or part thereof, at the University of Durham or any other institution. The material contained herein is the sole work of the author except where formally acknowledged by reference.

Abstract

A series of complexes of the type $[Rh(diphos)(C_7H_8)](BF_4)$ **(1)** have been synthesised and two of these species [diphos = $Bu^t_2P(CH_2)_2PBu^t_2$, $Cy_2P(1,2\text{-}trans\text{-}cyclopentane)PCy_2$] have been characterised by X-ray crystallography. The influence of the chelating diphosphine on the structural characteristics and NMR parameters of these compounds has been investigated.

Complexes of the type **(1)** are active catalysts for the hydroformylation of 1-hexene(120°C, 450psi 2:1 H_2:CO). However, they are inactive for the related hydroesterification process and this is attributed to the stability of $[Rh(diphos)(CO)_2]^+$ under the reaction conditions.

Detailed studies of the reactions of type **(1)** complexes with H_2 have been undertaken. The products from these reactions are dependent on both the diphosphine and the solvent employed. In THF and CD_2Cl_2, dimeric hydrides were observed, whilst in $CDCl_3$ hydrido-chloro-complexes of the type $[Rh_2(diphos)_2(\mu\text{-}Cl)H_2]^{2+}$ were formed. In the former solvents, three types of hydrides have been identified by NMR studies, namely $[Rh_2(diphos)_2H_6]$, $[Rh_2(diphos)_2H_4]$ and $[Rh_2(diphos)_2H_4]^{2+}$.

The oxidative-addition reactions of alkyl-, acyl- and formyl-halide with Rh(I) complexes have been investigated. The reaction with $ClCO_2Me$ with $[Rh(dppe)Cl]_2$ and $[Rh(dppe)]_2(BF_4)_2$ led to the formation of diphosphine-rhodium(III)-halide species $(H_3NOH)[Rh(dppe)Cl_4]$ and $[Rh_2(dppe)_2(\mu\text{-}Cl)_3Cl_2](BF_4)$ respectively. Alternative routes to these complexes have been investigated starting from $RhCl_3.3H_2O$/diphosphines and a series of the novel halide bridged dimers have been characterised, including by X-ray crystallography and their reaction chemistry explored.

In the synthesis of the cationic rhodium complexes from neutral chloro-complexes with $AgBF_4$, the novel silver complexes $[Ag_2(\mu\text{-}Bu^t_2P(CH_2)_3PBu^t_2)_2](BF_4)_2$, $[\{Ag(H_2O)\}_2(\mu\text{-}Bu^t_2P(CH_2)_2PBu^t_2)](BF_4)_2$, and $[Ag(C_6D_6)_3BF_4]$ have been isolated as by-products and characterised by X-ray crystallography.

Contents

Abbreviations

r.t.	Room temperature
GC	Gas Chromatography
MS	Mass Spectroscopy
NMR	Nuclear Magnetic Resonance
VT	Variable Temperature
AcAc	Acetylacetone
NMP	N-methylpyrrolidone
NBD	Norbornadiene: 2,2,1 hepta-2,5-diene
COD	Cycloocta-1,5-diene
TACN	Triazacyclononane
Cp*	Pentamethylcyclopentadienyl
DMP	3,5 Dimethylpyrazole
diphos	Any Chelating Phosphine
dBpm	1,1-Bis(di-*tert*-butylphosphino)methane
dppm	1,1-Bis(diphenylphosphino)methane
etdp	N,N,-Bis(diphenylphosphido)ethylamine
dBpe	1,2-Bis(di-*tert*-butylphosphino)ethane
dcpe	1,2-Bis(dicyclohexylphosphino)ethane
dcpcp	*trans*-1,2-Bis(dicyclohexylphosphino)cyclopentane
d*i*ppe	1,2-Bis(di*iso*propylphosphino)ethane
dppe	1,2-Bis(diphenylphosphino)ethane
dptf	1,2-Bis(di{trifluorotolyl}phosphino)ethane
dpf	1,2-Bis(di{pentafluorophenyl)phosphino)ethane
chiraphos	2,3-Bis(diphenylphosphino)butane
cyphos	1,2-Bis(diphenylphosphino)-1-cyclohexylethane
dipamp	1,2-Bis(*o*-anisylphenylphosphino)ethane
norphos	*trans*-2,3-Bis(diphenylphosphino)norborn-5-ene
prophos	1,2-Bis(diphenylphosphino)-propane
dBpp	1,3-Bis(di-*tert*-butylphosphino)propane
dcpp	1,3-Bis(dicyclohexylphosphino)propane
d*i*ppp	1,3-Bis(di*iso*propylphosphino) propane
dppp	1,3-Bis(diphenylphosphino)propane
dBpf	1,2-Bis(di*iso*propylphosphino)ethane
dBppf	1,1'-Bis(phenyl-*tert*-butylphosphino)ferrocene

d*i*ppf	1,1'-Bis(di-*iso*-propylphosphino)ferrocene
dppf	1,1'-Bis(diphenylphosphino)ferrocene
Boxylyl	1,4-Bis(di-*tert*-butylphosphino)*ortho*-xylene
d*i*ppb	1,4-Bis(di*iso*propylphosphino)butane
dppb	1,4-Bis(diphenylphosphino)butane
diop	4,5-Bis(diphenylpropylphosphino)methyl-2,2'dimethyl-1,3 dioxolane
*i*Prdiop	4,5-Bis(di*iso*propylphosphino)methyl-2,2'dimethyl-1,3 dioxolane
cydiop	4,5-Bis(dicyclohexylphosphino)methyl-2,2'dimethyl-1,3 dioxolane
binap	1,1'-Bis(diphenylphosphino)binapthalene
triphos	1,1,1-tris((diphenylphoshino)methyl)methane
PPy_3	Tripyridylphosphine

Introduction

Transition metals are active catalysts for a variety of reactions. Of particular interest are those reactions involving carbon monoxide. Notable success has been achieved in these reactions using the late transition metals, especially those based on rhodium, palladium and platinum.[1] An early example of catalytic carbonylation was in the 1920's with the Reppe process for the formation of esters and carboxylic acids from alkenes.[2] However, this used the highly toxic $Ni(CO)_4$ as a catalyst and operated at high temperatures and pressures. Since this time there has been a drive in industry to operate under moderate conditions, and to target clean technology, avoiding toxic materials where possible.

For example, methyl methacrylate[3] (MMA, the precursor to perspex) is currently made via the acetone-HCN route (see equation 1).

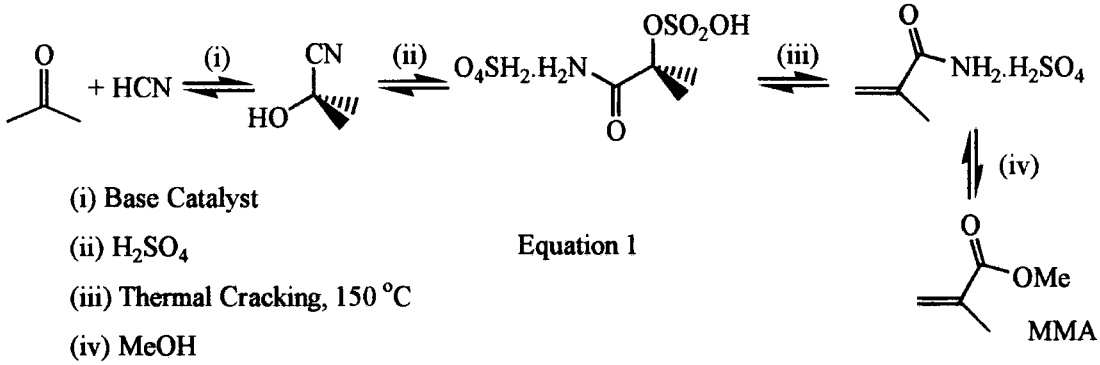

(i) Base Catalyst
(ii) H_2SO_4
(iii) Thermal Cracking, 150 °C
(iv) MeOH

Equation 1

The starting materials for this process are cheap by-products of other industries. However, HCN possesses a certain toxicity, and large quantities of H_2SO_4 are consumed. Additionally the intermediates are easily hydrolysed to produce undesirable side products. It is possible to convert acetone-cyanohydrin [$Me_2C(OH)CN$] to MMA in the absence of H_2SO_4. However, this requires careful control of both catalyst and conditions, details of which are not in the public domain. There are several alternative routes to this important chemical. The heterogeneous-transition-metal based oxidation of *iso*butene with air, is operated in the Far East, where this starting material is readily available (see equation 2). Alternatively, the HF, H_2SO_4 or BF_3 catalysed hydroesterification of propene and

subsequent heterogeneous-transition-metal catalysed oxidative dehydrogenation can be used to produce the free acid (see Equation 3).

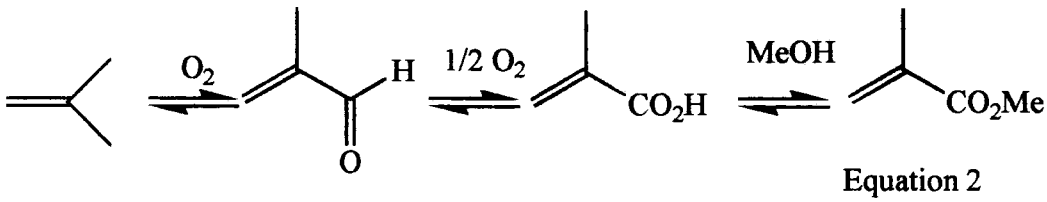

Equation 2

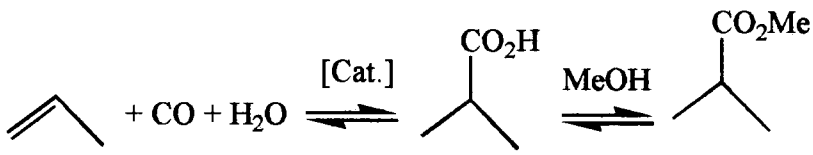

Equation 3

Later developments in the synthesis of MMA proceed *via* the homogenous, late transition-metal-catalysed carbonylation of unsaturated substrates, either directly from methyl acetylene (see Equation 4) using a Pd-phosphine catalyst, or by a two-stage process from ethene (see Equation 5). The second step in this last process is the base catalysed condensation of methanal and the ester[4] to form MMA.

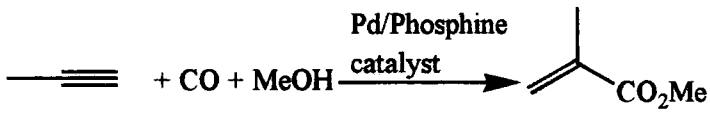

Equation 4

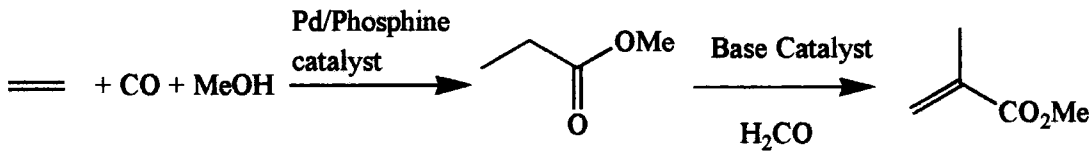

Equation 5

Improvements in the two-stage ethene process have recently been patented by ICI. Using a palladium-diphosphine catalyst high rates and selectivity to the propionic ester can be achieved. However, the high rates and selectivity could only be achieved with specific diphosphines, promoted by small quantities of organic acids. A similar exacting dependence on the nature of the phosphine was discovered by Drent/Shell,[5] for the catalytic production of CO/ethene co-polymer. By changing the phosphine

from a mono-phosphine (PPh_3) to a chelating phosphine ($Ph_2P(CH_2)_nPPh_2$), the selectivity towards the polymer was very high; production of the side product, methyl propionate was minimised.

There is an isoelectronic relationship between Rh(I) and Pd(II) (both are d^8-metals, and in the second row of the transition elements in the periodic table). So it would not be unreasonable for them both to display similar stoicheometric and catalytic reactions, and indeed both CO/ethene co-polymerisation and the hydroesterification of ethene to form methyl propionate have both been observed with rhodium mono-phosphine catalysts. However, the rates and selectivity were less than desirable.

This thesis is concerned with the chemistry of rhodium-chelating phosphine compounds similar to those employed in the ICI methyl propionate process. In particular the reactions of these species with carbon monoxide, hydrogen and other molecules capable of generating potential catalytic intermediates has been investigated.

This work consists of ten chapters. Chapter 1 contains an overview of rhodium chemistry with particular emphasis on rhodium-phosphine complexes, and the role of the phosphine in determining reactivity. Chapters 2-9 contain the experimental data collected in this work and discussion/interpretation of these results, whilst Chapter 10 contains the conclusions drawn from the experimental work. In particular, Chapter 2 is concerned with the synthesis and characterisation of the diphosphine (diphos) derivatives [Rh(diphos)(C_7H_8)](BF_4) **(1)** and their reaction with carbon monoxide. These molecules are attractive as starting materials for several reasons: (i) they are active catalysts for a wide variety of processes, including hydroformylation;[6] (ii) the norbornadiene is easily displaced, and this complex can bind all of the reactants necessary for the synthesis of methyl propionate, (iii) the steric and electronic influence of the diphosphine can be systematically altered to 'tune' the properties and reactivity of the complex. Chapter 3 contains details of the silver phosphine complexes isolated during the synthesis of **(1)**, and their characterisation by X-ray crystallography.

In Chapter 4 the catalytic carbonylation activity of complexes of the type **(1)** and related molecules is investigated, especially hydroformylation and hydroesterification. Chapters 5,6, and 7 are concerned with the generation of possible catalytic intermediates such as rhodium-hydrides, rhodium-alkyls and rhodium-acyls from the direct oxidative addition of the appropriate reactants (for example H_2, acyl-, and alkyl-halides) to Rh(I) complexes.

In Chapter 8 alternative syntheses of the novel diphosphine Rh(III) halide species reported in chapter 7 are proposed and the derivatisation of these products is examined. Chapter 9 contains a crystallographic study of the diphosphine Rh(III) halide species reported in Chapters 7 and 8.

---

[1] F.R. Hartley, "Studies in Inorganic Chemistry, Chemistry of the Platinum Group Metals, Recent Developments," Elsevier, Oxford, 1991.
[2] H.M. Colquhoun, D.J. Thompson, M.V. Twigg, "Carbonylation in Direct Synthesis of Carbonyl Compounds," Plenum Press, London, 1991.
[3] G. Eastham, M.Sc. Thesis, "Studies Related to the Oxidative Coupling of Carbon Dioxide and propane at Nickel(0)", Durham University, 1994.
[4] United States Patent Office 3,840,558, A.J.C. Pearson, Monsanto Company.
[5] E. Drent, J.A.M. Van Broekhoven, M.J. Doyle, *J. Organomet. Chem.*, **417**, (1991), 235-251.
[6] C.F. Hobbs, W.S. Knowles, *J. Org. Chem.*, **46**, (1981), 4422-4427.

Chapter 1

Rhodium Phosphine Chemistry

1.1 Rhodium Chemistry

Rhodium is only present to the extent of 0.0001% in the Earth's crust. Even so, this element along with the other platinum group metals (principally Ir, Pd and Pt) have been extensively studied due to their catalytic applications. However, it is not the aim of this review to cover all known rhodium chemistry, as this has been extensively covered elsewhere,[1,2,3,4] but to focus on the chemistry of rhodium phosphine complexes.

Rhodium has the ground state electronic configuration of $[Kr]4d^8 5s^1$. Complexes of this metal have been observed in oxidation states from -1 to +6 (for example $[Rh(CO)_4]^-$ and RhF_6 respectively). However, the bulk of organometallic rhodium chemistry is dominated by the +1 and +3 oxidation states. This behaviour contrasts with the other elements in the Rh triad, where the +4 state is relatively stable for Ir, and the +1 oxidation state is relatively unstable for Co. Consequently this chapter will concentrate on rhodium in the +1 and +3 oxidation states, and the interchange between these two. Rh(I) (d^8) complexes tend to be square planer whilst those of Rh(III) (d^6) are octahedral or five co-ordinate, and are normally 16/18 electron systems.[5]

There are three important classes of reactions of relevance to the present work: nucleophilic substitution, oxidative addition (and reductive elimination), and migratory insertion (and migratory de-insertion), and each will be discussed separately below.

1.1.1. Nucleophilic Substitution

Nucleophilic attack may occur either at the metal, or at the ligand. When a nucleophile attacks the metal either a current ligand may be displaced to provide a co-ordination site or, if a complex contains bridging ligands, the bridge can be broken.

For example, the L type 2-electron ligand CO reacts with $[Rh(ethene)_2Cl]_2$ to displace ethene, and form $[Rh(CO)_2Cl]_2$. In this instance the halide bridge remains intact,[6] and a high pressure of CO is required subsequently to break it. However, in the presence of CO and dppe the halide bridge in $[Rh(COD^*)Cl]_2$ **(1)** cleaves to form $[Rh(dppe^*)(CO)Cl]$.[7] Complex **(1)** reacts with the chelating phosphine etdp, to displace the chloride ion and form the stable cationic 16-electron complex $[Rh(etdp^*)(COD)](Cl)$.[8] Substitution reactions are not limited to L type ligands. For example, complex **(1)** reacts with allylmagnesiumbromide to form the η^3-allyl (LX) complex $[Rh(COD)(\eta^3\text{-}C_3H_5)]$.[9] Other transition metal complexes can act as nucleophiles. For example, $[Rh(dppe)Cl]_2$ reacts with $[Cp_2TaH_3]$ to form the mixed transition metal complex $[\{TaCp_2\}\{Rh(dppe)\}(\mu\text{-}H)(\mu\text{-}Cl)]$,[10] in which the Ta-H bonds act as the nucleophile and dihydrogen is lost in the process.
Transition metals with low spin d^6 octahedral configurations are kinetically stable and inert towards substitution reactions.[11] Consequently any reactions that do occur are controlled by the rate of dissociation of the ligands from the metal. However, $RhCl_3.3H_2O$ does react readily with L type ligands, such as SR_2 and PR_3 to form stable complexes of the type $[RhL_3Cl_3]$.[12]

An alternative to nucleophilic attack at the metal is the inter-molecular nucleophilic attack at a ligand which is promoted by co-ordination to the metal. For example, $[Rh(PPh_3)_2(CO)_2](BF_4)$ reacts with sodium methoxide in methanol to form the alkoxycarbonyl complex $[Rh(PPh_3)_2(CO)(CO_2Me)]$,[13] and rules have been established

---

* COD = 1,5-cyclooctadiene; dppe = 1,2-Bis(diphenylphosphino)ethane;
etdp = N,N,-Bis(diphenylphosphido)ethylamine.

governing the position of attack on co-ordinated polyenes when there are several possible sites of attack of the nucleophile.[5] The nucleophile always attacks the open face; polyenes react before polyenyl; open ligands react before closed and usually in the terminal position.

1.1.2. Oxidative Addition/Reductive Elimination

Oxidative addition to Rh(I) complexes to form Rh(III) complexes, and the reverse process, reductive elimination, are usually facile reactions. Both of these reactions are very important in catalytic rhodium chemistry, and reductive elimination is the last step in many postulated catalytic cycles. However, of the two reactions there are more documented examples of oxidative addition. The nature of the products from the oxidative addition of a molecule XY to a Rh(I) complex is dependent on the polarity of the XY bond. If XY is polar, then X and Y will occupy mutually *trans* positions in the product formed. However, if XY is non-polar, addition will occur in a concerted fashion and X and Y will occupy mutually *cis* positions.[11] For example, H_2 and HCl oxidatively add to $[Rh(dppp)_2](BF_4)$ to produce *cis* and *trans* products respectively (see Equation 1).[14]

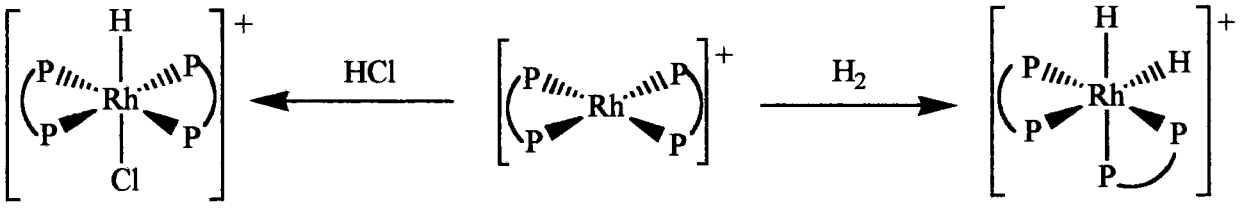

Equation 1

These results are consistent with a concerted reaction mechanism for the addition of H_2 *via* a three centred intermediate. The reaction with HCl proceeds *via* a non-concerted process. Electrophilic attack of the proton occurs prior to the addition of the halide ion, which occupies the vacant position in the five co-ordinate intermediate.

Organo-halide species (RX) will oxidatively add to rhodium complexes, for example $[Rh(PEt_3)_2(CO)Cl]$ reacts with CH_2I_2 to form *trans*-$[Rh(PEt_3)_2(CO)(CH_2I)(Cl)I]$.[15] The rate of addition to these species is dependent on the strength of the C-X bond.

Oxidative addition of RX is observed when X = I, Br, Cl, but the rate of the reaction is in the order I >> Br > Cl. Even C-H bonds can oxidatively add to some rhodium complexes. For example $[Rh(PMe_3)_3Cl]$ reacts with aldehydes to form a hydrido-Rh(III)-acyl species (see Equation 2) in a concerted fashion.[16]

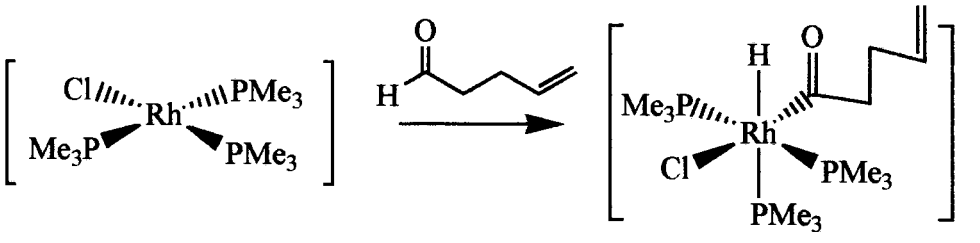

Equation 2

The reverse of oxidative addition is reductive elimination. Actual examples of this reaction involving rhodium are sparse due to the reactivity of the species involved. However, Halpern *et al.* have observed, at low temperature, intermediates in the hydrogenation of prochiral olefins (see Equation 3). When complex **(2)** is warmed from -78°C in methanol, elimination occurs and the catalyst is regenerated.[17]

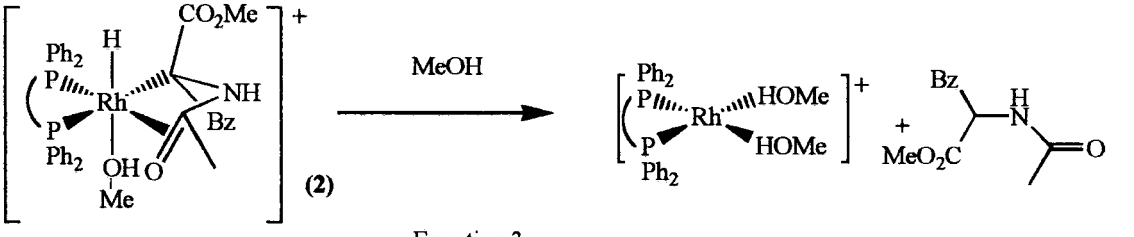

Equation 3

1.1.3. Migratory Insertion

This concerns the movement of an X type (1-electron) ligand onto an L type ligand or the insertion of an L type ligand into a metal-X bond to leave a new X type ligand. This reaction is frequently reversible and may be encouraged by adding an extra ligand to fill the vacant co-ordination position created. For example, addition of PR_3 to [CpRh(CO)X(Me)] promotes the migration of the methyl group onto the carbonyl and

an acyl complex [CpRh(PR_3)X(COMe)] is formed.[18] The rate of this reaction is dependent on both the electronegativity of X (Cl > Br > I) and the basicity of the phosphine ($PMePh_2$ > PPh_3 > $P(OPh)_3$). Equally, the reverse reaction may be encouraged by the removal of a ligand from the co-ordination sphere of the metal. For example, removal of a halide ligand from [Ir($PMePh_2$)$_3$(COC_3H_5)Cl_2] with NH_4PF_6 creates a vacant co-ordination position. Decarbonylation of the acyl group then occurs and a co-ordinatively saturated species *mer*-[Ir($PMePh_2$)$_3$(CO)(C_3H_5)Cl](PF_6) is formed.[19] Other factors can influence the course of migratory deinsertion reactions, and the decarbonylation of [Rh{$Ph_2P(CH_2)_2OMe$}$_2$(COR)Cl](BPh_4) to form [Rh{$Ph_2P(CH_2)_2OMe$}$_2$(CO)(R)Cl](BPh_4) is dependent on the steric bulk of the R group on the acyl ligand. Decreasing the steric bulk of the R group, encourages the deinsertion of CO from the acyl due to reduced steric crowding in the product.[20]

1.2. Rhodium-Phosphine Interactions

There are two components to transition metal ligand bonding interactions. Sigma (σ) bonds involve orbitals that lie directly between the metal and the ligand, whilst π bonds utilise orbitals that do not lie directly between the two atoms. Both of these bonding modes are displayed by phosphines (see Figure 1).

Figure 1 Metal-Phosphorus Bonding Interactions

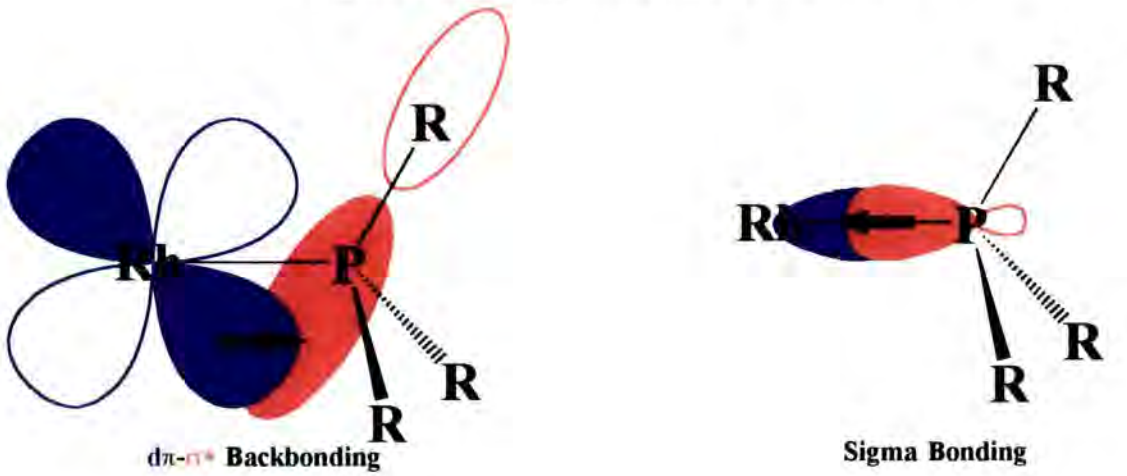

Sigma (σ) donation occurs from the lone pair on the phosphorus to the metal. At the same time electron density from the filled d orbitals on the metal is donated to the phosphine. The extra electron density is redistributed into the P-X anti-bonding (σ^*) orbitals.[†] Consequently metal to ligand backdonation results in an increase of the P-R bond distances.[21] The extent to which $d\pi$-σ^* backdonation occurs is dependent on both the substituents (X) on the phosphine and the oxidation state of the metal. The degree of backdonation to a phosphine PX_3 is in the order $PF_3 >> P(OR')_3 > P(Aromatic)_3 > P(Alkyl)_3$.[11] This corresponds to a decrease in the P-X bond strength, consequently the $\sigma^*_{(P\text{-}X)}$ is lower in energy, and there is more efficient overlap with the d orbitals of the metal. The backbonding properties of PF_3 are similar to those of CO, whilst those of trialkyl phosphines are limited. As the oxidation state of the metal is reduced, the d orbitals on the metal responsible for back donation become significantly more populated. Backdonation to the ligands is increased, which leads to an increase in the P-X bond length and a decrease in the P-M bond length, as observed for complexes in low oxidation states.[21] So far only electronic factors have been considered. However, when very bulky phosphines (for example PBu^t_3) are used, steric interactions can occur, resulting in increased M-P bond lengths and a reduction in the number of ligands co-ordinated to the metal. For mono-phosphines this was quantified by the Tolman cone angle.[22] However, due to the *cis* configuration observed for chelating phosphines, a more useful tool is the bite angle (defined as the angle between the two M-P bonds). Recently it has been suggested that M-P bonds can bend in mono-phosphine complexes, due to steric interactions with other ligands in the compound,[23] and in *cis* chelating phosphine complexes due to the conformational restrictions imposed by the chelate ring.[24]

[†] However if the d orbitals on the phosphorus are of similar energy to the P-X antibonding orbitals then it is likely that hybridisation will occur.

1.3. The Chemistry of Rhodium Chelating Phosphine Complexes

Rhodium phosphine complexes are interesting both for their catalytic and stoicheometric reactions. However, the aim of this review is to cover only the chemistry concerned with diphosphines. In particular those involved in chelating interactions, and mono, poly and diphosphines in other situations will only be mentioned by way of comparison.

1.3.1. Co-ordination Modes of Diphosphines

There are four possible modes of co-ordination for a bidenate phosphine (see below), determined by the steric and electronic requirements of the complex.

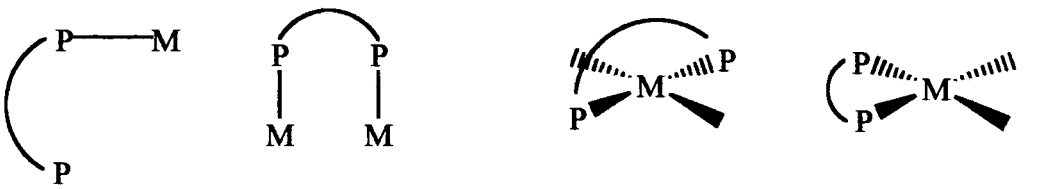

(A) monodentate **(B)** bridging **(C)** chelating *trans* **(D)** chelating *cis*

Type **(A)** complexes with the diphosphine involved in only one interaction with a metal are rare and these molecules are often fluxional due to the nucleophilic nature of the pendant phosphine. A more commonly observed co-ordination mode is the bridging systems **(B)** which is most frequently found for dppm (see Figure 2) and other phosphines with a single carbon atom in the backbone.

Figure 2. Bridging Dppm Complexes

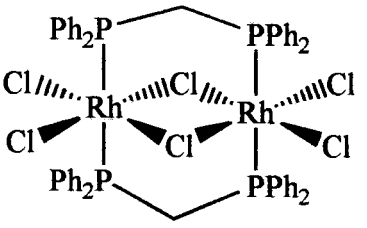

$[Rh_2(dppm)_2Cl_6]$[25]

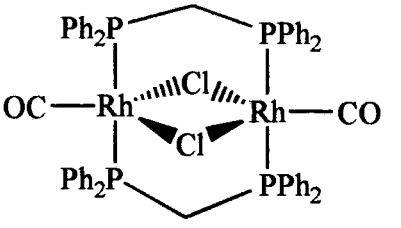

$[Rh_2(dppm)_2(CO)_2Cl_2]$[26]

However, under certain circumstances phosphines with longer backbones can form bridging species. For example the dppb complex $[Rh_2(dppb^{‡})_2(\mu\text{-dppb})(CO)_4](PF_6)_2$ containing two chelating, and one bridging diphosphine has been characterised by X-ray crystallography.[27]

The commonest bonding mode for diphosphines is *cis* chelation. However, *trans* chelation can occur if there are more than four carbon atoms in the backbone of the phosphine. Even if this is the case, *trans* chelation will only occur if it is enforced, such as for complexes **(3)**,[28] **(4)**[29] and **(5)**[30] (see Figure 3).

Figure 3. *Trans* Chelating Rhodium Diphosphine Complexes

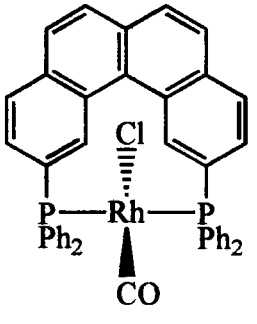

(3)

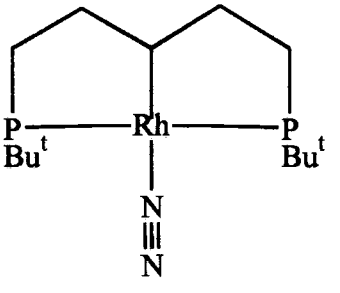

(4)

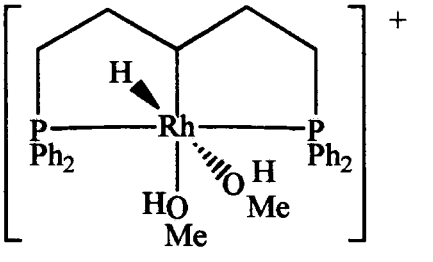

(5)

‡ dppb = 1,2-Bis(diphenylphosphino)butane; dppm = 1,2-Bis(diphenylphosphino)methane

1.3.2. The Synthesis of Rhodium Diphosphine Complexes

Rhodium diphosphine complexes are conveniently synthesised by the displacement of other ligands from a suitable rhodium salt. $RhCl_3.3H_2O$ reacts with mono-phosphines to produce a variety of rhodium(III) phosphine complexes and these have been extensively studied.[31,32,33,34] The nature of the product is dependent on both the stoicheometry of the reaction and the nature of the phosphine. For example $RhCl_3.3H_2O$ is reduced by PPh_3 in methanol to form the Rh(I) complex $[Rh(PPh_3)_3Cl]$.[35] In other cases halide bridged species such as $[Rh_2(PBu^n{}_3)_4(\mu\text{-}Cl)_2Cl_4]$ can be formed.[36] The products from the reaction with chelating phosphines are less well documented. The stoicheometric reaction of dppm with $RhCl_3.3H_2O$ produces the solvate adduct $[Rh(dppm)(MeOH)Cl_3]$ with the solvent *cis* to both phosphines.[37] Dppe reacts with $RhCl_3.3H_2O$ in methanol, in the presence of HCl and an alkyl ammonium salt to produce $[Rh(dppe)_2Cl_2][Rh(dppe)Cl_4]$ in low yield.[38] A more efficient route to the cation $[Rh(diphos)_2Cl_2]^+$ is to heat $RhCl_3.3H_2O$ with excess phosphine in refluxing ethanol.[39]

A more frequently employed route to rhodium diphosphine complexes is the substitution of alkene ligands in rhodium(I) complexes. For example, $[Rh(ethene)_2Cl]_2$ reacts with one equivalent of diphos to form the chloride bridged species $[Rh(diphos)Cl]_2$. However, reaction with excess phosphine leads to cleavage of the halide bridge and $[Rh(diphos)_2](Cl)$ is formed.[40] Rh(III) diphosphine complexes can then be formed by the oxidation of the Rh(I) complexes.[41,42]

1.3.3. The Reaction Chemistry of Rhodium Chelating Diphosphine Complexes

Chelating diphosphine rhodium complexes undergo a variety of reactions common to general rhodium chemistry. However, by tailoring the stereochemical and electronic properties of the chelating phosphine the reactivity of the complex can be modified, and the products from the reaction directed towards a desired end. Even relatively

small changes in the phosphine can produce a pronounced effect on the products of a reaction. This section is concerned with the effect that modifications in the phosphine can produce on the reactivity of rhodium complexes in stoicheometric reactions.

1.3.3.1. The Synthesis of Rhodium Hydrides

$[Rh(diphos)(diene)]^+$ **(6)** type complexes react with hydrogen gas, the diene being lost as an alkane. The nature of the products from this reaction is dependent on the phosphine and the solvent employed. Hydrogenation of aryl[§] substituted phosphine complexes in co-ordinating solvents (such as, methanol) forms disolvato-species $[Rh(diphos)(Solvent)_2]^+$, whilst in non-co-ordinating solvents, η^6-arene bridged dimers are formed.[43] No hydrides are observed for this reaction except when the phosphine can chelate *trans* across the complex (for example, with $Ph_2P(CH_2)_5PPh_2$).[30] In this case the rhodium can insert into a C-H bond in the backbone of the phosphine and a hydride forms (complex **(5)**). When **(5)** is treated with hydrogen gas, the metal-carbon bond is reduced and a *trans* dihydride is formed. The *trans* dihydride formed is similar to the product from the hydrogenation of the analogous mono-phosphine complexes (see below).[44]

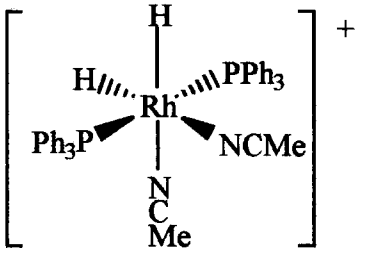

It is clear that the lack of hydrides in the *cis* chelating phosphine systems is due to the enforced *cis* conformation of the phosphine, since any hydride formed would always be *trans* to a phosphine and both hydrides and phosphines display a large *trans* effect.[11] The behaviour of the aryl substituted chelating phosphines contrasts with that of the alkyl substituted phosphines, which form hydrides in non-coordinating solvents, similar

[§] $R_2P(CH_2)_nPR_2$; aryl substituted R is Ph, alkyl substituted R is an alkyl group

to those observed for iridium diphosphine complexes.[45] After hydrogenation of the d*i*ppe derivative of complex **(6)** in $CDCl_3$, hydride resonances have been observed in the proton NMR, although the nature of the product is unclear.[46] Hydrogenation of $[Rh(di ppe^{**})(C_7H_8)](ClO_4)$ in methanol does produce hydrides and the perchlorate bridged dimer $[Rh_2(di ppe)_2(\mu\text{-}H)_2(H)_2(\mu\text{-}ClO_4)](ClO_4)$ has been identified by X-ray crystallography.[47] Introducing ferrocene into the backbone of the phosphine again changes the reactivity.[48] Hydrogenation of the dBpf, dBppf, dppf** derivatives of complex **(6)** leads to the formation of fluxional tetrahydrides in solution. However, in the solid state these complexes crystallise as the dimeric penta-hydride species of the type $[Rh_2(diphos)_2(\mu\text{-}H_3)(H)_2]^+$.[49]

The bis-diphosphine species $[Rh(diphos)_2]^+$ react with hydrogen to form *cis*-dihydride products $[Rh(diphos)_2(H)_2]^+$. Generally the stability of these *cis*-dihydrides is dependent on the size of the chelate ring. Hydrides were not observed at 1atm. hydrogen pressure using diphos = dppm and dppe, whereas the dppb, and diop†† hydride derivatives are only stable in the solid state. However, the dppp hydride complex does form and is stable in solution even in the absence of hydrogen gas.[14]

Neutral dimeric hydride species can be formed from the hydrogenation of the allyl derivatives $[Rh(diphos)(\eta^3\text{-}C_3H_5)]$ (diphos = d*i*ppe, d*i*ppp, d*i*ppb**).[9] There are two products formed in this reaction, a dimeric dihydride of the type $[Rh_2(diphos)_2(\mu\text{-}H)_2]$, and a tetrahydride of the type $[Rh_2(diphos)_2(\mu\text{-}H)_3H]$. The stability and reactivity of these complexes is dependent on the electronic and steric properties of the phosphine. For the d*i*ppe and d*i*ppp derivatives, the tetrahydride is unstable with respect to loss of hydrogen in the absence of a hydrogen atmosphere, whilst the complex $[Rh_2(di ppb)_2(\mu\text{-}H)_3H]$ is stable even in a vacuum. In this respect the behaviour of the d*i*ppb species most resembles that of the mono-phosphine analogue PPr^i_3.[50] The

---

** d*i*ppe = 1,2-Bis(di*iso*propylphosphino)ethane; d*i*ppp = 1,2-Bis(di*iso*propylphosphino)propane; d*i*ppb = 1,2-Bis(di*iso*propylphosphino)butane; dBpf = 1,1'-Bis(di*tert*butylphosphino)ferrocene; dBppf = 1,1'-Bis(phenyl*tert*butylphosphino)ferrocene; dppf = 1,1'-Bis(diphenylphosphino)ferrocene.

†† diop = 4,5-Bis(diphenylpropylphosphino)methyl-2,2'dimethyl-1,3 dioxolane.

reactivity of the dihydrides with alkenes has been investigated. The d*i*ppp derivative will only react with ethene, whilst the d*i*ppe derivative will react with all but the bulkiest of alkenes. The product from the ethene reaction is the bridged species $[\{Rh(di ppe)\}_2(\mu\text{-}H)(\mu, \sigma, \eta^2\text{-}CHCH_2)]$.[51] The difference in reactivity has been attributed to electronic effects. Interestingly, unlike $P(NMe_2)_3$,[52] the related chelating phosphite analogue $(Pr^iO)_2P(CH_2)_2P(Pr^iO)_2$ and mono phosphite analogues are both unreactive towards alkenes.

1.3.3.2. Reactions of Rhodium Diphosphine Complexes with CO

With CO a similar reactivity trend to that observed with hydrogen is noted for $[Rh(diphos)_2]^+$ (diphos = dppm, dppe, dppp, dppb) complexes.[14] The dppe derivative is completely unreactive. However, the dppm and dppp species do react to form 18-electron complexes of the type $[Rh(diphos)_2(CO)]^+$. These complexes are stable as solids, but lose CO in solution if a CO atmosphere is not maintained. The reaction with the dppb complex produces the dimer $[Rh_2(dppb)_3(CO)_4]^{2+}$ with the loss of one of the chelating phosphines.[53]

1.3.3.3. Reactions Of Rhodium Diphosphine Complexes with O_2

The dppe, and dppp derivatives of the type $[Rh(diphos)(NBD)](BF_4)$ are unreactive in solution towards molecular oxygen. However the PPy_3 analogue quickly reacts, and an equilibrium is established between the oxygenated and deoxygenated products.[54]

$$[Rh(PPy_3)_2(NBD)](BF_4) + O_2 \rightleftharpoons [Rh(PPy_3)_2(NBD)(O_2)](BF_4)$$

If the diene ligand is removed from $[Rh(dppe)(NBD)](BF_4)$ by hydrogenation, exposure to oxygen results in the formation of $[Rh(dppe)(H_2O)_2O_2]^+$. Addition of

N_2O_4 or SO_2 to this oxygenated species results in the formation of $[Rh(dppe)(H_2O)_2(NO_3)_2]^+$ and $[Rh(dppe)(H_2O)_2(SO_4)]^+$ respectively.[54]

The reaction of complexes of the type $[Rh(diphos)_2]^+$ towards O_2 in solution is dependent on the phosphine. For the phosphines dppm, dppe and dppp, the dioxygen adduct $[Rh(diphos)_2O_2]^+$ is formed. However, these species are only stable as solids; in solution, in the absence of an oxygen atmosphere the oxygen ligand is lost. The behaviour of the dppb species differs from that of the smaller ring chelates, reaction with oxygen is slower, and oxidation of the chelating phosphine ligands occurs to form the diphosphine dioxide product.[14]

1.3.3.4. Reactions Of Rhodium Diphosphine Complexes with Lithium Reagents

[Rh(diphos)Cl] (diphos = dBpe[‡‡] or d*i*ppe) reacts with a range of lithium reagents (RLi) to displace the halide ion and form a series of mixed Rh-Li complexes, for example complex **(7)**.[55]

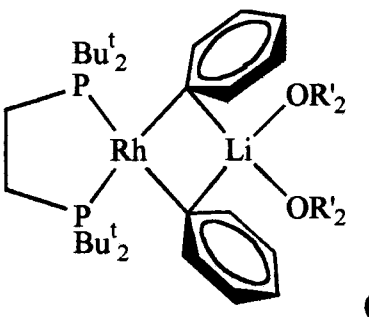

(7)

Complex **(7)** is thermally stable and does not react with alkenes or RLi, although hydrolysis with *i*PrOH affords the dimeric, hydride bridged species $[\{Rh(dBpe)\}_2(\mu\text{-}H)_2]$. This contrasts with the behaviour of the d*i*ppe analogue which is thermally unstable and undergoes exchange reactions with free RLi reagents. This difference in behaviour has been attributed to the reduced steric bulk of the d*i*ppe analogue.[55]

[‡‡] dBpe = 1,2-Bis(di*tert*butylphosphino)ethane.

1.3.4. The Catalytic Chemistry of Rhodium Chelating Diphosphine Complexes

Section 1.3.3. was concerned with the influence of the phosphine on the reaction chemistry of rhodium diphosphine complexes. This section is concerned with the influence that the phosphine can exert on the catalytic activity of rhodium complexes. Rhodium chelating phosphine complexes are used in a great many catalytic processes including hydrogenations, carbonylations, cyclisations and isomerisations (see below). In catalytic reactions the influence of the phosphine can be considerably more pronounced than in stoicheometric reactions, and small changes in the basicity or steric bulk of the phosphine can have dramatic effects.

1.3.4.1. Hydrogenation Reactions Catalysed by Rhodium Diphosphine Complexes

One of the most extensively studied catalytic processes is the homogenous catalytic hydrogenation of alkenes. In particular asymmetric hydrogenation has been studied due to the relative ease with which chiral multiplication can be achieved under mild conditions (1atm H_2, r.t.).[56] Excellent results have been achieved by the incorporation of chirality into chelating phosphines.[57] Particular success has been achieved using substrates that can chelate to the rhodium. For example methyl(z) α-acetamidocinnamate (MAC) can co-ordinate *via* the alkene double bond and the amido oxygen.[58] Using these systems enantiomeric excesses (e.e.) of 99.95% can be achieved.[54] The rhodium precursor complexes used to achieve these results are typically of the type $[Rh(diphos)(diene)]^+$**(6)**. Interestingly only the chiral aryl derivatives have been developed in this area and the mechanism of chiral transfer is believed to proceed *via* the creation of a chiral pocket by the aryl groups. The prochiral substrate can then form two diastereomers one of which is more stable than the other. It has been demonstrated that the less stable diastereomer reacts more quickly and leads to the majority of the product.[59,60] More fundamental studies on the

mechanism of hydrogenation have been investigated by Halpern and Brown.[59-61] The results of these studies indicate that the mechanism for hydrogenation with chelating phosphines is different to that observed for the mono-phosphine systems observed by Schrock and Osborn.[61] Hydrogenation using rhodium mono-phosphine catalysts proceeds *via* the initial oxidative addition of H_2, whilst the diphosphine catalyst systems are believed to proceed *via* the initial co-ordination of the substrate, the "unsaturate" route.[61] As mentioned above, hydrogenation of complex **(6)** produces dimers or solvent adducts for aryl-diphosphine adducts but hydrides for the mono-phosphine analogues. However, the chelating phosphine species are considerably more active than the mono-phosphine analogues. This difference in reactivity is due to the enforced *cis* conformation required by the diphosphine ligands. Another fundamental difference between the mono and diphosphine species is that for the mono-phosphine species an equilibrium is established in solution between the cationic dihydride and a neutral monohydride (see Equation 4).

$$[Rh(PR_3)_2(H)_2(Solvent)_2]^+ \rightleftharpoons [Rh(PR_3)_2(H)(Solvent)] + H^+$$

(Equation 4)

Both of these hydride species are catalytically active for the hydrogenation of alkenes and the dihydride is considerably more active than the monohydride species. However, the monohydride is a far more active isomerisation catalyst than the dihydride.[62]

Investigations by Halpern on a series of complexes of the type **(6)** (diphos = $PPh_2(CH_2)_nPPh_2$) reveals that the rate of hydrogenation is dependent on the size of the chelate ring. As n increases from 2, through to 4, the rate of hydrogenation increases by a factor of ~10. The largest increase in rate comes from the increase in carbon backbone chainlength from 3 to 4.[63] A similar trend was observed for hydrogenation with the bis-chelate species of the type $[Rh(diphos)_2]^+$, where the order of activity was dppb > dppp > dppe > dppm. Interestingly, comparison of complexes of the types $[Rh(diphos)_2Cl]$ and $[Rh(diphos)_2](BF_4)$ indicated the reaction was considerably faster for the complex with the non co-ordinating anion, presumably due to the availability of

a vacant co-ordination position in the cationic rhodium(I) complex.[64] As well as showing activity for the hydrogenation of simple olefins, $[Rh(dppe)(C_7H_8)]^+$ is active for the partial hydrogenation of arene species under mild conditions.[65] Both anthracene and napthalene can be hydrogenated, although no activity is shown towards benzene itself.

Complexes of the type **(6)** are active precursors for the hydrogenation of carbonyl compounds to alcohols. However, activity is only observed with the stronger electron donating alkyl and not the aryl substituted diphosphines. Tani *et al.*[66] found that the rate of hydrogenation for simple ketones, under mild conditions using the chelating phosphine d*i*ppp, was several orders of magnitude faster than the essentially inactive mono-phosphine analogue PPr^i_3. A similar result was observed by Burk *et al.*,[67] for the catalytic activity of complexes of the type **(6)** using the ferrocenyl diphosphine d*i*ppf in the hydrogenation of benzaldehyde. They found that this complex was significantly more active than mono-phosphine analogues, and no deactivation of the catalyst occurred through decarbonylation of the substrate. The mechanism for this reaction is still unclear. However, the hydrogenation of non-enolisable ketones implies that it does not proceed *via* the hydrogenation of an enol.

An alternative to hydrogenation using molecular hydrogen is transfer hydrogenation, where an alcohol or similar molecule acts as a hydrogen donor (see Equation 5), and is oxidised to the corresponding aldehyde or ketone.

$$MePhC{=}O + Me_2CHOH \rightleftharpoons MePhCHOH + Me_2CO$$

(Equation 5)

Type **(6)** complexes can be used to catalyse this process in the presence of KOH. However, in solution these are converted into an active catalytic species of the type $[Rh_3(diphos)_3(OR)_2](BF_4)_2$.[68] The first reported example was $[Rh_3(dppe)_3(OMe)_2](BF_4)_2$ from the reaction of $[Rh(dppe)(MeOH)_2]^+$ and base.[59]

Several more have been reported and the stability of these species is dependent on the steric bulk of the facially bridging alkoxide ligands. In fact $[Rh_3(Binap^{\S\S})_3(OH)_2](BF_4)_2$ is so stable the hydroxyl proton will not exchange with D_2O. This complex has been implicated as the deactivated form of the catalytically active species in the isomerisation of allylamines;[69] the related enolate species $[Rh_3(dppe)_3(OC(CH_2)CH_3)_2](ClO_4)_2$ is responsible for the deactivation of the active species in hydrosilation of ketones.[70] The asymmetric transfer hydrogenation of ketones is not as efficient as the hydrogenation of alkenes (see above) and small changes in the carbon backbone of the phosphine can have dramatic effects on the rate and product distribution. For the catalytic transfer hydrogenation of ketones, prophos is more active than chiraphos. However, chiraphos produced higher optical yields.[67] An alternative hydrogen source is from the water-gas shift reaction, and phenylacetone has been successfully hydrogenated to the corresponding alcohol in the presence of CO, using $[Rh(dppe)(COD)]^+$ as the catalyst.[71]

1.3.4.2. Hydrosilation Reactions Catalysed by Rhodium Diphosphine Complexes

Asymmetric hydrosilation of ketones is an alternative method of introducing chirality into a substrate molecule. This is efficiently catalysed by $[Rh(diphos)(Solvent)_2]^+$ and $[Rh(diphos)(PR_3)_2]^+$ type complexes with a high regioselectivity towards 1,2-addition for α,β-unsaturated ketones (Equation 6).[63]

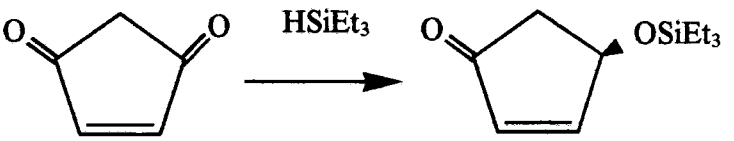

(Equation 6)

The rate of reaction shows a similar dependence on the phosphine to that observed for hydrogenation. The best rates are observed with the diop and dipamp analogues of **(6)**. These are at least ten times more active than dppe, cyphos, and chiraphos. However, the highest selectivities and e.e. are observed for chiraphos. If two

§§ binap = 1,1'-Bis(diphenylphosphino)binapthalene.

equivalents of monophosphine are introduced to form complexes of the type $[Rh(diphos)(PR_3)_2]^+$ similar activities can be achieved. However, these complexes are considerably more stable and no deactivation occurs in the presence of enolisable ketones. Just as the rate of reaction is dependent on the diphosphine component in type **(6)** complexes, a similar dependence is observed for the monophosphine component in these systems. PMe_3 derivatives are catalytically inactive and the best overall results are achieved with PPh_3.[63] Alkyne hydrosilation is efficiently catalysed with $[Rh(dBpm)Cl]_2$.[72] However, significantly greater rates of reaction can be achieved by the addition of two equivalents of a monophosphine, and this system shows a similar dependence on the phosphine basicity to that observed for ketone hydrosilation. Alkene hydrosilation is considerably slower than ketone hydrosilation. However, complexes of the type $[Rh(diphos)(Solvent)_2]^+$ are active for the *intra*-molecular hydrosilation of allylic silyl ethers into heterocycles.[73] If a prochiral alkene is employed then chiral products are formed. When the ligand binap is employed high enantioselectivities are attainable and these are superior to those observed with chiraphos.

1.3.4.3. Hydroformylation Reactions Catalysed by Rhodium Diphosphine Complexes

Rhodium mono-phosphine catalysts (for example, $[Rh(PPh_3)_2(CO)H]$) are highly active and selective for the hydroformylation of simple alkenes and this technology has been commercialised.[74] However these processes use large excesses of the mono-phosphine to stabilise the catalyst which would otherwise be deactivated.[75] Rhodium chelating phosphine complexes (for example, [Rh(diphos)(CO)H]) are generally more stable with respect to ligand dissociation than their mono-phosphine analogues, hence their attractiveness for chiral synthesis.[76] It has been found that by increasing the bite angle of the diphosphine the aryl groups on the phosphine exert an increased steric influence about the metal and this improves the yield of the normal product.[77,78] If chiral phosphines are employed and there is a secondary binding site for the metal in the

substrate then selectivities and e.e. strongly competing with those of the hydrogenation processes can be achieved. For example, at 100 atm. of 1:1 $CO:H_2$ and 60°C, the phosphine **(7)** has been used in conjunction with $[Rh(CO)_2AcAc]$ to promote the enantioselective hydroformylation of the conjugated diene **(8)**.[79]

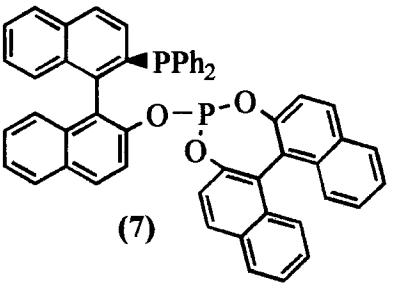

(7)

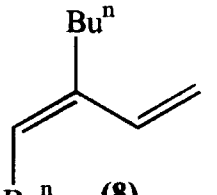

(8)

1.3.4.4. Cyclisation Reactions Catalysed by Rhodium Diphosphine Complexes

Complexes of the type $[Rh_2(diphos)_2](BF_4)_2$ are efficent r.t. catalysts for the intra molecular cyclisation of 4-pentenal to cyclopentanone[80] and butan-1,4-dial to a lactam[81] (see Equations 7 and 8) at r.t..

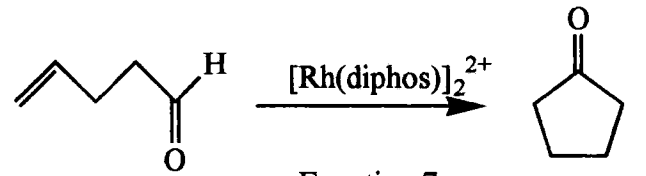

Equation 7

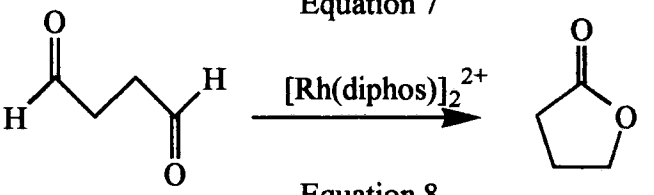

Equation 8

Chelating phosphine systems are significantly more active cyclisation catalysts than mono-phosphine systems. Mono-phosphine complexes {for example $[Rh(PPh_3)_3Cl]$} can only be operated catalytically under a pressure of ethene, and these systems are quickly deactivated by decarbonylation of the substrate.[80]

In both of the cyclisations (Equations 7 and 8), the reaction is believed to proceed *via* the initial activation of the aldehyde C-H bond. Unfortunately the intermediates from

these reactions cannot be isolated or observed spectroscopically. However, deuterium labelling studies on the aldehyde C-D in the pentenal system reveal that during the catalytic process this is distributed to all the positions in the product.[82] This indicates that rapid equilibria are established in solution, including decarbonylation, carbonylation, and β-hydride elimination steps. The rate of reaction is dependent on both the size of the chelate ring and the electron withdrawing nature of the substituents, in the order dcpe > dppb~dppp > dppe > dpf.*** However, increasing the basicity of the phosphine causes a corresponding increase in the rate of aldehyde decarbonylation and formation of the catalytically inactive $[Rh(diphos)(CO)_2]^+$ type complexes. In a similar manner to catalytic hydrogenation, this reaction does not occur in acetonitrile, due to unfavourable competition of the substrate with MeCN for co-ordination to the metal. However, unlike the catalytic hydrogenation of alkenes, this reaction is slow in methanol due to the acetalisation of the starting aldehyde which is catalysed by complexes of the type $[Rh(diphos)(Solvent)_2]^+$ and has been noted in other studies.[83]

When chiral phosphines are employed in complexes of the type $[Rh(diphos)(Solvent)_2]^+$, enantiomerically pure (e.e. 99%) products can be obtained from the cyclisation of 4-substituted 4-pentenals.[84] Interestingly, it was found that binap gave higher e.e. than chiraphos, which also gave the opposite product enantiomer. $[Rh(diphos)_2]^+$ type complexes are active catalysts for the decarbonylation of aldehydes.[85] However, in the presence of 4-substituted 4-pentenals, only cyclisation occurs.[86] Furthermore, it was found that $[Rh(chiraphos)_2]^+$ forms optically purer products than $[Rh(chiraphos)(Solvent)_2]^+$. For the cyclisation of racemic 3-substituted-4-pentenals with $[Rh(diphos)(Solvent)_2]^+$ type complexes, significantly lower e.e. were achieved, and this was attributed to the reversible interconversion between the isomers of starting material, occurring on the metal, and isomerisation to the corresponding 4-substituted 4-pentenal.[87]

*** dpf = 1,2-Bis(di{pentafluorophenyl}phosphino)ethane.

Other cyclisations have been investigated including the cyclisation of alkynoic acids to alkylidene lactones (see Equation 9).

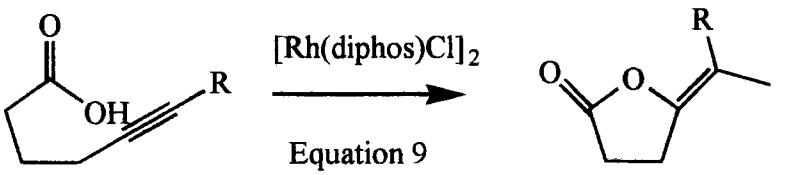

Equation 9

In this case considerable increases in rate and selectivity can be achieved using $[Rh(dcpe)Cl]_2$ under milder conditions than those required by mono-phosphine catalysts (e.g. $[Rh(PPh_3)_3Cl]$).[88] Unlike rhodium complexes, those of iridium are not active catalysts at r.t. and consequently these have been used to model the catalytic cycle, which is believed to proceed *via* the initial oxidative addition of the carboxylic acid group to the metal.[89]

1.3.4.5. Isomerisation Reactions Catalysed by Rhodium Diphosphine Complexes

Complexes of the type $[Rh(diphos)(solvent)_2]^+$ are efficient catalysts for the isomerisation of allylamines to optically pure enamines (see Equation 10).[90] This technology has been commercially developed as part of a route to (-) menthol, and ~1500 t/year are manufactured by this method.

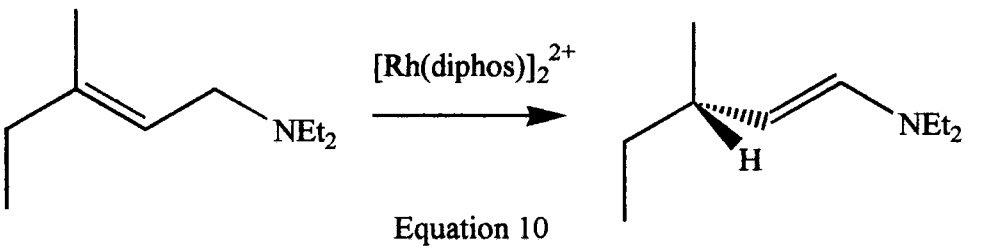

Equation 10

In a similar manner to the previous reactions, the activity of the catalyst is dependent on the phosphine. The best results are obtained with the aryl substituted diphosphines and increasing the basicity of the phosphine by substituting alkyl for aryl groups reduces the activity of the catalyst. This process generates a chiral product. In order

to produce a highly enantioselectivly pure product, a rigid chiral phosphine is required. Consequently the best results were obtained with the ligand binap which was considerably better than the more flexible diop. The activity of the catalyst is also dependent on the rhodium precursor, and $[Rh(dppe)Cl]_2$ and $[Rh(dppe)_2]^+$ are both inactive for this process. However $[Rh(binap)_2]^+$ is active at elevated temperatures (>80°C) and this complex is used in industry due to its increased stability over $[Rh_2(binap)_2]^{2+}$.

In a similar manner to allylamine isomerisation, allyl alcohols can be isomerised to aldehydes.[78] Once again $[Rh(diphos)]_2^{2+}$ type complexes are active for this process and the activity of the catalyst is dependent on the electronic and steric properties of the phosphine. In contrast to the allylamine isomerisation, the highest rates for this process are achieved with the electron rich diphosphine, dcpe.[†††] However, if the activity of the catalyst is reduced, it is possible to isolate the intermediate enol (see Equation 11). The enols formed have been shown to be stable in the absence of catalyst for up to two weeks at r.t.[91]

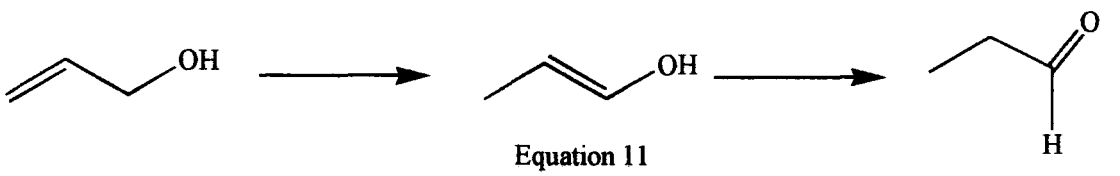

Equation 11

1.3.4.6. The Rhodium Diphosphine Catalysed Oxidation of Alkenes

The oxidation of alkenes with molecular oxygen represents an attractive route to the synthesis of ketones.[92] Complexes of the type $[Rh(diphos)(diene)]^+$ and $[Rh(diphos)_2]^+$ are efficient catalysts for this process, which operates under relatively mild conditions (25-70°C, 1 atm O_2, acidic, alcoholic media). However, under these conditions acetals and alcohols are produced as by products. An alternative method is to use Bu^tO_2H as the oxidant, and mechanistic studies indicate this is a metal rather

[†††] dcpe = 1,2-Bis(dicyclohexylphosphino)ethane.

than radical based process.[93] Unfortunately only $[Rh(dppe)(COD)]^+$ in its reduced form $[Rh(dppe)]_2^{2+}$ is an active catalyst for this process.

1.4. References

[1] N.N. Greenwood, A. Earnshaw, "Chemistry of the Elements," Pergamon Press, Oxford, 1986.
[2] F.R. Hartley, "Studies in Inorganic Chemistry 11, Chemistry of the Platinum Group Elements, Recent Developments", Elsevier Science, Oxford, 1991.
[3] G. Wilkinson, S.F.A. Gordon, A.W. Edward, R.P. Hughes, "Comprehensive Organometallic Chemistry, Volume 5, The Synthesis, Reactions, and Structures of Organometallic Compounds," Pergamon Press, Oxford, 1982.
[4] E.W. Abel, F.G.A. Stone, J.D. Atwood, G. Wilkinson, "Comprehensive Organometallic Chemistry II, Cobalt, Rhodium, and Iridium, Volume 8, A Review of the Literature 1982-1994," Pergamon Press, Oxford, 1982.
[5] R.H. Crabtree, "The Organometallic Chemistry of the Transition Elements", Wiley-Interscience, Chichester, 1988.
[6] J.A. McCleverty, G. Wilkinson, *Inorganic Syntheses*, **28**, (1990), 84-86.
[7] A.R. Sayer, *J. Chem. Soc. Dalton Trans.*, (1977), 120-129.
[8] R.J. Haines, E. Meintjies, *J. Chem. Soc. Dalton Trans.*, (1979), 367.
[9] M.D. Fryzuk, W.E. Piers, F.W.B. Einstein, T. Jones, *Can. J. Chem.*, **67**, (1989), 883-897.
[10] C.P. Casey, G.T. Whitaker, *Inorg. Chem.*, **29**, (1990), 876-879.
[11] A.G. Sykes, "Kinetics of Inorganic Reactions", Pergamon Press, Oxford, 1966.
[12] C.A. McAuliffe, "Transition Metal Complexes of Phosphorus, Arsenic, and Antimony Ligands," Macmillan, London, 1973.
[13] E.W. Ecans, M.B.H. Howlader, M.T. Atlay, *Transition Metal Chem.*, **19**, (1994), 183-186.
[14] B.R. James, D. Mahajan, *Can. J. Chem.*, **58**, (1980), 996-1004.
[15] R.C. Gash, D.J. Cole-Hamilton, R. Whyman, J.C. Barnes, M.C. Simpson, *J. Chem. Soc. Dalton Trans.*, (1994), 1963-1969.
[16] D. Milstein, *J. Chem. Soc. Chem. Commun.*, (1982), 1357-8.
[17] A.S.C. Chan, J. Halpern, *J. Am. Chem. Soc.* **102**, (1980), 838-840.
[18] D. Monti, M. Bassetti, G.L. Sunley, P. Ellis, P.M. Maitlis, *Organometallics*, **10**, (1991), 4015-4020.
[19] N.L. Jones, J.A. Ibers, *Organometallics*, **2**, (1983), 490-494.
[20] E. Lindner, Q.Y. Wang, H.A. Mayer, R. Fawzi, M. Steimann, *Organometallics*, **12**, (1993), 1865-1870.
[21] A.G. Orpen, N.G. Connelly, *Organometallics*, **9**, (1990), 1206-1210.
[22] C.A. Tolman, *Chem. Revs.*, **77**, (1977), 313.
[23] J. Powell, *J. Chem. Soc. Chem. Commun.*, (1989), 200.
[24] E. Linder, R. Fawzi, H.A. Mayer, K. Eichele, W. Willer, *Organometallics*, **11**, (1992), 1033-1043.
[25] F.A. Cotton, K.R. Dunbar, C.T. Eagle, L.R. Falvello, A.C. Price, *Inorg, Chem.*, **28**, (1989), 1754.
[26] F. Shafiq, R. Eisenberg, *Inorg. Chem.*, **32**, (1993), 3287-3294.
[27] L.H. Pignolet, D.H. Doughty, S.C. Nowicki, M.P. Anderson, A.L. Casalnuovo, *J. Organomet. Chem.*, **202**, (1980), 211-223.
[28] F.J.S. Reed, L.M. Venanzi, *Helv. Chim. Acta*, **60**, (1977), 2804-2814.
[29] A. Vigalok, Y. Bendavid, D. Milstein, *Organometallics*, **15**, (1996), 1839-1844
[30] J.M. Brown, P.A. Chaloner, A.G. Kent, B.A. Murrer, P.N. Nicholson, D. Parker, P.J. Sidebottom, *J. Organomet. Chem.*, **216**, (1981), 263-276.
[31] G.M. Intille, *Inorg. Chem.*, **11**, (1972), 695-702.
[32] F.A. Cotton, J.L. Eglin, S.J. Kang, *Inorg. Chem.*, **32**, (1993), 2332-2335.
[33] F.A. Cotton, S.K. Mandel, S.J. Kang, *Inorg. Chim. Acta.*, **206**, (1993), 29-39

[34] J. Chatt, N.P. Johnson, B.L. Shaw, *J. Chem. Soc. A*, (1964), 2281-3512.
[35] J.A. Osborn, G. Wilkinson, *Inorganic Syntheses*, **28**, (1990), 77-79.
[36] G. Chioccola, J.J. Daly, *J. Chem. Soc. A*, (1968), 1981.
[37] F.A. Cotton, K.R. Dunbar, C.T. Eagle, L.R. Falvello, A.C. Price, M.G. Verbruggen, S.J. Kang, *Inorg. Chim. Acta.*, **184**, (1991), 35-42.
[38] R.A. Cipriano, L.R. Hauton, W. Levason, D. Pletcher, N.A. Powell, M. Webster, *J. Chem. Soc. Dalton Trans.*, (1988), 2483-2490.
[39] V.M. Miskowski, J.L. Robbins, G.S. Hammond, H.B. Gray, *J. Am. Chem. Soc.*, **98**, (1976), 1301-2688.
[40] D.A. Slack, D.L. Egglestone, M.C. Baird, *J. Organomet. Chem.*, **146**, (1980).
[41] J. Chatt, B.L. Shaw, *J. Chem. Soc. A.*, (1966), 1437.
[42] R.F. Heck, *J. Am. Chem. Soc.*, **86**, (1964), 2796.
[43] J. Halpern, D.P. Riley, A.S.C. Chan, J.J. Pluth, *J. Am. Chem. Soc.*, **99**, (1977), 8057-8055.
[44] J.R. Shapley, R.R. Schrock, J.A. Osborn, *J. Am. Chem. Soc.*, **91**, (1969), 2816-2817.
[45] H.H. Wang, L.H. Pignolet, *Inorg. Chem.*, **19**, (1980), 1470-1480.
[46] I.R. Butler, W.R. Cullen, B.E. Mann, C.R. Nurse, *J. Organomet. Chem.*, **280**, (1985), C47-C50
[47] K. Tani, T. Yamagata, Y. Tatsuno, T. Saito, Y. Yamagata, N. Yasuoka, *J. Chem. Soc. Chem. Commun.*, (1986), 494-495.
[48] T.J. Kim, *Bull. Kor. Chem. Soc.*, **11**, (1990), 134-139.
[49] I.R. Butler, W.R. Cullen, T.J. Kim, F.W.B. Einstein, T. Jones, *J. Chem. Soc. Chem. Commun.*, (1984), 719.
[50] J. Wolf, O. Nurnberg, M. Schafer, H. Werner, *Z. Anorg. Allg. Chem.*, **620**, (1994), 1157-1162.
[51] M.D. Fryzuk, W.E. Piers, *Polyhedron*, **7**, (1988), 1001-1004; M.D. Fryzuk, T. Jones, F.W.B. Einstein, *Organometallics*, **3**, (1984), 185-191
[52] E.B. Meier, R.R. Burch, E.L. Muetterties, V.W. Day, *J. Am. Chem. Soc.*, **104**, (1982), 2661-2663.
[53] L.H. Pignolet, D.H. Doughty, S.C. Nowicki, A.L. Casalnuovo, *Inorg. Chem.*, **19**, (1980), 2172-2177.
[54] M. Bressan, F. Morandini, P.Rigo, *Inorg. Chim. Acta*, **121**, (1986), 219-222; M. Bressan, M. Molvillo, *Inorg. Chim. Acta*, **77**, (1983),L139-L142.
[55] A.A. Del Paggio, R.A. Anderson, E.L. Muetterties, *Organometallics*, **6**, (1987), 1260-1267.
[56] B.D. Vineyard, W.S. Knowles, M.J. Sabacky, G.L. Bachman, D.J. Weinkauff, *J. Am. Chem. Soc.*, **99**, (1977), 5946.
[57] D.P. Riley, *J. Organomet. Chem.*, **234**, (1982), 85-97.
[58] A.S.C. Chan, J.J. Pluth, J. Halpern, *Inorg. Chim. Acta*, **37**, (1979), L477-L479.
[59] A.S.C. Chan, J.J. Pluth, J. Halpern, *J.Am. Chem. Soc.*, **102**, (1980), 5952-5954.
[60] J.M. Brown, P.A. Chaloner, *J. Chem. Soc. Chem. Commun.*, (1980), 344-346.
[61] J.M. Brown, P.A. Chaloner, *J. Am. Chem. Soc.*, **102**, (1980), 3040-3048.
[62] R.R. Schrock, J.A. Osborn, *J. Am. Chem. Soc.*, **98**, (1976),2134-2143.
[63] C.R. Landis, J. Halpern, *J. Organomet. Chem.*, **250**, (1983), 485-490.
[64] B.R. James, D. Mahajan, *Can. J. Chem.*, **57**, (1979), 180-187.
[65] C.R. Landis, J. Halpern, *Organometallics*, **2**, (1983), 840-842.
[66] K. Tani, K. Suwa, E. Tanigawa, T. Yoshida, T. Okano, S. Otsuka, , *Chem. Lett.*, (1982), 261-264.
[67] M.J. Burk, T. Gregory, P. Harper, R.L. Lee, C. Kalberg, *Tetrahedron Lett.*, **35**, (1994), 4936-4966.
[68] R. Spogliarich, J. Kaspar, M. Graziani, *J. Catal.*, **94**, (1985), 292-296.
[69] T. Yamagata, K. Tani, Y. Tatsuno, T. Saito, *J. Chem. Soc. Chem. Commun.*, (1988), 466-468.
[70] T.E. Waldman, G. Schaefer, D. Riley, *ACS Symposium Ser.*, **517**, (1993), 58-74.
[71] J. Kaspar, R. Spogliarich, A. cernogaraz, M. Graziani, *J. Organomet. Chem.*, **255**, (1983), 371-376
[72] P. Hoffmann, C. Meier, W. Hiller, M. heckel, J. Reide, M.U. Schmidt, *J. Organomet. Chem.*, **490**, (1995), 51-70.
[73] S.H. Bergens, P. Noheda, J. Whelan, B. Bosnich, *J.Am. Chem. Soc.*, **114**, (1992), 2121-2128; *ibid.*, **114**, 2128-2155.

[74] R. Fowler, Br. Pat. 138 7657, Davy-Mckee; N. Harris, T.F. Shevels, U.S. Pat. 424 228, Davy-McKee; A.J. Dennis, G.E. Harrison, J.P. Wyber, U.S. Pat. 4496769, 1985, Davy-McKee; *ibid*, 4567306, 1986, Davy-McKee.

[75] R.M. Deshpande, S.S. Divekar, R.V. Ghalop, R.V. Chandharic, *J. Molec. Catal.*, **67**, (1991), 333-339.

[76] C.F. Hobbs, W.S. Knowles, *J. Org. Chem.*, **46**, (1981), 4422-4427.

[77] C.P. Casey, G.T. Whitaker, M.G. Melville, L.M. Petrovich, J.A. Gavney Jr., D.R. Powell, *J. Am. Chem. Soc.*, **114**, (1992), 5535-5543.

[78] T.J. Devon, Eur. Pat. 0375 573, 1990, Eastman Kodak Company.

[79] T. Horiuchi, T. Onta, K. Nozaki, H. Takaya, *J. Chem. Soc. Chem. Commun.*, (1996), 155-156.

[80] D.P. Fairlie, B. Bosnich, *Organometallics*, 7, (1988), 936-945.

[81] S.H. Bergens, D.P. Fairlie, B. Bosnich, *Organometallics*, **9**, (1990), 566-571.

[82] D.P. Fairlie, B. Bosnich, *Organometallics*, 7, (1988), 946-954.

[83] F. Gorla, L.M. Venanzi, *Helv. Chim. Acta*, **73**, (1990), 690-697; J. Ott, G.M.R. Tombo, B. Schmid, L.M. Venanzi, G. Wang, T.R. Ward, *Tetrahedron Lett.*, **30**, (1989), 6151-6154.

[84] R.W. Barnhart, X. Wang, P. Noheda, S.H. Bergens, J. Whelan, B. Bosnich, *J. Am. Chem. Soc.*, **116,** (1994), 1821-1830.

[85] D.H. Doughty, M.P. Anderson, A.L. Casalnuovo, M.F. McGuiggan, C.C. Tso, H.H. Wang, L.H. Pignolet, *Adv. Chem. Ser.*, **22**, (1982) 83-97.

[86] B.R. James, C.G. Young, *J. Organomet. Chem.*, **285**, (1985), 321-332.

[87] R.W. Barnhart, B. Bosnich, *Organometallics*, **14**, (1995), 4343-4348.

[88] D.M.T. Chan, T.B. Marder, D. Milstein, N.J. Taylor,*J. Am. Chem. Soc.*, **109**, (1987), 6385-6388.

[89] T.B. Marder, D.M.T. Chan, W.C. Fultz, J.C. Calabrese, D. Milstein, *J. Chem. Soc. Chem. Commun.*, (1987), 1885.

[90] S. Otsuka, K. Tani, *Synthesis*, (1991), 665-680.

[91] S.H. Bergens, B. Bosnich, *J. Am. Chem. Soc.*, **113**, (1991), 958-967.

[92] M. Bressan, F. Morandini, A. Morvillo, P. Rigo, *J. Organomet. Chem.*, **280**, (1985), 139-146.

[93] P. Muller, H. Idmounaz, *J. Organmomet. Chem.*, **345**, (1988), 187-199.

Chapter 2

The Synthesis and Characterisation of [Rh(diphosphine)(C_7H_8)](BF_4)

2.1. Introduction

As outlined in Chapter 1, complexes of the type [Rh(diphos)(C_7H_8)](BF_4) **(1)** provide versatile starting materials for many catalytic reactions. With a view to investigating their chemistry, particularly in the area of catalytic carbonylation, a range of type **(1)** complexes has been synthesised utilising different phosphines.

The synthesis of complexes of the type **(1)** from rhodium trichloride is summarised in Scheme 1. This reaction proceeds in high overall yield. However, there is the possibility of forming silver by-products. In some cases the silver by-products have been isolated and subsequently synthesised (see chapter 3) .

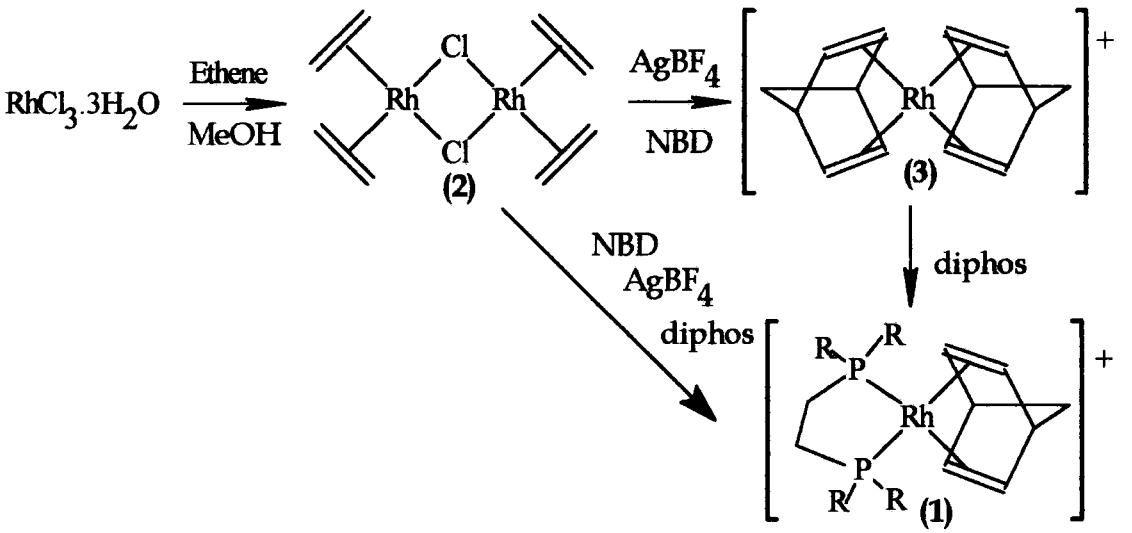

Scheme 1

2.2. Experimental

2.2.1. Synthesis of $[Rh(C_2H_4)_2Cl]_2$[1]

$RhCl_3.3H_2O$ (5.0g, 19mmols) was dissolved in water (7.5cm^3). To this was added methanol (125 cm^3). Ethene was bubbled through the solution for two days. During this time the colour changed from deep red to orange and a mustard coloured solid precipitated. At the end of the reaction the solid, $[Rh(C_2H_4)_2Cl]_2$ **(2)** was collected by filtration, washed with methanol (20cm^3),and then dried *in vacuo* (2.8g, 72%).

2.2.2. Synthesis of $[Rh(C_7H_8)_2](BF_4)$[2]

Complex **(2)** (0.7g, 1.78 mmols) was stirred as a suspension in dichloromethane (30 cm^3), and cooled in an ice bath. A solution of norbornadiene (NBD) (0.93cm^3) in dichloromethane (15cm^3) was added to the slurry. The solution turned deep red-brown on mixing and a gas (ethene) was evolved. The mixture was stirred for 30 minutes to ensure all of the ethene had been displaced and then excess $AgBF_4$ (1.00g, 5.14mmols) was added. Immediately on mixing a white solid (AgCl) was deposited and the solution turned deep red in colour. After 45 minutes the solution was filtered and THF (10cm^3) was added. The volume was reduced under reduced pressure to approximately 5cm^3 and yellow crystals were produced. The crystals were washed twice with THF (15cm^3) to remove any soluble silver impurities.[3] On drying *in vacuo*, the crystals changed from yellow to the deep red colour of $[Rh(C_7H_8)_2](BF_4)$ **(3)** (1.20g, 89%). Found C, 45.03; H 4.76. Calc. for $C_{14}H_{16}BF_4Rh$ C, 44.96; H, 4.31%.^{1}H NMR ($CDCl_3$): δ 5.66 (**4H**, d, =C*H*), 1.65 (**2H**, s, >CH_2), s 4.30ppm (**2H**, s, C*H*), (lit.,[4] δ 5.67 (**8H**, m), 4.28 (**2H**, br m) 1.65 (**4H**, t)) ppm.

FAB Mass Spectrum (methanol/glycerol matrix)

-ve ion: m/z 87 (100%, BF_4^-).

+ve ions: m/z 287 (64%, $Rh(C_7H_8)_2^+$), 195 (82, $Rh(C_7H_8)^+$), 102.9 (22, Rh^+).

2.2.3. Synthesis of $[Rh(Ph_2P(CH_2)_2PPh_2)(C_7H_8)](BF_4)^4$ (4)

1,2-bis(diphenylphosphino)ethane (dppe) (0.51g, 1.28 mmols) dissolved in dichloromethane ($6cm^3$) was slowly added to a solution of complex **(3)** (0.49g, 1.32 mmols) in dichloromethane ($10cm^3$). There was an immediate colour change on mixing the two solutions, from red to orange and an orange solid precipitated from the solution. The solid was recrystallised from dichloromethane-diethyl ether and dried *in vacuo*, (0.50g, 87%). The purity and identity of the product were assessed by comparison of phosphorus and proton NMR spectra with the literature data.[4] $^{31}P\{^1H\}$ NMR (CD_3OD): δ 57.5 (d, $^1J_{Rh-P}$ 158Hz), (lit., 57.3, d, $^1J_{Rh-P}$ 157Hz) ppm. ^1H NMR ($CDCl_3$): δ 7.56-7.54 (**20H**, m, Aryl *H*), 5.40 (**4H**, $^2J_{Rh-H}$ 17.5Hz, $=CH_2$), 2.51 (**4H**, d, $^2J_{P-H}$ 15Hz (PCH_2), 1.93 (**2H**, s, $=CH_2CH$), 1.82 (**2H**, s, CH_2), (lit.,[4] δ 7.75-7.55 (**20H**, m), 5.50 (**4H**, dd), 4.23 (**2H**, br), 2.50 (**4H**, dd $^2J_{P-H}$ 19 $^3J_{Rh-H}$ 1Hz), 1.84 (**2H**, br s)) ppm.

2.2.4. Synthesis of $[Rh(Ph_2P(CH_2)_3PPh_2)(C_7H_8)](BF_4)^4$ (5)

This was synthesised by a similar method to the dppe analogue. The solid was recrystallised from dichloromethane-diethyl ether and dried *in vacuo*, (0.79g, 81%) $^{31}P\{^1H\}$ NMR (CD_3OD): δ 18.8 (d, $^1J_{Rh-P}$ 149Hz), (lit.,[4] 19.6, d, $^1J_{Rh-P}$ 147Hz) ppm. ^1H NMR (CD_3OD): δ 7.99-7.53 (**20H**, m, *Aryl*), 4.84 (**4H**, dd $^2J_{Rh-H}$ 3, $^3J_{P-H}$ 2Hz, $=CH_2$), 4.08 (**2H**, s, PCH_2), 2.85 (**4H**, br s, PCH_2), 1.98 (**2H**, br m, CH_2), 1.68 (**2H**, br d, PCH_2CH_2), (lit.,[4] δ 7.65-7.55 (**20H**, m), 4.81 (**4H**, dd), 4.08 (**2H**, s, PCH_2), 2.85 (**4H**, br s, PCH_2), 1.98 (**2H**, br m, CH_2), 1.68 (**2H**, br d, PCH_2CH_2) ppm.

2.2.5. Synthesis of $[Rh(Ph_2P(CH_2)_4PPh_2)(C_7H_8)](BF_4)^4$ (6)

This was synthesised in a similar manner to the dppe analogue. The solid was recrystallised from dichloromethane-diethyl ether and collected by filtration then dried *in vacuo* (0.50g, 83%). The purity and identity of the product was confirmed by comparison of the NMR spectra with the literature $^{31}P\{^1H\}$ NMR (CD_3OD): δ 29.4 (d, $^1J_{Rh-P}$ 153Hz) ppm. (Lit.[4] δ 29.6 (d, $^1J_{Rh-P}$ 154Hz) ppm)

FAB Mass Spectrum (methanol/glycerol matrix)

-ve ion: m/z 87 (100%, BF_4^-)

+ve ions: m/z 620 (M^+,64%), 528.9 (54.3, $Rh(dppb)^+$), 102.9 (37.2, Rh^+)

2.2.6. Synthesis of $[Rh(Cy_2P(CH_2)_2PCy_2)(C_7H_8)](BF_4)$[4] (7)

This was synthesised in the same way as the dppe analogue. The solid (0.43g, 78%) was recrystallised from dichloromethane-hexane. The identity and purity was established from comparison of the proton and phosphorus NMR with the literature. $^{31}P\{^1H\}$ NMR (CD_3NO_2): δ 73.4 (d, $^1J_{Rh-P}$ 155Hz), (lit.,[4] d, 74.8ppm, $^1J_{Rh-P}$ 153Hz) ppm. ^1H NMR (CD_3NO_2): δ 5.67 (**4H**, d $^2J_{Rh-H}$ 5.0Hz, =C*H*$_2$), 2.06-1.17ppm (**52H**, m), (lit.,[4] δ 5.70 (**4H**, dd), 4.22 (**2H**, br s), 1.20-2.20 (**50H**, m) ppm.

FAB Mass Spectrum (methanol/glycerol matrix):

-ve ion: m/z 87 (100%, BF_4^-)

+ve ions: m/z 617 (M^+, 20.9%), 523 {15.4, $(M-C_7H_{10})^+$}, 357 {11.9, $(M-C_{23}H_{32})^+$}, 194.9 (16.4, $Rh(C_7H_8)^+$), 102.9 (5.1, Rh^+).

2.2.7. Synthesis of $[Rh(Cy_2P(CH_2)_3PCy_2)(C_7H_8)](BF_4)$ (8)

This was synthesised in the same way as the dppe analogue. The solid was recrystallised from THF-pentane. $[Rh(dcpp)(C_7H_8)](BF_4)$ **(8)** (yield 1.5g, 79.1%) $^{31}P\{^1H\}$ NMR (CD_3NO_2): δ 37.5 (d, $^1J_{Rh-P}$ 148Hz) ppm. ^1H NMR (CD_3NO_2): δ 5.37 (**2H**, d, $^3J_{Rh-H}$ 24.0Hz, *c*†), 4.13 (**1H**, s, *b*), 2.41 (**1H**, s, *a*), 1.99-1.64 and 1.43-1.28 (**25H**, m, *d-i*). $^{13}C\{^1H\}$ (CD_3NO_2): δ 81.8 (s, *c*), 71.3 (s, *b*), 55.8 (s, *a*), 38.0 (t, $J_{PP'-C}$ 12Hz, *g*), 31.7 (s, *e*), 29.8 (s, *d*), 27.3 (s, *i*), 28.6 (t, $J_{PP'-C}$ 6Hz, *h*), d 28.0 (t, $J_{PP'-C}$ 5Hz, *h*), 18.3 (t, *f*) ppm.

FAB Mass Spectrum (methanol/glycerol matrix):

-ve ion: m/z 87 (100%, BF_4^-)

+ve ions: m/z 631 (M^+,16%), 102.9 (22, Rh^+), 83.1 (44, Cy^+), 55.1 (100, $C_4H_7^+$).

† Letters denote the assignment of the resonances in this complex, see key over page.

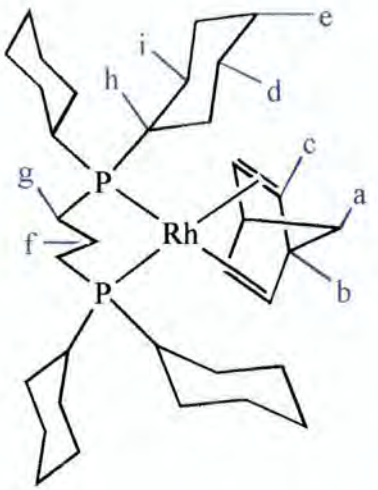

2.2.8. Synthesis of [Rh(Cy_2P(1,2-*trans*-cyclopentane)PCy_2)(C_7H_8)](BF_4) (9)

This was synthesised in a similar manner to the dppe analogue. The product, [Rh(dcpcp)(C_7H_8)](BF_4) **(9)** was recrystallised from dichloromethane-hexane, then by slow evaporation of a methanol-acetone solution (yield 0.91g, 84%). Found C, 53.88; H, 7.78. $C_{36}H_{60}BF_4P_2Rh$ requires C, 53.63; H 7.54%. $^{31}P\{^1H\}$ NMR (CD_3NO_2): δ 39.2 (d, $^1J_{Rh\text{-}P}$ 153Hz) ppm. ^1H NMR (CD_3NO_2): δ 5.72 and 5.32 (**2H**, s, *c*), 2.72-1.00ppm (**28H**, m, *a,b,d-l*), s 5.4 (s, CH_2Cl_2). $^{13}C\{^1H\}$ (CD_3NO_2) 88.4 and 81.3 (s, *c*), 71.6 and 68.7 (s, *b*), 56.9 (s, *a*), 49.3 and 49.1(d, *i*), 35.4, 35.3 and 33.4 (d, *h*), 33.3 and 32.3 (s, *e*) ppm, (see key to assignments below).

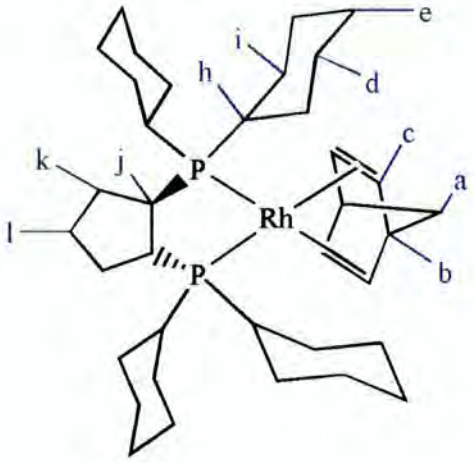

FAB Mass Spectrum (methanol/glycerol matrix):

-ve ion: m/z 87 (100%, BF_4^-).

+ve ions: m/z 657.24 (M^+,100%), 563 {58.2, $(M-C_7H_{10})^+$}, 573 {11.3, $(M-C_6H_{12})^+$}, 479 {26, $(M-C_{13}H_{22})^+$}, 395 {29, $(M-C_{19}H_{34})^+$}, 102.9 (13.1, Rh^+), 83.1 (17.1,Cy^+).

An X-ray crystal structure determination was performed by A. S. Batsanov on a single crystal of complex **(9)** obtained from recrystallisation in acetone-methanol (see Figure 1). The complex co-crystallised with one molecule of acetone which was highly disordered over several positions. Selected data are summarised below in Tables 1 and 2, and further information may be found in Appendix 2.

Table 1. Selected Bond lengths (Å) for Complex (9)

Bond	Distance	Bond	Distance
Rh-C(5)	2.202(5)	Rh-C(6)	2.209(5)
Rh-C(3)	2.213(5)	Rh-C(2)	2.218(5)
Rh-P(2)	2.309(1)	Rh-P(1)	2.323(1)
P(1)-C(11)	1.847(5)	P(1)-C(21)	1.849(5)
P(1)-C(01)	1.851(5)	P(2)-C(02)	1.849(5)
P(2)-C(31)	1.853(5)	P(2)-C(41)	1.855(5)
C(1)-C(2)	1.524(8)	C(1)-C(7)	1.545(8)
C(1)-C(6)	1.551(8)	C(2)-C(3)	1.371(8)
C(3)-C(4)	1.535(8)	C(4)-C(5)	1.534(7)
C(4)-C(7)	1.553(8)	C(5)-C(6)	1.371(8)
C(01)-C(02)	1.506(8)	C(01)-C(05)	1.558(8)
C(02)-C(03)	1.542(8)	C(03)-C(04)	1.547(8)
C(04)-C(05)	1.543(8)	C(11)-C(12)	1.538(7)
C(11)-C(16)	1.541(7)	C(12)-C(13)	1.526(8)
C(13)-C(14)	1.549(8)	C(14)-C(15)	1.515(9)
C(15)-C(16)	1.539(8)	C(21)-C(22)	1.539(8)
C(21)-C(26)	1.542(7)	C(22)-C(23)	1.525(8)
C(23)-C(24)	1.531(8)	C(24)-C(25)	1.531(8)
C(25)-C(26)	1.540(8)	C(31)-C(36)	1.532(8)
C(31)-C(32)	1.540(7)	C(32)-C(33)	1.529(8)
C(33)-C(34)	1.532(8)	C(34)-C(35)	1.518(9)
C(35)-C(36)	1.542(8)	C(41)-C(42)	1.546(8)
C(41)-C(46)	1.548(8)	C(42)-C(43)	1.533(8)
C(43)-C(44)	1.514(10)	C(44)-C(45)	1.523(9)
C(45)-C(46)	1.526(8)	B-F(1)	1.22(2)
B-F(2)	1.240(14)	B-F(4)	1.29(2)
B-F(3)	1.34(2)	C(1S)-C(2S)	1.30(2)
C(2S)-C(3S)	1.13(3)	C(2S)-C(3S)	1.20(2)
C(2S)-C(4S)	1.46(3)	C(2S)-C(4S)	1.57(3)

Figure 1. The Crystal Structure of [Rh(dcpcp)(C_7H_8)](BF_4) (9)

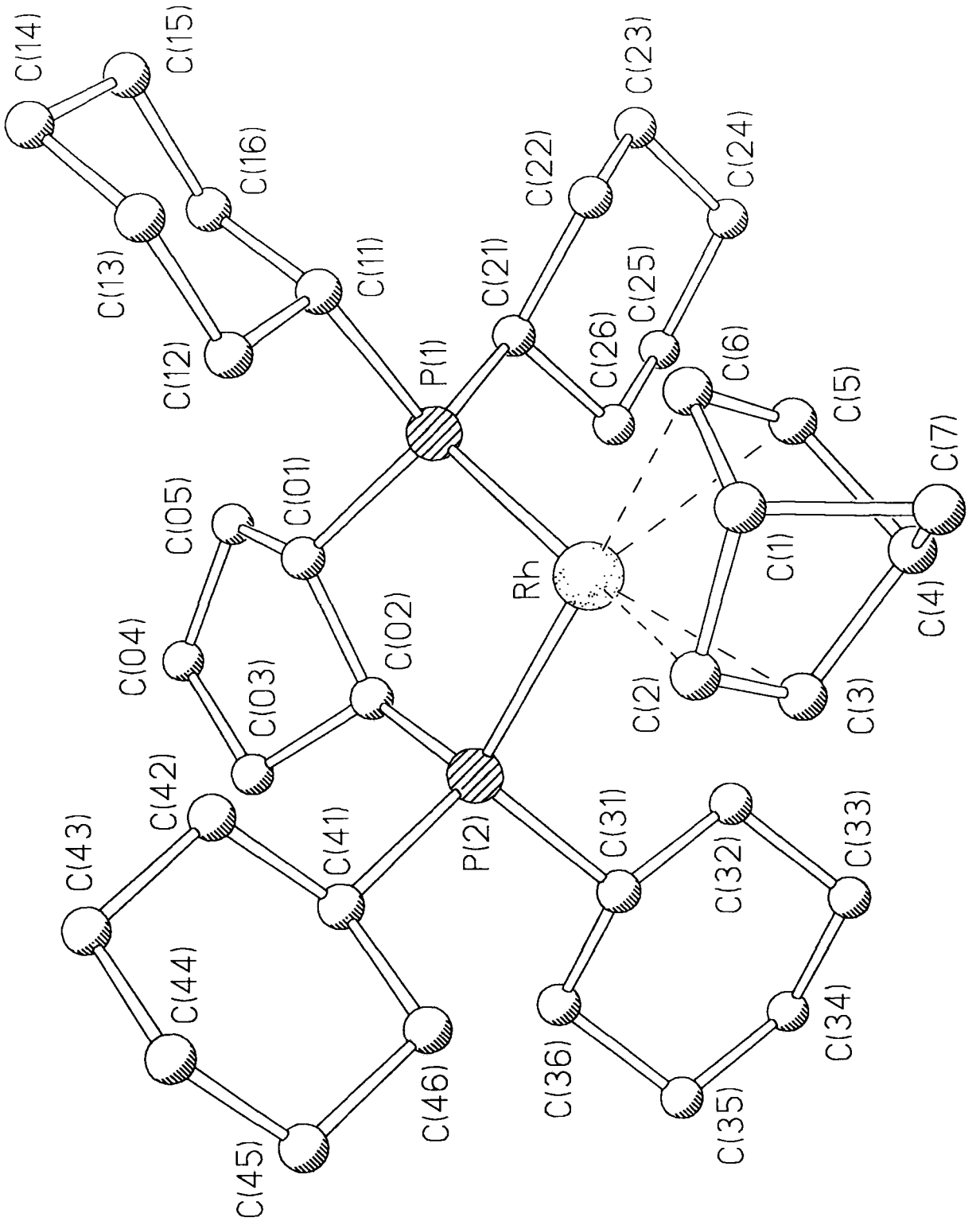

Table 2. Selected Bond Angles (°) for Complex (9)

Angle		Angle	
C(5)-Rh-C(3)	65.9(2)	C(6)-Rh-C(3)	77.5(2)
C(5)-Rh-C(2)	77.4(2)	C(6)-Rh-C(2)	65.7(2)
C(5)-Rh-P(2)	152.8(2)	C(6)-Rh-P(2)	167.3(2)
C(3)-Rh-P(2)	99.2(2)	C(2)-Rh-P(2)	104.4(2)
C(5)-Rh-P(1)	102.6(2)	C(6)-Rh-P(1)	100.4(2)
C(3)-Rh-P(1)	163.7(2)	C(2)-Rh-P(1)	156.8(2)
P(2)-Rh-P(1)	86.24(5)	C(11)-P(1)-C(21)	104.2(2)
C(11)-P(1)-C(01)	106.7(2)	C(21)-P(1)-C(01)	106.3(2)
C(11)-P(1)-Rh	111.0(2)	C(21)-P(1)-Rh	121.2(2)
C(01)-P(1)-Rh	106.6(2)	C(02)-P(2)-C(31)	106.5(3)
C(02)-P(2)-C(41)	106.7(2)	C(31)-P(2)-C(41)	105.7(2)
C(02)-P(2)-Rh	107.3(2)	C(31)-P(2)-Rh	110.6(2)
C(41)-P(2)-Rh	119.3(2)	C(2)-C(1)-C(7)	100.0(5)
C(2)-C(1)-C(6)	102.7(4)	C(7)-C(1)-C(6)	100.3(5)
C(3)-C(2)-C(1)	106.7(5)	C(3)-C(2)-Rh	71.8(3)
C(1)-C(2)-Rh	95.9(3)	C(2)-C(3)-C(4)	106.7(5)
C(2)-C(3)-Rh	72.2(3)	C(4)-C(3)-Rh	95.1(3)
C(5)-C(4)-C(3)	103.1(4)	C(5)-C(4)-C(7)	100.5(4)
C(3)-C(4)-C(7)	99.1(4)	C(6)-C(5)-C(4)	106.9(5)
C(6)-C(5)-Rh	72.2(3)	C(4)-C(5)-Rh	95.5(3)
C(5)-C(6)-C(1)	106.2(5)	C(5)-C(6)-Rh	71.6(3)
C(1)-C(6)-Rh	95.5(3)	C(1)-C(7)-C(4)	93.1(4)
C(02)-C(01)-C(05)	102.9(4)	C(02)-C(01)-P(1)	111.6(4)
C(05)-C(01)-P(1)	123.1(4)	C(01)-C(02)-C(03)	102.9(4)
C(01)-C(02)-P(2)	111.4(4)	C(03)-C(02)-P(2)	123.8(4)
C(02)-C(03)-C(04)	103.8(5)	C(05)-C(04)-C(03)	107.2(5)
C(04)-C(05)-C(01)	103.3(5)	C(12)-C(11)-C(16)	110.3(4)
C(12)-C(11)-P(1)	112.2(3)	C(16)-C(11)-P(1)	114.9(4)
C(13)-C(12)-C(11)	110.6(4)	C(12)-C(13)-C(14)	110.9(5)
C(15)-C(14)-C(13)	111.0(5)	C(14)-C(15)-C(16)	111.4(5)
C(15)-C(16)-C(11)	109.4(4)	C(22)-C(21)-C(26)	109.8(4)
C(22)-C(21)-P(1)	113.6(4)	C(26)-C(21)-P(1)	112.2(4)
C(23)-C(22)-C(21)	110.5(5)	C(22)-C(23)-C(24)	111.3(4)
C(25)-C(24)-C(23)	110.8(5)	C(24)-C(25)-C(26)	111.4(5)
C(25)-C(26)-C(21)	110.7(4)	C(36)-C(31)-C(32)	110.2(5)
C(36)-C(31)-P(2)	115.6(4)	C(32)-C(31)-P(2)	112.4(4)
C(33)-C(32)-C(31)	110.5(5)	C(32)-C(33)-C(34)	111.3(5)
C(35)-C(34)-C(33)	111.7(5)	C(34)-C(35)-C(36)	110.4(5)
C(31)-C(36)-C(35)	109.6(5)	C(42)-C(41)-C(46)	110.4(5)
C(42)-C(41)-P(2)	110.9(4)	C(46)-C(41)-P(2)	112.4(4)
C(43)-C(42)-C(41)	111.8(5)	C(44)-C(43)-C(42)	111.5(6)
C(43)-C(44)-C(45)	110.7(5)	C(44)-C(45)-C(46)	111.5(5)
C(45)-C(46)-C(41)	110.5(5)	C(3S')-C(2S)-C(1S)	109(2)
C(3S)-C(2S)-C(1S)	125.1(14)	C(3S)-C(2S)-C(4S)	137(2)

C(1S)-C(2S)-C(4S)	93(2)	C(3S')-C(2S)-C(4S')	135(3)
C(1S)-C(2S)-C(4S')	97(2)	F(1)-B-F(4)	109.7(14)
F(1)-B-F(2)	111.6(14)	F(1)-B-F(3)	113.9(14)
F(2)-B-F(4)	112(2)	F(4)-B-F(3)	107.0(14)
F(2)-B-F(3)	102.1(13)		

2.2.9. Synthesis of $[Rh(Bu^t_2P(CH_2)_2PBu^t_2)(C_7H_8)](BF_4)$ (10)

This complex was synthesised in a similar manner to the dppe analogue. The $[Rh(dBpe)(C_7H_8)](BF_4)$ **(10)** was recrystallised from dichloromethane-hexane and dried *in vacuo* (1.67g, 84%). Crystals of complex **(10)** suitable for X-ray analysis were isolated and their structure determined by C.W. Lehmann (for data, see Figure 2, Tables 3 and 4, Appendix 2). Found C, 49.67; H, 8.02. $C_{25}H_{48}BF_4P_2Rh$ requires C, 50.02; H, 8.06%. $^{31}P\{^1H\}$ NMR ($CDCl_3$): δ 84.2 (d, $^1J_{Rh-P}$ 153Hz) ppm. ^1H NMR ($CDCl_3$): δ 5.59 (**2H**, d, =C*H*$_2$), 4.17 (**1H**, s, C*H*), 1.96 (**2H**, d, P- C*H*$_2$), 1.83 (**1H**, s, >C*H*$_2$), 1.35 (**18H**, s, PC C*H*$_3$) ppm. $^{13}C\{^1H\}$ ($CDCl_3$): δ 80.3 (s, =$\underline{C}H_2$), 73.0 (s, >$\underline{C}H_2$), 54.3 (s, >$\underline{C}H$), 37.9 (m, P$\underline{C}CH_3$), 30.8 (s, PC$\underline{C}H_3$), 22.5 (t, $J_{PP'-C}$ 16Hz, P$\underline{C}H_2$) ppm.

FAB Mass Spectrum (methanol/glycerol matrix):

-ve ion: m/z 87 (100%, BF_4^-).

+ve ions: m/z 513 (M^+,84%), 195 {33, $Rh(C_7H_8)^+$}, 102.9 (2, Rh^+).

Table 3. Selected Bond Distances (Å) for Complex (10)

Bond	Distance	Bond	Distance
Rh(1)-C(55)	2.202(3)	C(10)-C(11)	1.544(4)
Rh(1)-C(54)	2.209(3)	C(20)-C(23)	1.530(4)
Rh(1)-C(52)	2.211(3)	C(20)-C(22)	1.532(4)
Rh(1)-C(51)	2.213(3)	C(20)-C(21)	1.535(4)
Rh(1)-P(1)	2.3504(7)	C(30)-C(31)	1.531(4)
Rh(1)-P(2)	2.3513(7)	C(30)-C(32)	1.532(4)
P(1)-C(1)	1.846(3)	C(30)-C(33)	1.536(4)
P(1)-C(10)	1.887(3)	C(40)-C(43)	1.531(4)
P(1)-C(20)	1.899(3)	C(40)-C(42)	1.542(4)
P(2)-C(2)	1.848(3)	C(40)-C(41)	1.543(4)
P(2)-C(40)	1.893(3)	C(51)-C(52)	1.370(4)
P(2)-C(30)	1.903(3)	C(51)-C(56)	1.522(4)
F(1)-B(1)	1.353(4)	C(52)-C(53)	1.539(4)
F(2)-B(1)	1.387(4)	C(53)-C(54)	1.531(4)
F(3)-B(1)	1.367(4)	C(53)-C(57)	1.544(4)
F(4)-B(1)	1.386(4)	C(54)-C(55)	1.373(4)

C(1)-C(2)	1.532(4)	C(55)-C(56)	1.533(4)
C(10)-C(13)	1.533(5)	C(56)-C(57)	1.544(4)
C(10)-C(12)	1.541(4)		

Table 4. Selected Bond Angles (°) for Complex (10)

Angle		Angle	
C(55)-Rh(1)-C(54)	36.28(12)	C(23)-C(20)-C(22)	106.6(2)
C(55)-Rh(1)-C(52)	76.77(12)	C(23)-C(20)-C(21)	108.5(2)
C(54)-Rh(1)-C(52)	65.40(11)	C(22)-C(20)-C(21)	108.6(2)
C(55)-Rh(1)-C(51)	64.64(11)	C(23)-C(20)-P(1)	106.8(2)
C(54)-Rh(1)-C(51)	76.70(11)	C(22)-C(20)-P(1)	112.3(2)
C(52)-Rh(1)-C(51)	36.09(12)	C(21)-C(20)-P(1)	113.7(2)
C(55)-Rh(1)-P(1)	106.16(8)	C(31)-C(30)-C(32)	108.2(2)
C(54)-Rh(1)-P(1)	99.13(8)	C(31)-C(30)-C(33)	109.5(2)
C(52)-Rh(1)-P(1)	150.52(9)	C(32)-C(30)-C(33)	107.0(3)
C(51)-Rh(1)-P(1)	169.31(9)	C(31)-C(30)-P(2)	113.1(2)
C(55)-Rh(1)-P(2)	151.38(9)	C(32)-C(30)-P(2)	107.0(2)
C(54)-Rh(1)-P(2)	168.82(9)	C(33)-C(30)-P(2)	111.8(2)
C(52)-Rh(1)-P(2)	105.62(8)	C(43)-C(40)-C(42)	108.6(2)
C(51)-Rh(1)-P(2)	100.04(8)	C(43)-C(40)-C(41)	109.4(2)
P(1)-Rh(1)-P(2)	85.85(2)	C(42)-C(40)-C(41)	106.8(2)
C(1)-P(1)-C(10)	102.98(13)	C(43)-C(40)-P(2)	110.3(2)
C(1)-P(1)-C(20)	103.82(12)	C(42)-C(40)-P(2)	107.1(2)
C(10)-P(1)-C(20)	110.35(13)	C(41)-C(40)-P(2)	114.4(2)
C(1)-P(1)-Rh(1)	108.24(9)	C(52)-C(51)-C(56)	106.9(3)
C(10)-P(1)-Rh(1)	116.78(10)	C(52)-C(51)-Rh(l)	71.9(2)
C(20)-P(1)-Rh(1)	113.29(9)	C(56)-C(51)-Rh(l)	96.9(2)
C(2)-P(2)-C(40)	102.26(12)	C(51)-C(52)-C(53)	106.3(3)
C(2)-P(2)-C(30)	104.42(12)	C(51)-C(52)-Rh(l)	72.0(2)
C(40)-P(2)-C(30)	110.09(13)	C(53)-C(52)-Rh(l)	95.9(2)
C(30)-P(2)-Rh(l)	113.65(9)	C(54)-C(53)-C(52)	102.1(2)
C(2)- P(2)- Rh(1)	107.96(9)	C(54)-C(53)-C(57)	100.5(3)
C(40)-P(2)-Rh(1)	117.01(9)	C(52)-C(53)-C(57)	99.7(2)
F(l)-B(l)-F(3)	112.8(3)	C(55)-C(54)-C(53)	106.4(2)
F(l)-B(l)-F(4)	109.7(3)	C(55)-C(54)-Rh(l)	71.6(2)
F(3)-B(1)-F(4)	110.3(3)	C(53)-C(54)-Rh(l)	96.2(2)
F(l)-B(l)-F(2)	107.7(3)	C(54)-C(55)-C(56)	106.7(3)
F(3)-B(1)-F(2)	106.9(3)	C(54)-C(55)-Rh(l)	72.2(2)
F(4)-B(1)-F(2)	109.3(3)	C(56)-C(55)-Rh(l)	97.1(2)
C(2)-C(l)-P(1)	113.6(2)	C(51)-C(56)-C(55)	101.2(2)
C(1)-C(2)-P(2)	113.7(2)	C(51)-C(56)-C(57)	100.4(3)
C(13)-C(10)-C(12)	109.1(3)	C(55)-C(56)-C(57)	100.7(2)
C(13)-C(10)-C(11)	109.7(3)	C(56)-C(57)-C(53)	93.3(2)
C(12)-C(10)-C(11)	106.9(3)	C(12)-C(10)-P(1)	107.2(2)
C(13)-C(10)-P(1)	109.4(2)	C(11)-C(10)-P(1)	114.4(2)

Figure 2. The Crystal Structure of $[Rh(Bu^t_2P(CH_2)_2PBu^t_2)(C_7H_8)](BF_4)$ (10)

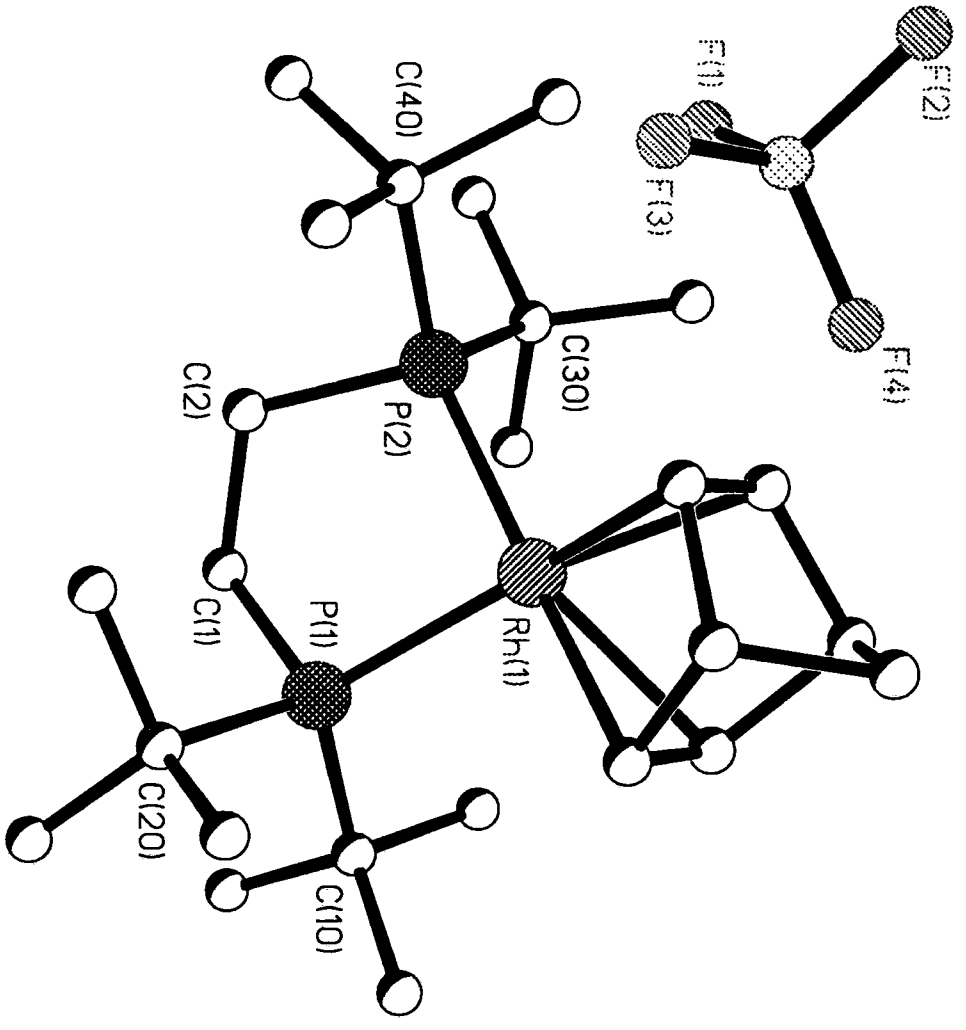

2.2.10. Synthesis of [Rh($Bu^t_2P(CH_2)_3PBu^t_2$)(C_7H_8)](BF_4) (11)

This was synthesised in a similar manner to the dppe analogue. The orange [Rh(dBpp)(C_7H_8)](BF_4) **(11)** was recrystallised from a THF-pentane mixture. (>80% yield). Found C, 50.51; H, 8.24. $C_{26}H_{50}BF_4P_2Rh$ requires C, 50.83; H, 8.20%. $^{31}P\{^1H\}$ NMR (CD_2Cl_2): δ 24.5 (d, $^1J_{Rh\text{-}P}$ 147Hz) ppm. $^{13}C\{^1H\}$ (CD_2Cl_2): δ 70.1-70.6 (m, =$\underline{C}H_2$), 52.9 (s, >$\underline{C}$ H_2), 69.0ppm (s, *THF*), 39.7ppm (m, $J_{PP'\text{-}C}$ 6.6Hz, P-$\underline{C}CH_3$), 30.8 (s, P-C$\underline{C}H_2$), 30.1 (s, *THF*), 23.0 (s, P-$CH_2\underline{C}H_2$), 27.1 (s, =C-$\underline{C}$H), 20.7 (t, $J_{PP'\text{-}C}$ 10Hz (P$\underline{C}H_2$) ppm. ^1H NMR ($CDCl_3$): δ 5.29 (**4H**, br d $^2J_{Rh\text{-}H}$ 3Hz, =C$\underline{H_2}$), 4.05 (**2H**, br s, C$\underline{H}$), 1.71 (**2H**, s, C$\underline{H_2}$) 1.80 (**6H**, m, PC$\underline{H_2}$C$\underline{H_2}$), 1.41 (**36H**, d $^3J_{P\text{-}H}$ 13Hz, PCC$\underline{H_3}$) ppm.

FAB Mass Spectrum (methanol/glycerol matrix):

-ve ion: m/z 87 (100%, BF_4^-)

+ve ions: m/z 527.4 (M^+,12.7%), 435.2 {100, $(M\text{-}C_7H_8)^+$}, 195 {8.57, $Rh(C_7H_8)^+$}, 102.9 (11.98, Rh^+).

2.2.11. Synthesis of [Rh(Bu^t_2P(*o*-xylene)PBu^t_2)(C_7H_8)](BF_4) (12)

This was synthesised as outlined above for the dppe analogue. The orange [Rh(Boxylyl)(C_7H_8)](BF_4).0.3(CH_2Cl_2) **(12)** was recrystallised from dichloromethane-diethyl ether-hexane (>85% Yield). Found C, 53.63; H,7.64. $C_{31.3}H_{52.6}BCl_{0.6}F_4P_2Rh$ requires C, 53.56; H, 7.55%. $^{31}P\{^1H\}$ NMR ($CDCl_3$): δ 23.1 (d, $^1J_{Rh\text{-}P}$ 148.Hz) ppm. ^1H NMR ($CDCl_3$): δ 7.33-7.30 (**2H**, m, *a*), m 7.20-7.17 (**2H**, m, *b*), 3.52 (**4H**, d $^2J_{P\text{-}H}$ 8.7Hz, *c*), 5.25 (**4H**, d $^2J_{Rh\text{-}H}$ 2.6Hz, *d*), 1.69 (**2H**, s, *e*), 4.00 (**2H**, br s, *f*), 1.50 (**18H**, d $^3J_{P\text{-}H}$ 12.6Hz, *g*), 5.3 (s, CH_2Cl_2) ppm. $^{13}C\{^1H\}$ ($CDCl_3$): δ 135.6 (s, *i*), 133.9 (s, *a*), 128.0 (s, *b*), 31.8 (s, *h*), 29.6 (t, $J_{PP'\text{-}C}$ 7Hz, *g*), 41.5 (d, $J_{PP'\text{-}C}$ 5Hz, *c*), 68.2 (d t $^1J_{Rh\text{-}C}$ 5Hz $J_{PP'\text{-}C}$ 5.9Hz, *d*), 52.0 (s, *e*), 69.1 (s, *f*) ppm (for key to assignments see below).

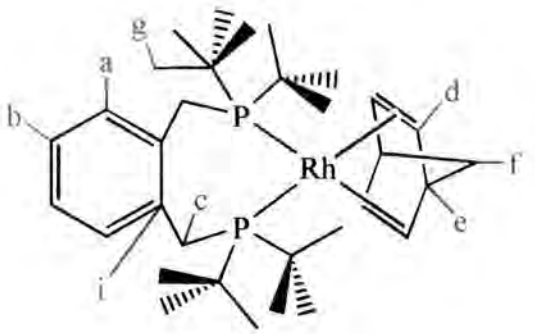

2.2.12. Synthesis of $[Rh(Cy_2PMe)_2(C_7H_8)](BF_4)$ (13)

Degassed sodium hydroxide solution (~1M, 25cm^3) was added to a slurry of dicyclohexylmethylphosphoniumiodide ($HPCy_2MeI$) (0.31g, 0.91mmols) in diethylether (50cm^3), and shaken until the white solid ($HPCy_2MeI$) had disappeared. The top layer was removed *via* cannula into a solution of complex **(3)** (0.17g, 0.46mmols) in dichloromethane (20cm^3). The solvent was removed after 30 minutes and the orange product dried *in vacuo*. Complex **(13)** was recrystallised from THF-diethylether. Found C, 55.38; H,8.26. $C_{33}H_{58}BF_4P_2Rh$ requires C, 56.10; H, 8.27%. $^{31}P\{^1H\}$ NMR ($CDCl_3$): δ 16.4 (d, $^1J_{Rh-P}$ 151Hz) ppm. ^1H NMR ($CDCl_3$): δ 4.88 (**4H**, s, =C*H*$_2$), 4.06 (**2H**, C*H*), 2.10, 1.87-1.75, 1.31, 1.11 (**52H**, m's) ppm. $^{13}C\{^1H\}$ NMR ($CDCl_3$): δ 78.1 (dd, $^1J_{Rh-C}$ 6, $^2J_{P-C}$ 4Hz, =CH), 63.4 (s, >CH$_2$), 54.0 (s, CH), 37.5 (t, $J_{PP'-C}$ 11Hz, PCH), 31.3, 29.1 (s, PCHCH$_2$), 28.0, 27.5 (m, PCHCH$_2$CH$_2$), 26.6 (s, PCH(CH$_2$)$_2$CH$_2$) ppm.

Synthesis of [HPCy$_2$Me](I)

Iodomethane (0.74cm^3) was slowly added to dicyclohexylphosphine (2.35g, 1.85mmols) dissolved in diethylether (50cm^3); a white solid quickly precipitated and the solution was stirred overnight. At the end of the reaction the solid was isolated by filtration, washed with diethylether and dried *in vacuo* (yield 2.61g 65%). $^{31}P\{^1H\}$ NMR ($CDCl_3$): δ 14.7 (s) ppm. ^1H NMR ($CDCl_3$): δ 7.39 (**1H**, ddt, $^1J_{P-H}$ 481Hz, P*H*), 2.74 (**3H**, m, PC*H*$_3$), 2.13-1.28 (**22H**, m, P*Cy*) ppm. $^{13}C\{^1H\}$ NMR ($CDCl_3$): δ 28.9 (d, $^1J_{P-C}$ 44Hz, PCH), 27.4 (d, $^2J_{P-C}$ 48Hz, PCHCH), 26.3 (m, PCHCHCH), 25.6 (s, PCHCHCHCH), 0.5 (d, $^1J_{P-C}$ 50Hz, PCH$_3$) ppm.

2.3. Reactions of Type (1) Complexes With Carbon Monoxide, Synthesis of Complexes of the Type $[Rh(diphos)(CO)_2](BF_4)$

2.3.1. The Reaction of Complex (10) with Carbon Monoxide

Complex **(10)** (~55mg) was placed in an NMR tube equipped with a Young's tap. The tube was then evacuated and deuterochloroform added by vacuum distillation. When the solution had reached room temperature, carbon monoxide was introduced to a pressure of 1 bar. Immediately on contact with the carbon monoxide the solution turned yellow in colour, due to the presence of $[Rh(dBpe)(CO)_2](BF_4)$ **(14)**. $^{31}P\{^1H\}$ NMR ($CDCl_3$): δ 108.6 (d $^1J_{Rh\text{-}P}$ 118Hz) ppm. ^1H NMR ($CDCl_3$): δ 1.41 (**9H**, d, PCC$\underline{H}_3$), 2.87 (**1H**,d m, PC$\underline{H}_2$) ppm. $^{13}C\{^1H\}$ ($CDCl_3$): δ185.9 (ddd, $^1J_{Rh\text{-}C}$ 60Hz $^2J_{P(trans)\text{-}C}$ 60Hz $^2J_{P(cis)\text{-}C}$ 16. Hz Rh-$\underline{C}$O), 30.3 (s, P-C$\underline{C}H_3$), 24.3 (t, $J_{PP'\text{-}C}$ 17Hz, P-$\underline{C}H_2$), 37.9 (m, $J_{PP'\text{-}C}$ 10, $^2J_{Rh\text{-}C}$ 5Hz, P-$\underline{C}CH_3$) ppm. $\nu_{(CO)}$ 2082(s), 2030 (s) cm^{-1}.

The reaction was repeated on a larger scale using a high pressure infra red cell. The vessel was pressurised up to 2000psi. However, even at this pressure, no extra carbonyl absorbtions were observed, indicating that it was not forming a five coordinate eighteen electron complex.

2.3.2. The Reaction of Complex (8) with Carbon Monoxide

Carbon monoxide was bubbled through a solution of complex **(8)** (0.20g, 0.27mmols) in a 1:1 mixture of methanol:diethylether (10mls) for 20minutes, and a pale orange solid was precipitated. The solid * $[Rh(dcpp)(CO)_2](BF_4)$ **(15)** was isolated by filtration and washed with diethylether (5mls) before drying *in vacuo* (0.15g, 81%). $^{31}P\{^1H\}$ NMR ($CDCl_3$): δ 22.1 (d, $^1J_{Rh\text{-}P}$ 113Hz) ppm. $\nu_{(CO)}$ 2082(s), 2026 (s), $\nu_{(BF)}$ (br vs) 1084 cm^{-1}.

* It was not possible to purify the dicarbonyl complex **(15)** completely and there always remained an impurity identified as the monocarbonyl complex $[Rh(dcpp)(CO)(Methanol)](BF_4)$ **(16)** $^{31}P\{^1H\}$($CDCl_3$): NMR δ 51.3 (dd, $^1J_{Rh\text{-}P}$ 113Hz, $^2J_{P\text{-}P}$ 23Hz). 41.5 (dd, $^1J_{Rh\text{-}P}$ 110Hz, $^2J_{P\text{-}P}$ 23Hz) ppm. $\nu_{(CO)}$ 1968, cm^{-1}.

2.3.3. The Reaction of Complex (11) with Carbon Monoxide

CD_3OD ($0.6cm^3$) was added to complex **(11)** (~50mg) in an NMR tube equipped with a Young's tap under an inert atmosphere. Hydrogen gas (1atm.) was introduced and the tube shaken until all the norbornadiene was converted into norbornane. The excess gas was removed under reduced pressure, and carbon monoxide introduced to form $[Rh(dBpp)(CO)_2](BF_4)$ **(17)**. The solution was sealed under 1atm of carbon monoxide (1atm.). $^{31}P\{^1H\}$ NMR (CD_3OD): δ 41.27 (d $^1J_{Rh-P}$ 116Hz) ppm. ^1H NMR (CD_3OD): δ 1.60 (**9H**, d $^3J_{P-H}$ 13.8Hz, $PCC\underline{H}_3$), 2.30ppm (**1H**, m, $PC\underline{H}_2$), 1.5-1.38 (m, $C_7\underline{H}_{12}$) ppm. $\nu_{(CO)}$ 2076(s), 2023 (s) cm^{-1}. (Shoulder also at $1968cm^{-1}$ due to the monocarbonyl).

2.4. Discussion

A range of essentially square-planar complexes of the type **(1)** has been synthesised, and two of these complexes $[Rh(dcpcp)(C_7H_8)](BF_4)$ **(9)** and $[Rh(dBpe)(C_7H_8)](BF_4)$ **(10)** have been structurally characterised. It was hoped to control the steric and electronic environment about the metal by changing the phosphine and, towards this end a variety of chelating phosphines have been used.

In complexes of the type $[Rh(diphos)(C_7H_8)]^+$ **(1)** the bonding of the metal to the ligands is dependent on the σ donor and π acceptor properties of the ligands. By keeping one of the ligands constant (the diene) and examining the effect upon it when the other ligand (the phosphine) is changed, an insight into the steric and electronic properties of the phosphine should be provided.

The π-acceptor character of a ligand is its ability to accept π-electron density from the metal. For phosphines this is the interaction of the d orbitals on the metal and the P-R σ* anti-bonding orbitals of the phosphine. In alkyl-phosphines these orbitals are much higher in energy than in aryl-phosphines leading to poor overlap and consequently little backbonding. Additionally for aryl phosphines the back-donated

electron density from the metal can be delocalised into the aromatic π*-orbitals.[5] The phosphines can be arranged in order of decreasing π acceptor properties, increasing σ-donor properties and increasing energy of the P-R σ* orbitals, in the order:

$$C_6F_5 > CF_3C_6H_4 > Ph > Cy \sim Bu^t$$

For the norbornadiene ligand σ donation comes from electrons in the carbon-carbon π-bonding orbitals and any backbonding to the diene is distributed into the anti-bonding π*-orbitals. As the backbonding to the diene increases, the s character of the bonds about the carbon becomes more evenly distributed and the strength of the carbon metal bond increases (the Rh-C bonds shorten).

Any increase in σ donation to the metal, is usually accompanied by an increase in π-back-donation to the ligands from the metal.[6] In the case of the alkyl substituted phosphines, its capacity for acceptance of electron density from the metal is limited. Consequently, the excess electron density is donated to the diene, leading to a weakening of the carbon-carbon double bond; the hybridisation about the carbon changes from sp^2 towards sp^3. As the capacity of the phosphine to participate in backbonding increases, so the metal can accept more electron density from the phosphine in the form of σ donation.

Table 5 contains selected bond lengths and distances for the type **(1)** complexes characterised in this work and the type **(1)** complexes reported in the literature. From a brief inspection of the data in Table 5, it becomes immediately apparent that the rhodium ligand bond lengths are influenced by both the nature of the backbone in the phosphine and the terminal substituents on the phosphorus atoms.

Table 5. Selected Bond lengths for Complexes of the Type [Rh(diphos)(C_7H_8)]$^+$ (1)

Complex (diphos =)	P-Rh (Å)	Mean C-Rh (Å)	C=C (Å)
(10) {dBpe = $Bu^t_2P(CH_2)_2PBu^t_2$}	2.351	2.091	1.372
(18) {cyphos = $Ph_2PCH(Cy)CH_2PPh_2$}[7]	2.292	2.187	1.314
(19) {dipamp = $[Ph(anisyl)PCH_2]_2$}[8]	2.290	2.214	1.365
(9) {dcpcp = Cy_2P(*trans*-1,2,-cyclopentane)PCy_2}	2.316	2.210	1.371
(20){norphos = Ph_2P(*trans*-2,3-norborn-5-ene)PPh_2}[8]	2.320	2.199	1.368
(21) {dppf = Ph_2P(1,1′ ferrocene)PPh_2}[9]	2.326	2.209	1.389
(22) {dBppf = $PhBu^tP$(1,1′ ferrocene)$PPhBu^t$}[12]	2.402	2.183	1.362
(23) {dBpf = Bu^t_2P(1,1′ ferrocene)PBu^t_2}[10]	2.462	2.171	1.377

The trends observed in the rhodium-ligand bond lengths can be rationalised in terms of the structure and bonding about the metal. There are two important trends that can be observed in the data in Table 5.

1. Increasing the σ-donor properties and decreasing the π-acceptor properties of the phosphine in the order Ph > Cy ~ Bu^t, increases the Rh-P and C=C bond lengths and decreases the Rh-C bond lengths, i.e. activation of the diene occurs.
2. Increasing the steric influence of the phosphine in the absence of changes in the electronic bonding properties of the phosphine, causes an overall increase in the metal-ligand bond lengths.

Trend 1 can be observed in the complexes **(10)**, **(18)** and **(19)**. Varying the phosphine from aryl substituted, complexes **(18)** and **(19)**, to alkyl substituted, complex **(10)**, increases the σ-donor properties and decreases the π-acceptor properties of the phosphine. This leads to a weakening (lengthening) of the Rh-P bonds due to reduced metal to phosphine π-backdonation, and consequently, the excess electron density on the metal is donated to the norbornadiene ligand. The increased dπ-π* bonding in the diene strengthens (shortens) the Rh-C bonds, increasing the Rh-C σ bond strength due to increased orbital overlap, and hence activation of the diene occurs. A similar trend is observed in complexes **(21)**, **(22)** and **(23)**. However, in these complexes, the larger ferrocene backbone of the phosphine increases the PRhP angle, and the substituents on

the phosphorus atoms are positioned closer to the diene, leading to increased steric interactions. Consequently, a general increase is observed in the metal ligand bond distances with respect to those complexes with smaller phosphine backbones, i.e. complexes **(10)**, **(18)** and **(19)**.

Trend 2 can be observed for complexes **(9)** and **(20)**, in which the corresponding ligand metal bond lengths are very similar. In these systems the enforced *trans* geometry in the backbone of the phosphine has several effects. The Rh-P bonds are slightly longer in the norphos complex **(20)** than in the dcpcp complex **(9)** and of a similar length to those in the dBpe complex **(10)**. The similarity of the Rh-P and Rh-C bond lengths in both these systems points to a similar electronic situation with regards to σ-donation and π-acceptance. The dcpcp complex, **(9)** is unlikely to participate in π-acceptance from the rhodium due to the high energy of the P-Cy σ*-orbitals. Consequently the similarity in the Rh-P bond lengths for the dcpcp and norphos complexes implies that the norphos complex, **(20)** is not participating in π-acceptance, even though the capacity for backdonation to this phosphine exists due to the relatively lower energy of the P-Ph σ*-orbitals. Although the Rh-P bonds are longer for complexes **(9)** and **(20)** compared with most other complexes (see Table 5), this is not reciprocated in a shortening of the Rh-C bonds which is observed for all of the other type **(1)** complexes. This probably implies that complexes **(9)** and **(20)** are more sterically constrained about the metal, leading to a general lengthening of the metal-ligand bond distances.

X-ray crystallography represents a powerful tool for investigating the effect variations in the phosphine can exert on the rhodium-ligand bonding in a rhodium-phosphine complex, and several trends have been established based on the data in Table 5 (see above). However, only a few type **(1)** complexes have been characterised in this manner, and the data are restricted to the solid state. Consequently, it is advantageous if spectroscopic solution measurements are employed to gauge the influence of the phosphine.

Phosphorus and rhodium are NMR active, with nuclear spins of I=1/2. Since coupling constants and chemical shifts are dependent upon the orbital contributions in the bonds about the desired element, it should be possible to gain structural information from the NMR spectra and determine whether the Trends 1 and 2 observed in the solid state are observed in solution, where we have a significantly larger basis set to compare. Selected NMR data are summarised in Table 6.

Table 6. Selected NMR Data for Complexes of the Type [Rh(diphos)(C_7H_8)]$^+$ (1)

Complex (diphos =)		δ_{p}‡ - ppm ($^1J_{Rh-P}$-Hz)	$\delta_{C=C}$§ (=$\underline{C}H_2$)	δ_{H}** ($^2J_{Rh-H}$-Hz)
(13)	(2PCy_2Me)	16.4 (151)	78.1	4.86
(32)	(2PPh_2Me)[11,4]	7.5 (158)	85.9	4.94
(24)	{dpf = $(C_6F_5)_2P(CH_2)_2P(C_6F_5)_2$}[4]	23.3 (168)	94.3	5.63
(25)	{dptf = $(CF_3Ph)_2P(CH_2)_2P(CF_3Ph)_2$}[4]	59.0 (159)	93	5.54
(19)	{dipamp = [Ph(anisyl)PCH_2]$_2$}[12]	50.9 (159)		
(4)	{dppe = $Ph_2P(CH_2)_2PPh_2$}	57.5 (158)	92.7	5.38 (17.5)
(7)	{dcpe = $Cy_2P(CH_2)_2PCy_2$}	73.4 (154)	87.3	5.67 (5.0)
(10)	{dBpe = $Bu^t_2P(CH_2)_2PBu^t_2$}	84.2 (153)	80.3	5.59
(9)	{dcpcp = Cy_2P(*trans*-1,2,-cyclopentane)PCy_2}	39.2 (153)	88.4, 81.3	5.72
(20)	{norphos = Ph_2P(*trans*-2,3-norborn-5-ene)PPh_2}[13]	25.8 (150) 24.9 (150)		
(21)	{dppf = Ph_2P(1,1′ ferrocene)PPh_2}[14]	14.8 (161)		
(22)	{dBppf = $PhBu^tP$(1,1′ ferrocene)$PPhBu^t$}[8]	32.5 (155)		5.25, 5.68
(23)	{dBpf = Bu^t_2P(1,1′ ferrocene)PBu^t_2}[8]	45.8 (148)		
(5)	{dppp = $Ph_2P(CH_2)_3PPh_2$}	18.8 (148)	89.3	4.81
(26)	{d*i*ppp = $Pr^i_2P(CH_2)_3PPr^i_2$}[15]	21.5 (148)		
(8)	{dcpp = $Cy_2P(CH_2)_3PCy_2$}	37.5 (148)	81.8	5.32
(11)	{dBpp = $Bu^t_2P(CH_2)_3PBu^t_2$}	24.5 (147)	70.4	5.29
(6)	{dppb = $Ph_2P(CH_2)_4PPh_2$}	29.4 (153)	87.3	4.59
(27)	{d*i*ppb = $Pr^i_2P(CH_2)_4PPr^i_2$}[10]	33.0 (152)		
(12)	{Boxylyl = Bu^t_2P(*o*-xylene)PBu^t_2}	23.1 (148)	68.2	5.25

‡ Where δp is the phosphorus chemical shift of the co-ordinated phosphine.

§ Where $\delta_{C=C}$ is the carbon chemical shift of the sp^2 hybridised carbon atoms in the NBD.

** Where δ_H is the proton chemical shift of the vinylic protons in the NBD.

(28)	(diop = see key below)[16]	16.2 (153)		
(29)	(etdiop = see key below)[17]	6.4 (150)		
(30)	(*i*prdiop = see key below)[10]	22.3 (152)		
(31)	(cydiop = see key below)[10]	16.5 (151)		

For the diop derivatives:

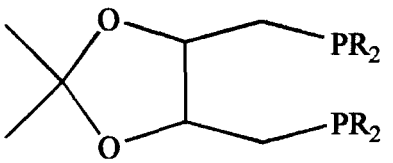

diop R = Ph, etdiop R = Et, *i*Prdiop R = *i*Pr, cydiop R = Cy

---

In addition to Trends 1 and 2 noted from the crystallographic data, close scrutiny of the NMR data presented in Table 6 reveals several more trends:

3. Increasing the σ-donor properties and decreasing the π-acceptor properties of the phosphine (replacing aryl groups on the phosphine with alkyl groups) shifts δ_p to higher frequency and decreases $^1J_{Rh\text{-}P}$. The exception to this is for complexes containing six and seven membered chelate rings where there is little or no change in $^1J_{Rh\text{-}P}$.
4. For the diop derivatives δ_P reaches a maximum value when *iso*propyl groups are employed (Pr^i > Cy > Ph >Et), whilst for the complexes containing six membered chelate rings the largest value of δ_P is observed for the cyclohexyl derivative (Cy > Bu^t > Pr^i > Ph).
5. Changing the aryl groups for alkyl groups decreases $\delta_{C=C}$, and this pattern is observed for all of the phosphines. $\delta_{C=C}$ decreases as the chelate ring size increases, when the other parameters on the phosphorus are kept constant.
6. Sterically restricting the backbone of the phosphine, e.g. for complexes **(9)** and **(20)** (diphos = dcpcp, norphos), causes a shift to lower frequency of ~ 30ppm in the phosphorus NMR spectra relative to the unrestricted complex. Additionally a decrease in $^1J_{Rh\text{-}P}$ is observed.

To understand these trends in the NMR data and relate them to Trends 1 and 2 observed in the structural studies it is first necessary to appreciate the origin of the differences observed in the NMR data.

There are two contributions to ligand metal bonding, σ-donation, and π-back-donation. The σ-contribution is dependent on the ability of the ligand to donate electrons to the metal, and for the metal to accept them. Usually σ-donation occurs through an s orbital or an s/p hybrid. If two elements are NMR active, then the coupling constant between them is dependent on the degree of s character in the bond, determined by Equation 1,[18]

$$^{1}J_{Rh\text{-}P} \alpha [^{3}\Delta E]^{-1}[S(O)_{Rh}]^{2}[S(O)_{P}]^{2}\sigma^{2} \qquad \text{Equation 1}$$

where $[^{3}\Delta E]$ is the singlet-triplet energy gap; $[S(O)_{Rh}]^{2}$, $[S(O)_{P}]^{2}$ and σ^{2} are the s electron densities at the rhodium and phosphorus nuclei, and in the Rh-P bond. It has been previously demonstrated that for sets of similar complexes, $[^{3}\Delta E]$, $[S(O)_{Rh}]^{2}$and $[S(O)_{P}]^{2}$ are essentially constant. Hence, variations in $^{1}J_{Rh\text{-}P}$ are mainly due to the σ^{2} term.[18] Consequently the Rh-P coupling constant ($^{1}J_{Rh\text{-}P}$) should provide a measure of the Rh-P bond strength; the greater the s character, the greater will be the magnitude of $^{1}J_{Rh\text{-}P}$, and therefore the greater the bond strength. The influence of the $d\pi\text{-}\sigma^{*}$ backbonding on $^{1}J_{Rh\text{-}P}$ is exerted by decreasing the Rh-P bond distance and hence improving the s orbital overlap which gives rise to the term, σ^{2} in Equation 1.

The decrease observed for the Rh-P bond distances in the structural studies with increasing σ donor properties of the phosphine, Trend 1, parallels Trend 3, the decrease in $^{1}J_{Rh\text{-}P}$ observed in the NMR studies, due to reduced s orbital overlap in the longer bonds (see Equation 1).

The smallest values of $^{1}J_{Rh\text{-}P}$ are observed for the weakest π-acceptor/potentially strongest σ-donor and bulkiest phosphines, which form the weakest Rh-P bonds, for example those with Bu^{t} groups, whilst the largest values in $^{1}J_{Rh\text{-}P}$ are observed for phosphines which are better π-acceptors and form the strongest Rh-P bonds, for

example those with C_6F_5 groups. If the backbone of the phosphine is kept constant, then a variation of 15Hz can be observed as the substituents on the phosphorus are changed in the order:

$$C_6F_5 > CF_3C_6H_4 > Ph > Cy \sim Bu^t$$

This variation in $^1J_{Rh\text{-}P}$ is much larger than the small fluctuations observed by variation of the solvent[††] indicating that in solution there is a real increase in the Rh-P bond distance as the σ-donor properties and π-acceptor properties of the phosphine are respectively increased and decreased.

The reduction of $^1J_{Rh\text{-}P}$ due to decreasing π-acceptor properties and increasing σ-donor properties of the phosphine is paralleled by a decreases in $\delta_{C=C}$, and this is due to an activation of the diene. As the phosphine accepts back less electron density, competition from the phosphine for backbonding is reduced; the metal pushes some of the electron density from the phosphine into the diene π*-orbitals. This weakens the carbon-carbon double bonds and rehybridisation of the vinylic carbons towards sp^3 occurs, resulting in a shift to lower frequency of $\delta_{C=C}$. The increase in back donation to the diene pulls the diene closer to the metal improving the orbital overlap for σ bonding and strengthening the Rh-C bond.

δ_H (=C$\underline{H_2}$), due to steric interactions of the vinylic protons with the phosphine, is not as instructive as the corresponding $\delta_{C=C}$ values for predicting changes in the metal-diene bonding, although there is a general trend to a lower frequency with increasing back donation to the diene. For example, co-ordination of NBD to the metal decreases δ_H from 6.94 (in free NBD[19]) to 4.59 (in complex **(6)**).

The greatest influence on $^1J_{Rh\text{-}P}$ is exerted by the ligands situated *trans* to the phosphine. Replacing the NBD group with two carbon monoxide ligands causes a

[††] From examination of other complexes in this thesis, fluctuations of $^1J_{Rh\text{-}P}$ with solvent can be limited to 2-3Hz at most.

dramatic difference in the metal-phosphorus bonding and this is reflected in the spectroscopic measurements obtained from these complexes. Table 7 contains selected data for complexes of the type $[Rh(diphos)L_2]^+$:

Table 7. Selected IR and NMR Data for Cationic Rhodium(I) Complexes of the Type [Rh(diphos)L$_2$]$^+$

Complex, (diphos =)	Phosphorus NMR data, δ_P - ppm ($^1J_{Rh-P}$ Hz)		ν(CO) (cm^{-1})
	L_2 = NBD	L_2 = 2CO	
(dppe = $Ph_2P(CH_2)_2PPh_2$)[4]	57.5 (158)	62.8 (121)	2100, 2055
(dcpe = $Cy_2P(CH_2)_2PCy_2$)[20]	73.4 (154)	85.2 (116)	2086, 2027
(dBpe = $Bu^t_2P(CH_2)_2PBu^t_2$)	84.2 (153)	108.6 (118)	2082, 2030
(dcpp = $Cy_2P(CH_2)_2PCy_2$)	37.5 (148)	22.1 (113)	2082, 2026
(dBpp = $Bu^t_2P(CH_2)_3PBu^t_2$)	24.5 (147)	41.3 (116)	2076, 2023

The electronic effects of the phosphine are more pronounced in the less sterically hindered cationic dicarbonyl complexes than in the NBD complexes. In the dicarbonyl complexes there is a correlation between rhodium-phosphorus bonding properties and the carbon-oxygen stretching frequencies in the IR spectra. Increasing the σ-donor properties and decreasing the π-acceptor properties of the phosphine,i.e. replacing aryl with alkyl groups shifts the CO stretch to lower wavenumbers by ~ $20cm^{-1}$. This is due to increased back donation to the carbon monoxide ligands, strengthening the metal carbon bonds and weakening the carbon oxygen triple bond (the extra electron density is distributed into the π*-orbitals of the CO ligands). Carbon monoxide is a much better π acceptor, but worse σ donor than norbornadiene and this can be observed by comparison of the $^1J_{Rh-P}$ values. In the NBD complexes $^1J_{Rh-P}$ is typically 30-40Hz smaller than in the analogous CO complexes. The strong back donation from the metal to the CO increases the crystal field splitting energy and consequently the singlet triplet-energy gap, $^3\Delta E$. The coupling constant is inversely proportional to $^3\Delta E$ (see Equation 1) and thus increasing $^3\Delta E$ causes a decrease in $^1J_{Rh-P}$. Unfortunately due to the lack of crystallographic data for the cationic dicarbonyl complexes, it is impossible to determine if $^3\Delta E$ is the only reason for the decrease in $^1J_{Rh-P}$, relative to

the NBD complexes, or if there is a contribution due to variation in the Rh-P bond distances in the CO complexes.

The chemical shift is dependent on the local electronic environment about the phosphorus. The electrons in the groups around the observed nucleus can shield or de-shield the nucleus from the applied magnetic field. This makes analysing chemical shifts difficult because they are dependent on the nature and disposition of the atoms in the local environment. However, the size of the chelate ring, and the nature of the substituents on the phosphorus atoms have a dramatic effect on the phosphorus chemical shift (δp).

The effect on the phosphorus chemical shift due to variations in the chelate ring size has been previously observed. However, the reasons for this variation still remain unclear.[21] The chemical shift, δp, can be broken down into two components as follows:

$$\delta p = \Delta + \delta f \quad \text{Equation 2}$$

where δf is the chemical shift of the non-complexed ligand and Δ is the co-ordination chemical shift, i.e. the difference between the chemical shift of the complexed and non-complexed ligand. A more useful term to define is Δr, which is the difference in chemical shifts between the chelated phosphine complex and a close equivalent phosphorus in a non-chelated analogue, for example, the PPh_2Me complex, **(32)** and the dppe complex, **(4)**.

$$\Delta r = \Delta_{\text{Chelating}} - \Delta_{\text{Non-chelating}}$$

Equation 3

Δr has been calculated for the aryl substituted phosphine complexes **(4),(5)** and **(6)** using complex **(32)** as the non-chelating analogue, and for the cyclohexyl derivatives using complex **(13)** as the nonchelating analogue (see Table 8).

The values of Δr observed here are similar to those observed for other transition metal-chelating aryl-phosphine complexes.[11] However, the increase in the co-ordination chemical shift (Δ) and the chelation chemical shift (Δr) for the cyclohexyl derivatives over the phenyl derivatives has not been commented on before. The magnitude of this difference is similar for both the two and three carbon-backboned phosphines (~+5, +10ppm respectively).

Table 8. Phosphorus Chemical Shift Analysis for Various Rhodium Phosphine Complexes of the Type [$RhP_2(C_7H_8)$][BF_4]‡‡

Complex (phosphine)††	δ_f[22]	δ_p	Δ§§	Δr***	Δd ††† (δ_{de}-δ_x)
(32) (PPh_2Me)	-28.0	7.5	35.5	0	-
(4) (dppe)	-13.2	57.5	70.7	50.0	0
(5) (dppp)	-17.5	18.8	36.3	11.3	38.7
(6) (dppb)	-17.8	28.4	46.2	20.9	29.1
(13) (PCy_2Me)	-18.3‡‡‡	16.4	34.7	0	-
(7) (dcpe)	-0.6[12]	74.8	75.4	58.4	0
(8) (dcpp)	-6.3§§§	37.5	43.8	21.1	37.3

Unfortunately it was impossible to calculate values of Δr for the *tert*-butyl phosphine complexes synthesised in this work due to the unavailability of data for the non-chelating analogue [$Rh(PBu^t_2Me)_2(C_7H_8)$][BF_4]. In order to compare the phosphorus chemical shift data, a new measure is required, Δd, the difference in phosphorus chemical shift between analogous complexes of the type [$Rh(diphos)L_2$]$^+$ having different numbers of carbon atoms in the backbone of the chelating phosphine (see Table 8). In table 9 values of Δd for both L_2 = 2CO and NBD are summarised.

‡‡ Where P_2 is either a diphosphine, or two mono-phosphines.
§§ Calculated using Equation 2 above.
*** Calculated using Equation 3 above.
††† Δd is difference in the chemical shift (δ_p) between the chelating phosphine derivative with two carbon atoms in the backbone of the phosphine and a chelating phosphine derivative with x carbon atoms in the backbone of the phosphine.
‡‡‡ Measuered in CD_2Cl_2. Formed *in situ* from the reaction of $HPCy_2MeI$ and poly-4-vinylpyridine (2% crosslinked).
§§§ Measured in diethylether.

Table 9. Comparative Phosphorus Chemical Shift Data for CO and NBD Rh(I) Phosphine Complexes of the Type [Rh(diphos)L_2]$^+$.

Substituents on the Chelating Phosphine	$\Delta d^{\dagger\dagger\dagger}$ (x=3) for L_2= NBD	$\Delta d^{\dagger\dagger\dagger}$ (x=3) for L_2= 2CO
Ph	38.7	54.6
Cy	36.9	63.1
Bu^t	63.7	67.4

The difference in the chemical shifts of the two and three carbon backboned complexes (Δd) is fairly constant for Cy and Ph derivatives, but anomalously large for the Bu^t derivatives of the NBD complexes, but not of the CO complexes. This difference in behaviour for the Bu^t complex with a three carbon backbone in the phosphine is probably due to a steric effect; there are significantly larger interactions between the phosphine and the norbornadiene than between the phosphine and the carbonyl ligands. Consequently, in the carbonyl complexes both the carbonyl and phosphine ligands can approach more closely to the metal, improving the orbital overlap and thus strengthening bonds.

A similar steric argument can be used to rationalise the phosphorus chemical shifts of the diop derivatives of complex **(1)**, Trend 4 . In these complexes the very bulky alkyl substituents (Cy and Bu^t) cause a reduction in the phosphorus chemical shift relative to the Ph derivative. This behaviour contrasts with that of the five membered chelates, and the ferrocenyl derivatives where the δp is shifted to higher frequency for both the Bu^t and Cy derivatives, and can be attributed to increased steric interactions with the norbornadiene ligand in the diop derivatives of complex **(1)**.

Whilst these are observations of the effects on δ_P caused by variations in the size of the chelate ring, the intrinsic reason behind these changes remains elusive, although several theories have been proposed.

In 1989 Powell[23] observed that the angle between two mono-phosphines subtended at the metal did not correlate with the Tolman cone angle,[24] and the CPC angles were

fairly resilient to compression. Consequently, when the steric bulk of the mono-phosphines was increased, the metal phosphorus bond "deformed" or "bent" to reduce any steric interactions with the other ligands bonded to the metal. Furthermore, there was a good correlation between the degree of M-P bending and the angle at the metal, increasing the PMP angle increased the degree of bond bending in the molecule.

Linder *et al*[25] examined the solution and solid state NMR of several chelating diphosphine complexes of Mo, W, and Pt and found a correlation between δp and β, where β is the angle subtended between the M-P vector and the normal to the plane containing the three carbon atoms α to the phosphorus atom. However, extending solid state phenomena into the solution state needs to be done with care. In the solid state large differences in bond lengths and angles can be caused by solid state packing forces. In attempting to correlate δ_P and β for the rhodium complexes in the present study, details of the crystal structures and NMR parameters were closely scrutinised. However, examination of crystal structures of identical molecules in slightly different environments**** revealed variations in β of +/- 5°, which invalidates any apparent correlation with solution state NMR measurements. In the solution phase, in which the NMR measurements contained in this work were obtained, the molecules are constantly bending and vibrating; consequently the magnitude of β is an average, and probably not that which is observed in the solid state. So, whilst bond bending is probably partly responsible for the chelation chemical shift, quantifying the degree of bending is problematic unless another solution state technique is used. For example infra-red spectroscopy could be employed to obtain the Rh-P bond length; the greater the degree of bond bending, and the longer the bond, the more the stretching frequency is shifted to lower wave numbers.

**** Using the Cambridge Crystallographic Data-Base.

2.5. Summary

A series of complexes of the type $[Rh(diphos)(C_7H_8)](BF_4)$ (diphos = dppe, dppp, dppb, dcpe, dcpp, dcpcp, dBpe, dBpp, Boxylyl) and $[Rh(diphos)(CO)_2](BF_4)$ (diphos = dBpe, dBpp, dcpp) has been synthesised. Two of these compounds ($[Rh(diphos)(C_7H_8)](BF_4)$ (diphos = dBpe, dcpcp) have been characterised by X-ray crystallography. For the complexes of the type $[Rh(diphos)(C_7H_8)](BF_4)$, the relationship between selected NMR data and X-ray crystallographic data has been examined and several trends have been observed. Increasing the σ-donor properties and steric bulk of the phosphine increases the Rh-P bond length (decreasing $^1J_{Rh-P}$) and activates the alkene (decreasing the $\delta_{C=C}$ for the =CH), reducing the Rh-C bond distances and increasing the C-C double bond length. Introducing steric restrictions into the phosphine backbone, e.g. by incorporating phosphorus atoms *trans* across a cyclopentane ring, causes a general lengthening of all metal-ligand bonds and a decrease in the phosphorus chemical shift (δ_p). The chelate chemical shifts (Δr) for complexes of the types $[Rh(diphos)(C_7H_8)](BF_4)$ and $[Rh(diphos)(CO)_2](BF_4)$ are dependent on the steric and electronic properties of the phosphine, and very bulky phosphines in the complexes of the type $[Rh(diphos)(C_7H_8)](BF_4)$ decrease Δr.

2.6. References

[1]R. Cramer, *Inorganic Synthesis*, **XV** , 14.
[2]T. G. Schenk, J.M. Downes, C.R.C. Milne, P.B. Mackenzie, H. Boucher, J. Whelan, B. Bosnich, *Inorg. Chem.* , **24** (1985) 2334-2337.
[3]See Chapter 3 .
[4]D.P. Fairlie, B.Bosnich, *Organometallics*, **7** (1988), 936-945.
[5] A.G. Orpen, N.G. Connelly, *Organometallics*, **9**, (1990), 1206-1210
[6] R.H. Crabtree, "The Organometallic Chemistry of the Transition Elements", Wiley-Interscience, Chichester, 1988.
[7] J.D.Oliver, D.P. Riley, *Organometallics*, **2**, (1983), 1032.
[8] J.S. Giovannetti, C.M. Kelly, C.R. Landis, *J.Am. Chem. Soc.*, **115**, (1993), 4040.
[9] W.R. Cullen, T.J. Kim, F.W.B. Einstein, T. Jones, *Organometallics*, **4**, (1985), 346.
[10] W.R. Cullen, T.J. Kim, F.W.B. Einstein, T. Jones, *Organometallics*, **2**, (1983), 714
[11] R.R. Schrock, J.A. Osborn, *J. Am. Chem. Soc.*, **93**, (1971), 2397-2407
[12] J.M. Brown, P.A. Chaloner, A.G. Kent, B.A. Murrer, P.N. Nicholson, D. Parker, P.J. Sidebottom, *J. Organomet. Chem.*, **216**, (1981), 263-276.
[13] E.P. Kypa, R.E. Davis, P.N. Juri, K.R. Shirley, *Inorg Chem.*, **20**, (1981), 3616.
[14] I.R. Butler, W.R. Cullen, T.J. Kim, S.J. Rettig, J. Trotter, *Organometallics.*, **4**, (1985), 972-980.

[15] K. Tani, E. Tanigawa, Y. Tatsuno, S. Otsuka, *J. Organomet. Chem.*, **279**, (1985), 87-101.
[16] D.A. Slack, I. Greveling, M.C. Baird, *Inorg. Chem.*, **18**, (1979), 3125-3132.
[17] K. Tani, K. Suwo, E. Tanigawa, T. Yoshida, T. Okano, S. Otsuka, *Chem. Lett.*, (1982), 265-268.
[18] P.S. Pregosin, "^{31}P and ^{13}C NMR of the Transition Elements," Pergamon Press, 1979.
[19] Neat, $CHCl_3$ reference.
[20] A. Del Zotto, L. Costella, A. Mezzetti, Pierluigi Rigo, *J. Organomet. Chem.* , **414**, (1991), 109-118.
[21] P.E. Garrou *Chem. Rev.*, **81**, (1981), 229-266.
[22] J.C. Tebby, "Handbook of Phosphorus-31 Nuclear Magnetic Resonance Data", CRC Press, Boston, 1991.
[23] J. Powell, *J. Chem. Soc. Chem. Commun.*, (1989), 200-202.
[24] C.A. Tolman, *Chem. Revs.*, **77**, (1977), 313.
[25] E. Lindner, R. Fawzi, H.A. Mayer, K. Eichele, W. Hiller, *Organometallics*, **11**, (1992), 1033-1043.

Chapter 3

The Synthesis and Characterisation of Silver Phosphine Complexes

3.1. Introduction

During the synthesis of $[Rh(diphos)(C_7H_8)](BF_4)$ **(1)** type complexes directly from $[Rh(ethene)Cl]_2$ **(2)** the silver ions used to remove the halide ions can compete with the rhodium for the norbornadiene and the phosphine reagents, to form soluble silver products. When excess norbornadiene and $AgBF_4$ are used in the production of the complex $[Rh(C_7H_8)_2](BF_4)$ **(3)**, the silver compound $[Ag_2(C_7H_8)_2](BF_4)_2$ **(4)** is formed and this has been previously reported in the literature.[1] This complex is light sensitive and decomposes in sunlight to produce silver metal. An alternative method to purify the rhodium complex **(1)** is to isolate the intermediate **(3)**, and this is facilitated by the greater solubility of the silver complex **(4)** than the rhodium complex **(3)** in THF.

When the phosphine is introduced to the rhodium precursor and silver ions are present, either as $AgBF_4$ or as complex **(4)**, then reaction with silver can occur. It has been shown previously that silver salts will react with chelating phosphines to yield $[\{Ag(diphos)\}_2]^{2+}$ **(5)** and $[Ag(diphos)_2]^+$ **(6)** ions respectively.[2]

This chapter is concerned with the isolation and characterisation of silver diphosphine complexes from the direct one-pot reactions of complex **(2)** to form type **(1)** complexes and in one case the subsequent synthesis of a silver diphosphine complex directly from silver tetrafluoroborate.

3.2. Experimental

3.2.1. Preperation of $[Ag_2(\mu\text{-}Bu^t_2P(CH_2)_3PBu^t_2)_2](BF_4)_2.2CH_2Cl_2$

The complex $[Ag_2(\mu\text{-dBpp})_2]$ $(BF_4)_2.2CH_2Cl_2$ **(7)** was isolated by partial crystallisation from a solution of $[Rh(dBpp)(C_7H_8)](BF_4)$ **(8)** in CD_2Cl_2 at -20°C. Complex **(7)** was isolated by filtration and dried *in vacuo*. Crystals suitable for X-ray crystallography were isolated and a structure determination performed by A. S. Batsanov (see Table 1, Appendix 3 and Figure 1). The $^{31}P\{^1H\}$ NMR spectrum was identical with that of an independently prepared sample (see below).

$[Bu^t_2P(CH_2)_3PBu^t_2]$ (0.42g, 1.27mmol) in diethylether ($4cm^3$) was added by cannula to a stirred suspension of silver(I) tetrafluoroborate (0.25g, 1.27mmol) in dichloromethane ($200\ cm^3$). The mixture was then stirred at r.t. in the dark for 2hrs. At the end of this period, the beige silver salt had reacted and a colourless solution formed. The solution was reduced in volume under reduced pressure to *circa* $50cm^3$, then filtered, before the volume was further reduced to *circa*. $15cm^3$. Slow addition of hexane caused the separation of colourless crystals of the title compound, which were removed by filtration. Cooling the filtrate to -15°C produced a second crop of crystals, shown to be identical to the first crop by spectroscopic methods. Yield: 0.50g (75%). Found: C, 39.27; H,7.33. $C_{40}H_{88}Ag_2B_2Cl_4F_8P_4$ requires C, 39.30; H, 7.26%. ^1H NMR ($CDCl_3$): δ 5.30 (s, $C\underline{H}_2Cl_2$), 1.88 (**4H**, br m, $PC\underline{H}_2$), 1.27 (**36H**, t, $^3J_{P\text{-}H}$ 7.2Hz, $PCC\underline{H}_3$), 1.18 (**2H**, s,$PCH_2C\underline{H}_2$) ppm. $^{13}C\{^1H\}$($CDCl_3$): δ 53.4 (s,$\underline{C}H_2Cl_2$), 29.8 (s, PC-$\underline{C}H_3$), 31.4 (m, P$\underline{C}$-CH_3), 33.8 (m, P$\underline{C}H_2$), 22.1 (m,$PCH_2\underline{C}H_2$) ppm. $^{31}P\{^1H\}$ ($CDCl_3$): δ 57.8 (d, $^1J\{^{107}Ag\text{-}P\}$ 467, $^1J\{^{109}Ag\text{-}P\}$ 539Hz) ppm

FAB Mass Spectrum (nitrobenzylalcohol matrix):

-ve ion: m/z 87 (100%, BF_4^-).

+ve ions: m/z 821.4 {3%, $(M\text{-}Bu^t)^+$}, 439.3 {100, $^{107}Ag(dBpp)^+$}, 57.0 (52, Bu^{t+})

Figure 1. The Crystal Structure of $[Ag_2(\mu\text{-}Bu^t{}_2P(CH_2)_3PBu^t{}_2)_2](BF_4)_2.2CH_2Cl_2$

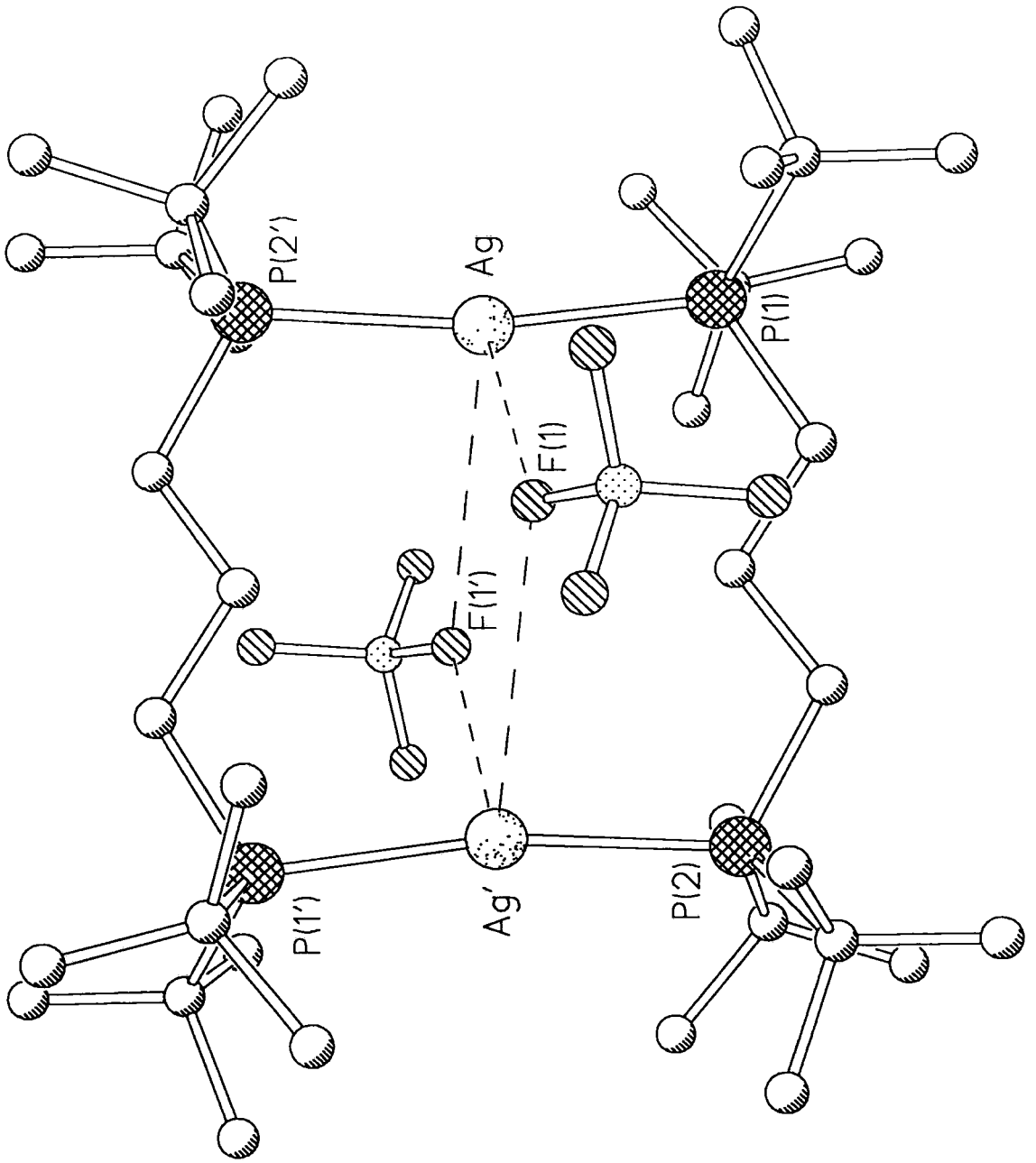

Table 1. Selected Bond Distances (Å) And Angles (°) for Complex (7)

Bond Distances (Å)		**Bond Angles (°)**	
Ag-P(2)	2.4056(14)	P(2)-Ag-P(1)	169.49(4)
Ag-P(1)	2.4059(13)	C(1)-P(1)-C(4)	104.1(2)
P(1)-C(1)	1.836(4)	C(1)-P(1)-C(8)	106.4(2)
P(1)-C(4)	1.877(4)	C(4)-P(1)-C(8)	112.9(2)
P(1)-C(8)	1.880(5)	C(1)-P(1)-Ag	110.93(14)
P(2)-C(3)	1.839(4)	C(4)-P(1)-Ag	111.4(2)
P(2)-C(16)	1.876(4)	C(8)-P(1)-Ag	110.9(2)
P(2)-C(12))	1.879(4)	C(3)-P(2)-C(16)	102.7(2)
P(2)-Ag	2.4056(14)	C(3)-P(2)-C(12)	106.2(2)
C(1)-C(2)	1.531(6)	C(16)-P(2)-C(12)	113.0(2)
C(2)-C(3)	1.533(6)	C(3)-P(2)-Ag	116.00(14)
C(4)-C(5)	1.534(6)	C(16)-P(2)-Ag	109.30(14)
C(4)-C(6)	1.541(7)	C(12)-P(2)-Ag	109.6(2)
C(4)-C(7)	1.544(6)	C(2)-C(1)-P(1)	114.6(3)
C(8)-C(9)	1.534(6)	C(1)-C(2)-C(3)	110.4(3)
C(8)-C(11)	1.537(7)	C(2)-C(3)-P(2)	115.3(3)
C(8)-C(10)	1.539(6)	C(5)-C(4)-C(6)	108.6(4)
C(12)-C(14)	1.530(6)	C(5)-C(4)-C(7)	109.7(4)
C(12)-C(15)	1.533(6)	C(6)-C(4)-C(7)	107.8(4)
C(12)-C(13)	1.533(7)	C(5)-C(4)-P(1)	114.3(3)
C(16)-C(17)	1.534(6)	C(6)-C(4)-P(1)	106.2(3)
C(16)-C(18)	1.539(6)	C(7)-C(4)-P(1)	110.1(3)
C(16)-C(19)	1.544(6)	C(9)-C(8)-C(11)	108.9(4)
Cl(1)-C(20)	1.806(7)	(9)-C(8)-C(10)	109.9(4)
C(18)-C(16)-C(19)	108.7(4)	C(11)-C(8)-C(10)	107.6(4)
C(17)-C(16)-P(2)	110.1(3)	C(9)-C(8)-P(1)	114.5(3)
C(18)-C(16)-P(2)	115.4(3)	C(11)-C(8)-P(1)	106.1(3)
C(19)-C(16)-P(2)	105.3(3)	C(10)-C(8)-P(1)	109.5(3)
C(17)-C(16)-C(19)	107.8(4)	C(14)-C(12)-C(15)	109.9(4)
		C(14)-C(12)-C(13)	109.1(4)
		C(15)-C(12)-C(13)	107.1(4)
		C(14)-C(12)-P(2)	114.5(3)
		C(15)-C(12)-P(2)	109.4(3)
		C(13)-C(12)-P(2)	106.6(3)
		C(17)-C(16)-C(18)	109.3(4)

3.2.2. The Isolation of $[(Ag_2(\mu\text{-}Bu^t_2P(CH_2)_2PBu^t_2)(H_2O)_2](BF_4)_2$ (10)

During the synthesis of $[Rh(dBpe)(C_7H_8)](BF_4)$ **(9)** directly from complex **(2)**, large colourless light sensitive crystals of $[(Ag_2(\mu\text{-}Bu^t_2P(CH_2)_2PBu^t_2)(H_2O)_2](BF_4)_2$ **(10)** grew from solution. The crystals were isolated by filtration and their X-ray crystal structure was determined by A. S. Batsanov (see Tables 2, Appendix 3 and Figure 2). There were insufficient crystals present to allow spectroscopic studies to be undertaken before decomposition had occurred to silver metal. Subsequent attempts to synthesise **(10)** independently from $AgBF_4$ and the diphosphine dBpe were fruitless. The phosphorus NMR spectrum of reaction solutions indicated that several products were present but none could be definitely assigned.

Table 2. Selected Bond Distances (Å) and Angles (°) for Complex (10)

Bond Distances		**Bond Angles**	
Ag-O	2.177(3)	O-Ag-P	169.78(9)
Ag-P	2.3472(9)	C(1)-P-C(6)	105.6(2)
P-C(1)	1.852(4)	C(1)-P-C(2)	104.1(2)
P-C(6)	1.868(4)	C(6)-P-C(2)	114.5(2)
P-C(2)	1.872(4)	C(1)-P-Ag	114.51(12)
C(1)-C(1)	1.532(7)	C(6)-P-Ag	109.79(13)
C(2)-C(3)	1.530(5)	C(2)-P-Ag	108.40(12)
C(2)-C(5)	1.536(6)	C(1)-C(1)-P	113.7(3)
C(2)-C(4)	1.541(6)	C(3)-C(2)-C(5)	109.0(4)
C(6)-C(8)	1.528(6)	C(3)-C(2)-C(4)	109.8(3)
C(6)-C(7)	1.535(6)	C(5)-C(2)-C(4)	108.6(4)
C(6)-C(9)	1.546(6)	C(3)-C(2)-P	110.1(3)
		C(5)-C(2)-P	105.3(3)
		C(4)-C(2)-P	113.9(3)
		C(8)-C(6)-C(7)	108.7(4)
		C(8)-C(6)-C(9)	110.2(3)
		C(7)-C(6)-C(9)	107.8(4)
		C(8)-C(6)-P	114.2(3)
		C(7)-C(6)-P	106.1(3)
		C(9)-C(6)-P	109.5(3)

Figure 2. The Crystal Structure of $[(Ag_2(\mu\text{-}Bu^t{}_2P(CH_2)_2PBu^t{}_2)(H_2O)_2](BF_4)_2$ (10)

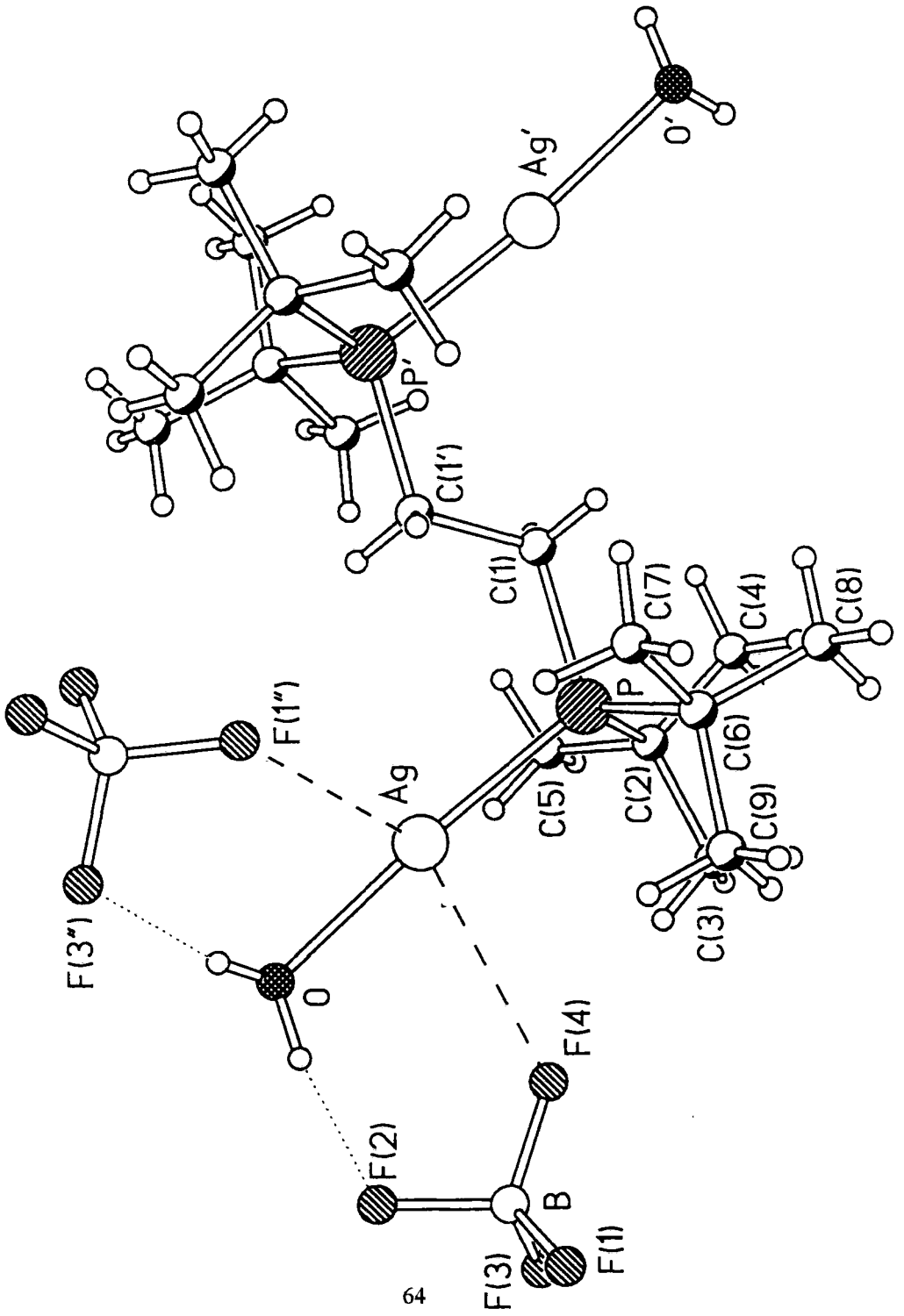

3.3. Discussion

The formation of soluble silver species is a problem during the synthesis of complexes of the type **(1)** due to the reaction of the silver ions with any excess norbornadiene[1] and diphosphine[2] used. The most efficient method of purification of the rhodium product is to isolate the intermediate $[Rh(C_7H_8)_2](BF_4)$ and remove the silver impurity **(3)** with THF in which the rhodium complex is only sparingly soluble. If the silver impurity is not removed at this stage then it can react later when the phosphine is introduced to form a silver phosphine complex. During this study two new silver phosphine species have been isolated, $[Ag_2(\mu\text{-dBpp})_2](BF_4)_2$ **(7)** and $[\{Ag(H_2O)\}_2(\mu\text{-dBpe})](BF_4)_2$ **(10)**.

Complex **(7)** consists of two silver ions bridged by two dBpp ligands to form a twelve membered ring, which is essentially planer (P-Ag-P, 170°) and the core $[Ag_2(L_2)_2]^{2+}$ unit is similar to the previously characterised complex $[Ag_2(\mu\text{-dppp})_2(NO_3)_2]$ **(11)** reported by Tiekiuk.[3] In complex **(7)** two solvent molecules (dichloromethane) sit above and below the plane of the silver complex, and these show some disorder.

There are weak interactions in complexes **(7)** and **(10)** between the silver atoms and fluorines on the tetrafluoroborate counterions. Similar weak Ag-F interactions have been observed in $[Ag_2(\mu\text{-}Bu^t_2PCH_2P\text{-}Bu^t_2)_2](PF_6)_2$[4] **(12)** (see Table 3).

Table 3. Secondary Interactions in Silver Complexes

Complex	Ag-F (Å)	O-F (Å)	H-F (Å)
(7)	3.218	-	-
	3.795		
(12)	2.992	-	-
(10)	2.834	2.730	1.818
	2.947	2.689	1.939

The magnitude of the $^{1}J(^{107}Ag\text{-}P)$ coupling constant (467Hz) in complex **(7)** is typical of sp hybridised two co-ordinate silver[4] bonded to phosphorus, and compares closely with the estimated value of 452Hz, based solely on s-orbital contributions to the coupling.[5] Thus the NMR data indicate that the solid state structure of complex **(7)** is retained in solution. Furthermore, complex **(7)** is air, moisture and light stable. The thermodynamic stability of complexes similar to **(10)** and **(11)** is found to be dependent on the size of the chelate ring, 12 membered rings possessing more stability than 10 membered rings.[2] The stability of complex **(10)**, which does not have a ring structure, contrasts with that of complex **(7)** which has a twelve membered ring, and complex **(10)** is probably only stable in the solid state due to secondary interactions with the BF_4^- counter-ion. Complex **(10)** contains only one diphosphine ligand, bridging two silver atoms, and *trans* to each phosphorus ligand is a water molecule.[6] Also, the protons in the water molecules and the silver atoms are engaged in secondary interactions with the BF_4^- counter-ion and these secondary interactions are stronger than those observed in complexes **(7)** and **(12)** (see Table 3). Complex **(10)** appears to be the first example of a P, O bonded, two co-ordinate silver complex, although $[Ag_2(diphos)]^{2+}$ complexes have been reported before[7].

3.4. Summary

During the synthesis of $[Rh(diphos)(C_7H_8)](BF_4)$ (diphos = dBpe, dBpp) complexes, two novel silver compounds $[Ag_2(\mu\text{-}dBpp)_2](BF_4)_2$ and $[\{Ag(H_2O)\}_2(\mu\text{-}dBpe)](BF_4)_2$ were isolated and characterised by X-ray crystallography. The dBpp complex has been independently synthesised from $AgBF_4$ and the phosphine, and characterised by NMR and elemental analysis.

3.5. References

[1] H.W.Quinn, *Can. J. Chem.*, 1968, **46**, 117-124.
[2] P.D. Di Bernado, G. Dolcetti, R. Portanova, M. Tolazzi, G. Tomat, *Inorg. Chem.*, 1990, **29**, 2859-2862;
[3] E.R.T. Tiekuik, *Acta. Crystallogr. Sect. C*, 1990, **C46**, 1933-4.
[4] H.H.Karsch and U.Schubert, *Z. Naturforsch. Teil B*, 1982, **37**, 186.
[5] M. Camalli, F. Caruso, *Inorg. Chim. Acta 1988*, **144**, 205.
[6] The source of this is probably the silver perfluoroborate itself which is very hygroscopic.
[7] Yang Hua-Hui, Zheng Lan-Sun, Zhang Ying, Zhang Peng, Zhang Qian-Er, *Jiegou Huaxue (J. Struct. Chem.)*, 1990, **9**, 137.

Chapter 4

Carbonylation Studies

4.1 Introduction

Rhodium complexes are active as catalysts for many reactions, including hydrogenation and carbonylation, for example in the synthesis of L-Dopa[1] and the Monsanto acetic acid process[2] respectively. In the former application phosphines are used as promoters. In general, through a judicious choice of precursor complex and phosphine, enhancements in both turnover frequency and selectivity are possible.[1]

This chapter is concerned with the carbonylation activity of the complexes reported in Chapter 1 especially [Rh(diphos)(C_7H_8)](BF_4) **(1)**. In particular two reactions have been attempted, alkoxycarbonylation (hydroesterification) and hydroformylation, each of which are presented separately below.

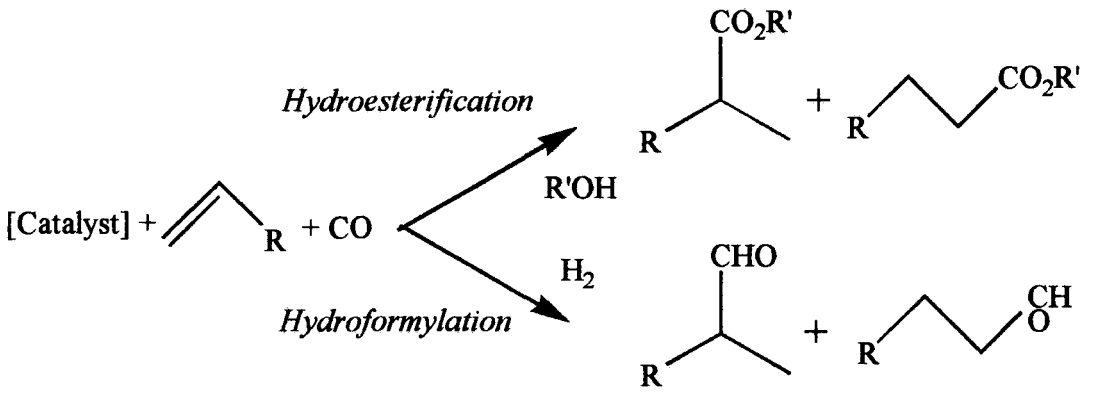

4.2 Hydroesterification

4.2.1 Attempts using [Rh(diphos)(C_7H_8)](BF_4) [1, diphos = dppe (2), dcpp (4)] and [Rh(C_7H_8)$_2$](BF_4) (3)

The complex (~40mg) dissolved in methanol (40cm^3) was transferred against a countercurrent of nitrogen *via* cannula into a 150cm^3 stainless steel autoclave equipped with an overhead Magnedrive stirrer. The solution was then treated with H_2 (500psi) for 15minutes to remove the norbornadiene. The stirring rate was standardised at 200rpm, and the total volume for the reactions was set at 40cm^3. A variety of conditions and diphosphines was investigated (see Table 1 for a summary of experiments performed). These included acidic, basic and neutral, and reaction temperatures from 100-175°C. The reaction time was varied between one and eight hours in-case the reaction was either very slow or there was an induction time required prior to catalysis. However, hydroesterification of either ethene or 1-hexene with CO and methanol was not observed. At the end of each reaction the vessel was vented and a sample of the product mixture (5cm^3) vacuum distilled and then analysed by GC-MS. In certain instances it was possible to obtain $^{31}P\{^1H\}$ NMR analysis of the reaction mixture. In all of the reactions analysed by this method only one phosphorus signal was observed, and this was consistent with the data previously obtained for [Rh(diphos)(CO)$_2$](BF_4) complexes.[3]

Table 1

Complex	Solvent/Reactants	Temperature (°C)	CO (psi)	ethene (psi)	Time (hrs)
(2)	MeOH	100 to 175	400	400	2
(2)	MeOH/HBF_4.Me_2O	100 to 175	400	400	1
(2)	MeOH/NaOMe 0.5M	175	400	400	1
Blank	MeOH/NaOMe 0.5M	175	400	400	1
Blank	MeOH/NMP/Hexene	175	450	-	2
(3)	MeOH	175	400	400	8
(4)	MeOH	175	400	400	8

Complexes used [Rh(dppe)(NBD)](BF_4) **(2)**, [Rh(NBD)$_2$](BF_4) **(3)**, [Rh(dcpp)(NBD)](BF_4) **(4)**

When basic conditions were employed a pressure drop was observed. However, this was due to the previously reported methoxide catalysed carbonylation of methanol to form methyl formate.[4] Blank reactions under identical conditions confirmed that the rhodium was not active for this reaction.

4.2.2 Under Monsanto Conditions, using [Rh(CO)$_2$(AcAc)]/Phosphine

The Monsanto company has previously claimed that [Rh(CO)$_2$(AcAc)] in the presence of trialkyl- phosphines (at 175°C, 700psi of 1:1 CO:ethene), is an active catalyst for the hydroesterification of alkenes.[5] In an effort to determine if the rhodium precursor complex was responsible for the lack of hydroesterification activity, the conditions employed in the Monsanto process were replicated, and the mono-phosphine was replaced by a chelating phosphine.

The rhodium complex and phosphine were quickly loaded as solids, in air, into the stainless steel 150cm^3 autoclave and the atmosphere replaced with nitrogen before methanol (40cm^3) was added *via* cannula. The autoclave was pressurised with CO (50psi) and heated to 175°C. When the reaction temperature was reached, a previously prepared reservoir of 1:1 CO:ethene (700psi) in a 1.1 litre autoclave attached to the reaction vessel was opened. The reaction was stirred for three hours and the pressure monitored. The results are summarised in Table 2. The phosphine to rhodium ratio was 2.5:1 for the monophosphine systems and 1:1 for the chelating phosphine systems.

Table 2 Summary of Reactions Investigated Under Monsanto Conditions

Precursor	Mass (mg)	Phosphine	Mass (mg)	Products
Rh(CO)$_2$(AcAc)	200	PCy_3	544	√
Rh(AcAc)$_3$	310	PCy_3	544	√
Rh(CO)$_2$(AcAc)	115	Boxylyl	172	X
Rh(CO)$_2$(AcAc)	100	dcpp	164	X
Rh(CO)$_2$(AcAc)	100	dppp	160	X

Products were only obtained for the monophosphine systems. A pressure drop was observed, although there was an induction period when [$Rh(AcAc)_3$] was the precursor. The product distribution using [$Rh(AcAc)_3$] was similar to that observed with $Rh(CO)_2(AcAc)$.

Table 3. Major Products and Distributions from Hydroesterification Reactions

Product	% Product in methanol solution (by Integration)	
	$[Rh(CO)_2(AcAc)]/PCy_3$	$[Rh(AcAc)_3]/PCy_3$
Methyl propionate	41.4	49.4
Methyl-butanoate and Methyl-2-methylpropionate	0.3	3.0
Methyl-2-methylpentanoate	6.8	3.9

4.3 Hydroformylation

The reactants and solvents were loaded into the 150cm^3 stainless steel autoclave in a similar manner to the hydroesterification experiments. The total liquid volume was maintained at 40cm^3. Both ethene and 1-hexene were used as the alkene. At the end of the reactions when 1-hexene was used, isomerised hexenes were detected. The H_2/CO was used as obtained in premixed cylinders. The results for the hydroformylation experiments are summarised in Table 4 below. No reaction was observed at temperatures below 100°C. The optimum conditions were found to be 120°C, 450psi 2:1 H_2:CO; increasing the temperature led to the formation of undesirable hydrogenation products. At the end of the reactions the phosphorus NMR spectra were obtained and this indicated the resting state of the catalyst to be [$Rh(diphos)(CO)_2$](BF_4), responsible for the only phosphorus signal obtained at the end of the reaction. The reaction time was either one (~70mg catalyst) or two hours (30mg catalyst). However, for a typical run the pressure in the vessel dropped quickly (15 or 30minutes respectively) due to the conversion of the alkene, CO and H_2 into aldehydes, implying the reaction was essentially over by the end of this time. The exception to this was when complex **(10)** was used, in which case the pressure dropped slowly over the whole period of time.

Key to Table 4

*Key to complexes: [Rh(dBpe)(C_7H_8)](BF_4) **(5)**, [Rh(dBpp)(C_7H_8)](BF_4) **(6)**, [Rh(dcpcp)(C_7H_8)](BF_4) **(7)**, [Rh(dcpe)(C_7H_8)](BF_4) **(8)**, [Rh(dppb)(C_7H_8)](BF_4) **(9)**, [Rh(Boxylyl)(C_7H_8)](BF_4) **(10)**.

†Ethene (300psi) was used in this reaction instead of 1-hexene.

‡The products were analysed by GC-MS at the end of the reaction, the ratio of the products being the integration of the GC peaks (flame ionisation detector). The integrals were not corrected for the varying response factors of the compounds observed.

§1:2:3 Subs ratio, is the ratio of the 1,2, and 3 substituted aldehyde isomers of $C_7H_{14}O$.

**The *n*:*b* ratio is the ratio of the *normal*(straight chained) to the *branched* (branched chain) products, i.e. the ratio of 1:(2+3).

#Key to products: unreacted isomerised hexenes **(S)**, propanal **(U)**, heptanol **(T)**, propanol **(V)**, 1,1-dimethoxyheptane, **(W)**, diethylketone **(X)**, 1-methyldimethoxyhexane **(Y)**, alkanes **(Z)**.

Table 4 Hydroformylation Results

Reaction No.	Complex*	Mass (mg)	Solvent/Reactants (Total Volume 40cm^3)	Temp. (^oC)	Time (Hrs)	CO (Psi)	H_2 (Psi)	*n:b* ratio**	Products‡ 1:2:3 subs§	Others#
1	**(5)**	68	31:9 NMP:1-hexene	100 to 150	1	150	300	21:12	21:11:1	**S**
2	**(5)**	64	31:9	120	1	225	225	31:15	31:14:1	**S**
3	**(5)**	69	21:10:9 NMP:MeOH:1-hexene	120	1	150	300	101:47	101:46:1	**S**
4	None	-	21:10:9	180	2	450	150	-	-	None
5	**(5)**	72	21:10:9	180	1	450	150	2:1	2:1	**T, W, Z**
6	**(6)**	28	21:10:9	120	2	150	300	2:3	2:2:1	**W**
7	**(5)**	30	27:13:0†	120	2	150	300	-	-	10**(U)**:1**(V)**:1**(X)**
8	**(4)**	25	21:10:9	120	2	150	300	1:1	3:2:1	**S**
9	**(7)**	31	21:10:9	120	2	150	300	1:1	3:2:1	**S**
10	**(8)**	24	21:10:9	120	2	150	300	10:6	10:5:1	**S**
11	**(9)**	31	21:10:9	120	2	150	300	7:1	7:1	**S, W**
12	**(10)**	30	21:10:9	120	2	150	300	3:2	9:5:1`	**S, W**
13	**(2)**	31	21:10:9	120	2	150	300	9:7	9:6:1	**S, W, Y**

4.4. Discussion

Complexes of the type **(1)** were inactive when tested as hydroesterification catalysts under a range of conditions, (including acidic, basic and neutral). Under Monsanto conditions,[5] in which the monophosphine species are active, the corresponding chelating phosphines are inactive. Consequently, the reason for the inactivity is the presence of the chelating phosphine. At the end of the reactions, NMR evidence indicated the rhodium was present as $[Rh(diphos)(CO)_2](BF_4)$ **(11)**, which appears to be a sink for this reaction due to its high stability under the conditions employed.

For catalysis to occur, the generation of an active catalytic species (for example a hydride) and co-ordination of the reactants (for example, ethene and CO) is necessary. Thus, at the outset, complex **(1)** was pre-treated with hydrogen gas to remove the norbornadiene as the saturated hydrocarbon norbornane, and generate a co-ordinatively unsaturated species $[Rh(diphos)(Solvent)_2]^+$ **(12)**. However, separate investigations of this type of complex (solvent=MeOH; see chapter 5) reveal that it is relatively stable (in methanol), and does not react (at r.t.) with either the solvent or hydrogen to form observable hydrides. Complexes of the type **(12)** (solvent = MeOH) react quickly when exposed to CO to form **(11)**, found to be very stable, especially in the presence of CO, preventing the co-ordination of other reactants and consequently catalysis occurring. Replacing the diphosphine in **(11)** for two mono-phosphines, causes a difference in reactivity. The cationic complex can now adopt a *trans* phosphine configuration stabilising the formation of hydrides,[6] and one of the phosphines can easily dissociate to create a vacant position for the alkene to co-ordinate. Comparison of the catalytic activity of PCy_3 and diphos / $[Rh(CO)_2(AcAc)]$ under Monsanto conditions[5] reveals that only the mono-phosphine systems are catalytically active. As mentioned above, this difference in catalytic activity can be ascribed to the ability of the mono-phosphine catalyst to adopt a *trans* configuration. The nature of the rhodium precursor can effect the course of the reaction. Two reactions were performed, using the precursors $[Rh(CO)_2(AcAc)]$ and $[Rh(AcAc)_3]$ and the mono-phosphine PCy_3. The product distributions for both of these systems are

similar. However, the yield of methyl propionate from the Rh(III) precursor is higher, even though it underwent an induction period, involving reduction to a Rh(I) species. The nature of the products indicates the reaction is proceeding *via* a hydride route, the active hydride species probably being formed initially from the oxidative addition of the methanol to a rhodium(I) complex. The two minor ester products $C_3H_7CO_2CH_3$ and $C_5H_{11}CO_2CH_3$ have an even number of carbon atoms in the 'acid' side of the molecule. If there was a hydride precursor, this indicates they could not come just from ethene and CO (this would give odd numbered acids, e.g. $C_2H_5CO_2CH_3$). The most likely source of this 'extra' carbon atom would be the methanol solvent present, *via* a rhodium-methyl species. However, this does invite the question of how does this species form. In the Monsanto acetic acid process a rhodium methyl species is formed by the oxidative addition of MeI to the nucleophilic $[Rh(CO)_2I_2]^-$. Such a reaction seems unlikely under these conditions due to the poor nucleophilicity of the rhodium precursor and the lack of a halide ion or similar group. One possibility is that methanol attacks a carbonyl group attached to the metal to form an alkoxycarbonyl, and this decomposes with the generation of CO_2 to form a rhodium-methyl complex.

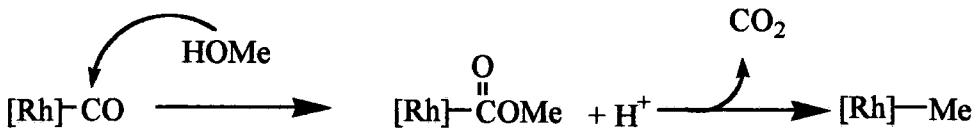

Similarly, the catalytic formation of long chain methyl-esters from the repeated insertion of ethene has been reported[7] for $[Rh(CO)(PPh_3)_3]$ and $[Rh(PPh_3)_3(CO)ClH]$ at 110°C, 1:1 ROH:HOAc, 1:1 CO:ethene (1000psi). However, unlike the Monsanto system, this system is active under acidic conditions. Additionally repeated insertions occur to such an extent that CO-ethene copolymers are formed in addition to methyl propionate which is the major product.

In contrast to their inactivity as catalysts under hydroesterification conditions, complexes of the type **(1)** are active catalysts for the hydroformylation of alkenes with CO, and H_2. However, this reaction requires relatively forcing conditions (120°C, 450psi 2:1 H_2:CO) for both ethene and 1-hexene.

Whilst no quantitative rate measurements were obtained, several qualitative observations were made due to the rate of the pressure change of the gases in the reaction vessel. When the reaction temperature was raised the rate of the reaction increased as might be predicted. However, this corresponded to a decrease in selectivity to the desired aldehydes due to the formation of hydrogenation products (alcohols and alkanes) and acetals that were not otherwise observed. Increasing the proportion of CO in the system from 33% to 50% decreases the rate of the reaction but has no significant effect on the normal to branched ratio of aldehydes. Changing the alkene from hexene to ethene increases the rate of the reaction. However, propanol and diethylketone are also produced as impurities when ethene is used. As mentioned above, the reaction involving the ligand Boxylyl is significantly slower than for the other phosphines. This may be related to the exceptional steric bulk of this phosphine because the phenyl substituted derivative [Rh(1,2-Bis(diphenylphosphino)*o*-xylene)$(CO)_2H$] has been patented as a hydroformylation catalyst due to its high rate of reaction.[8]

Examination of the product distributions reveals significant differences between the phosphine complexes, in particular the normal to branched ratio. This ratio for simple alkenes was previously found to be dependent on the size of the bite angle of the chelating phosphine. Increasing the bite angle increased the proportion of the normal product.[9] The results for the aryl derivatives (dppe and dppb) follow this trend, and the *n:branched (b)* ratio improves from 9:7 for complex **(2)** to 7:1 for complex **(9)**. The major products formed for complex **(2)** are the diacetals, compared to aldehydes for the other phosphines, although small amounts of diacetals are observed, as shown in Table 4. The result for the dppb complex, **(9)** is the best result obtained for all of the phosphine complexes investigated here with respect to rate and selectivity towards the *normal* product. The situation for the alkyl substituted phosphine complexes is quite the reverse to that observed for the aryl substituted phosphine complexes, with the *n:b* ratio favouring the branched product as the chelate ring size and bite angle are

increased. For the *tert* butyl derivatives (complexes **(5)** and **(6)**) the ratio changes from 2:1 to 2:3 whilst for the cyclohexyl derivatives (complexes **(8)** and **(4)**) it changes from 10:6 to 1:1. Interestingly, restricting the conformational freedom of the phosphine backbone (complex **(7)**) by the incorporation of a cyclopentane ring decreases the *n:b* ratio to 1:1, even though the bite angle is similar to that expected for the less constrained dcpe complex **(8)**.

At the end of the hydroformylation reactions the $^{31}P\{^{1}H\}$ NMR of the product liquor indicated the only species present were of the type **(11)**. The conditions required for hydroformylation using complexes of the type **(1)** are considerably more forcing than those required for $[Rh(PR_3)_2(CO)H]$.[10] At the end of the reactions described here, unreacted hexenes are always recovered, even though considerable quantities of gas remain. The accepted mechanism for hydroformylation is *via* a rhodium(I) hydride and this has been extensively studied using $[Rh(PPh_3)_3Cl]$ as the precursor.[10] To generate a hydride in the present system, it is necessary to oxidatively add hydrogen to the very stable dicarbonyl derived from complex **(12)** and this might be expected to form a rhodium(III) species **(13)**:

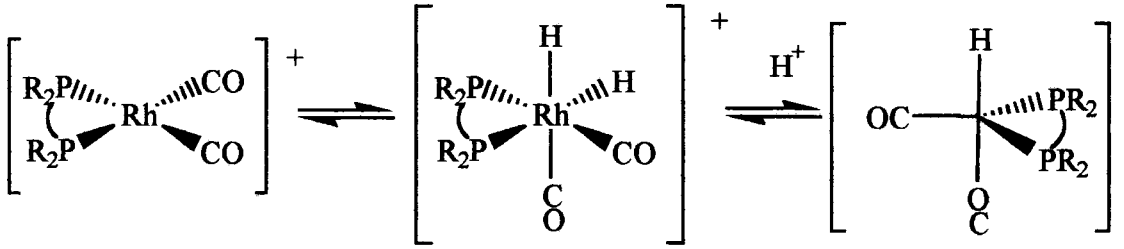

(11) **(13)** **(14)**

The bonding properties of **(13)**, which is a rhodium(III) complex, might be expected to be very different to those of the rhodium(I) complex **(11)**. In particular, the metal - carbon monoxide bonds are weakened due to decreased back donation from the metal in the higher oxidation state.[11] This would allow one of the CO ligands to be easily displaced by an alkene. Alternatively a proton could be lost to form a neutral rhodium(I) complex of the type **(14)**, similar to those species implicated in the catalytic cycle using rhodium(I) hydride-chelating phosphine or phosphite complexes.[12] It is not possible to tell from the data collected whether the hydroformylation proceeds *via*

a predominantly neutral rhodium(I) or a cationic rhodium(III) route, although it is quite possible that both are active species. Schrock and Osborn[13] observed a similar equilibrium when the mono phosphine analogues of complex **(1)** were employed as hydrogenation catalysts. They found that both the Rh(I) and the Rh(III) species were active hydrogenation catalysts, but that the Rh(I) species was a significantly more active isomerisation catalyst. Furthermore they found the isomerisation activity of the Rh(I) species was dependent on the phosphine employed, and the trialkylphosphines were the more active isomerisation catalysts. At the end of the reactions all of the remaining hexene had been isomerised to a statistical distribution of the isomers irrespective of the phosphine employed. This may point towards a rhodium(I) species as the active catalytic species in the present studies. However, under similar conditions[14] $[RhH(PEt_3)_3]$ is an efficient aldehyde hydrogenation catalyst whilst at 120°C little or no hydrogenation activity is observed for complexes of the type **(1)**. Interestingly, when the triaryl and trialkyl derivatives are compared, the *n*:*b* ratio is significantly higher for the triaryl species, and this was attributed to the higher isomerisation activity of the trialkyl species. So, whilst the improvement between the alkyl-phosphine and aryl-phosphine systems could be due to the higher isomerisation activity of the alkyl-phosphine species, this does not explain the decrease in the *n*:*b* ratio upon increasing the bite angle of the alkyl-phosphine species. Indeed by increasing the bite angle of the phosphine, the substituents are pushed around the metal and can interact with the other ligands on the metal more efficiently as is observed for the dppb system. This could imply a difference in mechanism. The alkylphosphine species are more likely to be Rh(III) complexes of the type **(13)** due to the electron rich nature of the phosphine ligand. Consequently, if the alkene binds *cis* to the two phosphorus atoms, then it will lie between the alkyl groups of the phosphine (see below). When the hydride ligand migrates onto the bound alkene, so long as it lies parallel to the rhodium-phosphine plane, the steric interactions with the phosphine in the two possible orientations are limited. By increasing the bite angle of the phosphine, the alkyl groups are pushed further around the sides of the molecule thus increasing the steric gap underneath the co-ordinated phosphine.

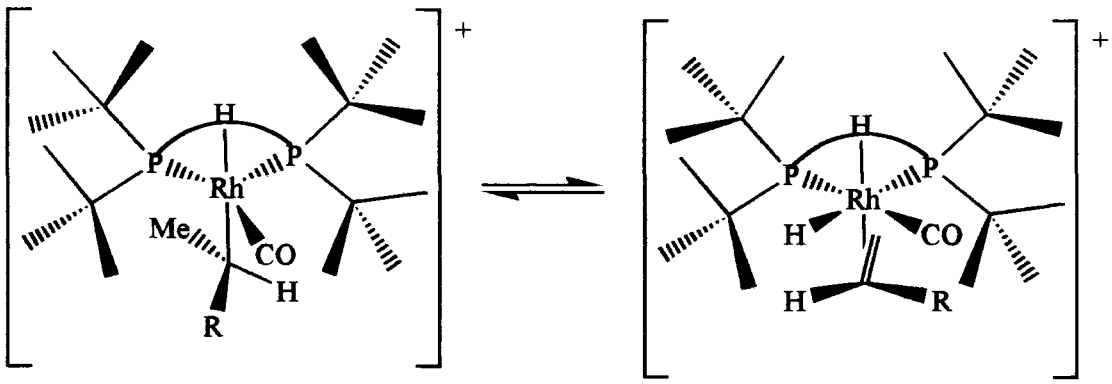

The exception to this is when Boxylyl is used as the chelating phosphine. This ligand contains an aromatic ring in the backbone, which must lie either above or below the rhodium-phosphine plane. This extra interaction blocks the steric gap and the *normal* product is once again favoured.

4.5. Summary

Complexes of the type **(1)** (diphos = dppe, dcpe, dcpcp, dBpe, dBpp, dcpp, dppb) are active catalysts for the hydroformylation of 1-hexene and ethene at 120°C, 450psi 2:1 H_2:CO. The rate of the reaction and the ratio of the product aldehydes from the hydroformylation of 1-hexene are both dependent on the nature of the phosphine. The best† results are obtained with the diphosphine dppb. For the aryl substituted diphosphines, increasing the size of the chelate ring increases the selectivity to the straight chain aldehyde product. This contrasts with the alkyl substituted diphosphines, where increasing the chelate ring size increases the selectivity towards the branched chain aldehyde products. This difference in behaviour stems from the establishment in solution of an equilibrium between a cationic Rh(III) and a neutral Rh(I) complex, both of which are catalytically active. Complexes of the type **(1)** and diphosphine/[$Rh(CO)_2(AcAc)$] systems are not catalytically active for the related hydroesterification reaction. However, the mono-phosphine, Monsanto catalyst PCy_3/[$Rh(CO)_2(AcAc)$] is active for hydroesterification. The inactivity of the

† With respect to rate of reaction and proportion of straight chain aldehyde produced.

diphosphine systems is due to the high stability of the cationic dicarbonyl $[Rh(diphos)(CO)_2]^+$. In the mono-phosphine systems, the phosphine ligands can adopt a *trans* configuration and/or dissociate from the complex allowing further reactions to occur and an active catalytic species to form.

4.6. References

[1] W.S. Knowles, M.J. Sabacky, B.D. Vineyard, D.J. WeinKauff, *J. Am. Chem. Soc.*, **97**, (1975), 5946-5942.
[2] D. Forster, *Adv. Organomet. Chem.*, **17**, (1979), 255.
[3] See Chapter 2
[4] S.P. Tonner, D.L. Trimm, M.S. Wainwright, N.W. Cant, *J. Mol. Catal.*, **18**, (1983), 215-222
[5] United States Patent Office 3,840,558, A.J.C. Pearson, Monsanto Company.
[6] See Chapter 5
[7] A. Sen, J. S. Brumbaugh, *J. Organomet. Chem.*, (1985), C5-C10.
[8] T.J. Devon, Eur. Pat. 0375 573 A1, 1990, Eastman Kodak Company
[9] C.P. Casey, G.T. Whiteker, M.G. Melville, L.M. Petrovich, J.A. Gavney Jr., D.R. Powell, *J. Am. Chem. Soc.*, **1992**, 114, 5535-5543.
[10] J.M. Brown, A.G. Kent, *J. Chem. Soc. Perkin Trans. II*, (1987), 1597-1607
[11] See Chapter 8
[12] G.J.H. Buisman, E.J. Vos, P.C.J. Kamer, and P.W.N.M. Van Leeuwen, *J. Chem. Soc. Dalton Trans.* (1995), 409-417.
[13] R.R. Schrock, J.A. Osborn, *J. Am. Chem. Soc.*, **98**, (1976), 2134-2143.
[14] J. K. MacDougall, D.J. Cole-Hamilton, *J. Chem. Soc. Chem. Commun.*, (1990), 165-167.

Chapter 5

The Synthesis, Characterisation and Reactivity of Rhodium Hydrides

5.1. Introduction

Complexes of the type [Rh(diphos)(C_7H_8)](BF_4) **(1)** have been shown to be active catalyst precursors for several processes including hydrogenation,[1,2,3] hydroformylation,[4] and hydrosilation.[5] In all of these processes hydrides are implicated as the active catalytic species, or as important intermediates in the catalytic cycle.[6,7]

The products from the reaction of complexes of the type **(1)** with hydrogen gas are dependent on the phosphine employed and the conditions used. In certain circumstances hydrides can be formed. This chapter is concerned with the nature and distribution of products from the reaction of complexes of the type **(1)** (diphos = dBpe, dBpp, dcpe, dcpp, dcpcp, Boxylyl) with hydrogen gas, and the effect of the solvent system used. The hydrides formed under these conditions are unstable in the absence of hydrogen gas, and often fluxional in solution; consequently they have been studied under an atmosphere of hydrogen gas by variable temperature (VT) phosphorus and proton NMR spectroscopy.*

* The windows used for phosphorus and proton NMR spectra, are 0-200ppm, and 12 to -30ppm respectively. See Appendix 1 for general experimental details.

5.2. The Hydrogenation of Type (1) Complexes in d^4-Methanol

The complexes of the type **(1)** (~50mg) were loaded in air into a resealable 5mm NMR tube equipped with a teflon tap, and the atmosphere replaced with N_2. CD_3OD (~0.5cm^3) was added in a glove box.* The nitrogen was removed *in vacuo* and replaced with hydrogen (1atm.).

5.2.1. Hydrogenation of [Rh(dBpp)(C_7H_8)](BF_4) (2) in CD_3OD

After hydrogenation the solution was deep red in colour. Even at -90°C the proton NMR did not show any signals in the hydride region (0 to -30ppm). However the proton NMR did show one interesting feature, a very temperature dependent signal at 5.03 ppm, probably due to the "OH" group of the solvent. This peak is enhanced relative to the methyl group due to rapid exchange *via* the rhodium with the hydrogen gas present. Further evidence for this comes from the comparison of the ^{13}C and ^{13}C {selective proton decoupled}† NMR spectra which show that the proton is not attached to any carbon atom. Only a doublet can be observed in the phosphorus NMR spectrum (see Figure 1, Page 83). $^{31}P\{^1H\}$ NMR (CD_3OD) (r.t.): δ 62.2 (d, $^1J_{Rh-P}$ 207Hz) ppm.

5.2.2. Hydrogenation of [Rh(Boxylyl)(C_7H_8)](BF_4) (3)

On addition of the hydrogen, the solution turned deep olive green in colour and remained so during the whole reaction. However, the complex formed exhibited reversible thermochroism, becoming deep red in colour when it was cooled down. The phosphorus NMR spectral changes (see Figure 2, Page 84) parallelled the thermochroism and the signal sharpened as the sample was cooled. Even at -90°C there were no hydride signals observed in the proton NMR spectrum. $^{31}P\{^1H\}$ NMR, (CD_3OD) (r.t.) δ 69.8 (br d, $^1J_{Rh-P}$ 245), (-90°C): 59.9 (d, $^1J_{Rh-P}$ 212) ppm.

---

* Methanol expands when frozen, consequently freeze thaw degassing and vacuum transfer was not used.

† Irradiating the signal at 5.03ppm in the proton NMR, and observing the ^{13}C NMR caused no change in the ^{13}C spectrum.

Figure 1. Variable Temperature $^{31}P\{^{1}H\}$ NMR for the Hydrogenation of [Rh(dBpp)(C_7H_8)](BF_4) (2) in CD_3OD

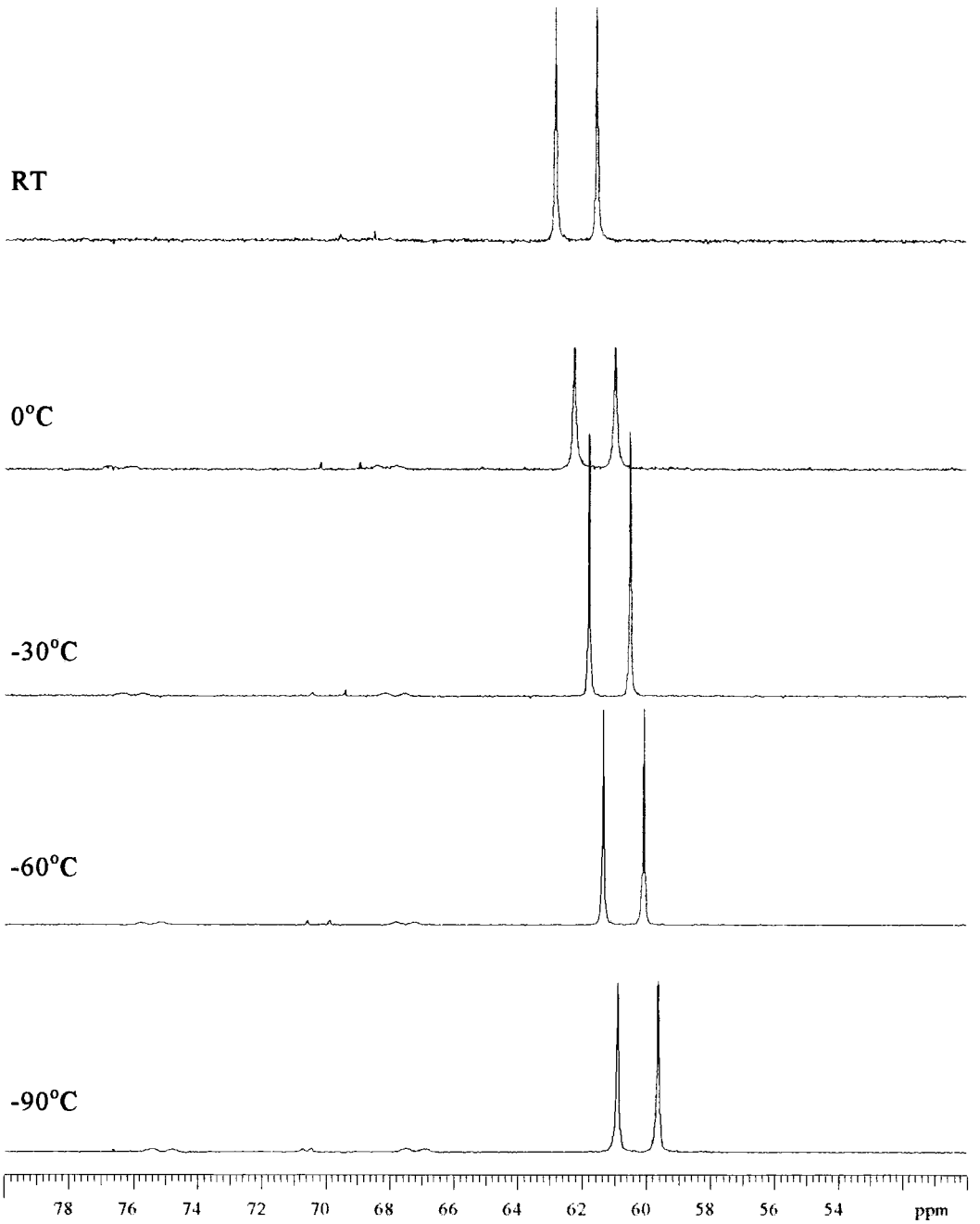

Figure 2. Variable Temperature $^{31}P\{^1H\}$ NMR for the Hydrogenation of [Rh(Boxylyl)(C_7H_8)](BF_4) (3) in CD_3OD

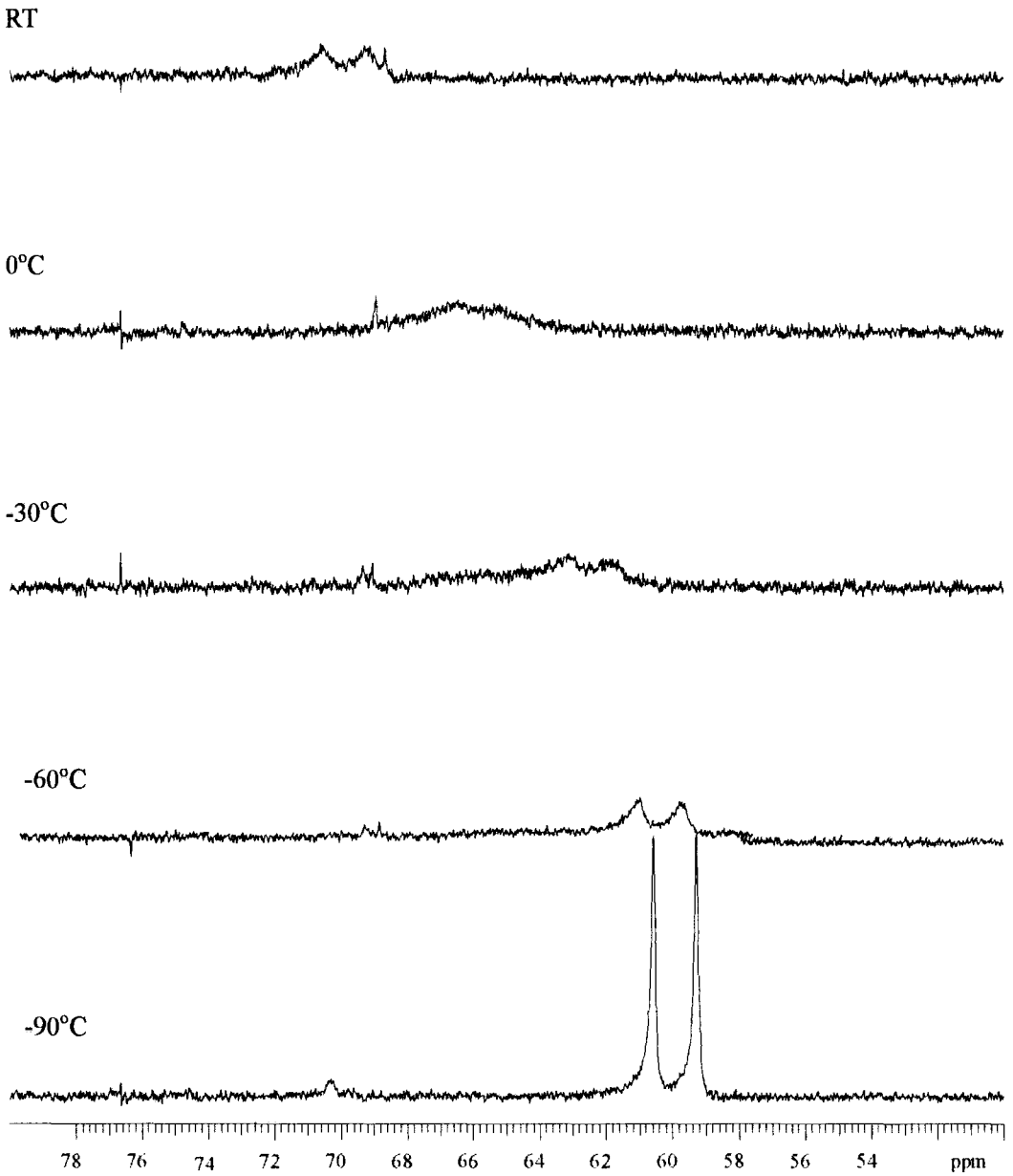

5.2.3. Discussion

The phosphorus NMR spectrum of the product from the reaction of complex **(2)** and hydrogen in methanol contains a single signal with a large rhodium phosphorus coupling constant (207Hz). The magnitude of the coupling constant implies the product is in the +1 oxidation state, and *trans* to a weakly co-ordinating ligand.[8]

Since no hydride signals can be observed it is resonable to formulate the product as the disolvate adduct observed previously in the $^{31}P\{^{1}H\}$ NMR spectra of various aryl substituted chelating phosphines[9] (see Equation 1).

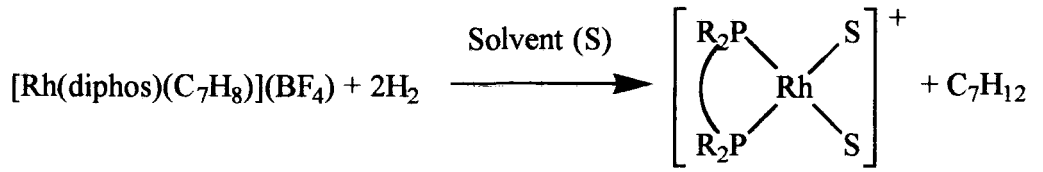

(1) **(4)**

(Equation 1)

In methanol solution, when the chelating phosphine has ferrocene in the backbone, hydrides have been observed as the major species.[10] However, with dBpp no hydrides are observed, although interestingly, there is an enhancement of the $CD_3O\underline{H}$ peak in the proton NMR spectrum. This enhancement could be due to exchange with the hydrogen gas present. This may be facilitated by the rhodium complex present in solution, either directly at the metal, or by protonation of the solvent and an equilibrium could be established in a similar manner to those observed when monophosphine complexes[11] are employed (see Equation 2).

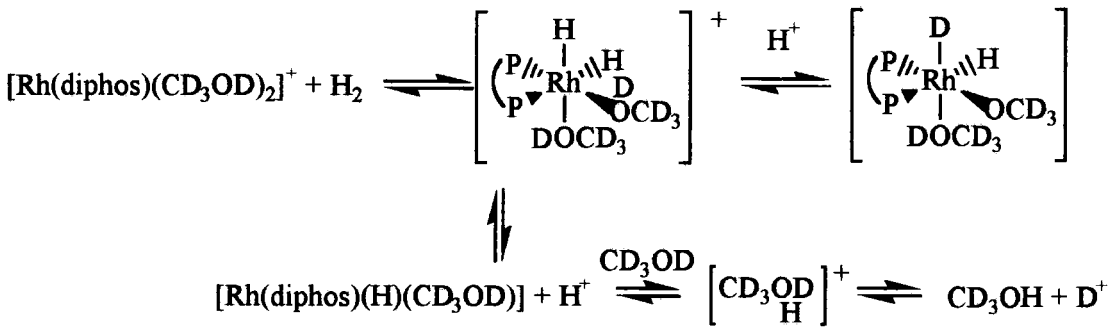

(Equation 2)

Further evidence for the reversible oxidative addition of hydrogen to complexes of the type $[Rh(diphos)S_2]^+$ **(4)** comes from the work of Brown[12] *et al*, who observed equilibration of *para* enriched hydrogen gas in the presence of **(4)** (diphos = diop) even though no hydride species could be observed either in the proton or the phosphorus NMR spectra.

The results for the hydrogenation of complex **(2)** contrast with those for [Rh(Boxylyl)(C_7H_8)](BF_4) **(3)**. After hydrogenation of complexes **(2)** and **(3),** complexes of the type **(4)** are observed. At r.t. $[Rh(dBpp)(CD_3OD)_2]^+$ is pale orange, whilst $[Rh(Boxylyl)(CD_3OD)_2]^+$ is olive green in colour; on cooling $[Rh(Boxylyl)(CD_3OD)_2]^+$ becomes orange-red in colour, and this thermochroism is reversible. At r.t. the phosphorus NMR spectrum of the green solution of complex **(4)** (diphos = Boxylyl) is a broad doublet. However, on cooling, this doublet sharpens as the colour of the solution changes from green to red. This anomolous behaviour can be explained in terms of a square-planar-tetrahedral isomerism. As the temperature is reduced the rate of exchange between the tetrahedral and square-planar isomers is reduced and the square-planar form predominates. A similar equilibrium and colour change is observed for $[Ni(PPh_3)_2Cl_2]$ which is green and tetrahedral at r.t., but on cooling the red square-planar form predominates.[13] The isomerisation of $[Rh(Boxylyl)(CD_3OD)_2]^+$ could be driven by a reduction in strain energy in the tetrahedral form where the ideal angles at the metal (109°) are closer to the large bite angle of the diphosphine Boxylyl. Alternatively the green colour could be due to a charge transfer complex, with the rhodium interacting with the benzene ring in the backbone of the phosphine, producing a consequent shift in the visible spectrum. However, it is unclear why this should be temperature dependent, and only occur at high temperature. Consequently the former reason for the observed phenomenon is more likely.

The behaviour of complexes **(2)** and **(3)** when reacted with hydrogen gas in methanol contrasts with that of [Rh(d*i*ppp)(C_7H_8)](ClO_4)[‡] which forms a hydride, isolated as yellow crystals.[14] The crystal structure corresponds to [{Rh(d*i*ppp)(H)(μ-H)}$_2$(μ-ClO_4)](ClO_4)[15] **(5)**, and the proton NMR data indicate that the structure is retained in solution.[16] In complex **(5)**, one of the perchlorate anions is bridging the two rhodium atoms, causing co-ordinate saturation to occur. Such a bridging group is unlikely to occur for a complex with the significantly less strongly

[‡] d*i*ppp = bis-1,3-(di-*iso*-propylphosphino)propane

co-ordinating anion than ClO_4^-, such as BF_4^- employed in the present studies. The lack of this stabilising bridging ligand may contribute to the lack of hydrides formed from the hydrogenation in methanol of complexes **(2)** and **(3).**

5.3. The Hydrogenation of [Rh(dBpe)(C_7H_8)](BF_4) (6) in d^8-THF

Generally, THF is a more weakily co-ordinating solvent than methanol. When complex **(6)** is hydrogenated in THF, two sets of signals are observed in the phosphorus NMR spectrum (see Figure 3, page 88), both with large $^1J_{Rh-P}$ (215, 213Hz at r.t.). These can be ascribed to mono- and di-solvent adducts, the signal with the larger coupling constant (215Hz) arising from the mono-solvent adduct. However, in the proton NMR spectrum (see Figure 4, Page 89) there are some weak hydride signals. The corresponding signals in the phosphorus NMR are too weak to be observed at r.t.. On cooling, the hydride peaks sharpen and both bridging and terminal hydrides are observed. The signal in the phosphorus NMR spectrum due to the mono-solvent adduct broadens and then sharpens again. Whilst this is occurring, a broad resonance appears in the phosphorus NMR spectrum, and the bridging hydride signals start to appear. This is rationalised in terms of a rapid exchange between the mono-solvent adduct and the hydride containing species at r.t.; as the sample is cooled, the exchange slows down and the resolution of the hydrides is enhanced. The structure of the hydride spectrum is very similar to the temperature variant portion of the spectrum observed in dichloromethane and the exact nature of the hydride species will be discussed below in Section 5.5.

Figure 3. Variable Temperature $^{31}P\{^1H\}$ NMR Study of the Hydrogenation of [Rh(dBpe)(C_7H_8)](BF$_4$) (6) in d^8-THF

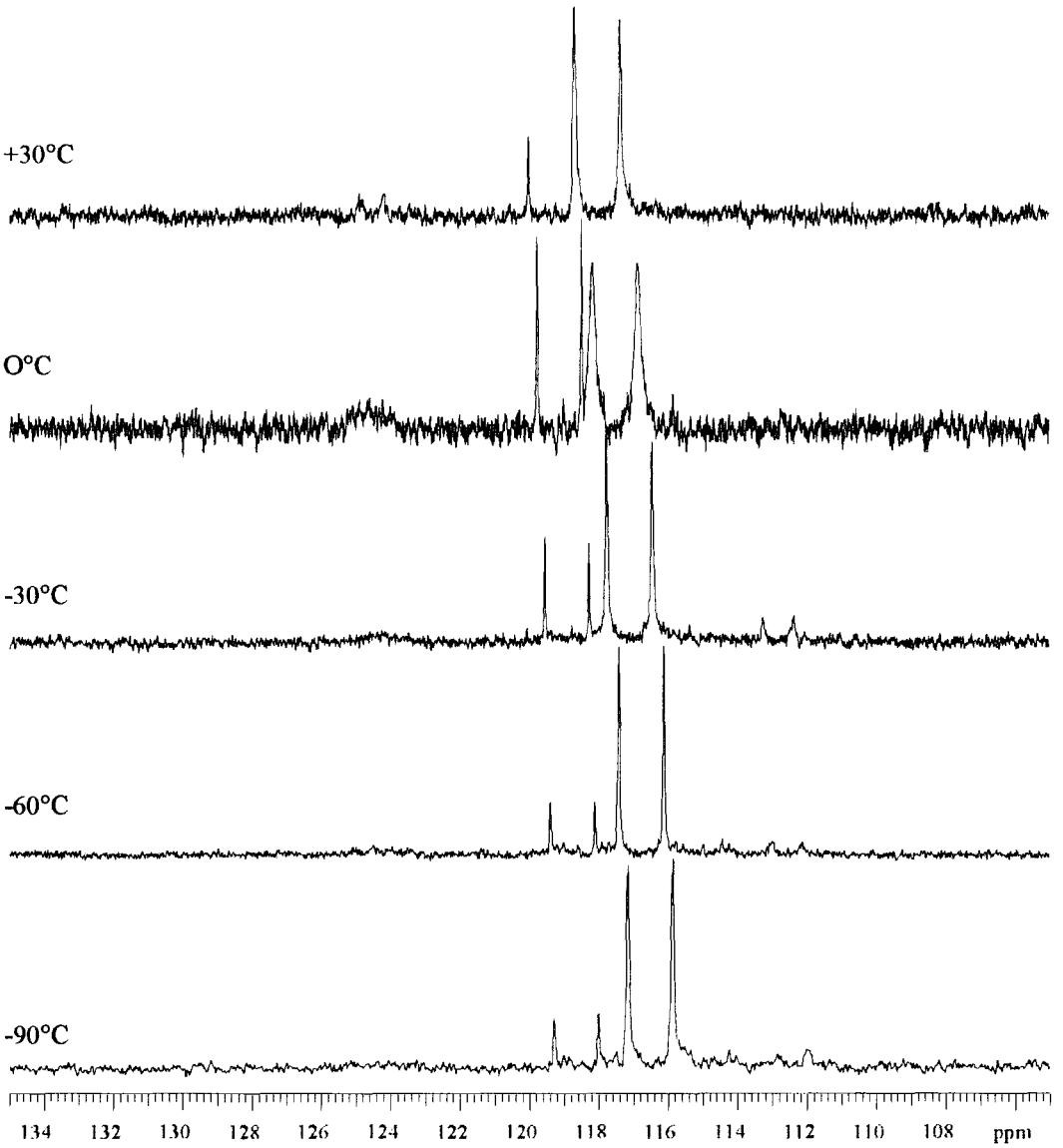

Data: $^{31}P\{^1H\}$ NMR (30°C): δ 119.4 (d, $^1J_{Rh-P}$ 215Hz), 118.0 (d, $^1J_{Rh-P}$ 213Hz); (-90°C) δ 118.6 (d, $^1J_{Rh-P}$ 206Hz), 116.5 (d, $^1J_{Rh-P}$ 210Hz), 112.0 (br s).

Figure 4. Variable temperature ^{1}H NMR Study of the Hydrogenation of [Rh(dBpe)(C_7H_8)](BF_4)(6) in d^8-THF

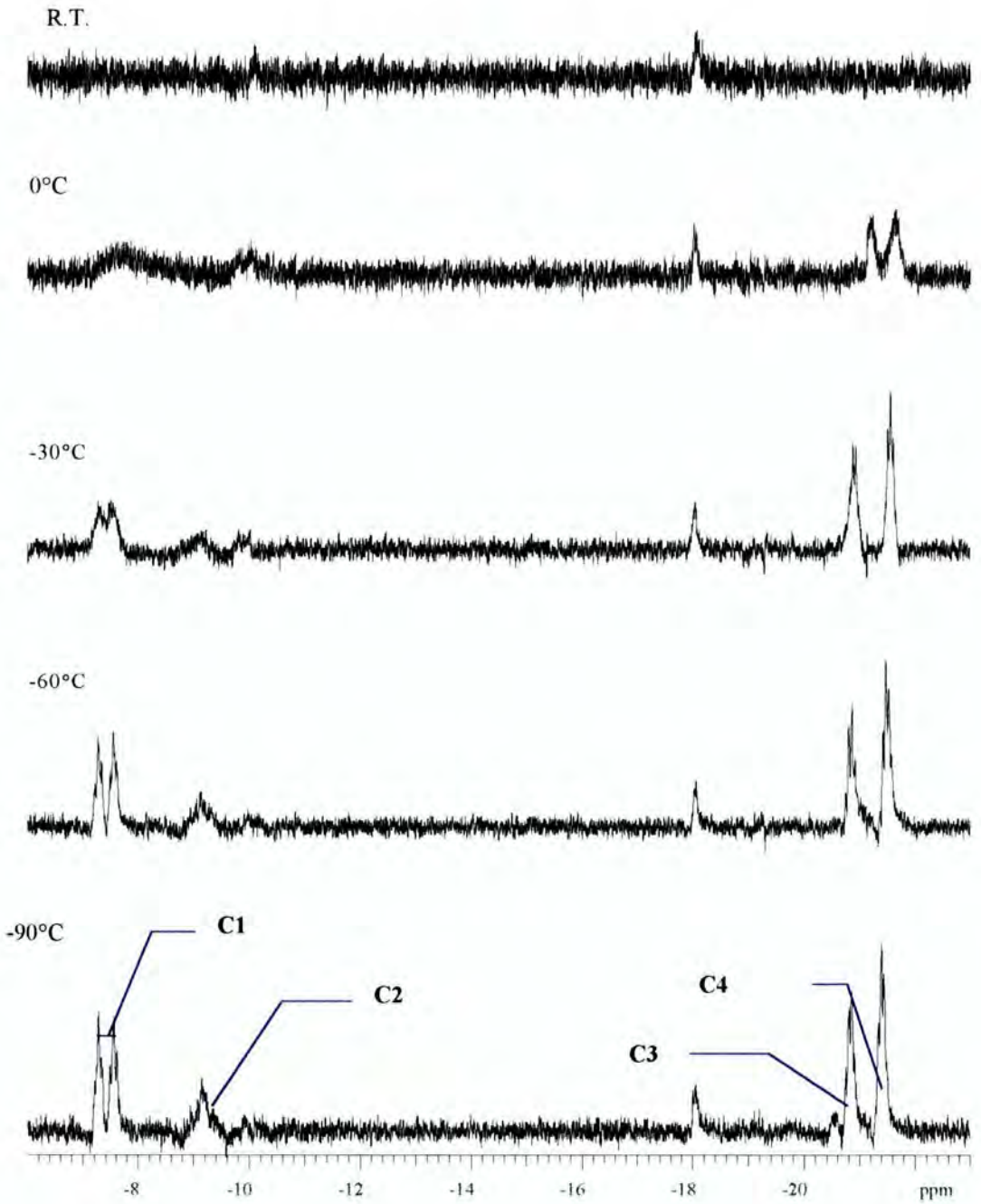

Data: ^{1}H NMR (C_4D_8O) (-90°C): δ -7.40 (dt, J_1 105, J_2 26Hz, **C1**), -9.15 (m, **C2**), -18.0 (br s), -20.80 (pq, **C3**), -21.39 (pq, **C4**).

5.4. The Hydrogenation of [Rh(dcpp)(C_7H_8)](BF_4) (7) in d^3-Nitromethane

The sample of complex **(7)** (~50mg) was placed in a 5mm NMR tube equipped with a teflon tap. This was evacuated and the CD_3NO_2 (~0.5cm^3) transferred in by vacuum-distillation. The solvent was freeze-thaw degassed three times before hydrogen gas (1atm.) was admitted. The tube was shaken and the products allowed to come to equillibrium (24hrs), before the VT $^{31}P\{^1H\}$ and ^1H NMR study began.
After hydrogenation the $^{31}P\{^1H\}$ signals were very weak, and the proton NMR showed only a single broad peak at 0°C. The data are summarised in the Table 1

The only observable signal in the phosphorus NMR spectrum at r.t., is a doublet, X (δ 40.8ppm) with a large Rh-P coupling constant (195Hz) due to the rhodium(I) solvent adduct [Rh(dcpp)(CD_3NO_2)$_2$](BF_4). On cooling to 0°C a hydride signal appears in the proton NMR spectrum and some additional peaks in the phosphorus spectrum (W, Y, Z). The hydride peak is broad and in the terminal hydride region (15 to -30ppm). If there are equilibria present in this system, similar to those observed in THF, the species involved cannot be 'frozen out' in this solvent because of its relatively high freezing point (-20°C). Consequently this made it inappropriate as a solvent for further studies.

Table 1. $^{31}P\{^1H\}$ and ^1H NMR Data for the Hydrogenation of Complex (7) in d^3 -Nitromethane

Peak	RT	δ - ppm (J - Hz) 0°C	-20°C
$^{31}P\{^1H\}$ NMR W		52.1 (br s)	51.2 (br s)
X	40.8 (d, 195)	No Change	No Change
Y		Broad Hump	37.4 (d, 168)
Z		Broad Hump	31.5 (br s)
^1H NMR		-18.44 (br s)	No Change

5.5 The Hydrogenation of Type (1) Complexes in d^2-Dichloromethane

The samples of type **(1)** complexes (diphos = dBpe, dBpp, dcpe, dcpp, dcpcp, Boxylyl) (~50mg) were placed in a 5mm NMR tube equipped with a teflon tap. This was evacuated and the CD_2Cl_2 (~0.5cm^3) transferred in by vacuum distillation. The solvent was freeze-thaw degassed three times before hydrogen gas (1atm.) was admitted. The tube was shaken and the products allowed to come to equilibrium (24 hours), before the variable temperature NMR study began. The VT phosphorus and proton NMR spectra may be found as indicated in Table 2. Full listings of the $^{31}P\{^1H\}$ and ^1H NMR experimental data are given in Appendix 4, and a complete analysis of the spectra may be found on page 104. Details of the hydrogenation experiments for each of the complexes given in Table 2 are discussed below.

Table 2. Locations of Spectra for the Hydrogenation of Type (1) Complexes in CD_2Cl_2

Complex	Phosphorus NMR (Page)	Proton NMR (Page)
[Rh(dBpe)(C_7H_8)](BF_4) **(6)**	Figure 5 (93)	Figure 6 (94)
[Rh(dBpp)(C_7H_8)](BF_4) **(2)**	Figure 7 (96)	Figure 8 (97)
[Rh(dcpe)(C_7H_8)](BF_4) **(8)**	Figure 9 (99)	Figure 10 (100)
[Rh(dcpp)(C_7H_8)](BF_4) **(7)**	Figure 11 (101)	Figure 12 (102)
[Rh(dcpcp)(C_7H_8)](BF_4) **(9)**	Figure 13 (103)	Figure 14 (103)
[Rh(Boxylyl)(C_7H_8)](BF_4) **(3)**	Figure 15 (113)	Figure 16 (114)

5.5.1. The Hydrogenation of [Rh(dBpe)(C_7H_8)](BF_4) (6) in CD_2Cl_2

After hydrogenation both the $^{31}P\{^1H\}$ (see Figure 5) and the proton (see Figure 6) NMR spectra contained a considerable number of signals, and these increased on cooling to -90°C. In order to ascertain which phosphorus signals were coupling to which hydride signals a series of selective phosphorus decoupling experiments was undertaken.

Selective Phosphorus Decoupling Experiments

The phosphorus signals were selectively and systematically decoupled to determine which hydrides were coupling or exchanging with the phosphorus environment under scrutiny. This experiment was performed at both room temperature and at -90°C, the results being summarised in Tables 3 and 4 below. For each hydride signal, X indicates no change was observed on selective irradiation of the phosphorus signal; √ indicates the coupling pattern of the hydride signal changed; ? indicates the coupling pattern may have changed, but this was not certain. Note, that not all of the hydride peaks have been successfully decoupled. This may be due to their broadness at the temperature at which the experiment was performed.

Table 3. Selective Phosphorus Decoupling Experiments at 30°C

^{1}H peaks[§]	A1	A2	B1
^{31}P peaks[§]			
A3	√	√	X
C5	X	X	X
B2	?	X	√
C3,C4	√	√	X
D	X	X	X

Table 4. Selective Phosphorus Decoupling Experiments at -90°C

^{1}H peaks[§]	C1	C2	A1	A2	C3	C4	B1
^{31}P peaks[§]							
C8	X	X	X	X	X	X	X
C9	X	X	X	X	X	?	X
A3	X	X	√	√	X	X	X
C5	√	√	√	X	X	X	X
B2	X	X	X	X	X	X	X
C6	√	√	√	√	X	?	X
C7	√	X	X	X	X	?	X
D	X	X	√	√	X	X	X

[§] See Figures 5 and 6 for the key of the signals used.

Figure 5. Variable Temperature $^{31}P\{^1H\}$ NMR Spectra for the Hydrogenation of [Rh(dBpe)(C_7H_8)](BF_4)

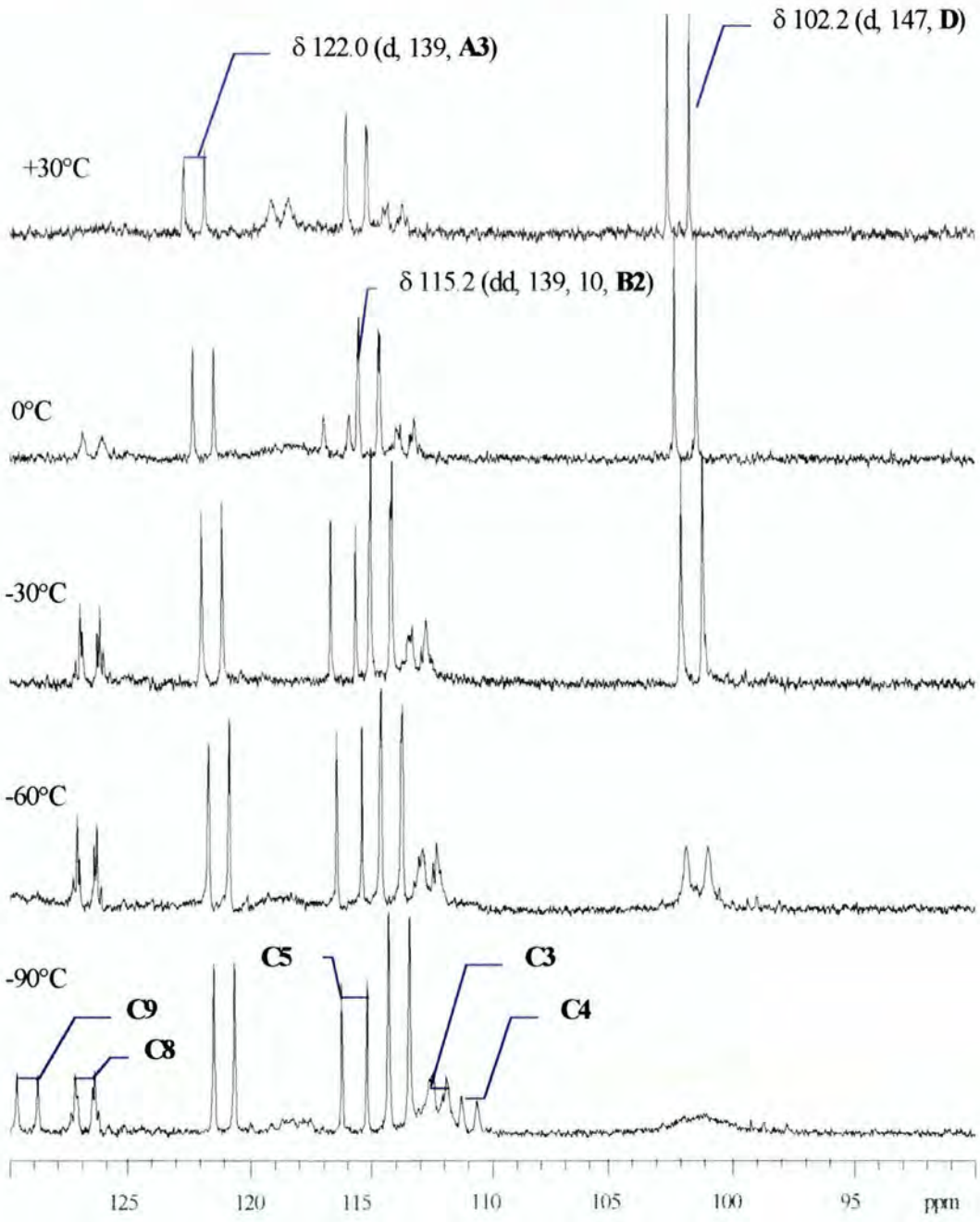

Data: At -90°C: $^{31}P\{^1H\}$ NMR: δ 115.7 (d, J_{Rh-P} 168Hz, **C5**), 112.2 (br d, J_{Rh-P} 84Hz, **C3**), 111.0 (br d, J_{Rh-P} 103Hz, **C4**).

Figure 6. Variable Temperature ^{1}H NMR Spectra for the Hydrogenation of [Rh(dBpe)(C_7H_8)](BF_4) in CD_2Cl_2

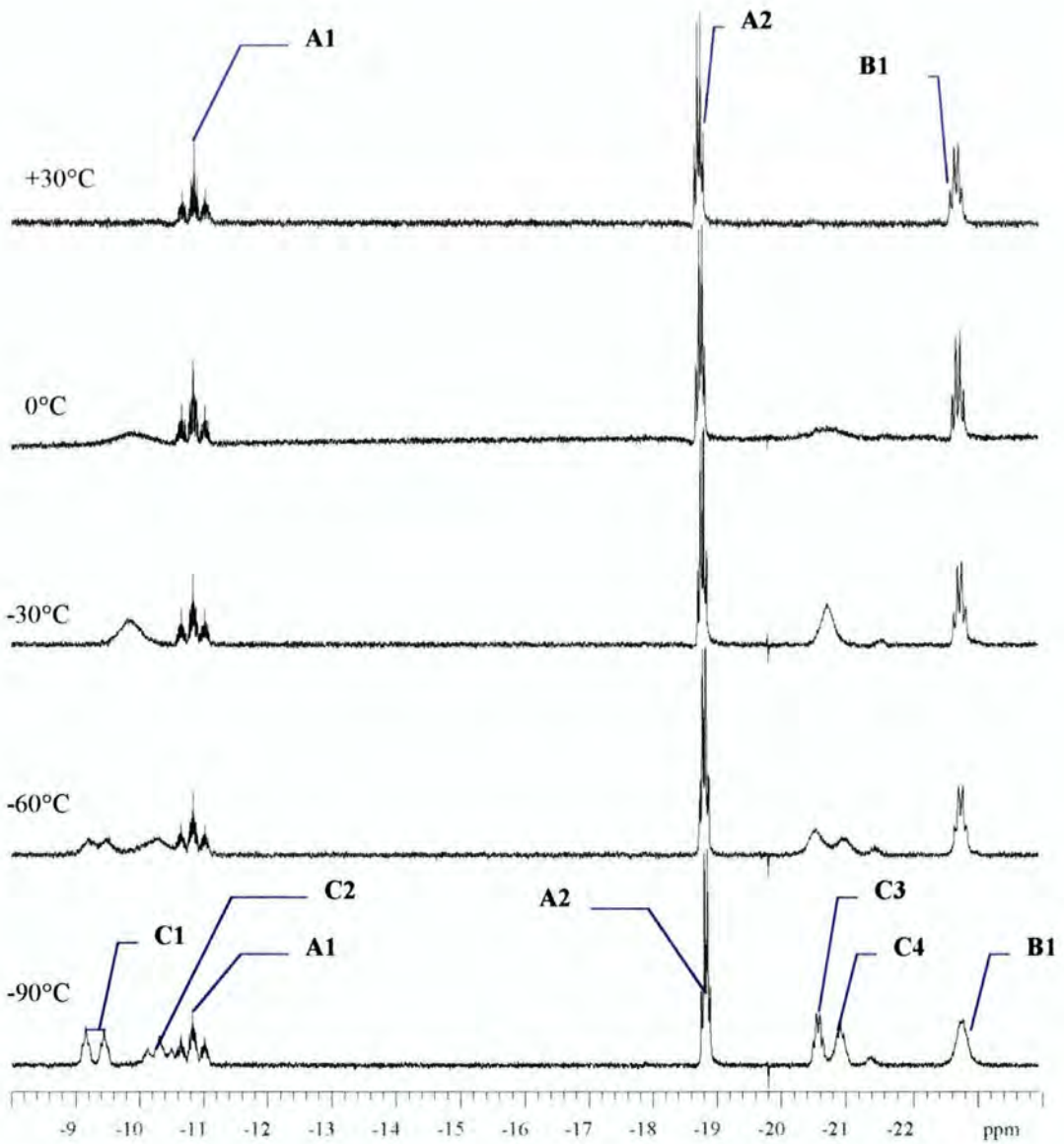

Data: ^{1}H NMR (r.t.): δ -10.85 (tm, $^2J_{P-H}$ 74.4, $^2J_{P-H}$ 7.2Hz, **A1**), -18.71 (dt, $^2J_{P-H}$ 18.8, $^1J_{Rh-H}$ 18.0Hz, **A2**), -22.7 (dt, $^2J_{P-H}$ 25.2, $^1J_{Rh-H}$ 23.6Hz, **A2**); (-90°C): δ -9.30 (br dt, $^2J_{P-H}$ 115Hz, **C2**), -10.30 (br tm, **C2**), -20.57 (br pq, J 22.4Hz, **C3**), -21.40 (br s, **C4**).

5.5.2. The Hydrogenation of [Rh(dBpp)(C_7H_8)](BF_4) (2) in CD_2Cl_2

After hydrogenation of complex **(2)** in CD_2Cl_2, the $^{31}P\{^1H\}$ (see Figure 7) and proton (see Figure 8) spectra are broad. However, on cooling to -90°C, several new signals appear. In a similar manner to experiments described in Section 5.5.1, selective phosphorus decoupling experiments were undertaken to establish the link between the hydride and phosphorus resonances. Irradiation of the phosphorus signals **C6** and **B2** (see Figure 7) affected the coupling of all of the hydride signals. This implies the hydrides were in the same molecules as the phosphorus signals. When the experiment was repeated at an increased concentration, the distribution in signal intensities of **B2**, **C6**, and **C7** changed in favour of **C6** and **C7**, (which remained in a 1:1 stoichiometry), indicating that **B2** was in a different molecule to **C6** and **C7**. A similar effect was observed in the proton spectrum. Resonances **C1**, **C2** and **C3** remained in the same ratio to one another whilst the proportion of **B1** present decreased. Consequently the phosphorus and proton NMR signals can be divided into two groups **C6**, **C7**, **C1-3**, and **B1**, **B2**.

Differentiation between classical and non classical hydrides {[M]-(H_2)} can be achieved by measuring the τ_1 relaxation time of the hydride signals. The τ_1 relaxation times are temperature dependent and were measured for the dBpp system at -90°C using the inversion recovery method. The minimum value of τ_1 is found by recording values of τ_1 at different temperatures. However, due to the similarity of the values obtained, measurements were only recorded at one temperature. A value of τ_1 of 250ms was observed for all of the hydride species in solution. If there was a non-classical hydride present, then a value of τ_1(minimum) of 30ms or less would be expected.[17,18] Consequently the large values of τ_1, together with the magnitude of the Rh-P coupling constants, implies that all of the phosphorus and proton signals arise from Rh(III) complexes (it is unlikely that a complex such as $[Rh(diphos)(H_2)_nS_y]^{3+}$ would form due to the lack of suitable anions present (there is only one BF_4^-, ion present per rhodium, and H^- would not be expected to be stable in a chlorinated solvent).

Figure 7. Variable Temperature $^{31}P\{^1H\}$ NMR Spectra for the Hydrogenation of [Rh(dBpp)(C_7H_8)](BF_4) (2) in CD_2Cl_2

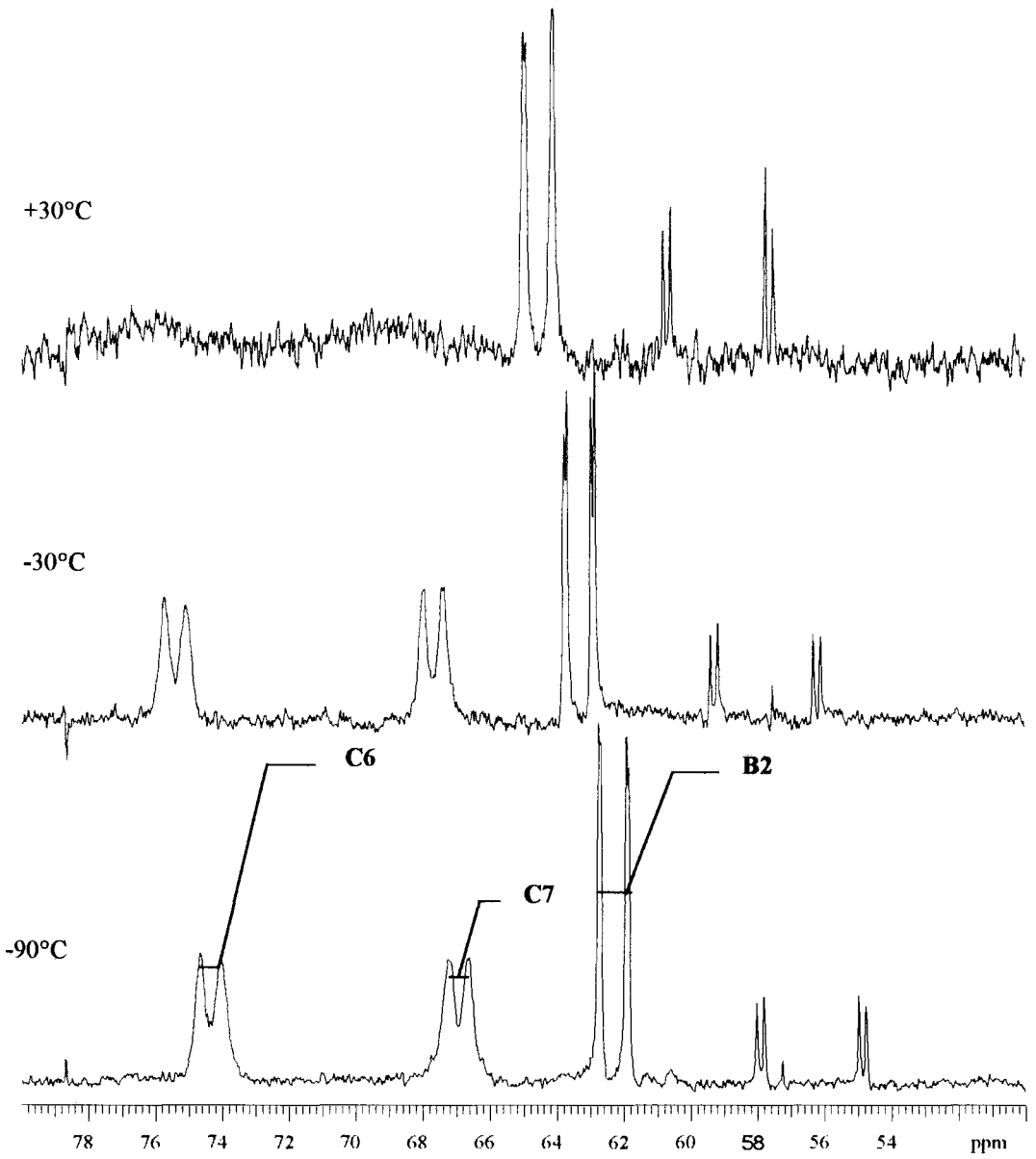

Data: $^{31}P\{^1H\}$ NMR (-90°C): δ 74.4 (**d**, J_{Rh-P} 94Hz, **C6**), 66.9 (**d**, J_{Rh-P} 102Hz, **C7**), 62.3 (**dd**, J_{Rh-P} 134, J_2 12Hz, **B2**).

Figure 8. Variable Temperature ^1H NMR Spectra for the Hydrogenation of $[Rh(dBpp)(C_7H_8)](BF_4)$ (2) in CD_2Cl_2

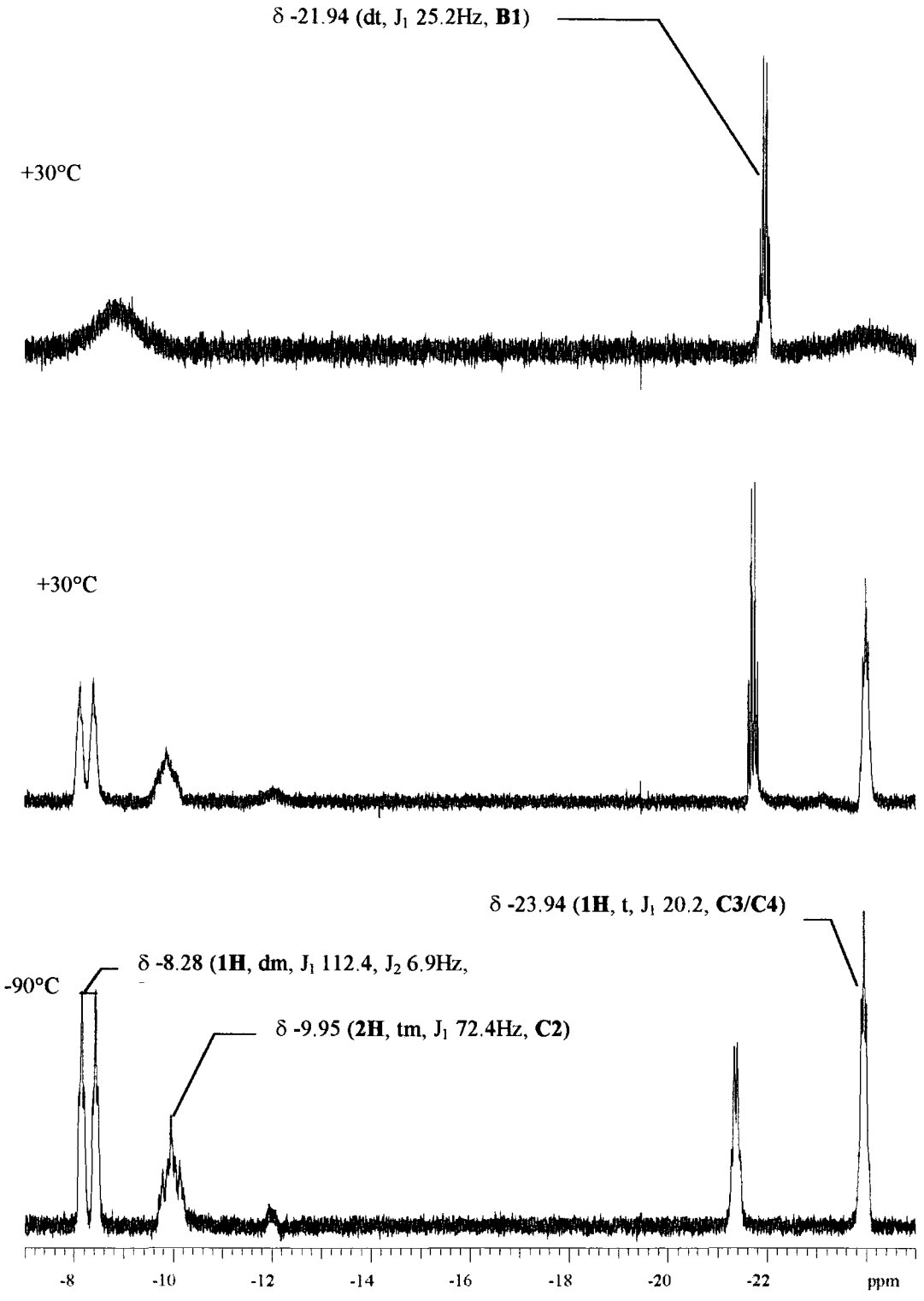

5.5.3. Hydrogenation of [Rh(dcpe)(C_7H_8)](BF_4) (8) in CD_2Cl_2

After the hydrogenation of complex **(8)** in CD_2Cl_2, several species were observed in the $^{31}P\{^1H\}$ (see Figure 9) and the hydride region of the proton (see Figure 10) NMR spectra. These signals broadened on cooling. Selective phosphorus decoupling of peak **A3** and the doublet at 97.0ppm at r.t. reduces the proton bridging signal **A1** to a triplet and the terminal **A2** to a doublet (J_{Rh-P} 20.8 and 22.4 Hz respectively), indicating these phosphorus environments are exchanging on the NMR timescale.

5.5.4 Hydrogenation of [Rh(dcpp)(C_7H_8)](BF_4) (7) in CD_2Cl_2

After hydrogenation of complex **(7)** in CD_2Cl_2 several signals were observed in the $^{31}P\{^1H\}$ (see Figure 11) and ^1H (see Figure 12) spectra. These signals were sharp at r.t.. However, on cooling the signals broadened significantly, indicating the low temperature limit had not yet been reached, and even at -90°C, chemical exchange between the complexes present was still relatively fast.

5.5.5 Hydrogenation of [Rh(dcpcp)(C_7H_8)](BF_4) (9) in CD_2Cl_2

After the hydrogenation of complex **(9)** in CD_2Cl_2, several groups of peaks could be observed in both the proton (see Figure 13) and phosphorus (see Figure 14) NMR spectra. However, both sets of spectra are complicated due to the presence of overlapping unresolved peaks. This is due in part to the chiral nature of the phosphine because diastereomers can be formed. Consequently, only the results obtained at -90°C are reported here (see Tables 5 and 6, page 104).

Figure 9. Variable Temperature $^{31}P\{^{1}H\}$ NMR Spectra for the Hydrogenation of [Rh(dcpe)(C_7H_8)](BF_4) (8) in CD_2Cl_2

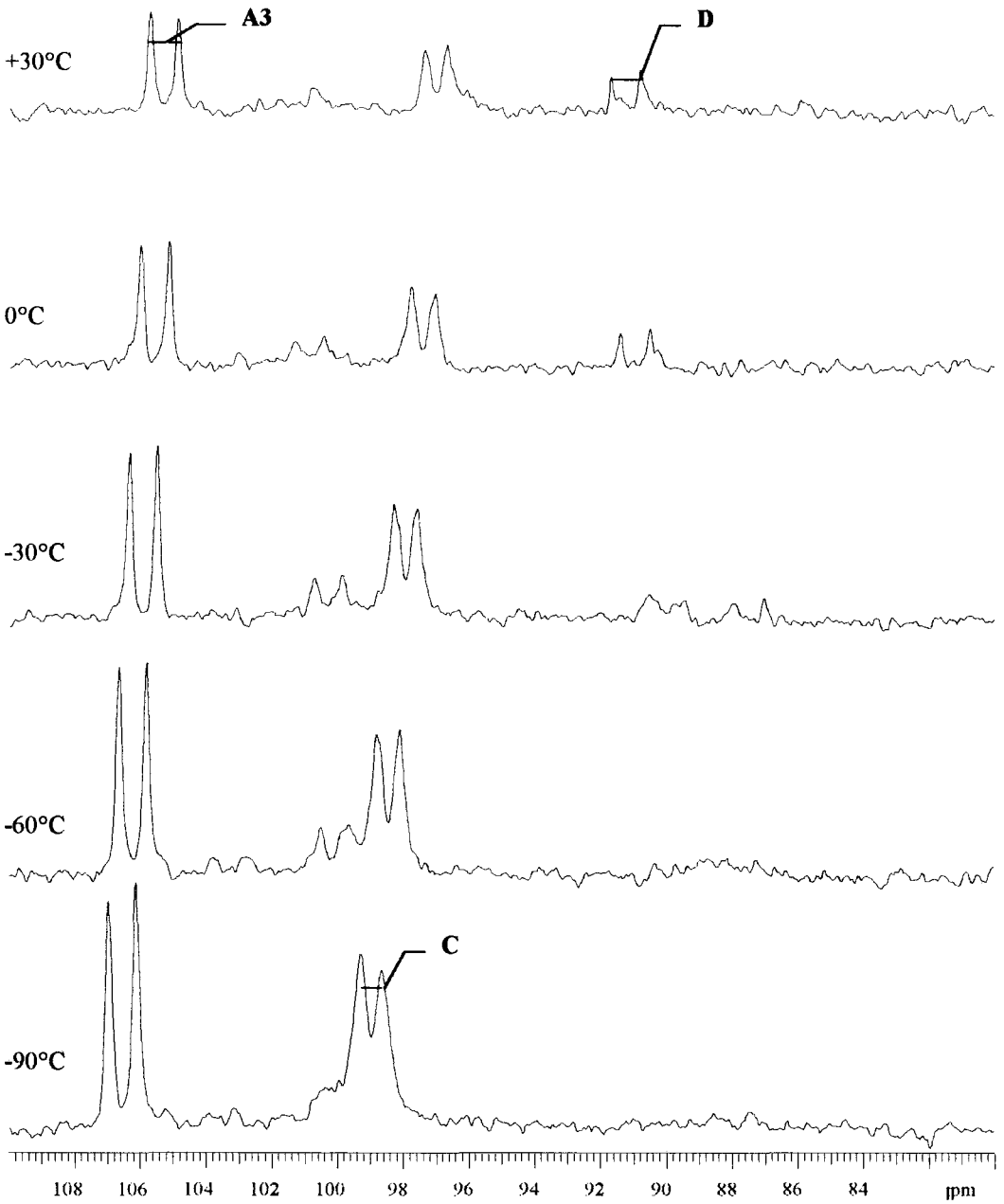

Figure 10. Variable Temperature ^1H NMR Spectra for the Hydrogenation of [Rh(dcpe)(C_7H_8)](BF_4) (8) in CD_2Cl_2

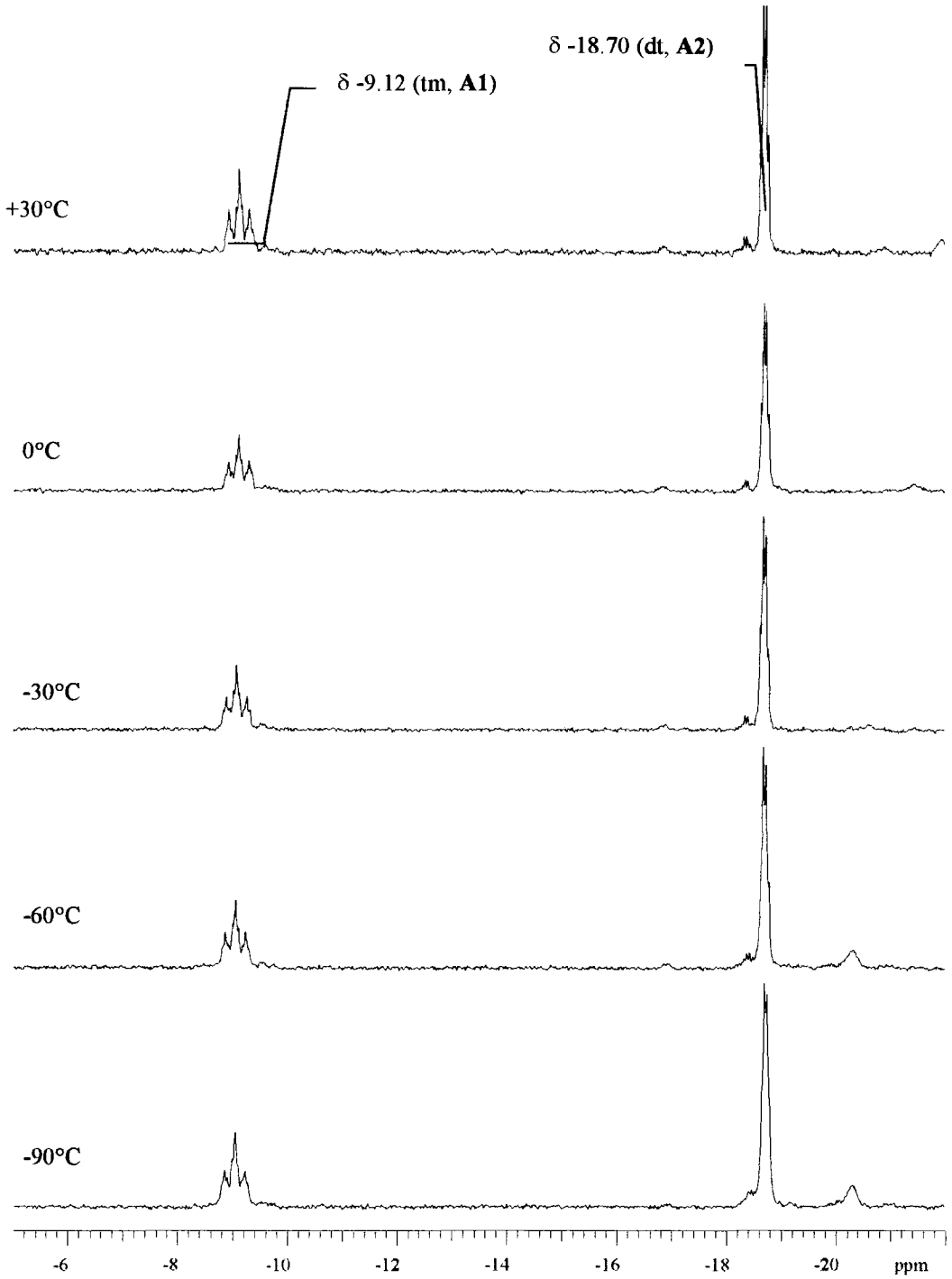

Figure 11. Variable Temperature $^{31}P\{^{1}H\}$ NMR Spectra of the Hydrogenation of [Rh(dcpp)(C_7H_8)](BF$_4$) (7) in CD_2Cl_2

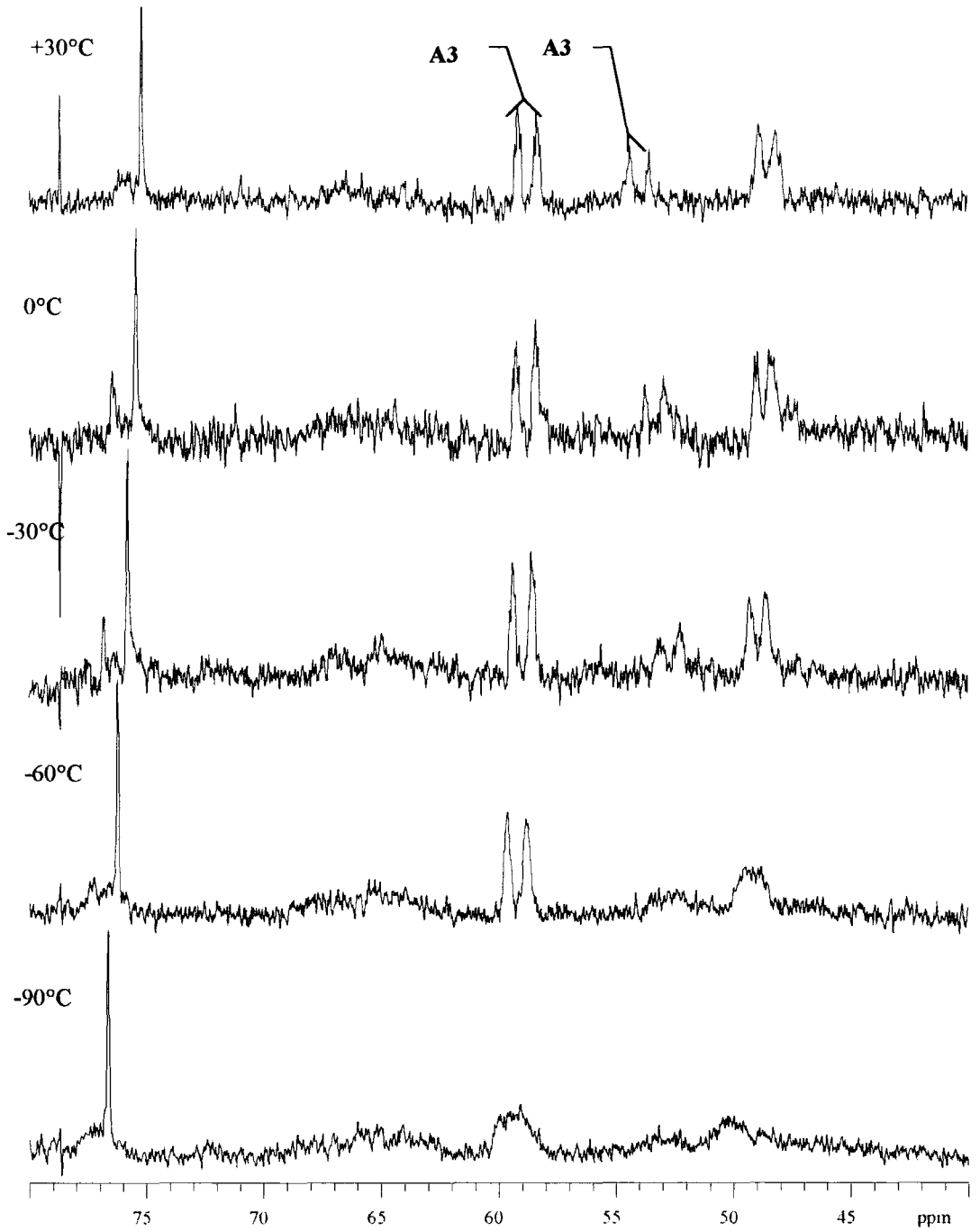

Figure 12. Variable Temperature ^{1}H NMR Spectra for the Hydrogenation of [Rh(dcpp)(C_7H_8)](BF_4) (7) in CD_2Cl_2

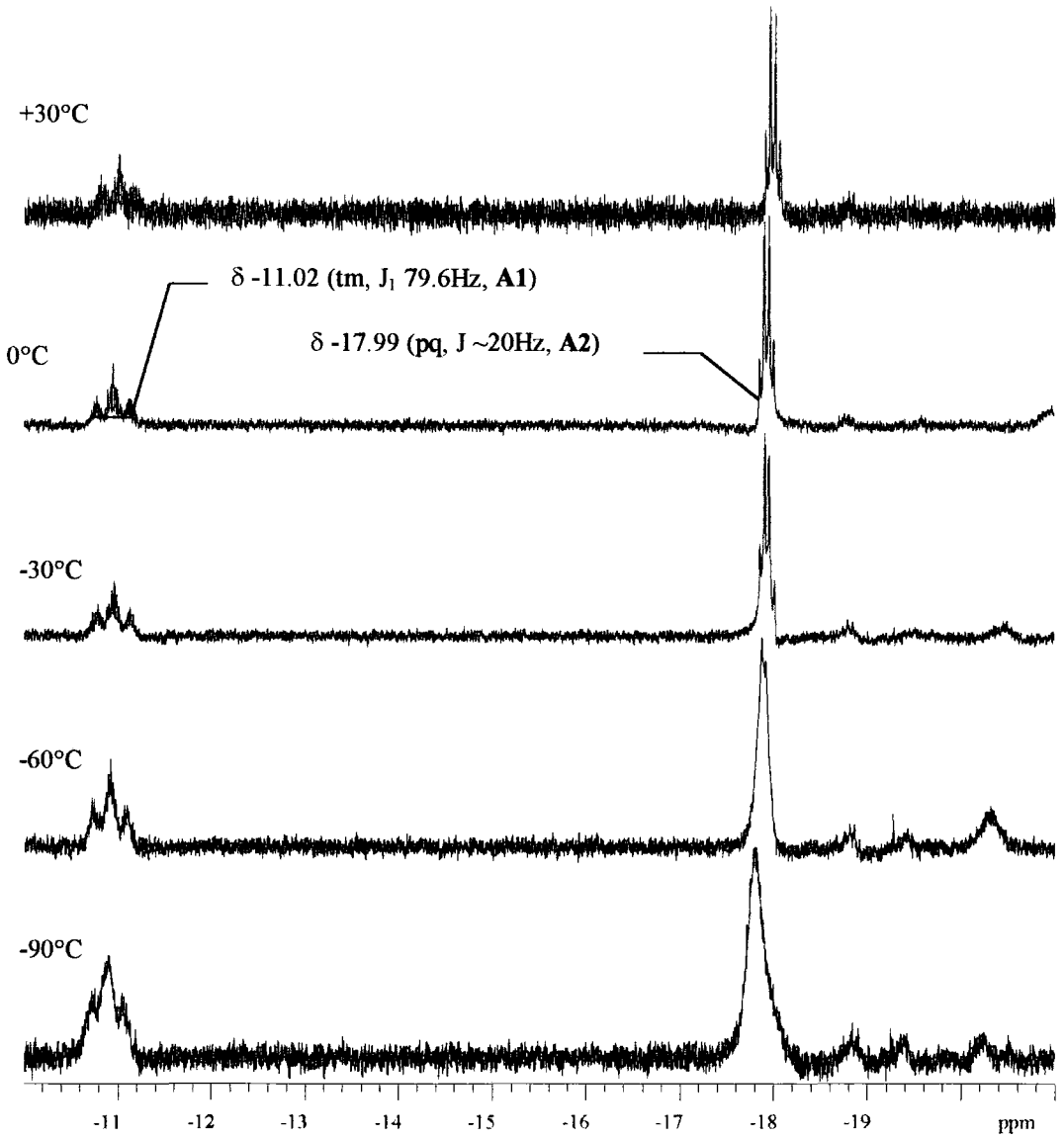

Figure 13. Low Temperature (-90°C) ^{31}P Coupled (Top) and (Bottom) ^{1}H {^{31}P Broad Band Decoupled} NMR Spectra for the Hydrogenation of [Rh(dcpcp)(C_7H_8)](BF_4) (8) in CD_2Cl_2

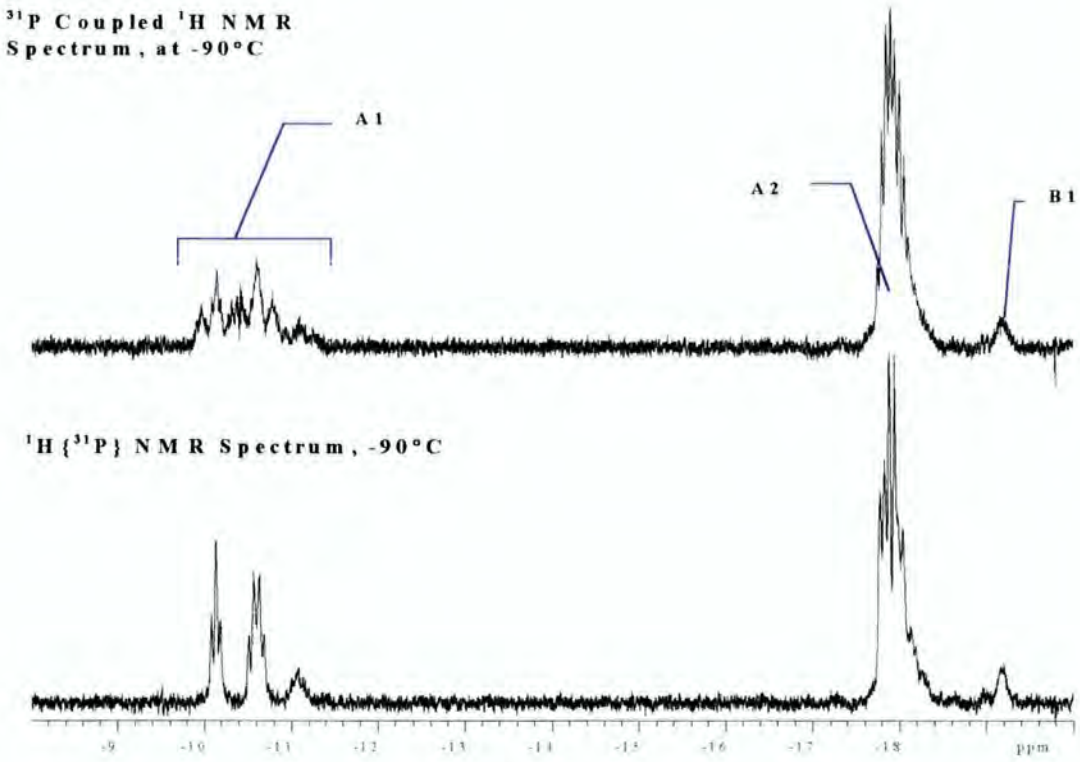

Figure 14. The $^{31}P\{^{1}H\}$ NMR Spectrum for the Hydrogenation of [Rh(dcpcp)(C_7H_8)](BF_4) (9) in CD_2Cl_2 at -90°C

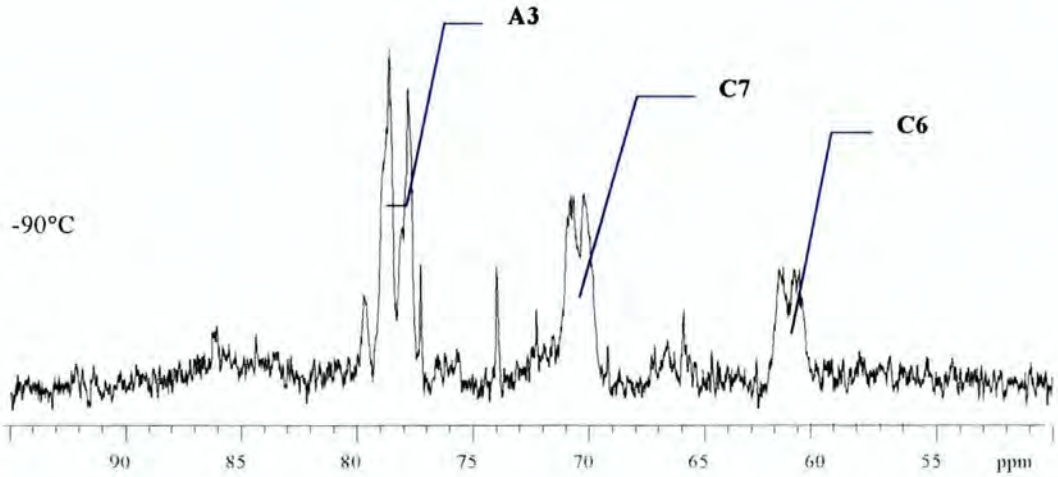

Table 5. Hydride Signals Observed After the Hydrogenation of Complex (9) in CD_2Cl_2, at -90°C.

^{1}H NMR Signal (see Figure 13)	-90°C δ - ppm (J - Hz) ^{31}P Coupled	^{31}P Decoupled
A1	-10.14 (tm, $^2J_{P-H}$ 71.6)	-10.13 (t, 20.2)
A1	-10.60 (tm)	-10.59 (q, 22.5)
A1	-11.04 (tm)	-11.07 (br s)
A2	-17.74-18.10 (m)	-17.80 (d, 21.2)
A2	"	-17.91 (d, 23.2)
A2	"	-18.01 (d, ~20)
A2	"	-18.11 (br s)
B1	-19.19 (br s)	-19.20 (br s)

Table 6. $^{31}P\{^1H\}$ NMR Signals Observed After the Hydrogenation of Complex (9) in CD_2Cl_2, at -90°C.

$^{31}P\{^1H\}$ NMR Signal (see Figure 14)	-90°C δ - ppm (J - Hz)
A3	78.2 (br dm, 133)
C7	70.5 (br dm, 86)
C6	61.4 (br dm, 142)

5.5.6 Discussion of the Hydrides formed from the Hydrogenation of Complexes of Type (1) in CD_2Cl_2

CD_2Cl_2 is a very weakily co-ordinating solvent and this favours the formation of hydrides. Close inspection of the $^{31}P\{^1H\}$ and ^{1}H NMR spectra permits the division of the signals present into three groups due to their coupling patterns, and behaviour with changing temperature.

Set A

- The signals in this group are essentially temperature invariant, although they can broaden on cooling to -90°C.
- These signals are not observed when dbpp or Boxylyl are the chelating phosphines employed.
- In the proton NMR there are two environments **A1** and **A2** (for example see Figure 6) in the ratio 1:2. **A1** is a sharp triplet of multiplets at ~ -11ppm ($^2J_{P-H}$

~75Hz). **A2** is a pseudo quartet (pq), at ~ -18ppm ($^1J_{Rh-H} \sim ^2J_{P-H} \sim 18Hz$). A pseudo quartet is a doublet of triplets where $^1J_{Rh-H} \sim ^2J_{P-H}$. However, since the couplings arise from different nuclei (Rh-H, and P-H) they are slightly different; this manifests itself such that the distance in hertz between the two central peaks is different to that between the central and outer peaks. Broad band phosphorus decoupling experiments reduce **A1** to a triplet, and **A2** to a doublet, due to the residual Rh-H couplings; The proton-proton couplings are not normally resolved. Signal **A1** arises from a hydride bridging two rhodium atoms and 0 to -15ppm is where bridging hydrides are normally found, whilst the hydride that gives rise to signal **A2** is attached to only one rhodium atom (hence a doublet, $I_{Rh} = 1/2$). δ -15 to -30ppm is the region normally associated with terminal hydrides for this type of species. In transition-metal complexes, proton-phosphorus coupling constants are larger if the proton is *trans* rather than *cis* to the phosphorus.[19] The large P-H coupling constant for signal **A1**, and the triplet multiplicity implies the proton is bridging and *trans* to two equivalent phosphorus atoms, whilst the small P-H coupling constant for hydride **A2** implies it is *cis* to two equivalent phosphorus atoms.

- The phosphorus $^{31}P\{^1H\}$ NMR spectra generally show several signals with similar coupling constants quite close to one another. Selective phosphorus decoupling experiments whilst monitoring the proton NMR spectrum provides a method for determining which phosphorus peaks are coupling to which proton peaks. For the signals **A1** and **A2** it appears that two phosphorus signals are coupling. However, only one of these signals, **A3**, like signals **A1** and **A2**, is temperature independent. The apparent coupling of signals **A1** and **A2** to the combined signal **C3** +**C4** is due to chemical exchange occurring slightly slower than that required to cause the signals **A3** and **C3** +**C4** to coalesce.
- In summary, set **A** signals are concerned with one phosphorus, one bridging hydride and one terminal hydride environment. The terminal hydrides are *cis*, and the bridging hydrides are *trans* to the phosphorus atoms.

Set B

- These signals are only observed when dbpp and dbpe are the phosphines employed.
- The signals in this group are usually sharp at r.t. but may broaden on cooling to -90°C.
- There is a single hydride species observed in the proton NMR giving rise to signal **B1**, a pseudoquartet at ~-23ppm (J_1 ~23Hz). This implies the hydride is *cis* to two phosphorus atoms and attached to a single rhodium atom.
- Selective decoupling experiments reveal a single phosphorus signal **B2** ($^1J_{Rh\text{-}P}$ ~ 140Hz) coupling to the hydride signal **B1**.
- The phosphorus signal sharpens into a doublet of doublets on cooling ($^1J_{Rh\text{-}P}$ 139Hz, J_2 ~10Hz). The origin of this second coupling is unclear, since it is not reciprocated in any phosphorus signal in the phosphorus NMR spectrum. The only other spin 1/2 nuclei present are Rh, H, and F in the BF_4^- counterion. The protons are broad band decoupled, which leaves F and Rh. Either the vacant co-ordination positions are being filled by weak co-ordination of a supposedly non co-ordinating counterion, or the species are dimerising *via* metal-metal bonds, essentially forming electron deficient clusters.
- In summary, set **B** signals arise from one terminal hydride and one phosphorus environment. The hydride ligands are located *cis* to the diphosphine ligand.

Set C

- These are observed for dcpcp, dbpp, dbpe in CD_2Cl_2, and dbpe in d^8-THF.
- At r.t. these signals are broad and often cannot be observed. As the sample is cooled, both the phosphorus and hydride spectra sharpen. Initially the hydride signals appear as broad singlets, one in the bridging , and one in the terminal hydride regions. However, on cooling to -90°C these split into two bridging environments **C1** and **C2**, and two signals in the terminal region **C3** and **C4**.
- Signal **C1** is a broad doublet of triplets at δ ~ -9 ($^2J_{P\text{-}H}$ ~ 114Hz) ppm indicating that this bridging hydride environment is *trans* to a single phosphorus atom.
- Signal **C2** is a broad triplet of multiplets δ ~ -10 ($^2J_{P\text{-}H}$~ 73Hz) ppm indicating this bridging hydride environment is *trans* to two similar phosphorus atoms.

- **C3** and **C4** are not resolved for the dBpp species even at -90°C. However, for dBpe in both dichloromethane and THF these signals are resolved into two pseudo quartets at $\delta \sim -21$ppm.
- Selective phosphorus decoupling experiments on the dBpe system indicate the broad phosphorus signal that appeared to be coupled with signals **A1** and **A2** at r.t. is coupling to signals **C1** and **C2**, the resolution is not sufficient to tell which phosphorus signals are coupling to **C3** and **C4**. In fact three phosphorus resonances **C5** ($^1J_{Rh\text{-}P}$ 168Hz), **C6** ($^1J_{Rh\text{-}P}$ 84Hz), and **C7** ($^1J_{Rh\text{-}P}$ 103Hz) appear to be coupling to **C1** and **C2**. All three of these resonances display a similar temperature dependence to the hydride resonances **C1-4**.
- The behaviour of dBpp is similar to that of dBpe, but due to the greater flexibility of the six membered chelate ring the signals are much broader at the low temperature limit. Additionally there are only two resonances in the phosphorus NMR **C6** ($^1J_{Rh\text{-}P}$ 84Hz), and **C7** ($^1J_{Rh\text{-}P}$ 102Hz).
- The integrals of both the phosphorus and hydride signals indicates that several species are present. The ratio of **C1**:**C2**:**C3**:**C4** is 1:1:1:1 for dBpe; **C1**:**C2**:**C3**+**C4** is 2:1:1 for dBpp.
- **C8** and **C9** are only present for dBpe, and these appear as the sample is cooled.
- At -90°C **C8** ($^1J_{Rh\text{-}P}$ 139Hz) is a simple doublet whilst **C9** is a complex doublet of multiplets ($^1J_{Rh\text{-}P}$ 132Hz).
- From selective decoupling experiments, it appears neither **C8** or **C9** appear to be coupling to the bridging hydrides, and due to the broad signals it is not possible to determine whether or not they are coupling to the terminal ones.
- In summary set **C** consists of at least two different rhodium species in rapid equilibrium. On cooling to -90°C, four proton and five phosphorus environments are resolved.

Set D

- This comprises of a single resonance in the phosphorus NMR spectrum (d, $^{1}J_{Rh-P}$ ~145Hz).
- The signal is only observed for the dcpe and dBpe systems.
- At room temperature the signal is sharp. However, on cooling the signal broadens into a broad singlet.
- from selective decoupling experiments **D** does not appear to be coupling to any observed hydride at r.t.. At -90°C, signal **D** is a broad singlet. For the dBpe system, selectively decoupling the broad signal **D**, appears to affect the coupling patterns of the hydride signals **A1** and **A2**.
- In summary, set **D** consists of a single rhodium species with equivalent phosphorus environments. This species is very fluxional and may be in equilibrium with the hydride species observed, although, it does not contain any hydride ligands.

Clearly there are several species present in solution, all of which are in equilibrium.

The $^{1}J_{Rh-P}$ values for signals **B2** suggest the rhodium is in the +3 oxidation state, whilst the NMR data suggest there is at least one hydride ligand attached which is *cis* to both phosphorus atoms. If we consider Equation 1 (page 85) again this could reasonably be assigned to the rhodium(III) cationic dihydride complexes of the type $[Rh(diphos)(H)_2(Solvent)_2]^+$ **(10)**. The hydride ligands appear to sit above and below the rhodium phosphine plane. This is because this isomer is likely to be the most stable with respect to reductive elimination of hydrogen gas. However, this model does not adequately explain the second smaller coupling constant observed for signal **B2**. As mentioned above this could be due to the dimerisation of the molecule, and the formation of a metal-metal bond, through which coupling can occur, either to the other rhodium atom, or to the phosphorus atoms on the other side of the dimer . Two and three bond couplings have been observed previously in rhodium dimers, for example $[\{Rh(dippe)\}_2(\mu\text{-}OPh)(\mu\text{-}H)]$[20] .

The $^{1}J_{Rh\text{-}P}$ values for signal **A3** suggest the rhodium is again in the +3 oxidation state. Since we have bridging hydrides the complex must be at least dimeric, and the 1:2 ratio of bridging to terminal hydrides, together with the high degree of symmetry required by the hydride and by the phosphorus resonances, leads to the conclusion that a co-ordinatively saturated dimeric species of the type **(11)** is present in solution. Such a structure is consistent with all of the data obtained.

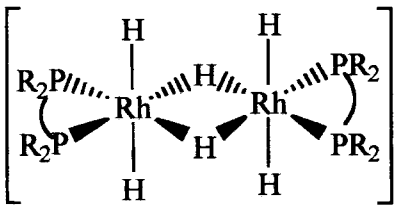

(11)

For the dcpcp system, the situation is more complex due to the formation of diastereotopic pairs. This is due to the chirality in the backbone of the phosphine. This phenomenon leads to the presence of several superimposed sets of signals in the NMR spectra. Broad band ^{31}P decoupled ^{1}H NMR spectra reveals the presence of a quartet in the bridging hydride region. This is probably due to the formation of a co-ordinatively saturated trimeric species similar to **(11)**, such as $[\{Rh(dcpcp)H_2\}_3(\mu_3\text{-}H)_2](BF_4)$ with facially bridging hydride ligands. The reason for the existence of this molecule, must be due to the steric restraints imposed on the molecule by the backbone of the phosphine since it is not observed for the related dcpe system.

At room temperature the hydride signals due to complexes of the type **(11)** (**A1**, **A2**) are affected by the selective decoupling of the broad phosphorus signals in set **C**. This leads to the conclusion that the transformation of type **(11)** complexes into the complexes responsible for the set of signals **C** is chemically straightforward. The fluxionality observed in the set of signals **C** is due to a degree of co-ordinative unsaturation in the molecule. The simplest way to achieve co-ordinative unsaturation is to lose dihydrogen from complex **(11)**. Since the solvent is such a poor ligand the molecule then rearranges to fill the vacant coordination positions. The most efficient method to do this, is to increase the number of bridging hydrides and decrease the

number of terminal hydrides. This is exactly what happens and this is reflected in the decrease in the bridging:terminal ratio from 1:2 to 1:1 or lower, with the formation of dimers of the type $[Rh_2(diphos)_2(H)_4]$ **(12)**. Fryzuk[21] observed previously that the size of the chelate ring played an important part in determining the conformation of complexes of the type **(12)**. For the *d*ippe and *d*ippp derivatives this was ascribed to the restriction of the bite angle imposed on the system when a five membered chelate ring was present. For the dBpp system the ratio of bridging to terminal hydrides (**C1+C2**:**C3+C4**) was not an integer value, at 3:1.75. This behaviour can be explained in terms of an approximately 1:1 ratio of complexes of the types **(12)** and $[Rh_2diphos)_2H_5]^+$ **(13)**.

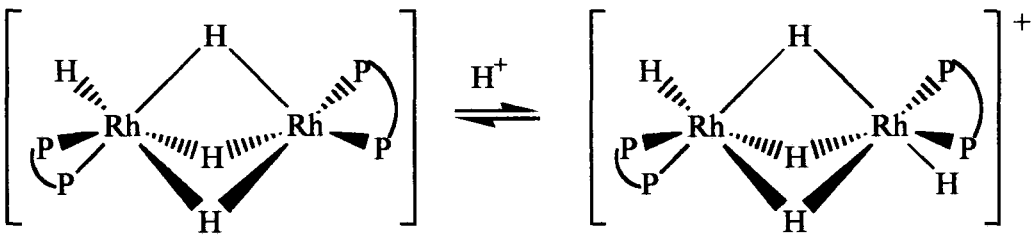

(12) **(13)**

Cationic penta-hydride complexes of the type **(13)** have been previously observed for Ir[22] and Rh[23] systems with mono-phosphine ligands, and characterised by X-ray crystallography for the chelating phosphine, dBpf.[24] Although, in solution complex **(13)** (diphos = dBpf) completely dissociates into complex **(12)** (diphos = dBpf). Type **(13)** complexes are isostructural with the novel complexes of the type $[Rh_2(diphos)_2(\mu\text{-}Cl)_3Cl_2]^+$ (diphos = dppe, dppp, dcpe) synthesised in this work by a variety of methods (see chapters 7,8 and 9). Even at -90°C the exchange of the phosphorus and proton environments in types **(12)** and **(13)** complexes is still quite rapid, and two broad doublets are observed in the phosphorus NMR, signals **C6** and **C7**. Each of these corresponds to one of either the type **(12)** or type **(13)** complexes. However, the hydride signals for complexes of the types **(12)** and **(13)** are superimposed, consequently only one set of resonances is observed.

The situation for dBpe is more complicated than for dBpp. The proton NMR spectra of the dBpe system are remarkably similar to those of the dBpp system. However,

there are significantly more signals present in the phosphorus NMR spectrum of the dBpe system, namely **C5-C9**, due to the conformational restrictions imposed by the phosphine. Several other isomers of complex **(12)** (diphos = dBpe) are present, and the ratio of the complexes **(12)**:**(13)** has also changed. Selective phosphorus decoupling experiments indicate that signals **C5**, **C6**, and **C7** are all coupled to the bridging hydrides. Signal **C5** arises from a Rh(I) species, and decoupling experiments indicate it is only coupling to the hydride environment *trans* to two phosphines **(C2)**. To account for this and the increased proportion of terminal hydrides present, other isomers of complex **(12)** (diphos = dBpe) must be present. For example, complexes of the type $[Rh_2(diphos)_2(\mu\text{-}H)_2H_2]$ **(14)**.

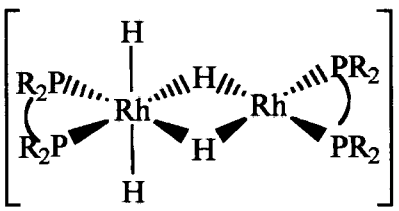

(14)

The signals **D**, **C8** and **C9** cannot be assigned to a particular structure in the dBpe system for two reasons; firstly even at -90°C all of the inter- and intra-molecular exchange has not been frozen out. Secondly, the information available from selective phosphorus decoupling experiments is limited by the broadness of the signals when the decoupling experiment occurs which obscures the coupling pattern. Consequently it is impossible to ascertain whether signals **D**, **C8** and **C9** are coupling to any terminal hydrides. However, it does seem resonable from the magnitude of $^1J_{Rh\text{-}P}$ (135-147Hz), that these three signals all correspond to phosphorus bound to rhodium in the +3 oxidation state.

It is interesting to note that the NMR signals for a given hydride species having cyclohexyl groups instead of *tert*-butyl groups on the phosphorus are much broader at any given temperature. This could be due to the relatively smaller steric bulk of the cyclohexyl phosphines which leads to a smaller activation energy for site exchange.

5.5.7. The Exception. The Hydrogenation of Complex (3) in CD_2Cl_2

The products from the reaction of [Rh(Boxylyl)(C_7H_8)](BF_4) **(3)** with hydrogen in CD_2Cl_2 have not been discussed so far, due to its apparently anomalous behaviour. When this complex is hydrogenated it forms olive green solutions (see Figures 15, page 113 and 16, page 114 for the variable temperature $^{31}P\{^1H\}$ and ^1H NMR spectra respectively) and these are of a similar hue to those observed in deuteromethanol. Hydrides are observed in CD_2Cl_2 but not in CD_3OD. When complex **(3)** is exposed to hydrogen gas in the solid state, the colour also changes from deep red to green, but the nature of the product has not been investigated.

The major signal at r.t. in the phosphorus NMR spectrum is a doublet at δ 73.6 ppm (d, $^1J_{Rh\text{-}P}$ 229Hz) **E1**. In the proton NMR only one signal, a broad singlet **E2**, is visible at r.t. in the terminal region, and this is temperature invariant. The poor resolution of the hydride signals does not permit selective phosphorus decoupling experiments, consequently we can only assume that signals **E1** and **E2** are from related structures from their similar behaviour with changing temperature. The magnitude of $^1J_{Rh\text{-}P}$ is indicative of Rh(I), whilst the lack of resolution in the proton NMR, even at -90°C implies exchange between possible hydride sites is very rapid and complex **(15)** is a reasonable formulation for the 'average' signal observed under experimental conditions at r.t.

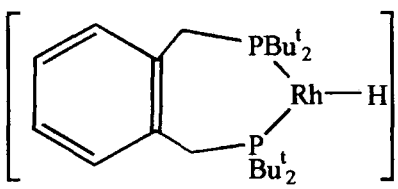

(15)

The monomeric complex **(15)** would be stabilised by the large steric bulk of the *tert*-butyl groups on the phosphine, which are pushed around the sides of the metal by the large bite angle of this relatively rigid phosphine.

Figure 15. Variable Temperature $^{31}P\{^{1}H\}$ NMR Spectra for the Hydrogenation of [Rh(Boxylyl)(C_7H_8)](BF_4) (3) in CD_2Cl_2

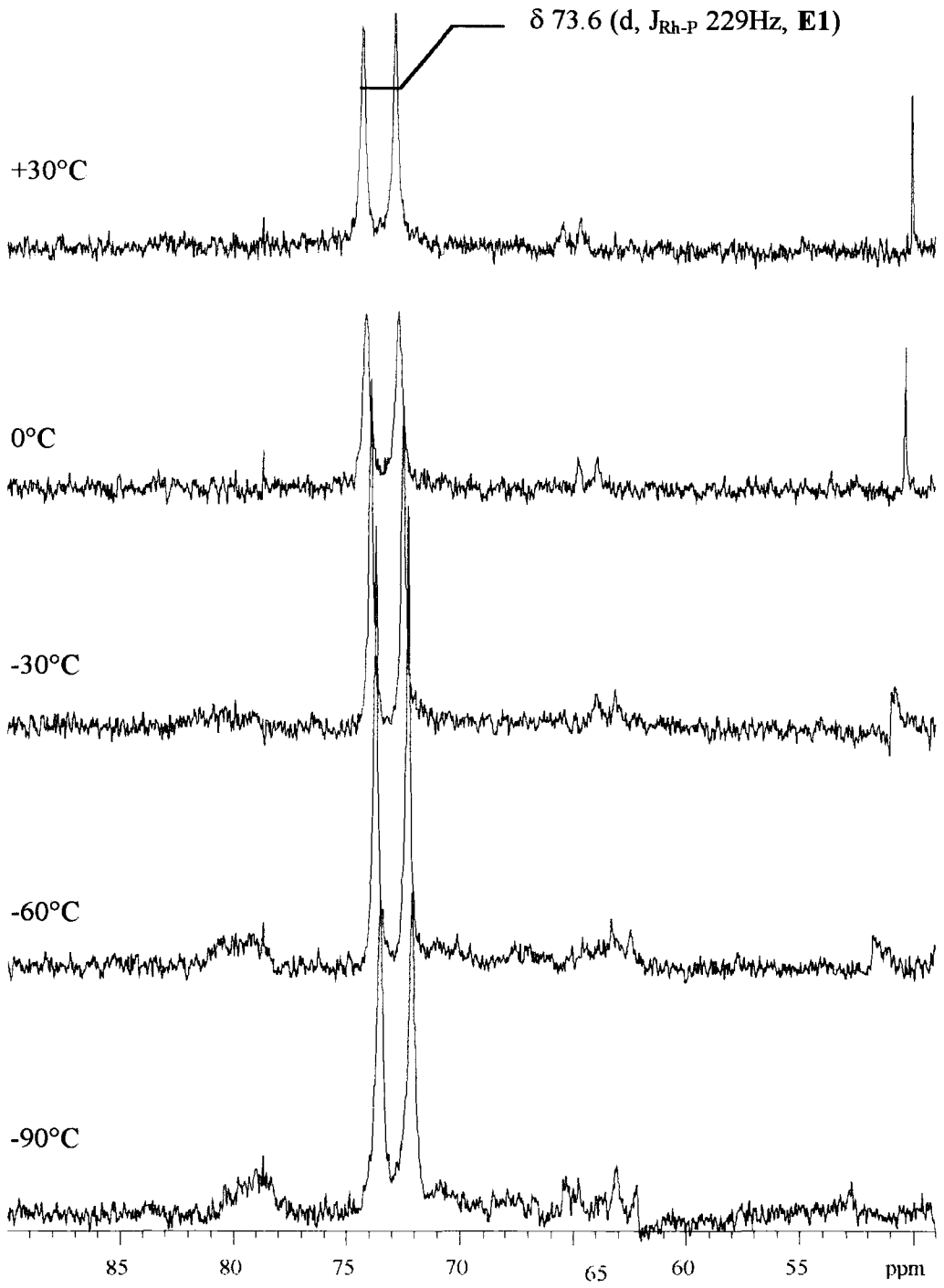

Figure 16. Variable Temperature ^1H NMR Spectra for the Hydrogenation of [Rh(Boxylyl)(C_7H_8)](BF_4) (3) in CD_2Cl_2

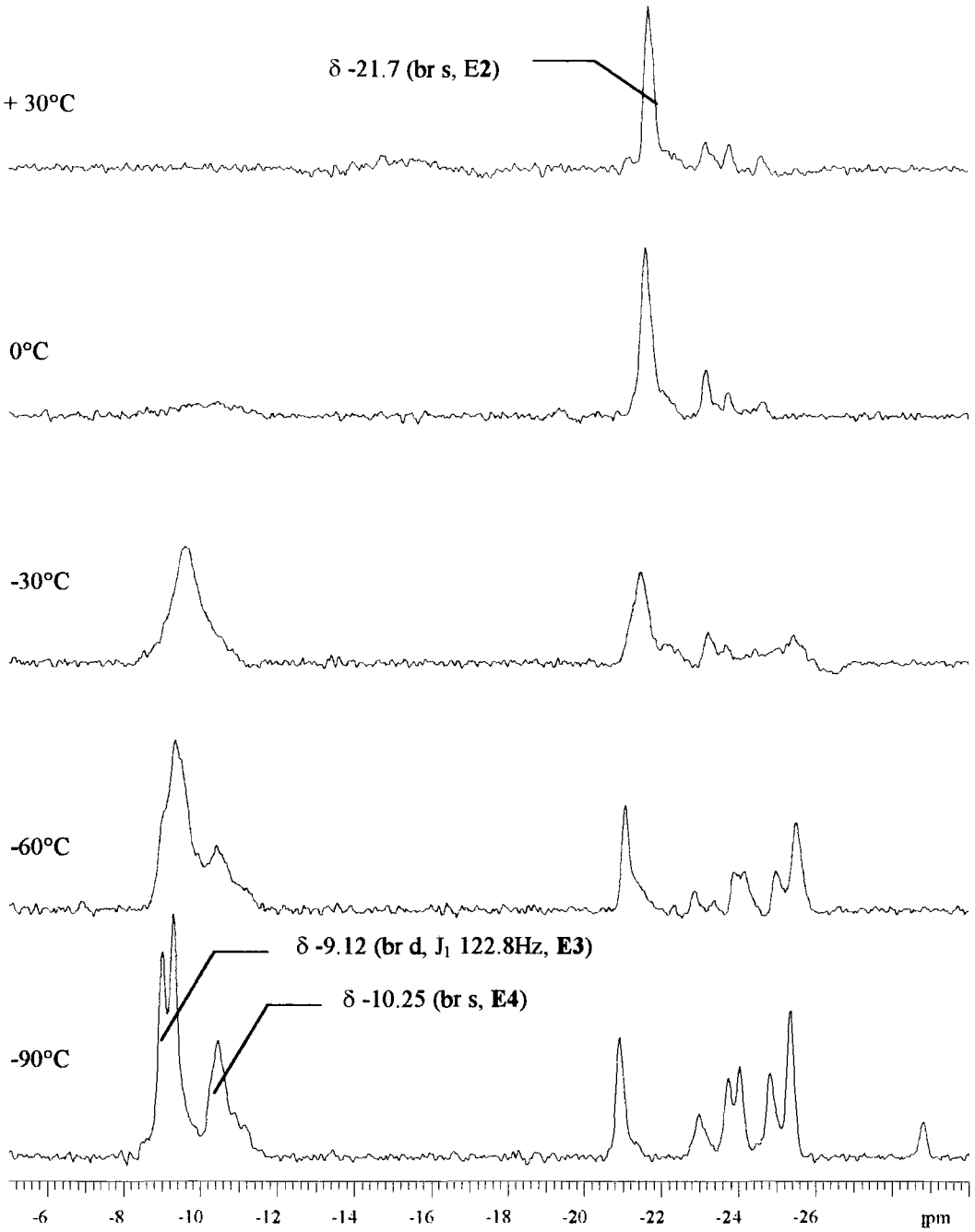

Rh(I) hydride bridged dimers $[Rh(diphos)H]_2$ **(16)** (diphos = $R_2P(CH_2)_{2\text{ or }3}PR_2$, R = *i*Pr or OR') have been observed by Fryzuk *et al.*[25] from the hydrogenation of the corresponding allyl derivatives $[Rh(diphos)(C_4H_7)]$. Interestingly, complex **(16)** is deep red for the phosphite derivative,[26] but deep green for the phosphine[15,19] derivative in both the solid and solution states.

As the products from the hydrogenation of complex **(3)** in CD_2Cl_2 are cooled, a broad singlet appears in the proton NMR which then separates into two bridging hydride signals **E3** and **E4**. Signal **E3** is a doublet of multiplets implying the bridging hydride giving rise to it is *trans* to a single phosphine, whilst signal **E4** is a broad singlet, implying that the bridging hydride giving rise to it is *trans* to two phosphorus atoms. To reduce steric repulsions a dimer structure could twist from a square planar geometry towards a tetrahedral geometry. This would push the *tert*-butyl substituents away from one another and increase the angle between two ligands from 90° to 109°. The expansion of the PMP angle is likely to be favoured by chelating phosphines with large backbones, such as Boxylyl. The two forms of the hydride bridged dimer are represented by the signals **E3** and **E4**; signal **E3** is the tetrahedrally distorted isomer whilst signal **E4** is the planar isomer. The broadness and lack of coupling patterns in the remaining signals in the proton and phosphorus NMR at -90°C, is probably due to rapid interconversion of the species giving rise to these signals, and prevents further assignments of the spectra.

5.6. The Reaction of the Hydrides Generated in CD_2Cl_2 with Ethene and CO.

5.6.1. The Reaction of CO and Ethene with the Hydrogenation Products of $[Rh(Boxylyl)(C_7H_8)](BF_4)$ (3) in CD_2Cl_2.

The hydrides formed from the reaction of $[Rh(Boxylyl)(C_7H_8)](BF_4)$ **(3)** in CD_2Cl_2 were reacted with ethene (1atm.) after removal of the excess hydrogen. No colour change from olive green was observed on addition of the ethene. However, the r.t.

$^{31}P\{^{1}H\}$ NMR spectra changed, and only broad features were observed, indicating the products were fluxional on the NMR timescale. Unfortunately, a VT NMR study was not obtained for this reaction $^{31}P\{^{1}H\}$ NMR (CD_2Cl_2) (r.t.): δ 71 (br s).

The ethene was removed under reduced pressure and carbon monoxide introduced, causing an immediate change in colour of the solution from olive green to orange. The NMR signals were sharp and two new products were detected. $^{31}P\{^{1}H\}$ NMR (CD_2Cl_2) (r.t.) δ 82.5 (**14P**, d, $^{1}J_{Rh-P}$ 125Hz,); 40.7 (**5P**, d, $^{1}J_{Rh-P}$ 121Hz). See below for a discussion of these results

5.6.2. The Reaction of Ethene with the Hydrogenation Products of [Rh(dBpp)(C_7H_8)](BF_4) (2) in CD_2Cl_2.

The hydrides formed from the reaction of [Rh(dBpp)(C_7H_8)](BF_4) **(2)** in CD_2Cl_2 were reacted with ethene (1atm.) after removal of the excess hydrogen by a single freeze-thaw cycle. The sample was immediately cooled to -90°C and the $^{31}P\{^{1}H\}$ and ^{1}H NMR spectra collected as the sample was warmed to r.t. (see Figures 17/18, pages 117/118, and Appendix 4 for full listings of $^{31}P\{^{1}H\}$and ^{1}H NMR signals). After the VT NMR data had been collected, H_2 was reintroduced to the system and the original r.t. NMR hydride spectrum was restored.

5.6.3. Discussion of the Products from the Reaction of Ethene and CO with the Hydrogenation Products of Type (1) Complexes in CD_2Cl_2

The products from the reaction of ethene with the hydrogenation products of the type **(1)** complexes in CD_2Cl_2 are dependent on the phosphine employed; the dBpp system reacts differently to the Boxylyl system. The $^{31}P\{^{1}H\}$ NMR spectrum for the Boxylyl system at r.t.indicates that reaction has occurred, but the signals are broad; no useful information was gained.

Figure 17. VT $^{31}P\{^{1}H\}$ NMR Spectra for the Reaction of Ethene with the Hydrogenation Products of [Rh(dBpp)(C_7H_8)](BF_4) in CD_2Cl_2

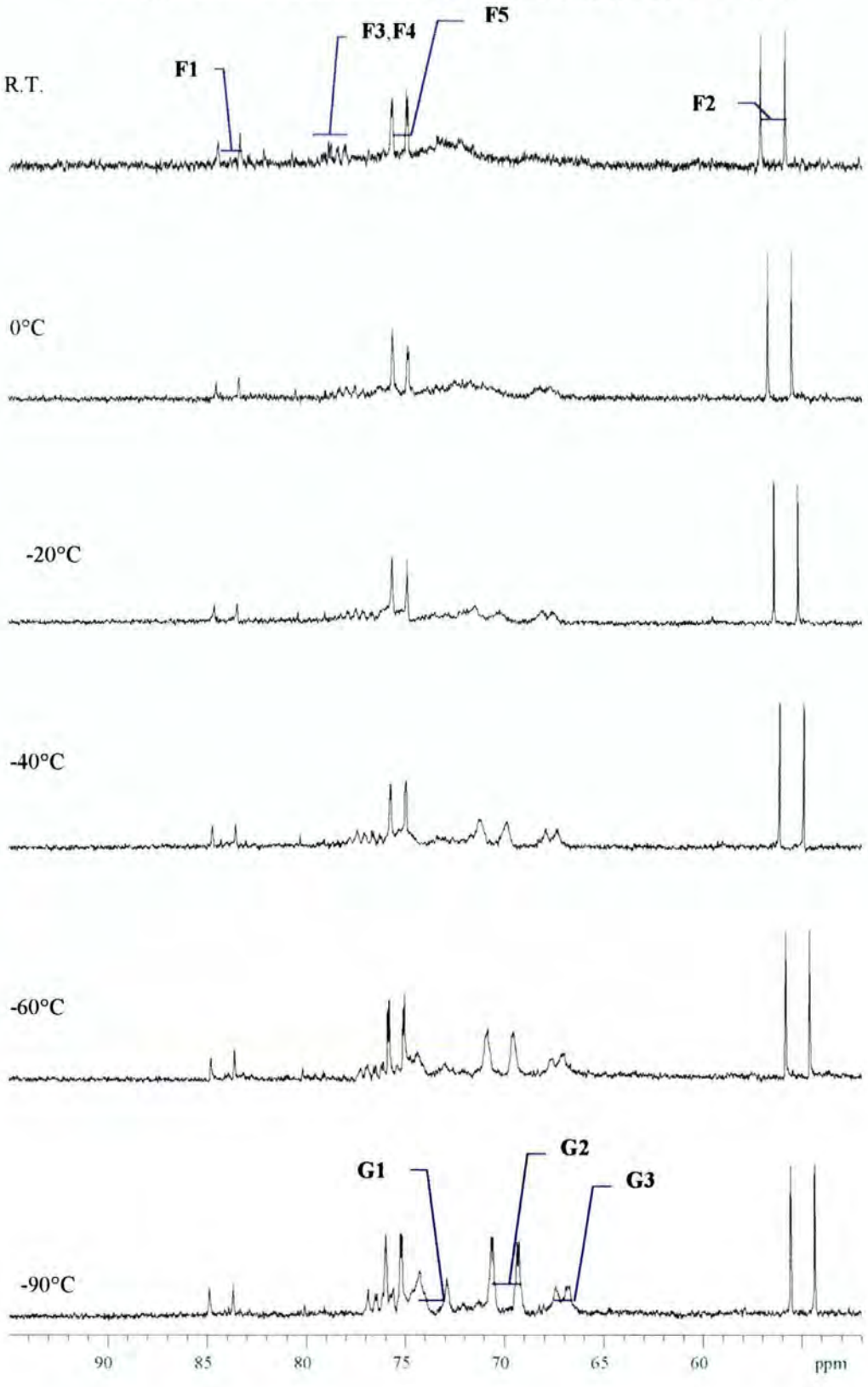

Figure 18. Variable Temperature ^1H NMR Spectra for the Reaction of Ethene with the Hydrogenation Products of $[Rh(dBpp)(C_7H_8)](BF_4)$ in CD_2Cl_2

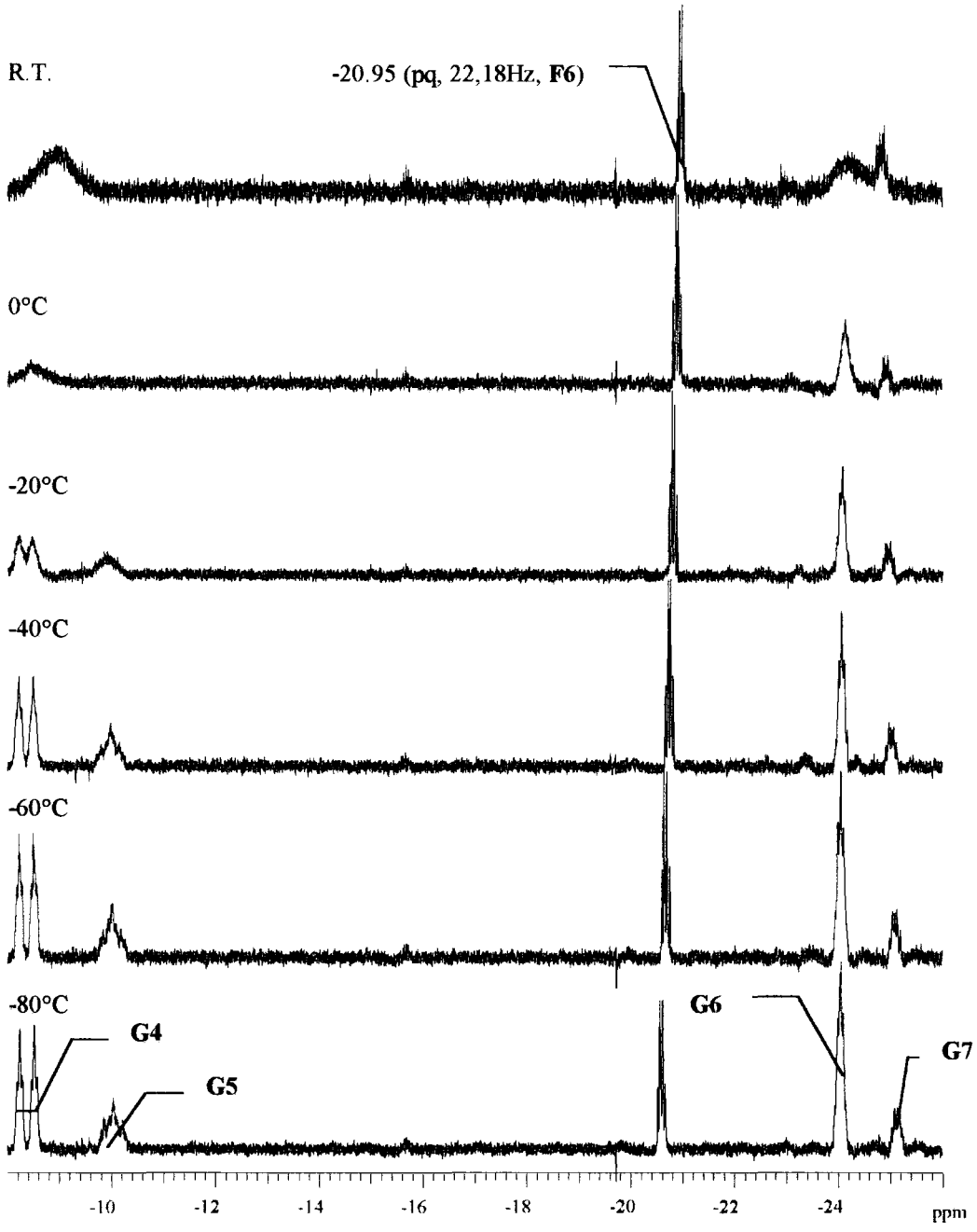

The green colour previously observed for the hydrogenation products of complex **(3)** in CD_2Cl_2 is present after the reaction with ethene, indicating a degree of isostructurality between reactants and products. This may mean that the product from the reaction with ethene is tetrahedral in solution, which leads to the conclusion that the rhodium must be in the +1 oxidation state. A species similar to those observed by Fryzuk[27], in which there is one bridging hydride ligand and a bridging alkenyl group acting as bridging ligand, *via* an η^1 Rh-C σ bond and an η^2 interaction with the carbon-carbon double bond could be formed; such as [{Rh(Boxylyl)}$_2$(μ-H)(σ,η^1,η^2 $CHCH_2$)] **(17)**.

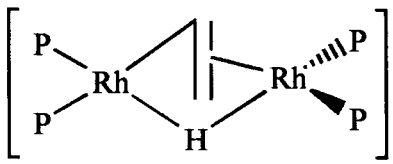

(17)

In contrast to the Boxylyl systems, there are several sets of new signals observed in the $^{31}P\{^1H\}$ and ^1H NMR spectra for the dBpp system, and both bridging and terminal hydride species are shown to be present. However, it is impossible to unambiguously assign the signals above 1 ppm in the proton NMR spectrum due to the large variety of signals present. Two dimensional correlation experiments were attempted for the hydride systems at both -90°C and r.t. , but were singularly unsuccessful due to the large variation in phosphorus-proton coupling constants present. We can treat these signals in a similar manner to those observed for the hydrides in CD_2Cl_2, and divide them into sets according to their behaviour with temperature:

Set F

- These signals are temperature invariant.
- Signals **F1** and **F2** are sharp doublets ($^1J_{Rh\text{-}P}$ 193, and 199Hz) in the phosphorus NMR spectrum. The data imply that they are due to Rh(I) species with a degree of symmetry, and the ligands *trans* to the phosphorus atoms are the same. The lack of change of the signals with changing temperature implies the ligands are either exchanging very quickly even at -90°C or not exchanging at all.

- Signals **F3**, and **F4** are multiplets in the phosphorus NMR spectra, arising from coupling to each other, although they represent a relatively small fraction of the total signals present.
- **F5** is a doublet of doublets ($^1J_{Rh-P}$ 123, J_2 13Hz) in the phosphorus NMR spectra, similar in appearance to signal **B2** observed in the NMR spectra of the hydride starting complex. However, this signal is shifted ~10ppm to higher frequency and $^1J_{Rh-P}$ is ~10Hz smaller.
- The hydride signal **F6** is a pseudo-quartet similar to that observed for signal **B1** in the NMR spectra of the hydride species.
- In summary, the temperature invariant signals comprising set **F** represent several species, one of which still contains hydride ligands.

Set G

- These signals change/appear as the temperature is reduced.
- Signals **G1**, **G2** and **G3**, coalesce at r.t. to form a broad feature in the phosphorus NMR spectrum. At -80°C, signal **G1** is a doublet ($^1J_{Rh-P}$ 210Hz), **G2** is a doublet of doublets of doublets ($^1J_{Rh-P}$ 212Hz) and **G3** is a broad doublet ($^1J_{Rh-P}$ 98Hz). The magnitude of $^1J_{Rh-P}$ for these three species indicates signals **G1**, and **G2** arise from a a phosphine co-ordinating to a Rh(I) species whilst signal **G3** arises from a Rh(III) complex.
- Signal **G4** is a doublet of triplets in the hydride bridging region of the proton NMR spectrum ($^2J_{P-H}$ 122.8Hz), implying it is *trans* to a single phosphorus atom, in a similar manner to signal **C3** in the NMR spectra of the starting hydride system.
- Signal **G5** coalesces at r.t. with signal **G4**. At -80°C, signal **G5** is a multiplet in the bridging hydride region, the ratio of the signals **G4** to **G5** being approximately 2:1.
- signals **G6** and **G7** are multiplets at -80°C in the terminal hydride region, similar to signals **C3** and **C4** in the NMR spectra of the hydride species. At r.t., signals **G6** and **G7** coalesce into a single broad feature.
- In summary, set **G** consists of several isomers of a Rh(I) species containing hydride ligands and these are in rapid equilibrium at r.t.

Whilst there are many similarities between the hydrogenation products of $[Rh(dBpp)(C_7H_8)](BF_4)$ in CD_2Cl_2 and the products from the reaction of these with ethene described here, they are not the same. In general the phosphorus NMR signals are shifted to higher frequency in the ethene system, perhaps due to the co-ordination of ethene to these hydride complexes, or migratory insertion of ethene into the Rh-H bonds to form alkyl species.

The large singlet at 0.72ppm in the proton NMR is due to the presence of ethane. Clearly for alkanes to be produced, alkyl species must have been formed at some stage. Signals **F5** and **F6** have similar coupling patterns to signals **B1** and **B2** in the hydride system, although they are shifted slightly in frequency. From this it would be reasonable to suppose that the species giving rise to signals **F5/F6** and **B1/B2** are similar, the difference arising from one of the hydride ligands being substituted for an alkyl ligand. However, it is impossible to tell from the spectra whether the alkyl ligand is in a bridging position.

Since there are no more temperature independent hydride signals unassigned, this means the signals **F1** and **F2** must arise from either a Rh(I) cationic complex or a complex containing alkyl ligands, a Rh(I) species being indicated by the magnitude of the $^1J_{Rh\text{-}P}$ values. Furthermore, the rhodium phosphorus coupling constants for signals **F1** and **F2** are too large for an alkene to be co-ordinated *trans* to the phosphine (cf. $[Rh(diphos)(C_7H_8)](BF_4)$ **(1)** $^1J_{Rh\text{-}P}$ 160-145Hz). It seems unlikely that a monomeric $14e^-$ complex such as $[Rh(diphos)]^+$ would exist in solution, although it could dimerise through metal-metal bonds. Consequently $[\{Rh(dBpp)\}_2(\mu\text{-}C_2H_5)_2]$ **(18)** is proposed as the species giving rise to signals **F1** and **F2**.

The temperature dependent signals, set **G**, bear a similar resemblance to the set of signals, **C**, observed in the NMR spectra of the hydride system, but there is an increased proportion of Rh(I) environments present. Unfortunately, selective decoupling experiments were not obtained for these systems, so it is not possible to tell

which phosphorus signals are associated with which hydride signals. Nevertheless the values of $^{1}J_{Rh\text{-}P}$ for signals **G1**, and **G2** are very large, much larger in fact than those reported for Rh(I) hydride species of the type $[Rh(diphos)(\mu\text{-}H)]_2$. Perhaps these large coupling constants can be explained in terms of a dimer $[Rh(dBpp)]_2^{2+}$. At low temperatures, two forms of this species can be observed, due to the cationic dimer twisting to reduce intramolecular repulsions between the *tert*-butyl groups. Finally the phosphorus signals **G3**, and the hydride signals **G4-G7** could arise from a series of isomers of $[Rh_2(dBpp)_2(\mu\text{-}R)_3R]$, where R is either a hydride or an alkyl ligand, due to the similarity of the coupling patterns of the hydrides to the hydride signals arising from $[Rh_2(dBpp)_2(\mu\text{-}H)_3H]$, which have been reported previously in this Chapter.

The Reaction with CO

When the ethene products, reported in section 5.6.1. were exposed to carbon monoxide, two non-fluxional species were formed. The rhodium-phosphorus coupling constants for both peaks fit well with those observed previously for complexes of the type $[Rh(diphos)(CO)_n]^{+}$[28]. However, in view of the fact that the chemistry of complexes containing the Boxylyl ligand is heavily influenced by its steric properties when compared to electronically similar phosphines, it is not unreasonable to assume the species at a higher field (and larger coupling constant) is due to a terminal mono-carbonyl adduct. A trigonal arrangement of the ligands about the metal, due to the steric bulk of the phosphine is the lowest energy conformation for the mono-carbonyl adduct. The inherent symmetry of this arrangement, creates a similar electronic environment for each phosphine, hence the appearance of only one doublet in the phosphorus NMR spectrum. This behaviour towards CO differs from complex **(17)** which forms $[Rh(dippe)(\mu\text{-}CO)]_2$ *via* an intermediate hydride and carbonyl bridged species.[20] However, it should be remembered that for the systems reported in this chapter, any neutral hydrides are formed by the dissociation of a proton, and that proton is not removed at any stage in the reaction. Consequently stable cationic

species can be formed by protonation of a neutral hydride with or without the subsequent loss of H_2.

5.7. Summary

The reactions of [Rh(diphos)(NBD)](BF_4) (diphos = dBpe, dBpp, dcpe, dcpp, dcpcp, Boxylyl) with hydrogen gas (1atm.) have been investigated by variable temperature proton and phosphorus NMR spectroscopy. The nature of the products are dependent on the solvent and the diphosphine employed in the reaction. Usually several products are formed in rapid equilibrium with each other, and with the hydrogen gas present.

In methanol the complexes [Rh(diphos)(NBD)](BF_4) (diphos = dBpp, Boxylyl) form di-solvent adducts of the type [Rh(diphos)($MeOH)_2$](BF_4) instead of hydride containing products. The Boxylyl derivative exhibits reversible green (r.t.) to red (-90°C) thermochroism, due to a tetrahedral-square-planar equilibrium and this is mirrored in the phosphorus NMR spectrum. This contrasts with the dBpp adduct which is red at all temperatures. The reaction of [Rh(dBpe)(NBD)](BF_4) in THF leads to the formation of both hydrides and solvent adducts. The hydrides formed are similar to those observed in dichloromethane. In the weakly co-ordinating CD_2Cl_2 all of the [Rh(diphos)(NBD)](BF_4) (diphos = dBpe, dBpp, dcpe, dcpp, dcpcp, Boxylyl) complexes investigated form hydrides when exposed to hydrogen gas. Three major hydride complexes can be distinguished in solution, of the types [Rh_2(diphos)$_2H_6$], [Rh_2(diphos)$_2H_4$] and [Rh(diphos)H_2]$^+$, although several isomers of each species can be observed. The distribution of the hydride species is dependent on the steric bulk of the phosphine; increasing the steric bulk favours the formation of the dimeric tetra-hydride. The behaviour of the Boxylyl system is again exceptional, due to its combination of steric and electronic properties and green instead of red solutions are observed. Furthermore, the predominant species in solution are Rh(I) as opposed to Rh(III).

Reaction of the hydrides with ethene in CD_2Cl_2, for the dBpp system results in the formation of fluxional, Rh(I) and Rh(III) alkene, alkyl and alkyl-hydride adducts. Addition of CO to the alkyl adducts in the Boxylyl system causes the rapid formation of complexes of the type $[Rh(Boxylyl)(CO)_{1 \text{ or } 2}]^+$.

5.8. References

[1] J. Halpern, *Science*, **217**, (1982), 401-407.
[2] B.D. Vineyard, W.S. Knowles, M.J. Sabacky, G.L. Bach, D.J. Weinkauff, *J. Am. Chem. Soc.*, **99**, (1977), 5946-5952.
[3] K. Tani, K. Suwa, E. Tanigawa, T. Yoshida, T. Okano, S. Otsuka, *Chem. Lett.*, (1982), 261-264.
[4] C.P Casey, G.T. Whitaker, M.G. Melville, L.M. Petrovich, J.A. Gavney, and D.R. Powell, *J. Am. Chem. Soc.* . **114**, (1992), 5535-5543.
[5] T.E. Waldman, G. Schaefer, D. Riley, *A.C.S. Symposium Series*, **517**, (1993), 58-74.
[6] A.S.C. Chan, J. Halpern, *J. Am. Chem. Soc.* . **102**, (1980), 839-840.
[7] J.M. Brown, P.A. Chaloner, *J. Chem. Soc. Chem. Commun.*, (1980), 344-346.
[8] P.S. Pregosin, "^{31}P and ^{13}C NMR of the Transition Elements," Pergamon Press, 1979.
[9] B.R. James, *Adv. Organomet. Chem.*, **17**, (1979), 319.
[10] J. M. Brown, P.A. Chaloner, A. G. Kent, B.A. Murrer, P.N. Nicholson, D. Parker, P. J. Sidebottom, *J. Organomet. Chem.* , **216**, (1981), 263-276.
[11] T. J. Kim, *Bull. Korean Chem. Soc.* , **11**, (1990), 134-139.
[12] J.M. Brown, L.R. Canning, A.J. Downs, A.M. Forster, *J. Organomet. Chem.*, **255**, (1983), 103-111.
[13] C.A. McAuliffe, " Transition Metal Complexes of Phosphorus, Arsenic, and Antimony Ligands", McMillan Press, London, 1973.
[14] K. Tani, E. Tanigawa, Y. Tatsuno, S. Otsuka, *J. Organomet. Chem.*, **279**, (1985), 87-101.
[15] K. Tani, T. Yamagata, Y. Tatsuno, T. Saito, Y. Yamagata, N. Yasuoka, *J. Chem. Soc. Chem. Commun.*, (1986), 494-495.
[16] K.Tani, E. Tanigawa, Y. Tatsuno, S. Otsuka, *J. Organomet. Chem.*, **279**, (1985), 87-101.
[17] R.H. Crabtree, *Angew. chem. Int. Ed. Engl.*, **32**, (1993), 789
[18] U.E. Bucher, T. Lengweiler, D. Nanz, W. Von Philipsborn, and L.M. Venanzi, *Angew. chem. Int. Ed. Engl.*, **29**, (1990), 548
[19] R.H. Crabtree, "The Organometallic Chemistry of the Transition Elements", Wiley-Interscience, Chichester, 1988.
[20] M.D. Fryzuk, M. Jang, T. Jones, F.W.B. Einstein, *Can. J. Chem.*, **64**, (1986), 174-179
[21] M.D. Fryzuk, W.E. Piers, T. Jones, F.W.B. Einstein, *Can. J. Chem.*, **67**, (1989), 883-897
[22] H.H. Wang, L.H. Pignolet, *Inorg. Chem.*, **19**, (1980), 1470-1480.
[23] J. Wolf, O. Nurnberg, M. Schafer, H. Werner, *Z. Anorg. Allg. Chem.*, **620**, (1994), 1157-1162.
[24] I.R. Butler, W.R. Cullen, T.J. Kim, F.W.B. Einstein, T. Jones, *J. Chem. Soc. Chem. Commun.*, (1984), 719
[25] M.D. Fryzuk, T. Jones, F.W.B. Einstein, *Organometallics*, **3**, (1984), 185-191.
[26] M.D. Fryzuk, *Can. J. Chem.*, **61**, (1983), 1347-1351.
[27] M.D. Fryzuk, W.E. Piers, , *Polyhedron.*, **7**, (1988),1001-1014
[28] See chapter 2, section 3.

Chapter 6

The Synthesis of Hydrido-Chloro-Complexes, An NMR study

6.1. Introduction

The products from the hydrogenation of [Rh(diphos)(C_7H_8)](BF_4) **(1)** type complexes in $CDCl_3$ are radically different from those observed in other solvents (see chapter 5). This difference arises from the partial chlorination by the $CDCl_3$ of the initial hydrides formed. The final product for most phosphine systems investigated in $CDCl_3$ is a hydride-containing species. This chapter is concerned with the synthesis and characterisation of hydrido-chloro complexes from the reaction of rhodium hydrides with chloroform, and from the reaction of a range of rhodium diphosphine precursors with HCl. The chemistry discussed here, and the reaction pathways proposed are summarised in Scheme 1 (page 126).

It proved impossible to isolate the hydrido-chloro-rhodium complexes, which were found to be very reactive and fluxional in solution. Consequently, they were studied as formed in deuterochloroform by VT phosphorus and proton NMR spectroscopy. In a typical experiment, a type **(1)** complex (~50mg) contained in an NMR tube equipped with a Young's teflon tap, was dissolved in $CDCl_3$ (~0.5cm^3), added by vacuum distillation. After three freeze/thaw cycles, hydrogen gas (1atm.) was introduced at r.t. and, after the system had come to equilibrium (24 hours), the products were monitored by ^1H and $^{31}P\{^1H\}$ NMR spectroscopy. In some cases several phosphorus signals were observed and selective phosphorus decoupling experiments were performed to ascertain which proton signals were coupling to which phosphorus signals.

Scheme 1 Proposed Reaction Sequences and Products for the Hydrogenation of Type (1) Complexes in $CDCl_3$

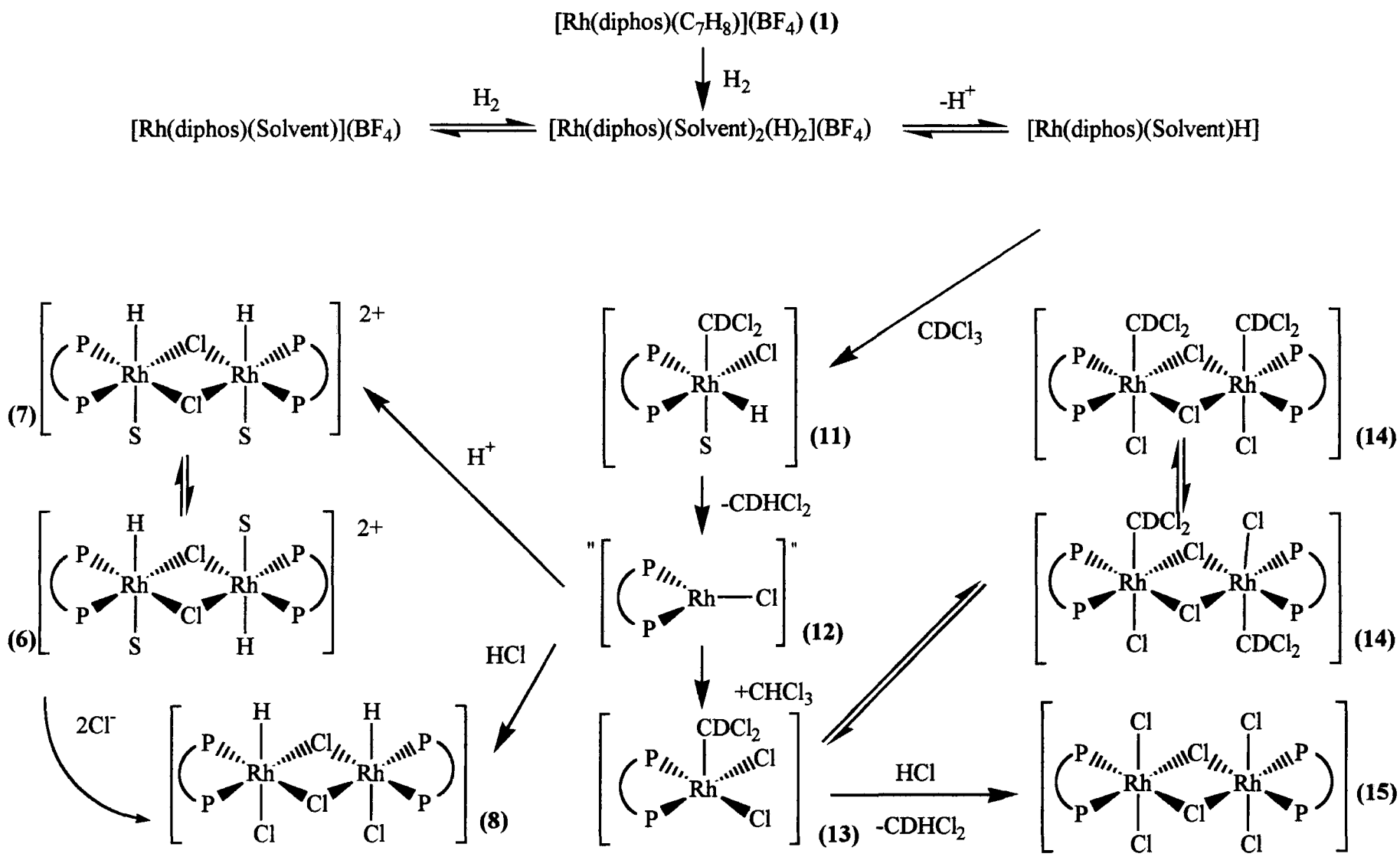

6.2. Results and Discussion

The reaction of type **(1)** complexes with hydrogen in chloroform produces a range of products. The most important of these are the hydrido-chloro-rhodium complexes. This reaction was carried out for four rhodium diphosphine complexes and the NMR spectra for these systems can be found as indicated in Table 1; full listings of the VT $^{31}P\{^{1}H\}$ and ^{1}H NMR data are recorded in Appendix 5.

Table 1.

Complex	Phosphorus NMR (Page)	Proton NMR (Page)
[Rh(dBpe)(C_7H_8)](BF_4) **(2)**	Figure 4 (133)	Figure 1 (129)
[Rh(dcpe)(C_7H_8)](BF_4) **(3)**	Figure 5 (134)	Figure 2 (130)
[Rh(dBpp)(C_7H_8)](BF_4) **(4)**	Figure 6 (135)	Figure 3 (131)
[Rh(Boxylyl)(C_7H_8)](BF_4) **(5)**	Figure 7 (142)	Figure 8 (143)

In order to confirm the nature of the products formed by the hydrogenation of type **(1)** complexes in deuterochloroform, a series of experiments was undertaken using HCl gas and suitable rhodium precursors. The complexes used were the hydrogenation products of type **(1)** complexes (see Chapter 5), characterised in the solvents CD_2Cl_2 and d^8-THF (reactions **a**, **b**), and $[Rh(dppe)Cl]_2$ (for reaction **c**):

a. $[Rh_m(dBpp)_n(Hydride)_x](BF_4)_y^{*} + HCl \xrightarrow{CD_2Cl_2} [Rh_2(dBpp)_2Cl_2H_2(S)_2](BF_4)_2$

b. $[Rh_m(dBpe)_n(Hydride)_x](BF_4)_y^{*} + HCl \xrightarrow{d^8\text{-THF}} [Rh_2(dBpe)_2Cl_2H_2(S)_2](BF_4)_2$

c. $[Rh_2(dppe)_2Cl_2] + HCl \xrightarrow{CD_3OD} [Rh_2(dppe)_2Cl_4H_2]$

* m = n = 1 or 2; x = 1-6; y = 3m-x.

After the hydrogenation of type **(1)** complexes in $CDCl_3$, the NMR (^1H, ^{31}P; VT, decoupled) data are consistent with the presence of two related compounds of the type $[Rh(diphos)(S)_2(\mu\text{-}Cl)_2H_2]^{2+}$ in equilibrium with each other, and the data will be represented with reference to the two structures **(6)** and **(7)** below (S is a weakily co-ordinating solvent molecule or a vacant co-ordination position).

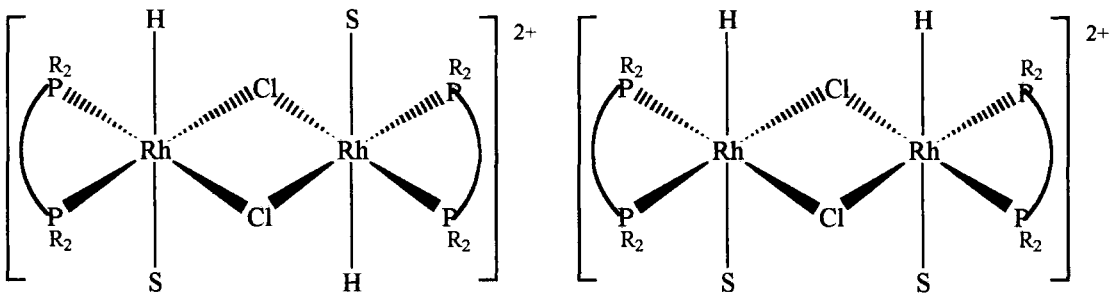

***Trans* (6)** ***Cis* (7)**

Figures 1 and 2 show the variable temperature (VT) proton NMR spectra for the hydrogenation in $CDCl_3$ of the dBpe and dcpe complexes **(2)** and **(3)** respectively. At r.t. only a single broad hydride signal in the terminal hydride* region is observed, corresponding to the hydride ligands in complexes **(6)** and **(7)**. On cooling the sample to -50°C, the hydride signal observed at r.t. splits into two, signals **B1** and **B2**. Two signals are observed at -50°C, because the rate of exchange between complexes **(6)** and **(7)** is now slower than the NMR timescale. The coupling pattern of these signals, corresponds to a triplet of doublets (pseudo-quartet). This coupling pattern is consistent with a hydride ligand coupling to a single rhodium atom (hence a doublet) and two equivalent phosphorus atoms (hence a triplet). The P-H coupling constant is quite small (~ 25Hz) and consequently the hydride ligand in complexes **(6)** and **(7)** is *cis* to the phosphorus atoms. Two hydride signals are observed because the hydride ligands in complexes **(6)** and **(7)** are magnetically inequivalent. The signals **B1** and **B2** are in the ratio 3:1, implying that one of the isomers predominates.

* The hydride region here is regarded as 0 to -30ppm; terminal hydrides for similar systems (see Chapter 5) appear in the region -15 to -30ppm.

Figure 1. Variable Temperature Proton NMR Study of the Hydrogenation of [Rh(dBpe)(C_7H_8)](BF_4) (2) in $CDCl_3$

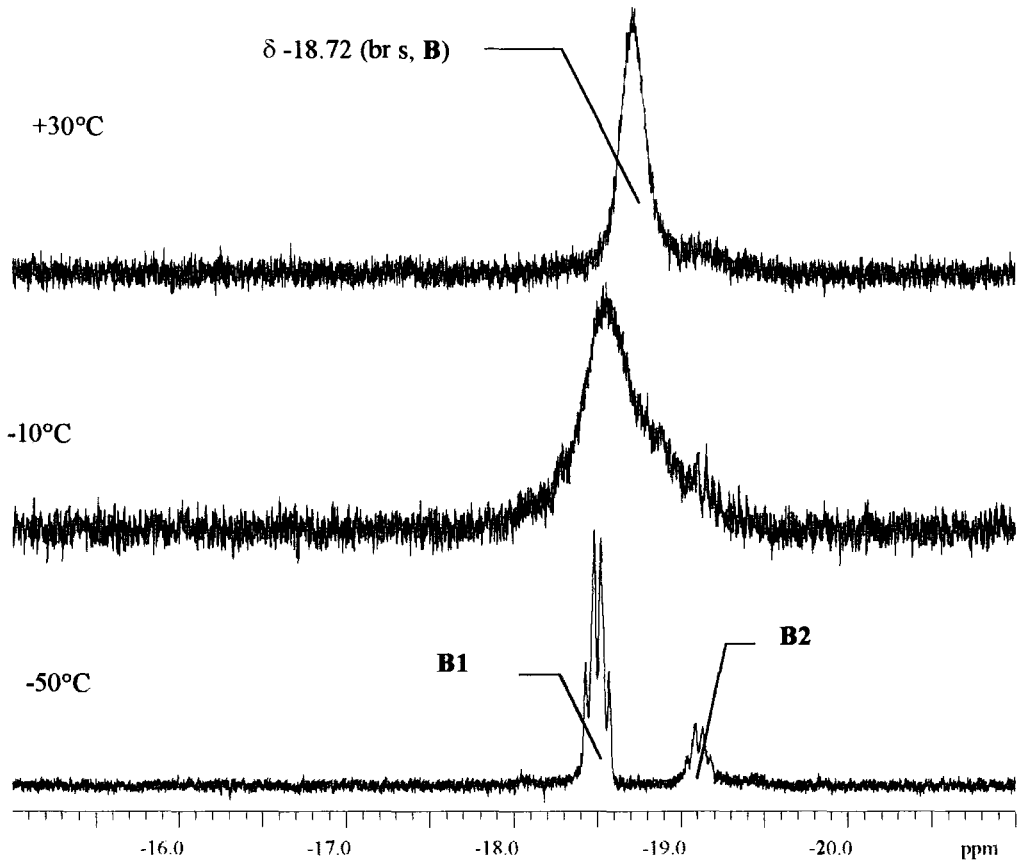

See Appendix 5 for full listings of $^{31}P\{^1H\}$ and ^1H NMR data for the hydrogenation of complex **(2)** in $CDCl_3$.

Figure 3 contains the VT proton NMR spectra for the hydrogenation of the dBpp complex, **(4)** in $CDCl_3$. In contrast to the dBpe and dcpe systems which form five membered chelate rings, only one hydride signal is observable at -50°C for the dBpp system which forms a six membered chelate ring. However, the hydride signal is in a similar position, with similar Rh-H and P-H coupling constants to the dBpe and dcpe hydride signals (see Table 2), indicating there are structural similarities.

Figure 2. Variable Temperature ^1H NMR Study of the Hydrogenation of [Rh(dcpe)(C_7H_8)](BF_4) (3) in $CDCl_3$

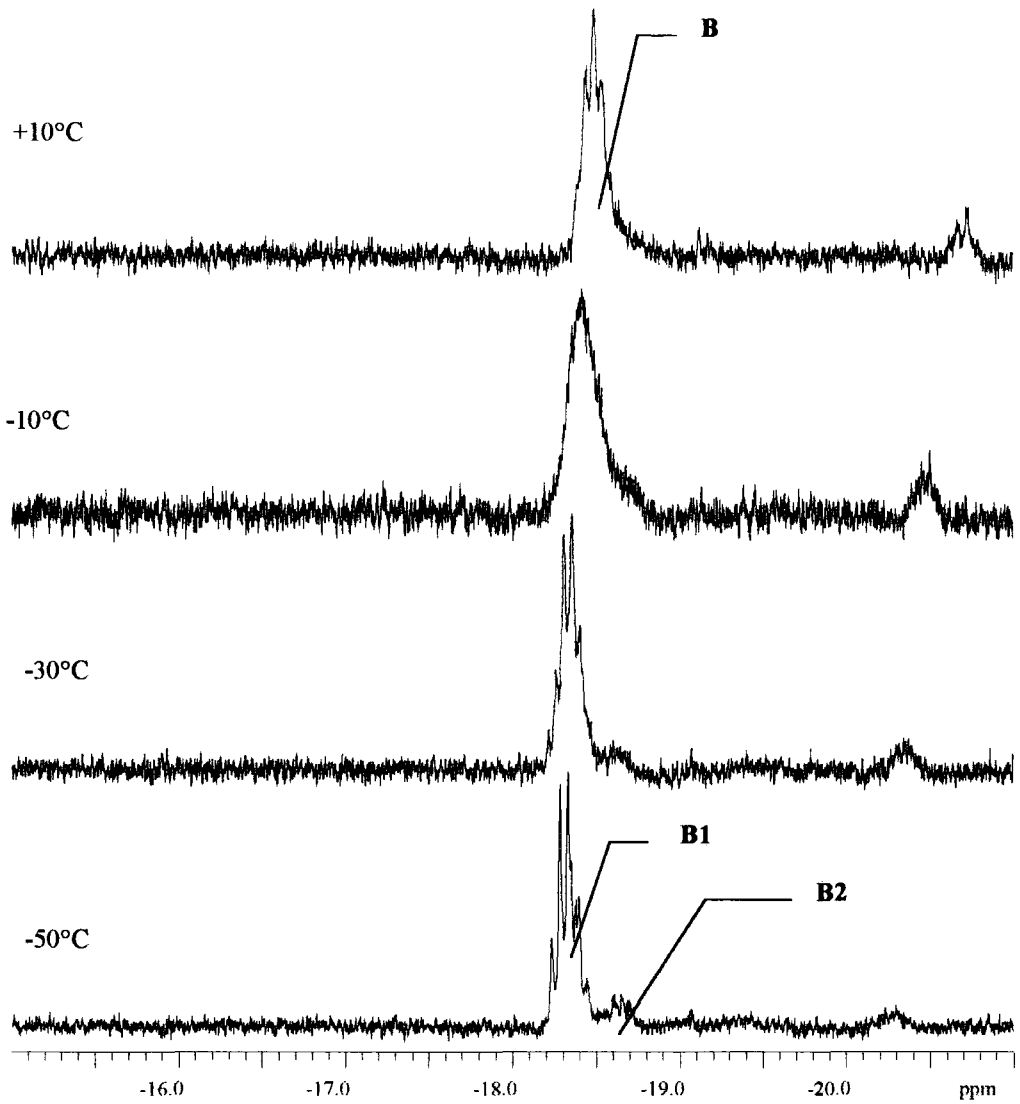

The difference in behaviour in the larger chelate system (dBpp) is due to the increased size of the chelate ring, which in turn increases the steric interactions of the Bu^t groups with the rest of the molecule. This could have two effects: at -50°C, exchange between complexes **(6)** and **(7)** is still faster than the NMR timescale due to a decreased activation energy for this process; the increased steric interactions may cause one isomer to predominate in solution.

Figure 3. Variable Temperature ^1H NMR Study of the Hydrogenation of $[Rh(dBpp)(C_7H_8)](BF_4)$ (4) in $CDCl_3$

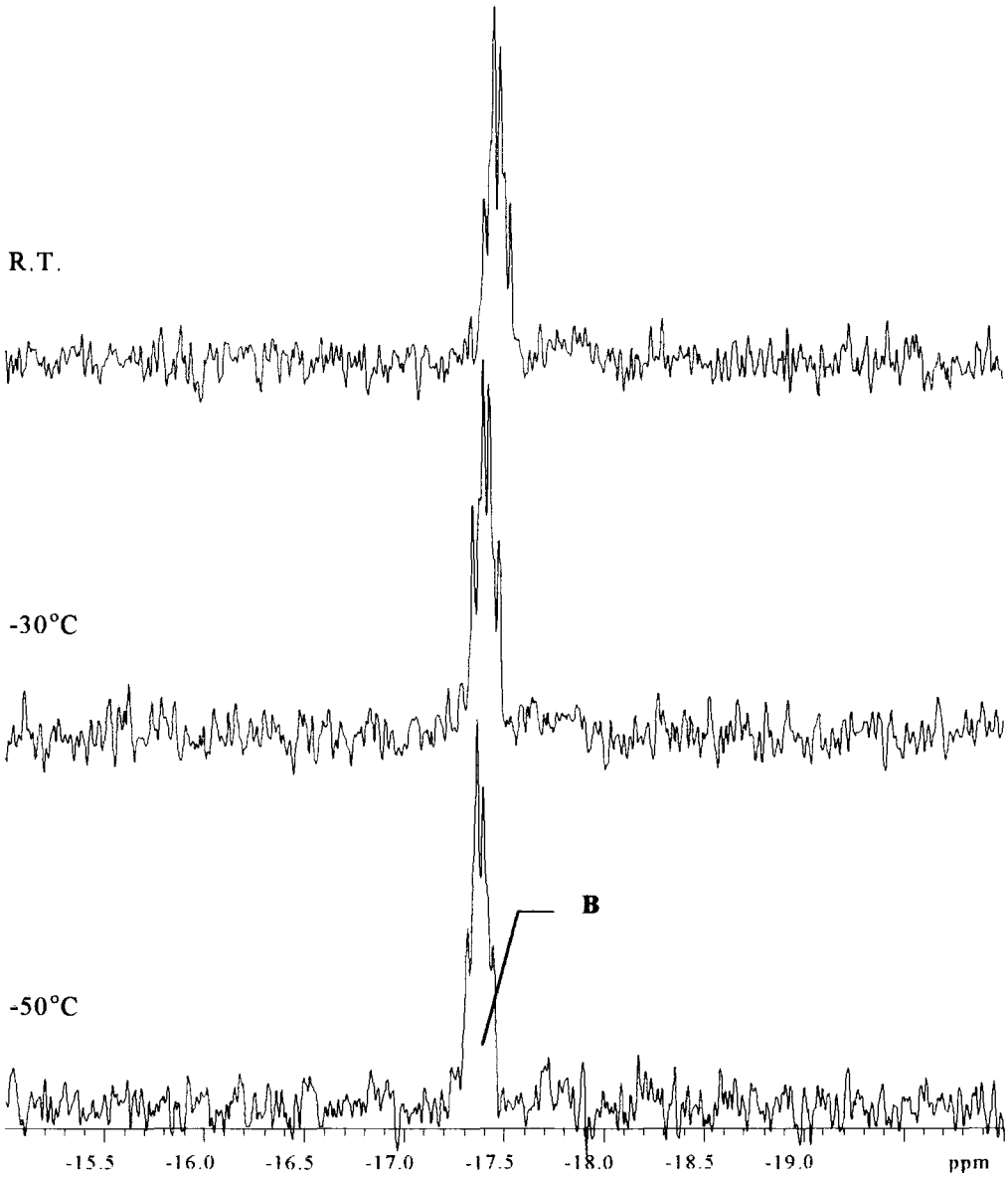

Selective decoupling of doublet **A** in the phosphorus NMR reduces multiplet **B** in the proton NMR to a broad singlet, indicating these two signals are coupled.

Selected NMR data from these reactions and from the hydrogenation of type **(1)** complexes in $CDCl_3$ are summarised in Table 2.

Table 2 Summary of Important NMR Data at -50 °C for the Hydrido-Chloro-Rhodium Complexes

Phosphine (Reaction)	$^{31}P\{^1H\}$ -ppm, (*, J_{Rh-P}, J_β Hz)	δH -hydride -ppm (†,* , J - Hz)
dBpe hydrogenation of **(2)**	113.3 (dd, 136, 18)	-18.48 (**3P**, dt, 22.2, 15.2), -19.06 (**1P**, dt, 17.6).
dcpe hydrogenation of **(3)**	100.2 (dd, 135,17)	-18.35 (dt, 19.6)
dBpp hydrogenation of **(4)**	67.7 (dd, 136, 19)	-17.5
Boxylyl hydrogenation of **(5)**	54.9 (dd, 133, 22)	indeterminate (-18.16 ?)
dBpp **(a)**	61.2 (d, 136)	-18.58 (dt, 23.6, 11.2)
dBpe **(b)**	110.1 (d, 136)	
dppe **(c)**	51.6 (d, 118)	-16.6 (br s)

* Coupling Pattern
† Relative Intensity by Integration

Figures 4 and 5 contain the proton decoupled phosphorus NMR spectra from the hydrogenation in $CDCl_3$ of the dBpe and dcpe complexes, **(2)** and **(3)** respectively. For both of these systems there are a great many phosphorus signals present. However, complexes of the type **(6)** and **(7)** only give rise to the signals denoted, **A**. The temperature dependence of the signals **A** (Figures 2/3) parallels that of the hydride signals **B** (Figures 5/6). At r.t. the exchange between complexes **(6)** and **(7)** is rapid and a single doublet is observed due to Rh-P coupling. As the sample is cooled to -50°C, the rate of exchange between complexes **(6)** and **(7)** slows down and the signal **A** first broadens, then splits into two, **A1** and **A2**. Signals **A1** and **A2** in the ratio 3:1 respectively, arise from complexes **(6)** and **(7)**. Consequently it is not unreasonable to assume that the larger signal **A1** arises from the same complex as the larger hydride signal **B1**. Therefore, the smaller phosphorus and hydride signals **A2**, and **B2** , must arise from the other isomer.

Figure 4. $^{31}P\{^{1}H\}$ Variable Temperature NMR study of the Hydrogenation of $[Rh(dBpe)(C_7H_8)](BF_4)$ (2) in $CDCl_3$

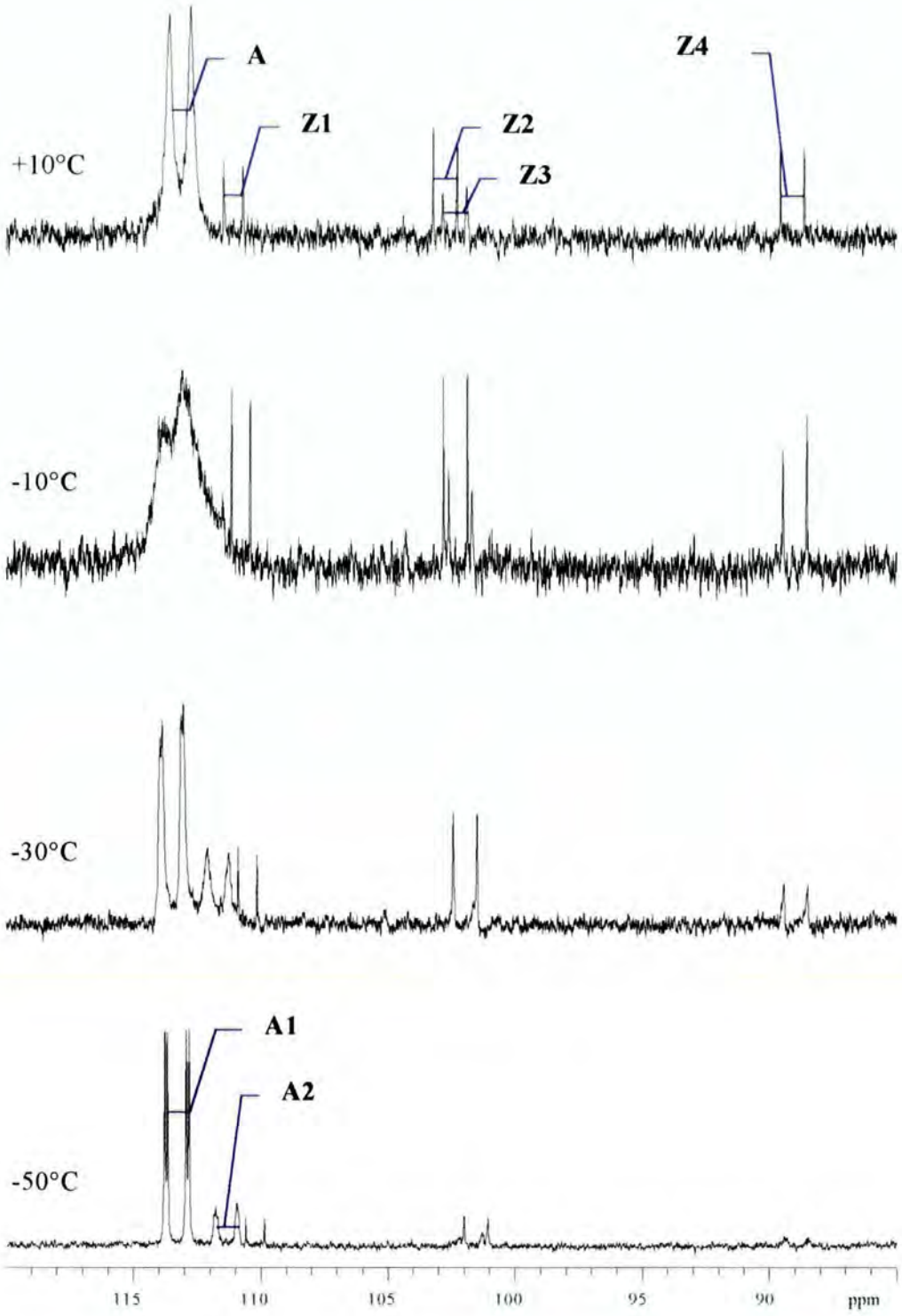

Figure 5. Variable Temperature $^{31}P\{^{1}H\}$ NMR Study of the Hydrogenation of $[Rh(dcpe)(C_7H_8)](BF_4)$ (3) in $CDCl_3$

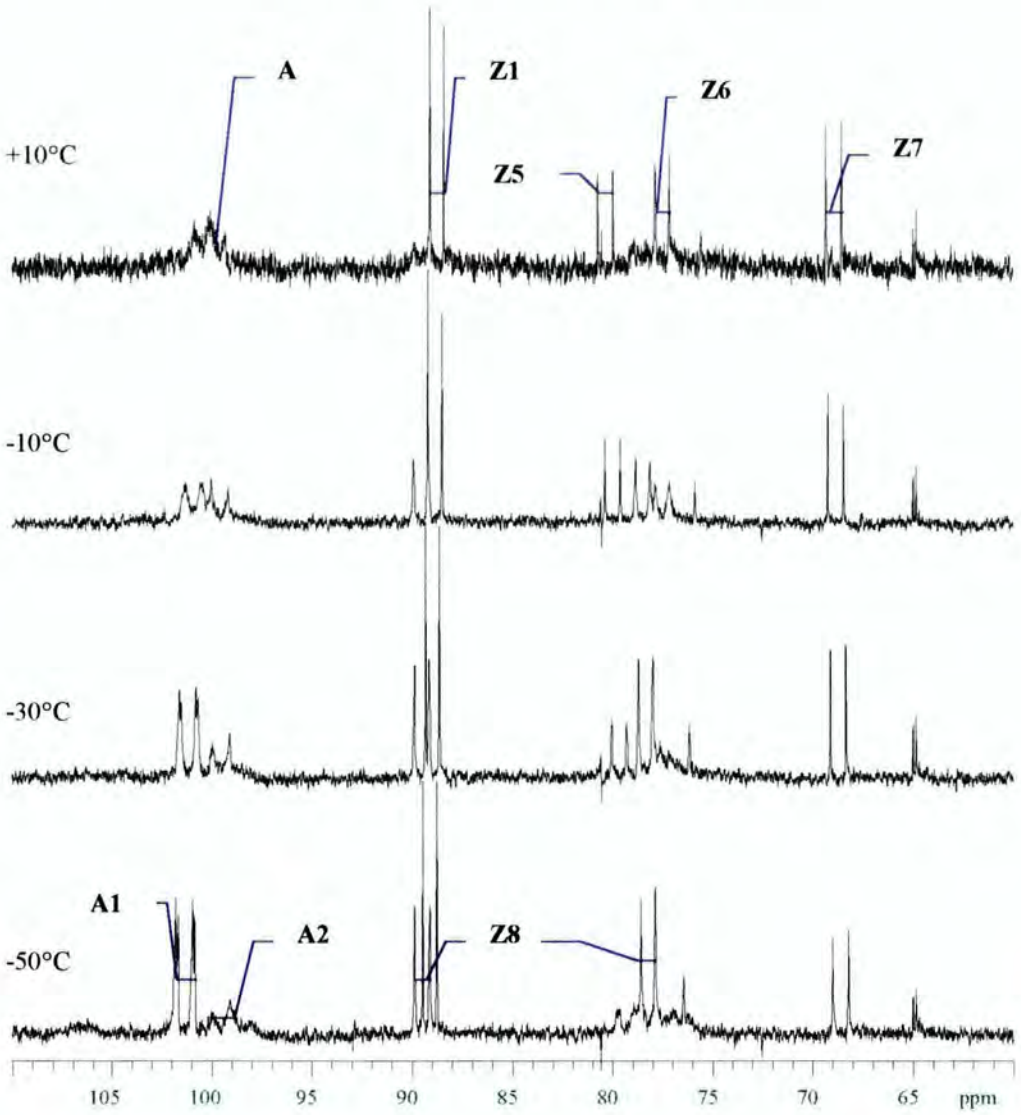

Figure 6. Variable Temperature $^{31}P\{^{1}H\}$ NMR Study of the Hydrogenation of [Rh(dBpp)(C_7H_8)](BF_4) (4) in $CDCl_3$

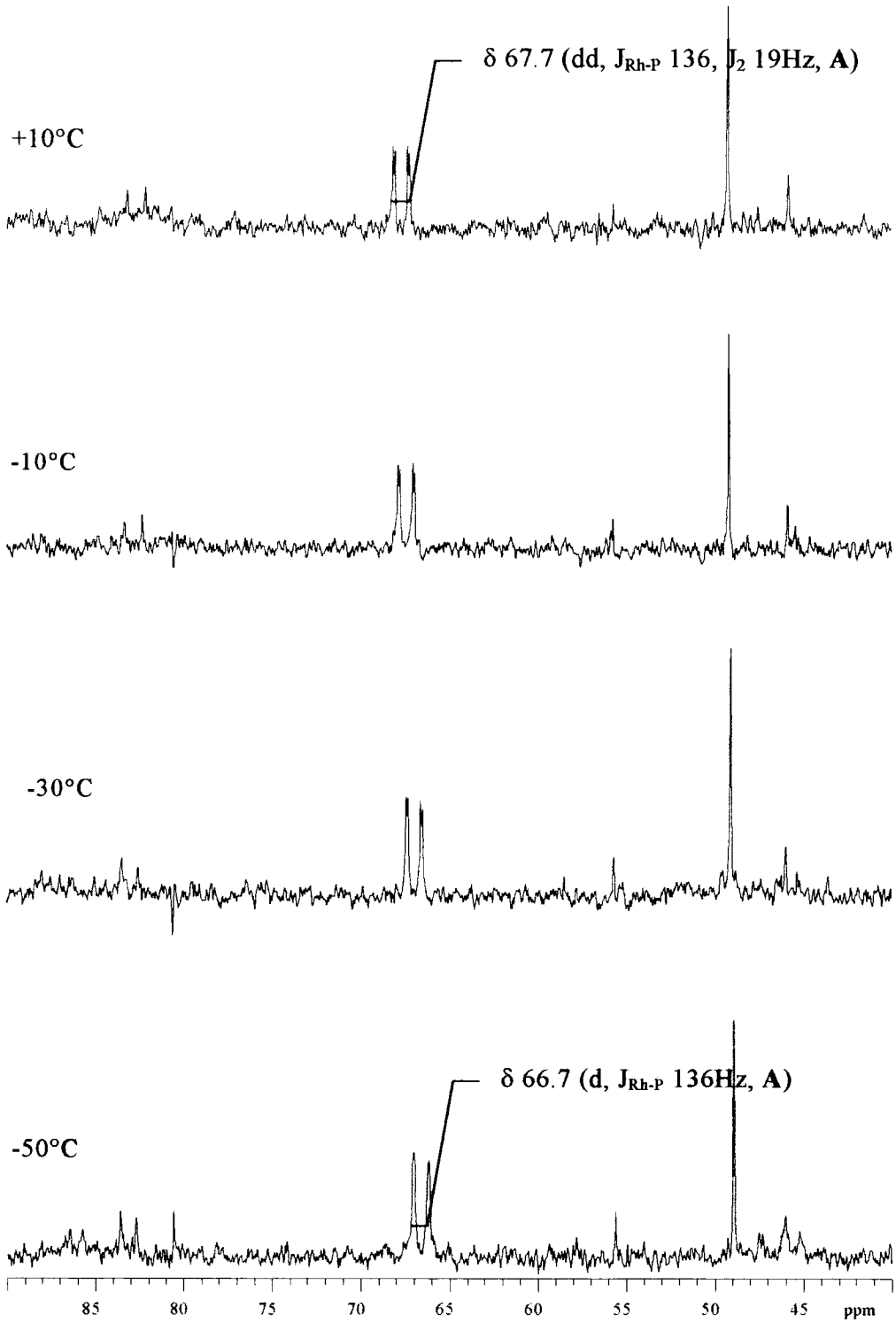

Selective decoupling of the phosphine's protons in the dBpe system at r.t., splits the doublet **A** into a doublet of doublets due to coupling to the hydride ligand, indicating that there is only one hydride ligand attached to each rhodium atom.

Figure 6 contains the proton decoupled phosphorus NMR spectra from the hydrogenation in $CDCl_3$ of the dBpp complex, **(4)**. These spectra are much cleaner than those obtained for the dcpe and dBpe systems. Similar to the ^1H NMR spectra of the dBpp system, only one resonance is observed in the phosphorus NMR spectra and this can be explained in a similar manner. Selective decoupling of the phosphorus signal **A** at -50°C reduces the hydride signal **B** from a pseudo-quartet to a broad doublet due to residual Rh-H couplings. This indicates that the hydride ligand is indeed in a terminal position; the phosphorus and hydride resonances arising from the same molecule.

In all three of these (dBpe, dcpe, dBpp) systems, the major signal at -50°C, **A1**, is a doublet of doublets ($^1J_{Rh\text{-}P}$ ~136, J_β ~18Hz). The magnitude of $^1J_{Rh\text{-}P}$ is quite small (~136Hz), indicating that the rhodium in complexes **(6)** and **(7)** is in the (+3) oxidation state. Coupling constants of this magnitude have been observed for Rh(I) species with strong π acidic ligands *trans* to the phosphine (for example, CO[1]). However, the magnitude of $^1J_{Rh\text{-}P}$ observed here is more indicative of P *trans* to Cl for a Rh(III) complex,[2] though is larger than those observed for the related species $[Rh_2(dppp)_2(\mu\text{-}I)_2(I)_2(H)_2]$.[3] The size of the Rh-P coupling constant and the large values of the phosphorus chemical shift, δ indicate that the phosphines are still chelating, whilst the occurrence of only one doublet in the phosphorus NMR implies the phosphorus atoms in the chelating phosphine are magnetically equivalent and symmetrically related.

In solution the *cis* complex **(7)** can bend about the Cl-Cl axis, causing solvent to be lost and the positions marked S to overlap. The rhodium-rhodium interaction thus

formed gives rise to the smaller couping constant observed (β) (see Table 2).† Bending about the Cl-Cl axis is not as favourable for the *trans* complex **(6)**, and if this did occur the two positions marked S would not overlap and consequently the metal-metal interaction would not form. Hence the larger signals observed in solution, **A1**, and **B1** are due to the *cis* complex **(7)** because (β) is observed for signal **A1**, whilst the smaller signals **A2** and **B2** are due to the *trans* complex **(6)**.

Further structural evidence for the complexes of the type **(6)** and **(7)** comes from the reaction of the hydrides‡ formed in CD_2Cl_2 or d^8-THF with HCl gas. On the addition of $HCl_{(g)}$ a new species forms and the previous NMR signals disappear. This new species resonates at approximately the same δ value in the phosphorus NMR spectrum and with an identical Rh-P coupling constant to the hydrido-chloro-rhodium complexes **(6)** and **(7)**, indicating a degree of isostructurality. This is reinforced by a hydride signal in a similar region to those of complexes **(6)** and **(7)** (see Table 2).

Complex $[Rh_2(dppe)_2(\mu\text{-}Cl)_2Cl_2H_2]$ **(8)** has been synthesised from the oxidative addition of $HCl_{(g)}$ to $[Rh(dppe)Cl]_2$.

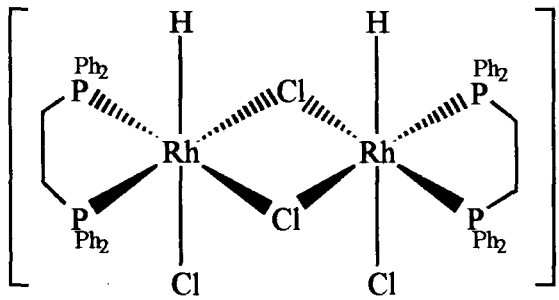

(8) [*cis* isomer is shown here]

† (β) must derive from coupling of the phosphorus atoms to another nucleus with spin I=1/2. There are five of these in the system: Rh, P, H, C, and F. Since the coupling involves all of the signal, this precludes ^{13}C which has only 1% natural abundance. If (β) was due to P-P coupling, then we would expect to observe two doublets of doublets in the phosphorus NMR. However, this is not the case. The synthesis of hydride complexes (Chapter 5) with hydride signals at significantly lower chemical shifts precludes the possibility that the broad band proton decoupler is not covering all of the hydride signals. Consequently (β) does not arise from a P-H coupling. This coupling is not reciprocated in the fluorine NMR spectrum, consequently the coupling constant (β) must derive from the interaction with another rhodium atom.

‡ See Chapter 5

Complex **(8)** has a much smaller Rh-P coupling constant than complexes **(6)** and **(7)**, and this is in good agreement with the value of $^{1}J_{Rh\text{-}P}$ found for the structurally characterised dppp analogue $[Rh(dppp)Cl_2H]_2$ **(8)** ($^{1}J_{Rh\text{-}P}$ 125Hz).[4] In the CD_2Cl_2 and THF systems (reactions **a** and **b**) there is a large excess of HCl present in solution§ which could exchange with the hydride and chloride ligands already present in the complex in a manner that destroys the small coupling constant, **(β)** by breaking the metal-metal bond through which it is transmitted. The related species *cis* and *trans*-$[Rh_2(triphos)_2(\mu\text{-}Cl)(H)_2]^{2+}$ have been reported before from the reaction of the corresponding tetra-hydride and dichloromethane.[5] However, these species, unlike complexes **(6)** and **(7)**, are not fluxional on the NMR timescale at r.t. due to the stabilising effect of the extra phosphine ligand, which blocks the otherwise vacant co-ordination site. Interestingly, the reaction between type **(1)** complexes and hydrogen in $CDCl_3$ has been examined previously[6] for chelating ferrocenyl-phosphines and 1,2 bis(di*iso*propylphosphino)ethane (d*i*ppe) derivatives. It was found that the ferrocenyl-phosphine system behaved differently to d*i*ppe system, and the final product from the reaction of the d*i*ppe system gave a doublet of triplets in the proton NMR spectrum, δ -17.30 ($^{1}J_{Rh\text{-}H}$ 22, $^{2}J_{P\text{-}H}$ 25Hz) ppm. Unfortunately, no phosphorus NMR data were given and this was tentatively assigned as the fluxional hydride - $[(dippe)RhH_4]^{+}$.[6] Considering the similarity of the data for the d*i*ppe system, to the results obtained in this work, and the experimental conditions used, it would not be unreasonable to assume that the d*i*ppe species was wrongly assigned, and is instead, one of the series of type **(6)** and **(7)** complexes reported here.

So far only the hydride containing species observed in the phosphorus NMR has been discussed. However, the hydrogenation of the type **(1)** complexes in chloroform produces some other minor species (marked ***Zn*** in the spectra, see Figures 4 and 5).

Chlorination of the dBpe system with CCl_4 converts both the major species, complexes **(6)** and **(7)** and minor species, ***Zn*** to a single product ($^{31}P\{^{1}H\}$ NMR δ 110.3 ppm, d,

§ This appears as a broad singlet at ~4.9ppm.

$^1J_{Rh\text{-}P}$ 136Hz) and the hydride signals can no longer be observed. The terminal hydride ligands are replaced by chloride ligands to form $[Rh_2(dBpe)_2(\mu\text{-}Cl)_2Cl_2]^{2+}$. Evidence for this structure comes from the phosphorus chemical shift and the Rh-P coupling constant which are are very similar to those observed for the complexes **(6)** and **(7)**, indicating a degree of isostructurality. Further chlorination to form $[Rh_2(dBpe)_2(\mu\text{-}Cl)_2Cl_4]$ can be ruled out, since $^1J_{Rh\text{-}P}$ for $[Rh_2(dBpe)_2(\mu\text{-}Cl)_2Cl_2]^{2+}$ is much larger than for complexes of the type $[Rh_2(diphos)_2(\mu\text{-}Cl)_2Cl_4]$ reported in Chapters 7 and 8 ($^1J_{Rh\text{-}P}$ ~118Hz).

The chlorination with carbon tetrachloride is generally accepted to be a radical reaction, affecting both metal-hydrogen and metal-carbon bonds. Since the species ***(Zn)*** react with CCl_4 but do not contain hydride ligands, then perhaps they possess alkyl ligands derived from the $CDCl_3$ solvent. Further evidence for the presence of alkyl ligands in the species ***Zn*** comes from the magnitude of the Rh-P coupling constants, which at ~145Hz are very similar to previously observed rhodium(III)-acyl species, of the type $[Rh(diphos)(COMe)Cl_2]$.[4,7]

There are essentially two possibilities regarding the source of the halide ligand required for the complexes of the types **(6)** and **(7)**; either it is present in the chloroform ($CHCl_3$ will hydrolyse in the presence of light and water to produce HCl), or it could come from the oxidative addition of the chloroform to a rhodium(I) species (see Scheme 1). However, since efforts were made to keep the chloroform dry,† and the results were consistent when repeated using different batches of chloroform, it appears more plausible that the chloride ligands came from the oxidative addition of chloroform to a Rh(I) complex.

† The solvent was dried over pre-dried molecular sieves, freeze-thaw degassed prior to use, stored in the dark and vacuum distilled into the NMR tube.

When the mono-phosphine derivatives of type **(1)** complexes (diphos = $2PR_3$) are treated with hydrogen gas, two hydrides form:[8]

$$\textit{trans}\text{-}\ [Rh(PR_3)_2H_2(solvent)_2]^+ \rightleftharpoons [Rh(PR_3)_2H] + H^+$$

(9) **(10)**

Equation 1

The equilibrium between complexes of the types **(9)** and **(10)** is dependent on the basicity of the phosphine used. We might expect a similar equilibrium to be established after the hydrogenation of type **(1)** complexes. However, due to the enforced *cis* conformation of the chelating phosphine, complexes of the type **(9)** are destabilised, and this pushes the equilibrium to the right {see Scheme 1, (Page 126)}.

Rh(I) complexes are susceptible to oxidative addition, and even dichloromethane has been known to add to $[Rh(dppe)Cl]_2$[9], whilst $[Rh(PEt_3)_2(CO)(CH_2I)(Cl)I]$ is formed from the oxidative addition of CH_2I_2 to $[Rh(PEt_3)_2(CO)Cl]$.[10] It is not unreasonable to assume that chloroform could oxidatively add to complexes similar to **(10)** to form a rhodium (III) species of the type $[Rh(diphos)(CHCl_2)Cl(H)]$ **(11)**. A type **(11)** complex could then eliminate dichloromethane to form complexes of the type $[Rh(diphos)Cl]_2$** **(12)**. This could then lead to the formation of the observed products (see Scheme 1 for the proposed products and reaction pathways). Protonation of type **(12)** complexes gives the hydrido-chloro-rhodium(III) species, of the types **(6)** and **(7)** (see Scheme 1). Alternatively chloroform can oxidatively add to type **(12)** complexes to form saturated Rh(III) alkyl complexes (responsible for the signals ***Zn***), such as $[Rh(diphos)(CHCl_2)Cl_2]$ **(13)** , which can dimerise, and several isomers of the type, *cis* and *trans* $[Rh_2(diphos)_2(CHCl_2)_2(\mu\text{-}Cl)_2Cl_2]$ **(14)** may be present.

The reaction of hydrogen with $[Rh(Boxylyl)(C_7H_8)](BF_4)$ **(5)** in $CDCl_3$ is not quite so simple as those outlined above (see Figures 7 and 8, pages 142 and 143 respectively). The large bite angle and rigid backbone of the phosphine produce significantly more

** This complex may be monomeric or dimeric in solution, see Chapter 7 for further discussion of these species.

complicated NMR spectra. However, these can be understood if the above model is applied and these extra steric factors are taken into account.

A complex of the type $[Rh(diphos)(S)(H)Cl]_2^{2+}$ **(6/7)** forms in solution (phosphorus signal **D4**), but is no longer the major product and the dimer is broken up due to the large steric bulk of the phosphine.

The proton NMR indicates there is one bridging hydride environment and four terminal hydride environments present. The spectra are still broad and it is difficult to relate specific proton peaks to specific phosphorus peaks. Certainly one of the terminal hydrides belongs to species **(6)/(7)**, and from comparison of the proton chemical shift data this could be signal **C3**, which leaves four hydride environments to assign.

Assignment of the remaining signals to specific structures is complicated by the lack of data concerning P-H coupling constants and the large number of phosphorus environments present. However, from the magnitude of $^1J_{Rh-P}$ it is possible to state that, all of the remaining unassigned phosphorus environments are in molecules containing rhodium in the +3 oxidation state. The presence of the bridging hydride signal **C1** could imply the presence of a bridged species of the type $[\{Rh(diphos)\}_2(\mu\text{-}Cl)_2(\mu\text{-}H)H_2]^+$ **(16)** and complexes of this nature have been observed before in iridium phosphine systems.[11] The proton signal **C2** has a very large P-H coupling constant, indicating that it is *trans* to a single phosphine and this could be due to a monomeric form of the dimers of the types **(6)** and **(7)**. Further evidence for an equilibrium of this type is reinforced by the broadening of all of the major phosphorus peaks as the sample is warmed from -50°C to r.t.

Figure 7. Variable Temperature $^{31}P\{^{1}H\}$ NMR Study of the Hydrogenation of [Rh(Boxylyl)(C_7H_8)](BF_4) (5) in $CDCl_3$

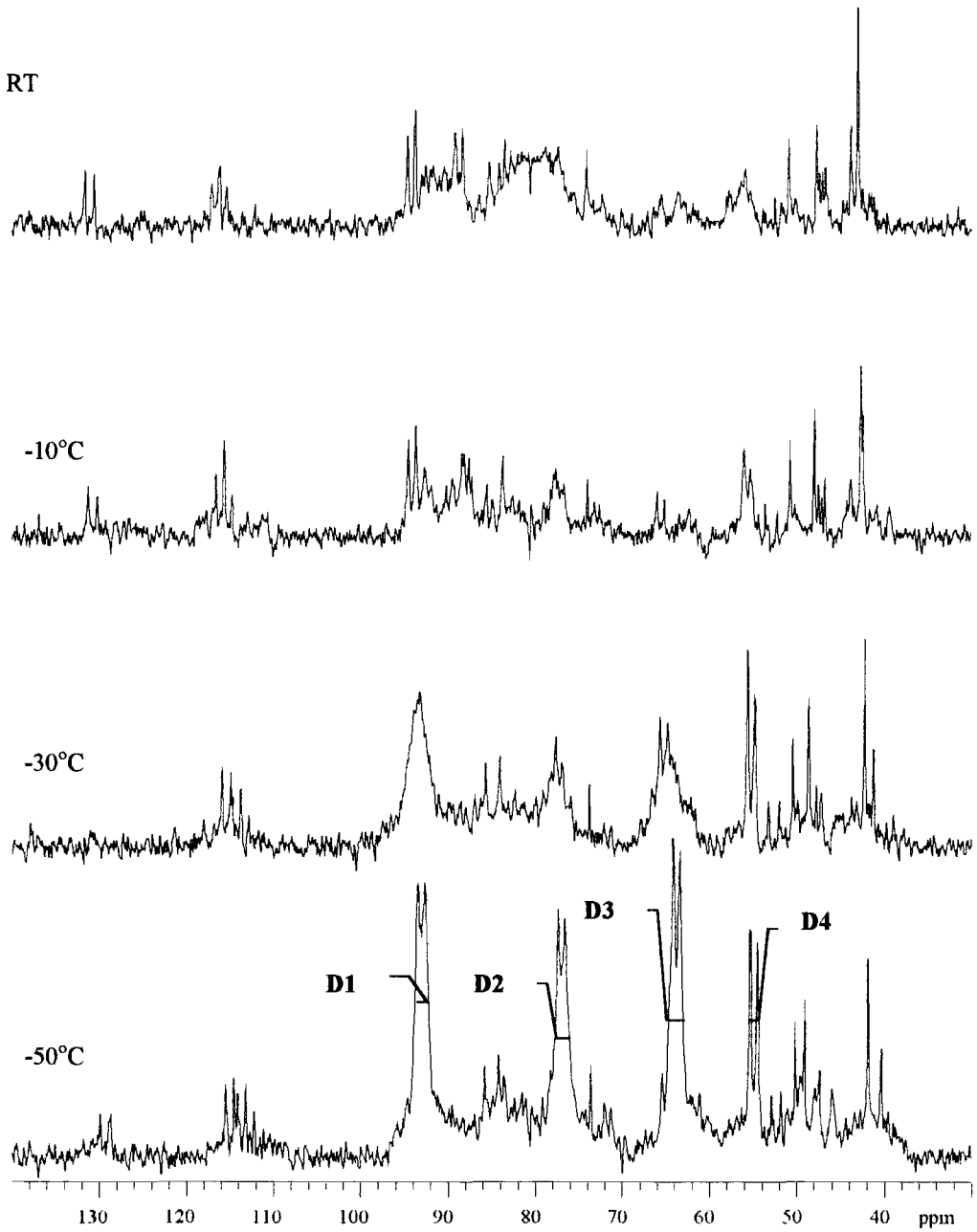

Figure 8. Variable Temperature Proton NMR Study of the Hydrogenation of [Rh(Boxylyl)(C_7H_8)](BF_4) (5) in $CDCl_3$

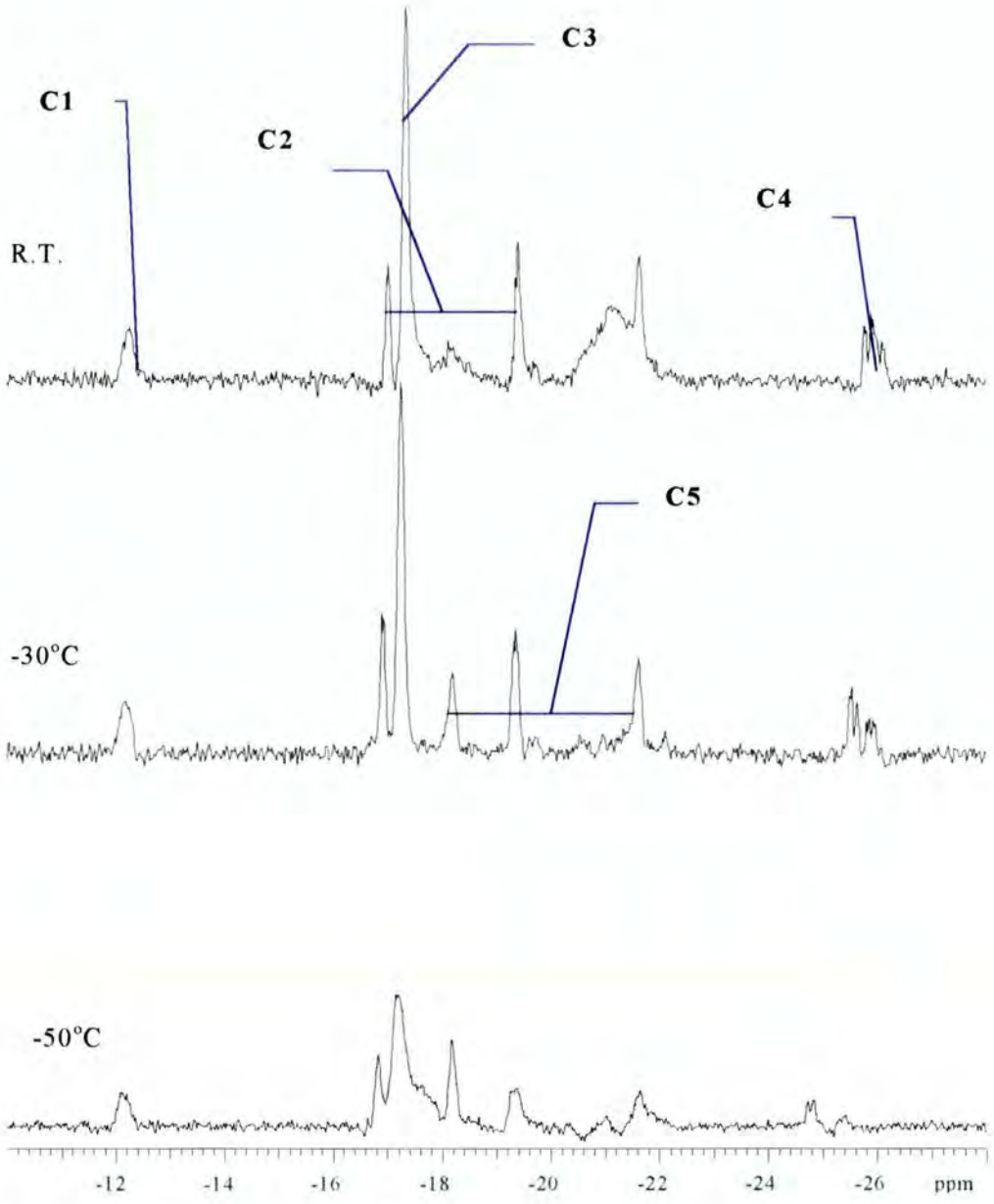

For full listings of VT $^{31}P\{^1H\}$ and ^1H NMR data see Appendix 5

6.3. Experimental

6.3.1. The Reaction of the Hydrogenation Products of [Rh(dBpp)(C_7H_8)](BF_4) (3) in CD_2Cl_2 with HCl

The hydrogenation products of complex **(3)** in CD_2Cl_2 were exposed to a partial vacuum for 30 seconds to remove the excess gaseous hydrogen, before hydrogen chloride gas was introduced. The tube was sealed under $HCl_{(g)}$ (1atm.) and shaken. The phosphorus and proton NMR spectra were essentially invariant with temperature. The only temperature variant signal was a broad hump at ~4.9ppm in the proton NMR which broadened on cooling and moved to higher field. Selective decoupling of the *tert*-butyl protons and other protons associated with the phosphine, followed by observation of the phosphorus NMR at r.t. shows splitting of the phosphorus signal from a doublet, to a doublet of doublets $^1J_{Rh-P}$ 136, $^2J_{P-H}$ 23Hz, indicating only a single proton was attached to each rhodium atom.

$^{31}P\{^1H\}$ NMR (CD_2Cl_2) (r.t.): δ 61.2 (d, $^1J_{Rh-P}$ 136Hz) ppm. ^1H NMR (CD_2Cl_2) (r.t.): δ -18.58 (t d, $^2J_{P-H}$ 11.2, $^1J_{Rh-H}$ 23.6), 1.48 (d, $^3J_{P-H}$ 30.1Hz, PCC$\underline{H}_3$), 1.54 (d, $^3J_{P-H}$ 30.1Hz, PCC$\underline{H}_3$) ppm.

6.3.2. The Reaction of the Hydrogenation Products of [Rh(dBpe)(C_7H_8)](BF_4) in d^8-THF with HCl

The hydrogenation products of complex **(2)** in CD_2Cl_2 were exposed to a partial vacuum for 30 seconds to remove the excess gaseous hydrogen, before hydrogen chloride gas was introduced. The tube was sealed under of $HCl_{(g)}$ (1atm.) and shaken. The phosphorus NMR spectrum revealed there was only a single species present.

$^{31}P\{^1H\}$ NMR (d^8-THF): δ 110.1 (d, $^1J_{Rh-P}$ 136Hz) ppm.

6.3.3. The Reaction of $[Rh(dppe)Cl]_2$ with HCl in d^4-Methanol

$[Rh(dppe)Cl]_2$ (~50mg) was loaded into a resealable NMR tube and the atmosphere replaced with N_2, before CD_3OD (~0.5cm^3) was added under an inert atmosphere. The solution was briefly exposed to a vacuum before HCl was introduced (1atm), and the tube sealed then shaken. The solution changed from orange to yellow in colour and a pale yellow solid was produced. The phosphorus NMR spectrum of the sample showed there was one major species present in solution. $^{31}P\{^1H\}$ NMR (CD_3OD): δ 54.1 (d, $^1J_{Rh\text{-}P}$ 117Hz).

It was not possible to obtain a reasonable proton spectrum due to hydrogen-deuterium exchange between the solvent and the $HCl_{(g)}$ introduced. To overcome this problem, the solid was isolated by filtration and dried in a stream of nitrogen before it was dissolved in $CDCl_3$ and the NMR spectra examined. $^{31}P\{^1H\}$ NMR ($CDCl_3$): δ 51.6 (d, $^1J_{Rh\text{-}P}$ 118Hz) ppm. ^1H NMR ($CDCl_3$): δ -16.6 (br s) ppm.

6.3.4. The Attempted Isolation of the Hydrido-Chloro-Rhodium(III) Products from the Hydrogenation of $[Rh(dBpe)(C_7H_8)](BF_4)$ (2) in $CDCl_3$

Hydrogen was bubbled through a solution of $[Rh(dBpe)(C_7H_8)](BF_4)$ (0.15g) in dichloromethane (15cm^3), the solution turning from orange-red to deep red in colour. The solvent was removed under reduced pressure, and the residue dissolved in chloroform (10cm^3), the solution being filtered to remove a greasy red solid. The solution was reduced in volume to ~5cm^3 and then diethyl ether (10cm^3) was added to precipitate a solid product. After isolation by filtration, the product was dried *in vacuo*. The phosphorus NMR spectrum of the precipitate showed there were two products present, corresponding to peaks **A** and **Z3** (see Figure 4. page 145) which had been observed previously in the direct hydrogenation of complex **(2)** in $CDCl_3$. When the hydrogen atmosphere was removed, peak **A** lost and peak **Z3** gained in intensity. When a hydrogen atmosphere was replaced, peak **A** gained in intensity whilst peak **Z3** lost intensity. Attempts to crystallise the product were unsuccessful

and the hydrogenation product of complex **(2)** decomposed before any further information could be obtained.

6.3.5. Reaction of the Products from the Hydrogenation of Complex (2) in $CDCl_3$ with CCl_4

CCl_4 was added by vacuum distillation to an NMR tube containing the products from the hydrogenation of complex **(2)** in $CDCl_3$. Reaction occurred immediately and the phosphorus NMR spectrum revealed there was only one rhodium species present, and the hydride signal in the proton NMR had disappeared. $^{31}P\{^1H\}$ NMR ($CDCl_3$): δ 110.3 (d, $^1J_{Rh\text{-}P}$ 136Hz) ppm.

6.4. Summary

Hydrogenation of [Rh(diphos)(NBD)](BF_4) (diphos = dBpe, dBpp, dcpe, Boxylyl) in $CDCl_3$ forms hydrido-chloro-Rh(III) complexes of the type $[Rh(diphos)(\mu\text{-}Cl)_2H_2]^{2+}$ from the partial chlorination of the initial hydride products by the solvent, $CDCl_3$. Alternative synthetic pathways to these complexes have been investigated using HCl(g) and a reaction mechanism is proposed. The hydrido-chloro-complexes are fluxional on the NMR timescale and have been studied by VT NMR. During the hydrogenation reaction utilising diphosphines with five membered chelate rings (dcpe, dBpe) several other, non hydride products are produced, which are believed to contain Rh-C bonds. When the Boxylyl ligand is employed, the reaction contrasts with those observed for other diphosphines and this contrast is attributed to the electronic and steric properties endowed by this diphosphine.

6.5. References

[1] See Chapter 2.2
[2] F.A. Cotton, J.L. Eglin, S.J. Kang, *Inorg. Chem.*, **32**, (1993), 2332-2335.
[3] K. G. Moloy, J.L. Peterson, *Organometallics*, **14**, (1995), 2931-2936.
[4] K.G. Moloy, R.W. Wegman, *Organometallics*, **8**, (1989), 2883-2892.
[5] C. Bianchini, A. Meli, F. Laschi, J.A. Ramirez, P. Zanello, A. Vacca, *Inorg. Chem*, **27**, (1988), 4429-4435.
[6] I.R. Butler, W.R. Cullen, B.E. Mann, C.R. Nurse, *J. Organomet. Chem.* **280**, (1985), C47-C50.
[7] N.L. Jones, J.A. Ibers, *Organometallics*, **2,** (1983), 490-494;; D.A. Slack, D.L. Egglestone, M.C. Baird, *J. Organomet. Chem.*, **146**, (1978).
[8] R.R. Schrock, J.A. Osborn, *J. Am. Chem. Soc.*, **98**, (1976),2134-2143
[9] M.D. Fryzuk, *Organometallics*, **10**, (1991), 3767-3769.
[10] R.C. Gash, D.J. Cole-Hamilton, R. Whyman, J.C. Barnes, M.C. Simpson, *J. Chem. Soc. Dalton Trans.*, (1994), 1963-1969.
[11] R.H. Crabtree, H. Felkin, G.E. Morris, *J. Organomet. Chem.*, **141**, (1977), 205-215.

Chapter 7

Oxidative Addition Reactions of Rhodium Chelating Phosphine Species

7.1. Introduction

Rhodium(I)-phosphine complexes readily undergo oxidative addition reactions with organohalide molecules to form Rh(III) alkyl species. Rhodium(III)halo-alkyl species have been previously studied because of their participation in several catalytic processes, including the Monsanto acetic acid process,[1] and the reductive carbonylation of methanol to form ethanal.[2] This chapter is concerned with the synthesis of rhodium(III) alkyl, acyl and alkoxycarbonyl complexes by the oxidative addition of RX to Rh(I) complexes that are potential intermediates in the hydroesterification of alkenes. The reactions reported in this chapter are summarised in Scheme 1 below, together with a summary of the results.

Scheme 1

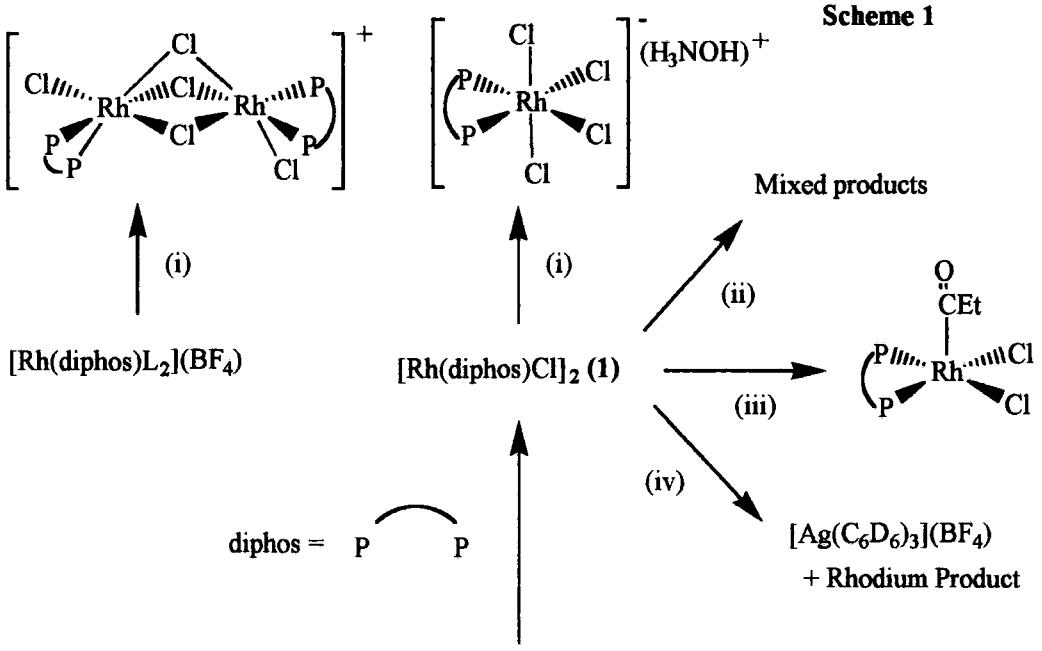

(i) $ClCO_2Me$; (ii) $Br(CH_2)_2CO_2Me$; (iii) ClCOEt; (iv) $EtCl/AgBF_4$.

7.2. Preparation of Precursors

7.2.1. Synthesis of $[Rh(C_8H_{12})Cl]_2$[3] (2)

Freshly distilled cyclooctadiene ($3cm^3$) was added to $RhCl_3.H_2O$ (2.0g, 7. 6mmol) dissolved in degassed 5:1 ethanol:water ($20cm^3$). The solution was heated to 90°C for 18 hours. During this time the solution lightened from red to orange in colour and a yellow precipitate formed. The solid, complex **(2)** was collected by filtration and dried *in vacuo*. 1.79g (96%). Found C, 38.94; H,4.97. $C_{16}H_{24}Cl_2Rh_2$ requires C, 38.95; H, 4.91%.

7.2.2 Synthesis of $[Rh(dppe)Cl]_2$[4] (3)

Complex **(2)** 0.2g (0.41mmol) was dissolved in degassed toluene ($3cm^3$) under nitrogen at 70°C. To the stirred solution was added a solution of dppe (0.32g, 0.80mmol) in toluene ($4cm^3$). The reaction mixture was heated to 125°C for 3hours, and an orange crystalline solid had formed at the end of this time. Hexane ($4cm^3$) was added and the reaction mixture was cooled to -78°C over a period of 1hour. The crystals of complex **(3)** were collected by filtration and washed with hexane ($10cm^3$) and pentane ($10cm^3$) before drying *in vacuo*. Found C, 57.88 H,4.26. $C_{52}H_{48}Cl_2Rh_2$ calculated C, 58.17 ; H, 4.50 %. $^{31}P\{^1H\}$ NMR (C_6D_6): δ 73.2 (d, $^1J_{Rh\text{-}P}$ 198Hz) ppm. ^1H NMR (C_6D_6): δ 8.21-7.21 (m, $C_6\underline{H}_5$, **5H**), 1.96 (d, J 20Hz, P-C$\underline{H}_2$, **1H**). $^{13}C\{^1H\}$ NMR (C_6D_6): δ 28.0 (m, P$\underline{C}H_2$), 133.4 (m, P-C-$\underline{C}$H), 128.8 (m, P-C-CH-$\underline{C}$H), 131.0 (m, P-$\underline{C}$), 128.4 (m, P-C-CH-CH-$\underline{C}$H) ppm.

7.2.3 Synthesis of $[Rh(Boxylyl)Cl]_2$ (4)

The phosphine (0.28g, 7.09mmols), dissolved in dried and degassed diethylether ($15cm^3$), was added to a suspension of $[Rh(ethene)_2Cl]_2$ (0.14g 7.10mmols) in diethylether ($15cm^3$). Upon reaction, the solution became deep olive green. The reaction mixture was filtered, and degassed pentane ($30cm^3$) was added, to precipitate a green solid. The solid was collected by filtration and dried *in vacuo*. This compound was very air sensitive and decomposed in solution to give an orange product, which

hampered purification (yield > 50%). Compound **(4)** forms green solutions in THF, and methanol. The phosphorus NMR signals were broad indicating a degree of fluxionality at r.t. However, a VT $^{31}P\{^1H\}$ NMR study in d^4-methanol displayed only a single doublet even at -90°C. $^{31}P\{^1H\}$ NMR (d^8-THF): δ 80.7 (**5P**, d, $^1J_{Rh-P}$ 204Hz), 62.0 (**P**, br s). (CD_3OD) δ (r.t.) 78.8 (d, $^1J_{Rh-P}$ 209Hz), (-90°C) 78.2 (d, $^1J_{Rh-P}$ 206Hz) ppm. ^1H NMR (d^8 - THF): δ 7.20, 7.40 (**2H**, m, $C_6\underline{H}_4$), 3.46 (**2H**, dd, $^2J_{P-H}$ 8.5Hz, $^3J_{Rh-H}$ 1.7Hz, P-C$\underline{H}_2$), 1.60 (**9H**, d, $^3J_{P-H}$ 15Hz, P-CC$\underline{H}_3$) ppm.

7.3. Oxidative Addition Reactions

7.3.1. Reaction of Complex (3) with Ethylchloride.

$[Rh(dppe)Cl]_2$ (~ 50mg) was placed in an NMR tube equipped with a Young's tap. Deuterobenzene (~0.75cm^3) was added by vacuum distillation. The sample was freeze/thaw degassed and ethylchloride (1atm.) was introduced, and the tube was sealed. No reaction occurred, even when the mixture was heated to 60°C. $AgBF_4$ (excess) was added to the sample under nitrogen. The reaction quickly changed colour from orange to deep red to colourless. The phosphorus NMR of the resulting colourless solution indicated that a single phosphorus containing complex, **(5)** had formed at r.t.. $^{31}P\{^1H\}$ NMR (C_6D_6) δ 71.7 (br d, $^1J_{Rh-P}$170Hz, unidentified rhodium complex **(5)**) ppm.

Large cubic colourless crystals grew from solution. However, they appeared to dissolve in the perfluorinated oil used to protect the crystals from solvent loss and aerial oxidation during X-ray data collection procedures. The X-ray crystal structure was solved by A.S. Batsanov who found a novel silver complex $[Ag(C_6D_6)_3](BF_4)$ (see Appendix 6 for the crystallographic data and discussion).

7.3.2. Reaction of Complex (3) with Propionyl chloride.

Propionyl chloride was vacuum distilled into a degassed deuterobenzene solution of $[Rh(dppe)Cl]_2$ **(3)** in an NMR tube. When the solution was warmed to r.t., the

solution and the precipitate turned pale yellow in colour. The [Rh(dppe)(COEt)Cl_2] **(6)** was isolated by filtration and washed with toluene (1cm^3). Solution NMR studies were performed in nitromethane in which the product had a greater solubility. This reaction was successfully repeated on a larger scale and isolated in 85% yield. Found C, 53.77; H,4.53. $C_{27}H_{29}Cl_2OP_2Rh$ requires C, 53.65; H, 4.84 %. $^{31}P\{^1H\}$ NMR (CD_3NO_2): δ 71.9 (d, $^1J_{Rh\text{-}P}$ 145Hz) ppm. ^1H NMR (CD_3NO_2): δ 7.88 (m, P-C-C*H*), 7.58-7.42 (m, P-C-CH-C*H*-C*H*), 1.54 (t, $^3J_{HH}$ 2.8Hz, $COCH_2CH_3$), 3.38 (q, $^3J_{HH}$ 2.8Hz, $COCH_2CH_3$), 2.4, 3.2 (br m, P-CH_2) ppm. IR (KBr disc) $\nu_{(CO)}$ 1689cm^{-1}(s).

Reaction of [Rh(dppe)(COEt)Cl_2] with $AgBF_4$

Excess $AgBF_4$ was added to a sample of complex **(6)** (~50mg) dissolved in deuterobenzene. This caused the solution to turn yellow in colour and an off white solid was deposited. Phosphorus NMR of the supernatent liquid detected four phosphorus environments. The benzene was removed and the remaining solid dissolved in nitromethane to form a pale yellow solution and a bright white solid. When the phosphorus NMR of the solution was examined it showed a change in the distribution of species and the peaks were sharper.

Peak Positions and Intensities after dehalogenation of Complex (6) with $AgBF_4$

	δ (ppm) (Integral, $^1J_{Rh\text{-}P}$ -Hz)	
	d^6 Benzene	d^3 Nitromethane
A	80.6 (**704P**, br d)	75.8 (**180P**, 123)
B	67.7 (**150P**, br s)	68.4 (**61P**, 107)
C		65.2 **56P**, (106)
D	60.8 (**333P**, br d)	62.7 (**78P**, 104)
E	53.0 (**78P**, 93)	55.1 (**36P**, 91.9)

Reaction of dehalogenated mixture with CO

The sample (from the CD_3NO_2 solution, see above) was freeze thaw degassed and carbon monoxide (1 atm.) was introduced. Reaction occurred very quickly, and the major product identified as [Rh(dppe)$(CO)_2$](BF_4) **(7)** by comparison of the phosphorus NMR and IR spectroscopy with the literature data.[5] $^{31}P\{^1H\}$ NMR

(CD_3NO_2): δ 61.2 (d, $^1J_{Rh-P}$ 123Hz, **(7)**), 57.0 (dd, $^1J_{Rh-P}$ 85Hz, J_{Minor} 4Hz, **(8)**) ppm. IR (KBr disc) $\nu_{(CO)}$ (CD_3NO_2) 2038 and 2088 cm^{-1}. (lit.[5] $^{31}P\{^1H\}$ NMR (CD_3NO_2): δ 62.8 (d, $^1J_{Rh-P}$ 121Hz, **(7)**) ppm. $\nu_{(CO)}$ 2055 and 2100 cm^{-1}).

7.3.3. Reaction of Complex (4) with Propionyl chloride.

Propionyl chloride ($2cm^3$) was added to a solution of complex **(4)** (0.20g, 0.37 mmols) in toluene ($10cm^3$). Over a period of two days the solution slowly changed colour from deep red-green to pale orange, and an orange solid was precipitated. Hexane ($5cm^3$) was added before the solid was isolated by filtration. The solid was washed with hexane before drying *in vacuo*. The phosphorus and proton NMR spectra were broad due to the fluxional nature of the molecule. Found C, 45.52 H, 6.85%. $^{31}P\{^1H\}$ NMR ($CDCl_3$): δ 70.9 (br s) ppm. IR (KBr): 1739 (m), 1640 (m) cm^{-1}.

7.3.4. Reaction of Complex (3) with Methylchloroformate

Complex **(3)** (~50mg, 0.093 mmols) was placed in a re-sealable NMR tube, and CD_3NO_2 and $ClCO_2Me$ were added by vacuum distillation. On the addition of the methylchloroformate a reaction occurred to produce a product soluble in the nitromethane solvent. The phosphorus NMR spectrum indicated a single product was present **(9)**. $^{31}P\{^1H\}$ NMR (CD_3NO_2): δ 78.1 (br d, $^1J_{Rh-P}$ 137Hz, **(9)**) ppm.

After being left to stand for several days, large red crystals suitable for X-ray analysis formed The crystal structure was elucidated by A.S. Batsanov, and found to be the novel complex $(H_3NOH)[Rh(dppe)Cl_4]$ **(10)** (see Figures 1 and 2).[6] The hydroxylammonium ions are hydrogen bonded to the chloride ligands of the anion and there are four cation/anion pairs in the unit cell, in addition to some d^3-nitromethane solvent molecules.

Figure 1. The Crystal Structure of $(NH_3OH)[Rh(dppe)Cl_4]$ (10)

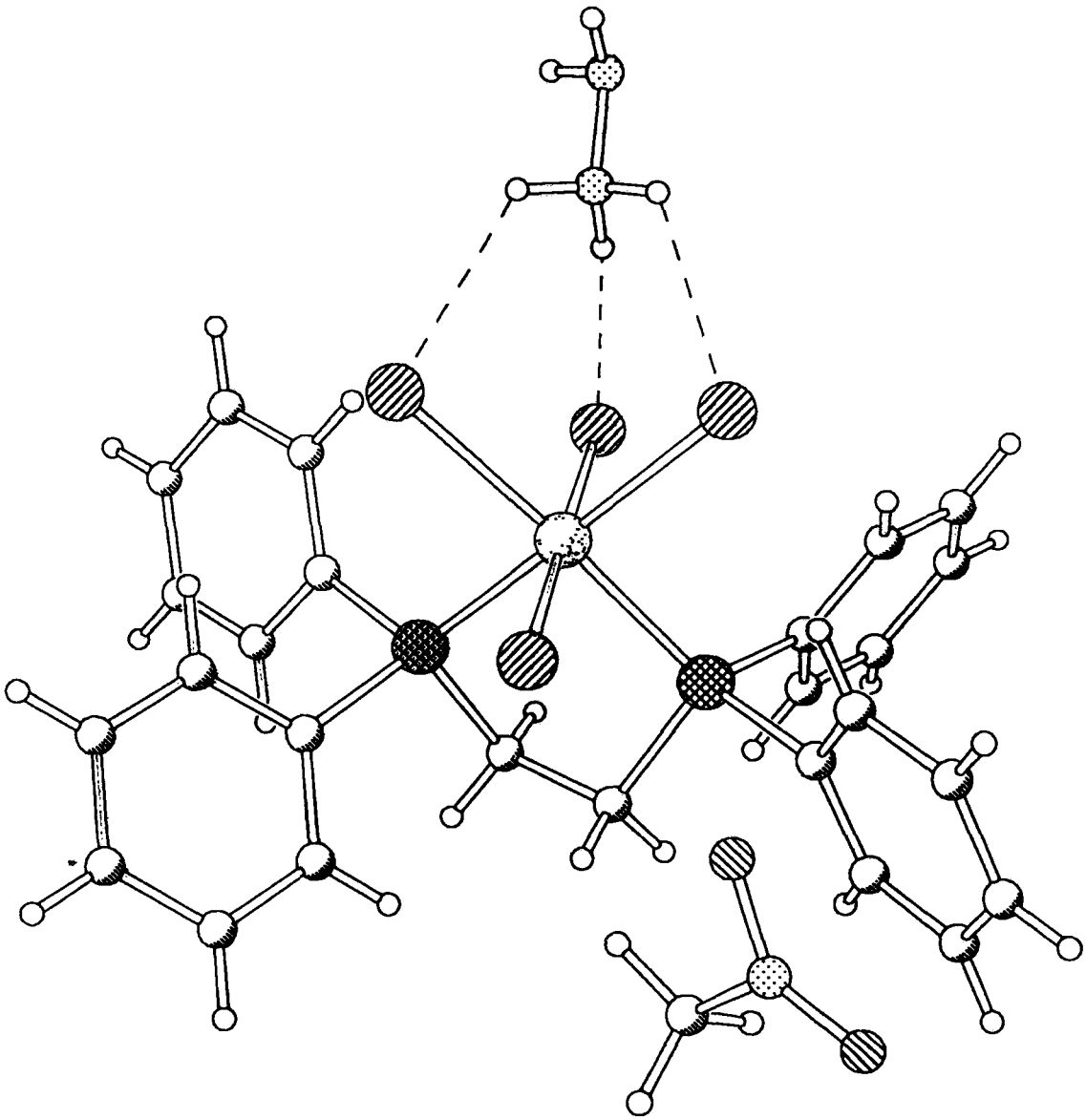

Figure 2. Crystal Packing diagram of the Unit cell for Complex $(NH_3OH)[Rh(dppe)Cl_4]$ (10)

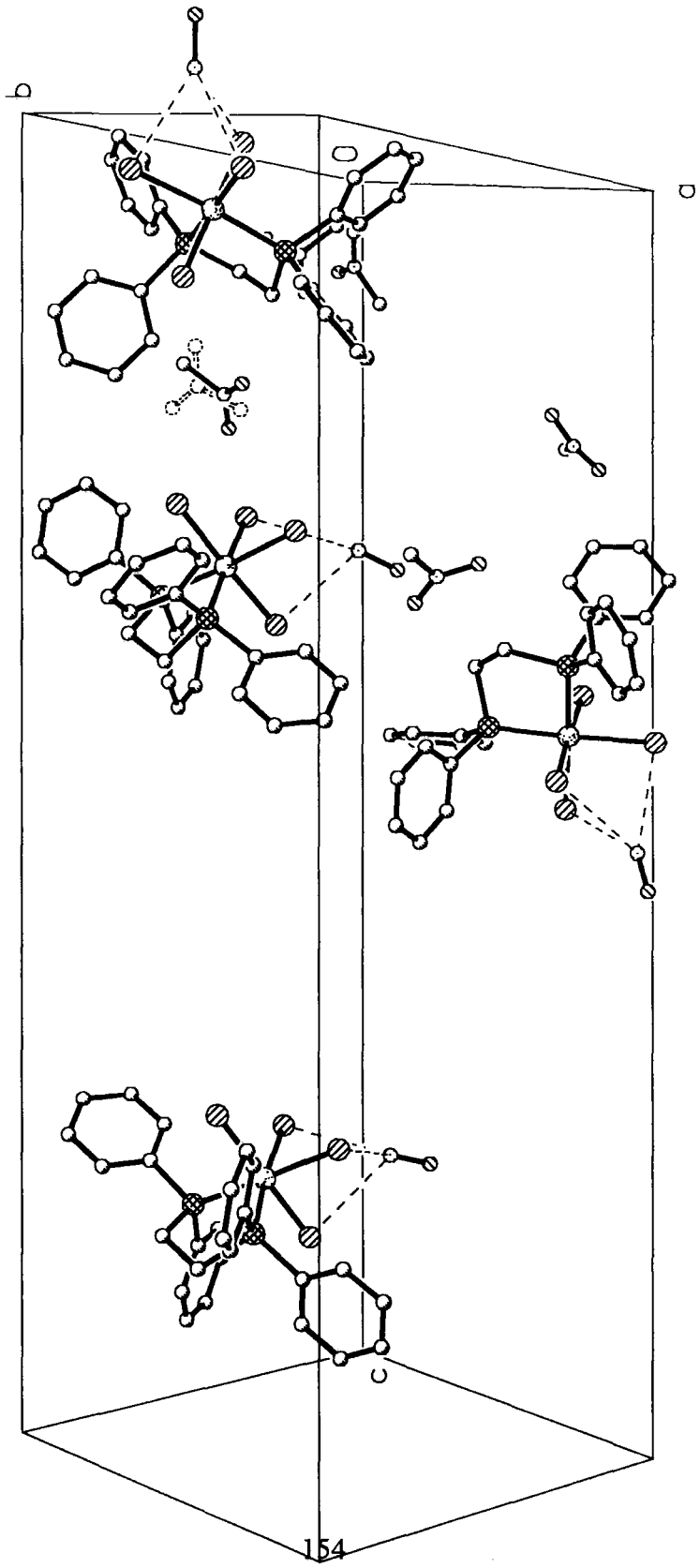

The crystals were removed from the NMR tube, and the phosphorus spectrum re-examined. It was found that in the intervening time period of several months, whilst sealed under N_2, that the phosphorus spectrum had changed completely. There were now three phosphorus environments present, assigned to two new complexes **(11)** and **(12)**. $^{31}P\{^1H\}$ NMR (CD_3NO_2): δ 67.2 (**32P**, dd, $^1J_{Rh\text{-}P}$ 100Hz, **(11)**), 66.0 (**29P**, dd, $^1J_{Rh\text{-}P}$ 99Hz, **(11)**), 55.5 (**38P**,dd, $^1J_{Rh\text{-}P}$ 117Hz, **(12)**) ppm.

7.3.5. Reaction of [Rh(dppe)(C_7H_8)](BF_4) (13) with Methylchloroformate

Hydrogen gas was bubbled through a solution of complex **(13)** (0.2g, 0.029 mmols) in methylchloroformate ($10cm^3$) for thirty minutes. At the end of this time the system was purged with nitrogen and heated to the temperature of refluxing $ClCO_2Me$ for one hour. The solution was filtered and the solvent removed *in vacuo*. The yellow $[Rh_2(dppe)_2Cl_5)](BF_4)$ **(14)** was recrystallised from a $CHCl_3$-CH_2Cl_2-hexane mixture, which produced crystals suitable for X-ray crystallography. The X-ray structure was solved by A.S. Batsanov , and found to be $\{[Rh_2(dppe)_2Cl_5)]\}_2(BF_4)(B_2F_7)$ **(14b)** (see Figure 3). There is a large margin of error on the crystal structure due to its high solvent content and large unit cell (9 solvent molecules and two Rh dimers per unit cell). Cyclic voltammetry of this complex in nitromethane shows a single non reversible oxidation at 0.2412V w.r.t. H/H^+.[†] Found C, 47.42; H, 3.65. $C_{53}H_{50}BCl_5F_4P_4Rh_2.CHCl_3$ requires C, 47.12; H, 3.65%. $^{31}P\{^1H\}$NMR (CD_3NO_2): δ 68.0 (dd, $^1J_{Rh\text{-}P}$ 126, $^3J_{P\text{-}P}$ 8Hz), 65.9 (dd, $^1J_{Rh\text{-}P}$ 126, $^3J_{P\text{-}P}$ 8Hz) ppm. ^1H NMR (CD_3NO_2): δ 3.40 (**4H**, br m, PC$\underline{H}_2$), 8.26-8.22 (**2H**, m,PCC$\underline{H}$), 7.91-7.86 (**2H**, m, PCC$\underline{H}$), 7.76-7.71 (**2H**, m, PCC$\underline{H}$), 7.61-7.38 (**14H**, m, Phenyl $\underline{H}$), 7.3 (C$\underline{H}$$Cl_3$) ppm. $^{13}C\{^1H\}$ NMR (CD_3NO_2): δ 26.9 and 25.3 (dd, $^1J_{P\text{-}C}$ 40, $^2J_{P\text{-}C}$ ~10Hz, P(1)$\underline{C}H_2$), 127.8 (d, $^1J_{P\text{-}C}$ 32Hz, P$\underline{C}$), 128.4 (d, $^1J_{P\text{-}C}$ 38Hz, P$\underline{C}$), 129.1 (d, $^1J_{P\text{-}C}$ 55, P$\underline{C}$), 131.4 (d, $^1J_{P\text{-}C}$ 62Hz, P$\underline{C}$), 130.3 and 129.8 (d, $^2J_{P\text{-}C}$ 13Hz, PC$\underline{C}$H), 130.1 and 129.9 (d, $^2J_{P\text{-}C}$ 11Hz, PC$\underline{C}$H), 133.4 (d, $^4J_{P\text{-}C}$ 3Hz, PCCHCH$\underline{C}$H), 133.7 and 133.9 (d, $^4J_{P\text{-}C}$ 3Hz, PCCHCH$\underline{C}$H), 134.3 and 135.0 (d, $^3J_{P\text{-}C}$ 9Hz, PCCH$\underline{C}$H), 134.5 and 134.6 (d, $^3J_{P\text{-}C}$ 6Hz, PCCH$\underline{C}$H) ppm.

[†] Many thanks to Dr. J.M. Rawson for the cyclic voltammetry measurement.

Figure 3. The Crystal Structure of $\{[Rh_2(dppe)_2Cl_5)]\}_2(BF_4)(B_2F_7)$ (14b)

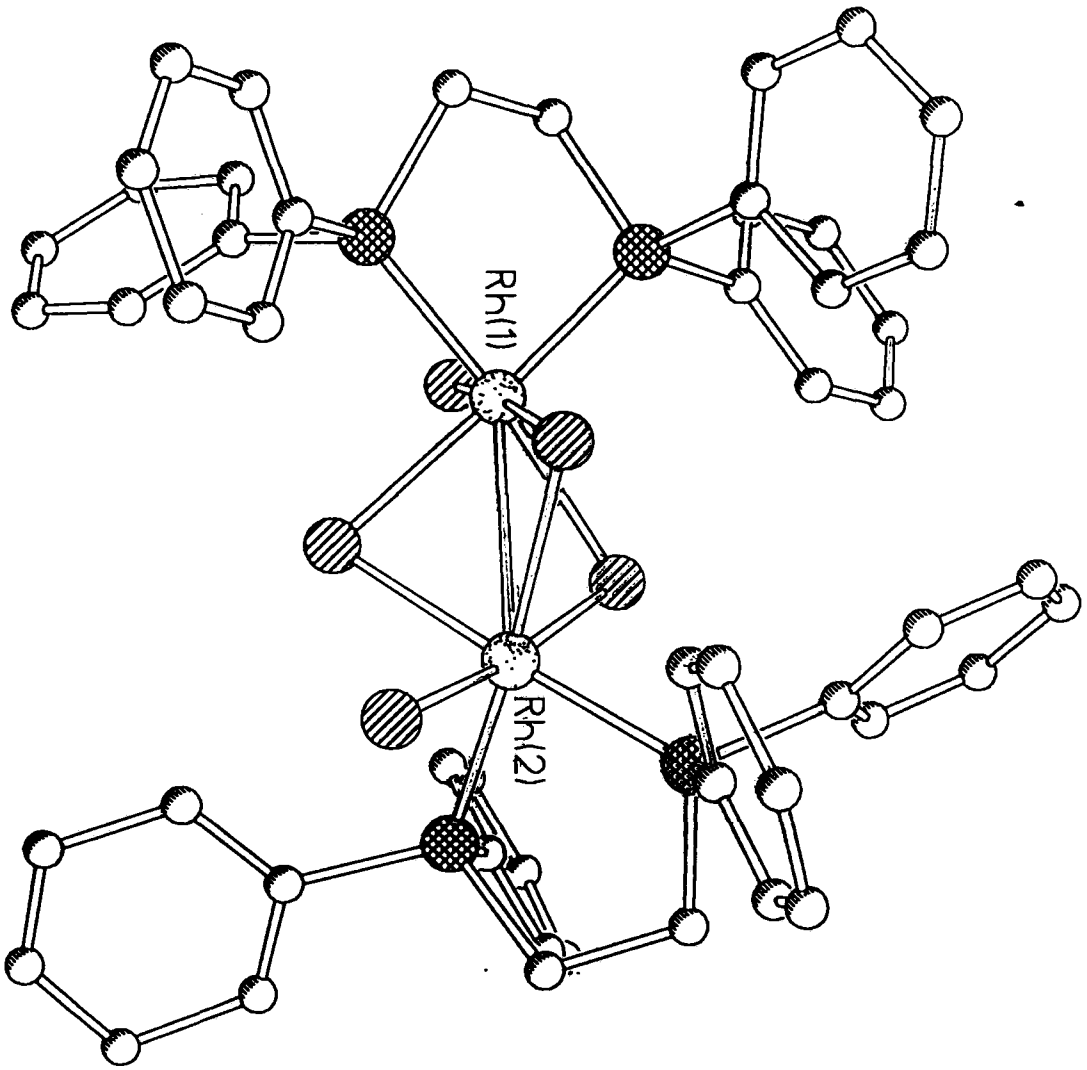

7.3.6. Reaction of $[Rh(dppe)_2]_2(BF_4)_2$ (15) with Methylchloroformate

Hydrogen was bubbled through a solution of complex **(12)** (0.2g) in dichloromethane ($10cm^3$) for ten minutes. The solvent was removed under reduced pressure and methylchloroformate ($10cm^3$) added to the solid, complex **(15)**. The reaction mixture was stirred for 30minutes , before the excess reagent was removed under reduced pressure. The yellow residue was recrystallised from a dichloromethane-hexane mixture. Analysis by phosphorus NMR showed the product to be **(14)** the same product as in 7.3.5.

7.3.7. Reaction of $[Rh(dppe)Cl]_2$ (3) with 3-Bromomethylpropionate

C_6D_6 was vacuum distilled into an NMR tube containing a sample of complex **(3)**. The solution was freeze/thaw degassed, then excess $Br(CH_2)_2CO_2Me$ was introduced by syringe. The reaction was followed throughout by phosphorus NMR. The product was only sparingly soluble and a yellow precipitate was always present. The initial phosphorus spectra showed there were many species present. Heating the mixture to ~66°C quickly reduced the number of species present. After 9 hours there were two signals in the phosphorus NMR due to complexes **(16A)** and **(16B)**. Presumably the system had reached equilibrium and further heating caused an increase in the number of products. $^{31}P\{^1H\}$ NMR (C_6D_6): δ 69.5 (**3P**, d, $^1J_{Rh-P}$ 143Hz, **(16A)**), 68.2 (**1P**, d, $^1J_{Rh-P}$ 128Hz, **(16B)**) ppm.

Repetition in Nitromethane

The reaction was repeated in deuteronitromethane, in an attempt to increase the solubility of the product, unfortunately the increase in solubility was quite small. The reaction was not heated, but left at r.t., and regularly shaken. After 15 days there was one major product, **(16A)**, detected in the phosphorus NMR spectrum, (yield, 75% by integration). $^{31}P\{^1H\}$ NMR (CD_3NO_2) δ 66.6 (d, $^1J_{Rh-P}$ 144Hz, **(16A)**) ppm.

Addition of CO

CO (1 atm.) was added to the products of the reaction of complex **(3)** with $Br(CH_2)_2CO_2Me$ in CD_3NO_2. This reacted slowly, and three signals in the phosphorus NMR were observed. $^{31}P\{^1H\}$ NMR (CD_3NO_2): 64.5 (dd, $^1J_{Rh-P}$ 97, J_2 19Hz), 62.3 (d, $^1J_{Rh-P}$ 115Hz), 63.4 (d, $^1J_{Rh-P}$ 110Hz) ppm.

7.4. Discussion

$[Rh(diphos)Cl]_2$ **(1)** can be made from the substitution reaction of $[Rh(alkene)_2Cl]_2$ with the appropriate diphosphine. The structure and reactivity of these compounds have been found to be dependent on the steric and electronic properties of the diphosphine.[7,8] The dramatic effect of the phosphine can be observed when the dppe and Boxylyl adducts of **(1)** are compared. In solution the dppe adduct **(3)** is pale orange in colour, whilst the Boxylyl adduct **(4)** is olive green. A green colour has been observed previously in this work, in the rhodium-Boxylyl-hydride studies,[‡] and was attributed to a tetrahedral arrangement about the metal. However, unlike the hydride complexes formed in CD_2Cl_2, the chloro complex **(4)** does not show any thermochromism.

7.4.1. Reaction of Acyl halides with Complex (1)

Complex **(1)** has been shown previously[9,10,11]to react with acyl halides to form stable rhodium(III) complexes. The reaction of complex **(3)** with propionyl chloride follows this same pattern and rapidly forms $[Rh(dppe)(COEt)Cl_2]$ **(6)**. The NMR and IR data observed for complex **(6)** indicates it is isostructural with previously reported $[Rh(P)_2(COR)X_2]$[§] type complexes (see Table 2), especially the structurally characterised complex $[Rh(dppp)(COPh)Cl_2]$ which has square based pyramidal geometry with an apical acyl group.[9]

[‡] See Chapter 5.

[§] Where P_2 is either diphos or $2PR_3$.

Table 2. Spectroscopic Data for [Rh(P$_2$)(COR)X$_2$]

Phosphine	R	X	υ(CO)-cm^{-1}	J_{Rh-P} - Hz
dppe	Et	Cl	1689	145
dppp[10]	Me	Cl	1705	136
dppp[9]	Ph	Cl	-	-
$PMePh_2$[11]	C_3H_5	Cl	1687, 1660	143
PPh_3[10]	Me	Cl	-	145

In contrast to complex **(3)**, complex **(4)** reacts slowly with propionyl chloride, and the product formed is fluxional on the NMR timescale (a broad hump in the phosphorus NMR spectrum occurs at 70.9ppm). There is no clearly assignable carbonyl stretch in the IR, due to the presence of the phenyl ring stretches. Indeed, the CHN analyses of this product are much lower than expected for this type of complex, questioning whether the product is an acyl derivative. Further chlorination may have occurred and a rhodium(III)-chloro species, similar to complexes **(10)** or **(14)** formed.

In the presence of $AgBF_4$, complex **(6)** dehalogenates to form several new species which are more soluble in nitromethane than toluene, indicating they are quite polar. If carbon monoxide is added to the system, the dehalogenated products react rapidly to form the very stable complex $[Rh(dppe)(CO)_2](BF_4)$. However, the magnitude of the Rh-P coupling constants (~100Hz) indicates that all the dehalogenated species are Rh(III) complexes. This means a reductive step must occur when the carbon monoxide is added, a potential reaction scheme being shown below.

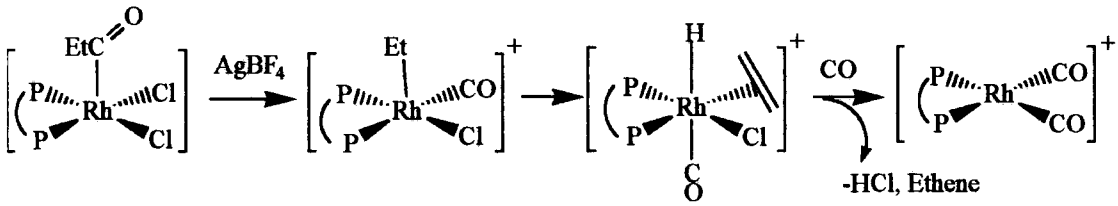

Following the dehalogenation of complex **(6)**, decarbonylation is envisaged, followed by β-hydride abstraction to form a six co-ordinate Rh(III) complex $[Rh(dppe)(ethene)(CO)(H)Cl]^+$. Reductive elimination of HCl will produce a four co-ordinate rhodium(I) complex, $[Rh(dppe)(ethene)(CO)]^+$ which in the presence of carbon monoxide will form $[Rh(dppe)(CO)_2](BF_4)$. This proposed scheme is supported by the reaction of the related complex $[Ir(PMePh_2)_3(COC_3H_5)Cl_2]$ with

excess NH_4PF_6, which forms the co-ordinatively saturated complex *mer*$[Ir(PMePh_2)_3(CO)(C_3H_5)Cl]$.[11]

7.4.2. Reactions of Alkylhalides with $[Rh(dppe)Cl]_2$ (3)

Complex **(3)** does not react with ethylchloride in d^6-benzene even if it is heated to 60°C. However reaction occurs on addition of silver tetrafluoroborate, and the colour of the solution changes from orange, through deep red to colourless, and colourless crystals grow. The phosphorus NMR spectrum of the solution is broad; the large phosphorus chemical shift indicates the phosphine is still chelating to the rhodium, whilst the magnitude of the $^1J_{Rh\text{-}P}$ coupling constant (170Hz) indicates the product is probably a Rh(I) complex. However, the colourless crystals did not contain rhodium, X-ray crystallography identifying them as $[Ag(C_6D_6)_3](BF_4)$ (see Appendix 6 for the crystallographic data), formed from the reaction of the deuterated solvent with the $AgBF_4$ that was added.

Colourless rhodium complexes are quite unusual, and previously observed examples have been Rh(III) hydrido-chloro complexes.[12] Reaction between EtCl and $[Rh(dppe)Cl]_2$ did not occur until silver tetrafluoroborate was added to the mixture; $AgBF_4$ has been previously used in this work to remove halide ions from neutral rhodium complexes. Consequently the product is probably cationic. Since there are silver ions present, which would abstract chloride ions to form a cationic rhodium complex and the phosphorus NMR is broad indicating exchange, the product may be a fluxional, mixed Rh(I)/Rh(III) dimer, with bridging hydride and chloride ligands, such as, $[\{Rh(dppe)\}_2(ethene)(\mu\text{-}H)(\mu\text{-}Cl)_2]^+$, formed *via* β-hydride elimination from the potential alkyl adduct $[\{Rh(dppe)\}_2(\mu\text{-}Et)(\mu\text{-}Cl)_2]^+$, possibly responsible for the transitory deep red colour observed.

The products derived from the reaction of $Br(CH_2)_2CO_2Me$ with complex **(3)** are as elusive as those observed with EtCl. However, $Br(CH_2)_2CO_2Me$ is more reactive than EtCl and reaction occurs slowly at r.t., without the assistance of $AgBF_4$, although the

reaction can be accelerated at elevated temperatures. The major product formed in this reaction appears as a doublet at δ 66.6 ppm (J_{Rh-P} 144Hz) in the phosphorus NMR spectrum. Both the chemical shift and the Rh-P coupling constant are very similar to those of the acyl species [Rh(dppe)(COEt)Cl_2] **(6)** reported in this chapter, indicating a degree of structural similarity. Clearly this species cannot contain an acyl group, but it would be reasonable to assume it is the desired product [Rh(dppe){$(CH_2)_2CO_2Me$}(Cl)Br]. However, if this is square based pyramidal, or octahedral (due to chelation of the alkyl ligand *via* the ester group) then two doublets of doublets should be observed in the phosphorus NMR (due to P *trans* to Cl, and P *trans* to Br). Since this is not observed at r.t., then either the molecule is highly fluxional or the molecule is trigonal bypyramidal with an apical alkyl group. It was not possible to isolate the oxidative addition product either in solution or in the solid state due to additional reaction occurring, as observed in the NMR experiments (see experimental, Section 7.3.7). These additional reactions can be explained in terms of β-hydride elimination from the alkyl group and the production of an alkene (CH_2=$CHCO_2Me$) and a hydride ligand, which may react further. When this mixture of products is exposed to CO (1atm.) several new complexes are formed. The signal at δ 62.3 (J_{Rh-P} 115Hz) ppm in the phosphorus NMR is probably due to the formation of [Rh(dppe)$(CO)_2$](Br), as both the chemical shift and coupling constant compare favourably with those previously reported for [Rh(dppe)$(CO)_2$](BF_4) **(7)** (δ 62.8 {J_{Rh-P} 121Hz) ppm).[8] This Rh(I) complex could easily be formed from the reductive elimination of HCl, or HBr from the above alkene complexes. The nature of the other two products is unclear. However, the Rh-P coupling constants are small indicating they may be hydrido- or alkyl-halo Rh(III) species.

7.4.3. Reaction of Rhodium(I) Complexes with Methylchloroformate

Complex **(3)** reacts quickly with methylchloroformate in d^3-nitromethane, the initial phosphorus NMR data indicates that the desired product [Rh(dppe)$(CO_2Me)Cl_2$] **(9)** has been formed. However, after a few days deep red crystals form due to further chlorination of this adduct by the excess methylchloroformate present, and these were

characterised as $(NH_3OH)[Rh(dppe)Cl_4]$ **(10)**. The structural aspects of complex **(10)** are dealt with elsewhere (see Chapter 9). In the solid state, there are four octahedral rhodium anions in the unit cell, hydrogen-bonding to four hydroxylammonium cations. (See Figures 1 and 2). The solution NMR of complex **(10)** shows there are several species present, designated complexes **(11)** and **(12)**, indicating that complex **(10)** may only be stable in the solid state due to hydrogen bonding interactions. Previous attempts to synthesise complex **(10)** have only met with limited success,[13] and analogues of **(10)** containing different chelating phosphines have only been isolated with very large monomeric or dimeric rhodium cations.[14] For example $[Rh(Btpe)Cl_4]^-$ was isolated as a salt with the cation $[\{Rh(Btpe)Cl\}_2]^{2+}$ from the oxidation of $[Rh(Btpe)(PPh_3)Cl]$ with chloroform.[** 15] In this work $[Rh(dcpe)Cl_4]^-$ was isolated as a salt with $[Rh_2(dcpe)_2Cl_5]^+$ as the cation.[14] Although no phosphorus NMR data is available for the Btpe system, examination of the dcpe complex synthesised in this project (see chapter 8), reveals that it is fluxional in solution due to intermolecular exchange of the halide ligands. In solution the dcpe system decomposes to form several cationic and neutral bridged species such as $[Rh_2(dcpe)_2Cl_5]^+$ and $[Rh_2(dcpe)_2Cl_6]$. Hence it is not unreasonable to assume that the complexes **(11)** and **(12)** are similar to these, being related to $[Rh_2(dppe)_2Cl_5]^+$ and $[Rh_2(dppe)_2Cl_6]$ respectively. However, the Rh-P coupling constants at r.t. for complex **(11)** are ~25Hz smaller than those observed for the authentically prepared $[Rh_2(dppe)_2Cl_5]^+$ **(14)**. This could arise due to interactions of the cationic dimer with the free chloride ions in solution and an average structure being observed.

$[Rh(dppe)(C_7H_8)](BF_4)$ **(13)** reacts with methylchloroformate in the presence of hydrogen to form the novel complex $[\{Rh(dppe)Cl\}_2(\mu\text{-}Cl)_3](BF_4)$ **(14)**,which contains two rhodium(III) units each with a chelating phosphine, a terminal chloride ligand, and three bridging halide ligands (see Figure 3). The phosphorus atoms are in different environments, and this is reflected in the phosphorus NMR where two doublets of

---

** Btpe is 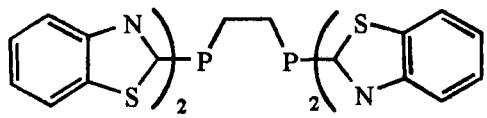

doublets can be observed. These signals are very close together, and in certain solvents can overlap, so the spectrum appears as a broad triplet. In the unit cell there are two rhodium dimers, eleven chlorinated solvent molecules and the counter ions BF_4^- and $B_2F_7^-$ leading to considerable disorder in the crystal. However, it is not clear from elemental analysis whether the unusual counterion $B_2F_7^-$ is present in all crystallites in the bulk sample.[††] Complex **(14)** is isostructural with the pentahydride rhodium(III) dimers observed previously by Kim[16] and Werner.[17] However, complex **(14)** appears to be the first all-halide form of $[Rh_2(diphos)_2X_5]^+$-type complexes containing chelating phosphines. The PEt_2Ph analogue of $[Rh_2(diphos)_2X_5]^+$ has been reported, but not characterised crystallographically.[18]

In an effort to understand the mechanism of the reaction of complex **(13)** with methylchloroformate, the experiment was repeated using $[Rh(dppe)(solvent)_2]^+$ instead. Spectroscopic evidence clearly indicated the product was complex **(14)** implying the reaction did not proceed *via* the chlorination of a rhodium hydride.

There are several possible routes for the reaction, and in Scheme 2, page 164 various possible reactions leading to the products charactersied are outlined. However, the first step must be the oxidative addition of methylchloroformate, $[Rh(dppe)]_2^{2+}$ will react to form a co-ordinatively unsaturated Rh(III) species, such as $[Rh(dppe)(CO_2Me)Cl(Solvent)_2]^+$ **(17)**.

[††] There are still solvent molecules incorporated into the crystal lattice of complex **(14)**, even after drying *in vacuo*. For example non stoicheometric amounts of $CHCl_3$ can be observed in the proton NMR. The presence of the solvent molecules reduces the calculated CHN values for complex **(14)** in a similar way to the presence of $B_2F_7^-$. Consequently the CHN data can be interpreted, within experimental error such that either $B_2F_7^-$ is present or $CHCl_3$ is present.

Scheme2. Proposed Reaction Pathways for the Oxidative Addition of Methylchloroformate to[Rh(dppe)Cl]$_2$ and [Rh$_2$(dppe)$_2$](BF$_4$)$_2$

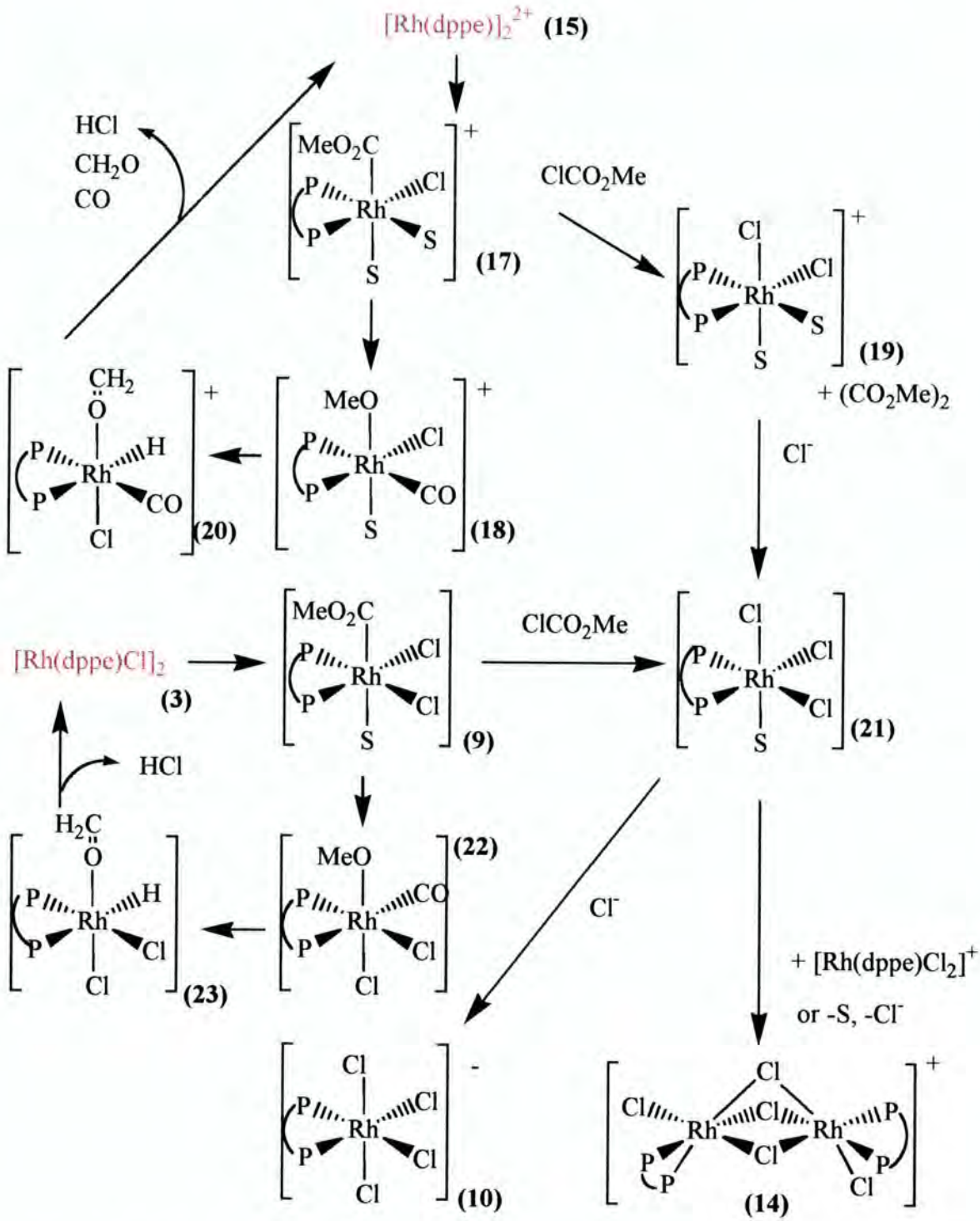

Note Complexes **(9)**, **(10)**, **(21)** (S = MeCN) and **(14)** have been characterised in this study,and complex **(21)** (S = MeCN, MeOH; diphos = dppm)synthesised in other studies

Due to the co-ordinative unsaturation of complex **(17)**, it would not be very stable or long lived; consequently, further reaction could occur, either decarbonylation to form $[Rh(dppe)(CO)(OMe)(Cl)]^+$ **(18)** or reaction with further $ClCO_2Me$ to form $[Rh(dppe)Cl_2]^+$ **(19)** and dimethyloxalate. Complex **(18)** could form a formaldehyde ligand through the dehydrogenation of the methoxy ligand and form a chloro-hydrido-rhodium(III) complex $[Rh(dppe)(OCH_2)(CO)(H)Cl](BF_4)$ **(20)**.
This is unlikely to be very stable and could lose CO, methanal and HCl to regenerate complex **(15)**. The chloride ions produced could react with complex **(19)** to form the neutral species $[Rh(dppe)(Solvent)Cl_3]$ **(21)**. This complex has been previously synthesised in this project when Solvent = MeCN; the dppm analogues (Solvent = MeCN, MeOH) have been reported elsewhere.[19] Alternatively, HCl can be generated by the hydrolysis of methylchloroformate by traces of water present in the solvent.

Possible pathways to the formation of other complexes formed are also outlined in Scheme 2. Reaction of complex **(21)** with complex **(19)** could form the dimeric species complex **(14)**. As described subsequently in Chapter 8, complex **(14)** appears to be more stable than a dimeric form of complex **(21)**. The mechanism for the formation of complex **(14)** can be extended to account for the occurrence of $(NH_3OH)[Rh(dppe)Cl_4]$ **(10)**. In this case the starting molecule is complex **(3)**, and HCl can be generated in a similar manner to that envisaged for complex **(15)**, proceeding *via* complexes $[Rh(dppe)(Solvent)(CO_2Me)Cl_2]$ **(9)**, $[Rh(dppe)(CO)(OMe)Cl_2]$ **(22)**, and $[Rh(dppe)(OCH_2)(H)Cl_2]$ **(23)**. Alternatively, complex **(9)** could react further with methylchloroformate to form complex **(21)**, and dimethyloxalate. Reaction of complex **(21)** with the HCl generated would then form the desired product, complex **(10)**, stabilised by the hydrogen-bonding interactions with the hydroxylammonium ion present.

The H_3NOH^+ cation is formed from the reaction of the methylchloroformate with the CD_3NO_2 solvent (see below). The $ClCO_2Me$ reacts with the nitronic acid form of the nitroalkane to liberate HCl and form a nitronic ester which is not very stable and

decomposes to form an oxime. The oxime may then be hydrolysed to hydroxylamine by traces of water present or methanol (from the hydrolysis of the methylchloroformate) in a similar manner to the acid catalysed Meyer[20] reaction to form an aldehyde (or an acetal if hydrolysed by methanol).[21]

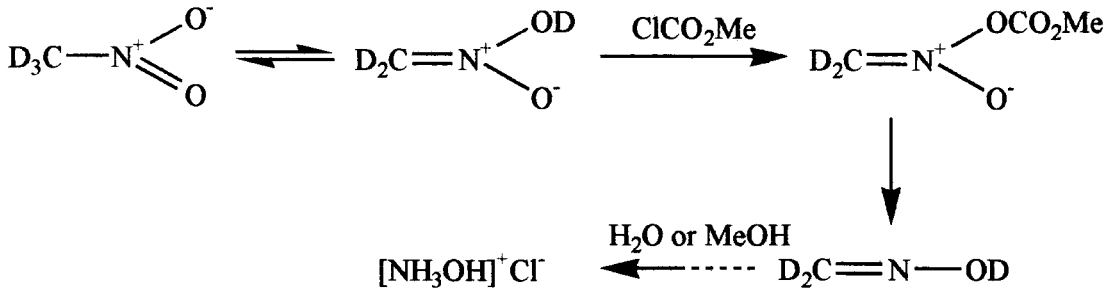

7.5. Summary

The complexes $[Rh(dppe)Cl]_2$ and $[Rh(Boxylyl)Cl]_2$ have been synthesised and their reactions with RX compounds investigated (RX = EtCOCl, EtCl, $Br(CH_2)_2CO_2Me$, $ClCO_2Me$). The oxidative addition of EtCOCl to $[Rh(dppe)Cl]_2$ produces the expected Rh(III) acyl. It was not possible to isolate rhodium products from the reactions with $Br(CH_2)_2CO_2Me$ and EtCl. The reaction with EtCl did not occur until $AgBF_4$ was added, at which point the novel silver complex $[Ag(C_6D_6)_3](BF_4)$ formed. Addition of excess $ClCO_2Me$ in d^3-nitromethane led to the formation of the novel hydrogen-bonded complex $(H_3NOH)[Rh(dppe)Cl_4]$, which was characterised by X-ray crystallography. However, VT NMR investigations reveal that it is not stable in solution and rapid equilibria are established by the loss of chloride ligands between dimeric, chloride bridged Rh(III) neutral and cationic species. Repeating the reaction of $ClCO_2Me$ with $[Rh(dppe)(C_7H_8)](BF_4)$ led to the formation of the related species $[Rh_2(dppe)_2Cl_5](BF_4)$ which was characterised by X-ray crystallography. A reaction mechanism has been proposed for the formation of $[Rh_2(dppe)_2Cl_5](BF_4)$ and $(H_3NOH)[Rh(dppe)Cl_4]$.

7.6. References

[1] R.H. Crabtree, "The Organometallic Chemistry of the Transition Metals", J. Wiley and Sons Interscience, Chichester, 1988.
[2] K.G. Moloy, and R.W. Wegman, *Organometallics*, **8**, (1989), 2883-2892.
[3] G. Giordano, and R.H.Crabtree, *Inorganic Synthesis*, (1991), **volume XIX,** 218
[4] M.D. Fryzuk, *Organometallics* **7**, (4), (1988), 936-945
[5] D.P. Fairlie, B. Bosnich, *Organometallics*, **7**, (1988), 936-945
[6] See Chapter 9 for a full crystallographic description.
[7] P. Hoffmann, C. Meier, U. Englert, M.U. Schmidt, *Chem. Ber.* , **125**, (1992), 353-365.
[8] P. Hoffmann, C. Meier, W. Hiller, M. Heckel, J. Reide, M.U. Schmidt, *J. Organomet. Chem* , **490**, (1995), 51-70.
[9] M.F. McGuiggan, D.H. Doughty, L.H. Pignolet, *J. Organomet. Chem.*, **185**, (1980), 241-249.
[10] D.A. Slack, D.L. Egglestone, M.C. Baird, *J. Organomet. Chem.* , **146**, (1978), 71-76
[11] N.L. Jones, J.A. Ibers, *Organometallics*, **2**, (1983), 490-494.
[12] B.R. James, D. Mahajan, *Can. J. Chem.* , **58**, (1980), 996-1004
[13] R.A. Cipriano, L.R. Hauton, W. Levason, D.Pletcher, N.A. Powell, M. Webster, *J. Chem. Soc. Dalton Trans.* , (1988), 2483-2490.
[14] See Chapters 8 and 9
[15] F. Mohammad, F.M. Al-Dulaymni, P.B. Hitchcock, R.L. Richards, *J. Organomet. Chem.* , **338**, (1988), C31-C34.
[16] T. J. Kim, *Bull. Korean Chem. Soc.* , **11**, (1990), 134-139.
[17] J. Wolf, O. Nurnberg, M. Schafer, H. Werner, *Z. Anorg. Allg. Chem.* , **620**, (1994), 1157-1162.
[18] E.B. McAslan, T.A. Stephenson, *Inorg. Chim. Acta*, **96**, (1985), L49-L51;J.A.S. Duncan, T.A. Stephenson, M.D. Walkinshaw, D. Hedden, D.M. Roundhill, *J. Chem. Soc. Dalton. Trans.*, (1984), 801-807
[19] F.A. Cotton, K.R. Dunbar, C.T. Eagle, L.R. Falvello, S.J. Kang, A.C. Price, M.G. Verbruggen, *Inorg. Chim. Acta*, **184**, (1991), 35-42.
[20] H. Feuer, "The Chemistry of the Nitro and Nitroso Groups: Part 1", J. Wiley and Sons, Interscience, London, 1969.
[21] S. Patai, "The Chemistry of the Functional Groups: Supplement F, The Chemistry of Amino, Nitroso, and Nitro Compounds, and their Derivatives", J. Wiley and Sons, Interscience, Chichester, 1982.

Chapter 8

The Synthesis and Reactivity of Rh(III) Compounds Containing Chelating Phosphines and Halide Ligands

8.1. Introduction

Several rhodium(III) halide complexes containing chelating phosphines have been synthesised by the oxidative addition of methylchloroformate to rhodium(I) complexes and reported in Chapter 7. In this chapter, the synthesis of these species directly from rhodium(III)chloride is explored and some of their reaction chemistry is examined. The reactions presented here are summarised in Scheme 1 below.

Scheme 1

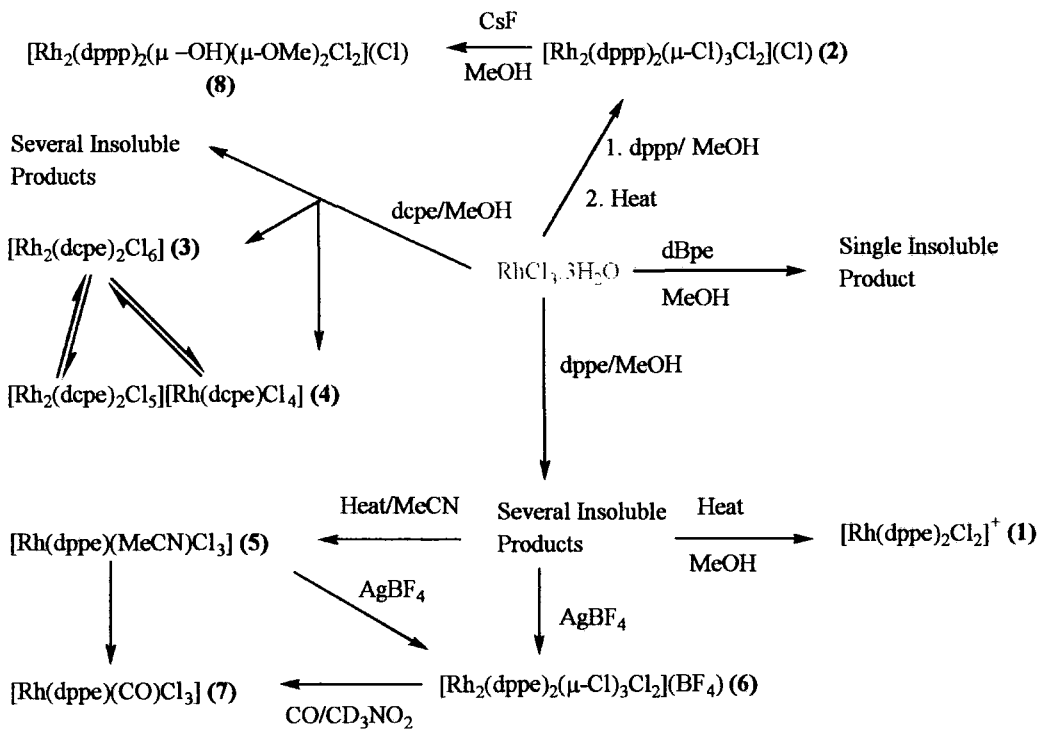

8.2. The Reaction of $RhCl_3.3H_2O$ with Chelating Phosphines.

8.2.1. Reaction with 1,2-Bis(diphenylphosphino)ethane (dppe)

Dppe (0.45g, 1.13 mmols) dissolved in methanol ($45cm^3$) was slowly added to a solution of $RhCl_3.3H_2O$ (0.30g, 1.14 mmols) in methanol ($10cm^3$). As the phosphine was added the solution lightened from deep red to pale peach in colour, and a salmon coloured solid precipitated from solution. The precipitate was isolated by filtration, washed with methanol ($5cm^3$), and dried *in vacuo*. The solid was found to be very insoluble in all solvents tried, and contained a mixture of complexes, making further purification and characterisation problematic. ^{31}P CP MAS NMR:[1] δ 48.3, 36.2, 7.9 ppm. Derivatisation of the insoluble product is discussed later in section 8.3.1.

Thermodynamic Equilibration

The salmon solid was heated in refluxing methanol for one hour; it slowly dissolved to give a clear orange solution. On cooling the salmon solid did not reappear and the solution was filtered. Analysis by phosphorus NMR indicated the presence of several species in the reaction mixture. The solvent was reduced to approximately $10cm^3$, and a yellow precipitate formed. The solid was washed with methanol ($5cm^3$) and dried *in vacuo*. After recrystallising from chloroform-diethylether, a single product, $[Rh(dppe)_2Cl_2]Cl$ **(1)**, was detected by proton, carbon and phosphorus NMR. This corresponded to the major product prior to purification (54% by phosphorus NMR). $^{31}P\{^1H\}$ NMR ($CDCl_3$): δ 37.1 (d, $^1J_{Rh\text{-}P}$ 84Hz, **(1)**) ppm. ^1H NMR ($CDCl_3$): 7.18-7.51 (m, P-$C_6\underline{H}_5$); 3.12 (m, P-$C\underline{H}_2$) ppm. $^{13}C\{^1H\}$ NMR ($CDCl_3$): δ 24.6 (m, P-$\underline{C}H_2$), 124.1, 127.4, 130.24 (s, P-C_6H_5) ppm.

Reaction In the Presence of $BzEt_3NCl$

The reaction of $RhCl_3.3H_2O$ and dppe in methanol was repeated in the presence of four equivalents of benzyltriethylammonium chloride in an effort to prepare the complex $(BzEt_3N)[Rh(dppe)Cl_4]$. Analysis of the reaction mixture by phosphorus NMR indicated the rhodium containing products were identical to those observed in the

absence of the alkyl-ammonium salt. When the mixture was heated in refluxing methanol, the products were identical by phosphorus NMR to those obtained after heating in the absence of the alkyl-ammonium salt.

8.2.2. Reaction with 1,3-Bis(diphenylphosphino)propane (dppp)

Dppp (1.07g, 2.59 mmols) dissolved in methanol (125cm^3) was slowly added to a solution of rhodium(III) chloride (0.70g, 2.60 mmols) in methanol (10cm^3). The solution was left to stir overnight, then heated to the temperature of refluxing methanol for one hour, causing the yellow solid produced previously to dissipate. The reaction solution was concentrated under reduced pressure to ~10cm^3. Diethylether (20cm^3) was added to the reaction mixture and a solid precipitated. The solution was then filtered. The solid was suspended in methanol and heated at the methanol reflux temperature for one hour before cooling and filtering. Addition of diethylether to the methanol solution precipitated a yellow solid, found by phosphorus NMR to be a single product **(2)**. After leaving the supernatant liquor to stand, crystals formed. These were suitable for X-ray diffraction and the structure was determined by A.S. Batsanov[2], and found to be $[Rh_2(dppp)_2(\mu\text{-}Cl)_3Cl_2](Cl).4(CH_3OH).3(H_2O)$ **(2)** (see Figure 1, page 171).[2] Found C, 51.14; H, 3.97. $C_{55}H_{56}Cl_6OP_4Rh_2$ requires C, 51.47; H, 4.63%. $^{31}P\{^1H\}$ NMR (CH_3OH): δ 24.8 (d, $^1J_{Rh\text{-}P}$ 116Hz) ppm.

Reaction with 1,2-Bis(di-*tert*-butylphosphino)ethane (dBpe)

DBpe (0.54g, 1.70 mmols) dissolved in degassed diethylether (40cm^3), was slowly added to a solution of $RhCl_3.3H_2O$ (0.45g, 1.70mmols) in degassed methanol (50cm^3). Upon contact of the two solutions a light brown precipitate formed and a deep red supernatant liquid remained. The reaction was then left to stir overnight. At the end of this time the reaction solution was reduced in volume (~10cm^3) and filtered. The brown precipitate was washed with methanol (5cm^3) and dichloromethane (5cm^3) before drying *in vacuo*. The unidentified solid was found to be *circa* 98% pure by integration of the phosphorus CP MAS NMR. ^{31}P CP MAS NMR: δ 40.9 (**98P**, s), 118.7 (**2P**, s) ppm.

Figure 1. Crystal Structure of $[Rh_2(dppp)_2(\mu\text{-}Cl)_3Cl_2](Cl).4(CH_3OH).3(H_2O)$ (2)

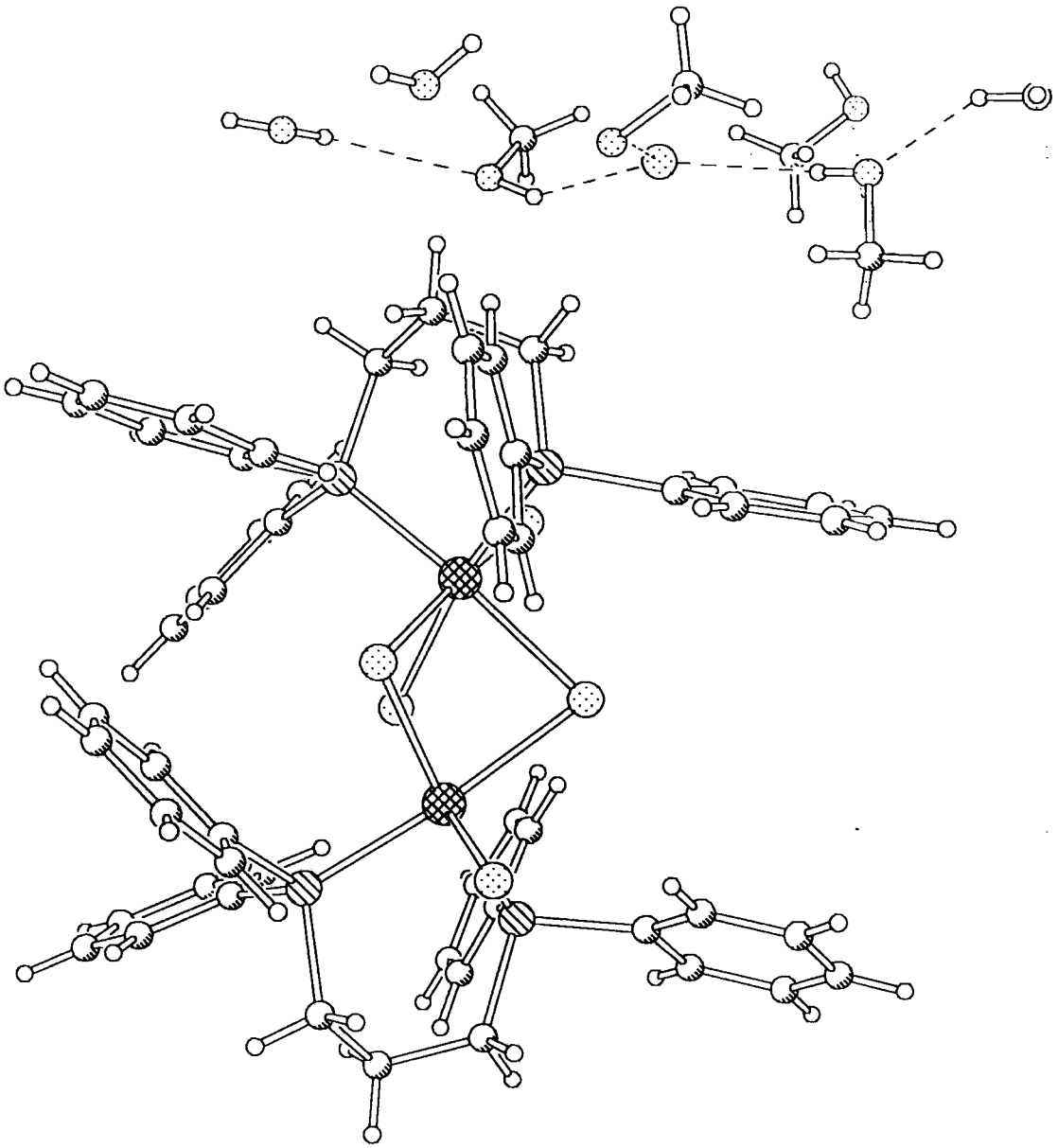

The filtrate was reduced to dryness under reduced pressure and washed with dichloromethane. The phosphorus NMR spectrum of the CH_2Cl_2 extract showed that there were several products present. Diethylether was added and large crystals grew. X-ray analysis of the crystals revealed them to be the phosphine oxide $[Bu^t_2P(O)(CH_2)_2P(O)Bu^t_2]$. $^{31}P\{^1H\}$ NMR ($CDCl_3$): δ 65.8 (s) ppm.

8.2.4. Reaction with 1,2-Bis(dicyclohexylphosphino)ethane (dcpe)

Dcpe (0.45g, 1.04 mmols) dissolved in degassed diethylether ($40cm^3$) was slowly added to a solution of $RhCl_3.3H_2O$ (0.27g, 1.04mmols) in degassed methanol ($50cm^3$). Upon contact of the two solutions a brown precipitate formed and an orange supernatant liquid remained. The mixture was stirred overnight before the solution was reduced in volume to ~$10cm^3$ and filtered. The brown precipitate (fraction 1) was washed with methanol ($5cm^3$), and dichloromethane ($10cm^3$) (which dissolved some of the solid (fraction 2)) before drying *in vacuo*. The solid was found to be insoluble in common organic solvents in a similar manner to the product from the reaction with dppe (section 8.2.1). Solid state phosphorus NMR indicated there were several species present. $^{31}P\{^1H\}$ MAS NMR: δ 82.5, 54.3, 19.6 ppm.

Phosphorus NMR indicated that fraction 2 contained a single rhodium containing species **(3)**. $^{31}P\{^1H\}$ NMR (CH_2Cl_2): δ 78.8, (d, J_{Rh-P} 118Hz, **(3)**) ppm.
The filtrate (fraction 3) was taken to dryness *in vacuo* and the methanol replaced with dichloromethane to give a deep red coloured solution. This was then filtered and the solution allowed to slowly evaporate, producing deep red crystals. Crystals suitable for X-ray analysis were identified, and the structure was elucidated by A.S Batsanov.[2] This indicated that the compound was $[Rh_2(dcpe)_2Cl_5][\ Rh(dcpe)Cl_4]$ **(4)** (see Figures 2 and 3, pages 173 and 174 respectively).

The crystals showed some solubility in deuterochloroform, but at room temperature the signals were broad. A V.T. $^{31}P\{^1H\}$ NMR experiment was performed (see Figure.4, page 175), and the results are summarised in Table 1.

Figure 2. The Crystal Structure of the Cation $[Rh_2(dcpe)_2Cl_5]^+$ (4).

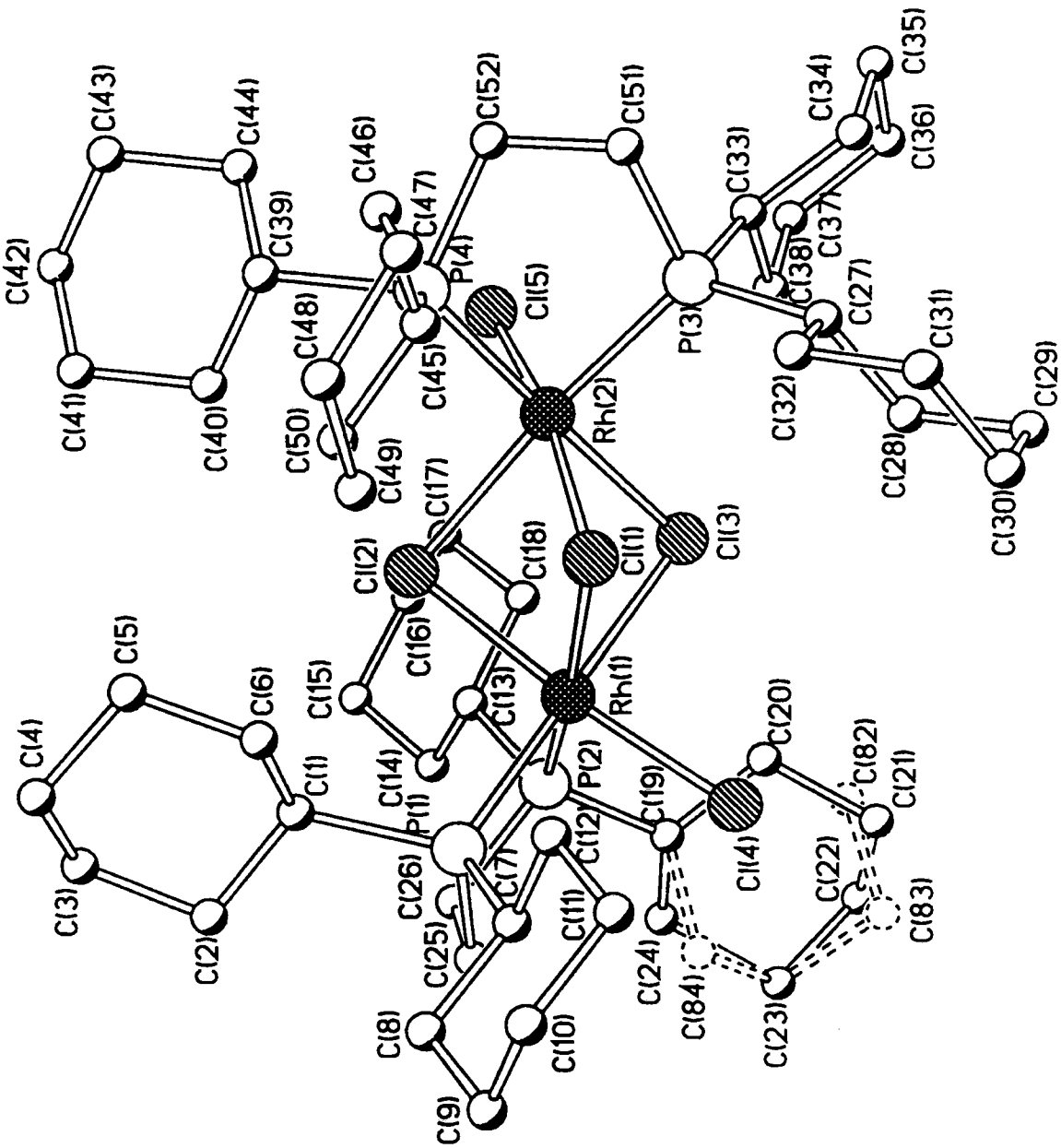

Figure 3. The Crystal Structure of the Anion $[Rh(dcpe)Cl_4]^-$ (4).

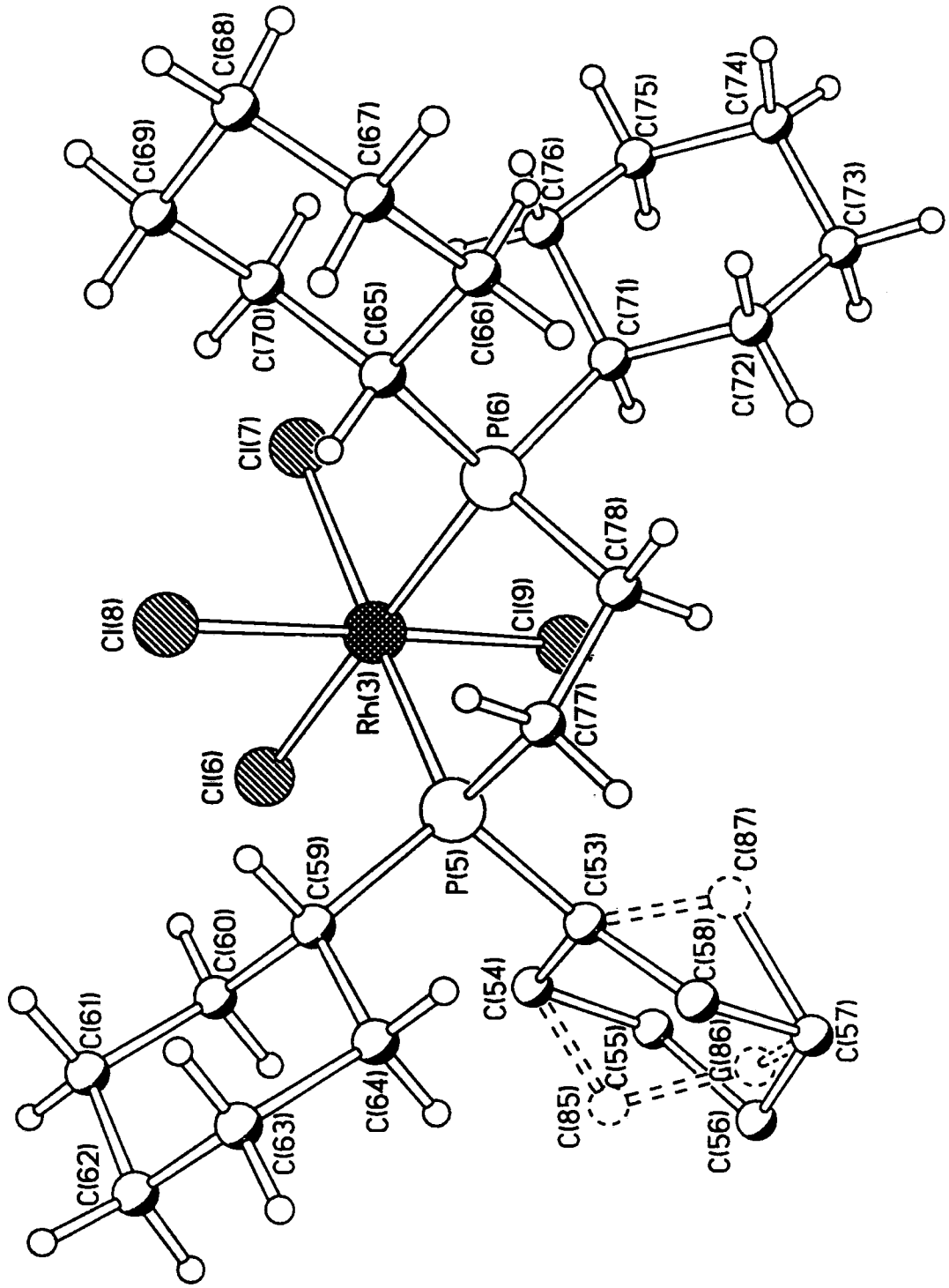

Figure 4. VT $^{31}P\{^{1}H\}$ NMR Specta of $[Rh_2(dcpe)_2Cl_5][Rh(dcpe)Cl_4]$ (4) in $CDCl_3$

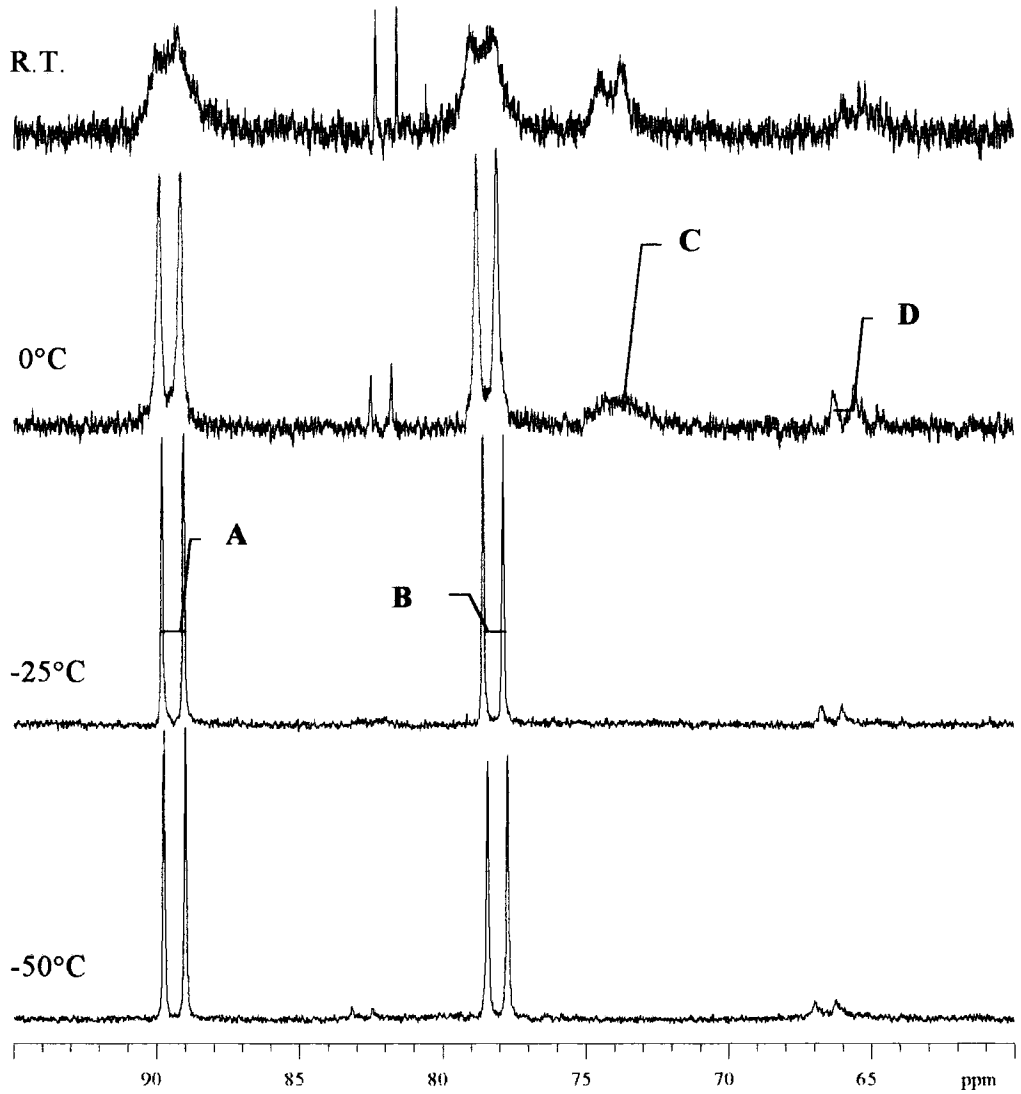

Table 1 VT $^{31}P\{^{1}H\}$ NMR Data for Complex (4) in $CDCl_3$

	δ - ppm (J, Hz)			
peak	RT	0°C	-25°C	-50°C
A	89.4 (**77P**, br s)	89.5 (**58P**, br d,122)	89.4 (**160P**, dd, 120)	No Change (**86P**)
B	78.7 (**79P**, br d, 118)	78.5 (**60P**, d, 117)	78.2 (**168P**, dd, 116)	No Change (**89P**)
C	74.2 (**37P**, br d, 123)	73.6 (**16P**, br s)	Disappeared	Disappeared
D	65.0 (**23P**, br s)	66.0 (**6P**, d, 123)	66.4 (**36P**, br dm, 123)	66.6 (**24P**, br d, 121)

8.3. Derivatisation of the Products from Reaction 8.2.

8.3.1. Synthesis of [Rh(dppe)(MeCN)Cl_3] (5)

The insoluble product from reaction 8.2.1 was heated in refluxing MeCN until the supernatant liquid and any remaining solid had turned from salmon to yellow in colour. The supernatant liquid was removed by filtration, and when left to stand, cubic crystals grew. These were analysed by X-ray crystallography by C.W. Lehmann, and found to be [(dppe)Rh(MeCN)Cl_3]. However, the crystal structure determination was of insufficiently good data (R= 18%) to determine any more than the relative orientation of the ligands (see Figure 5, page 177), and confirm the identity of the compound. Due to their relative insolubility the crystals were characterised by elemental analysis and solid state phosphorus NMR. Two phosphorus environments were identified in the ratio 1:1 due to the magnetic inequivalence of the phosphorus atoms in the unit cell. Found C, 51.99; H, 4.24; N, 2.85. $C_{28}H_{27}Cl_3NP_2Rh$ requires C, 52.05; H, 4.29; N,3.14%. CP MAS ^{31}P NMR: δ 52.0 (s), 48.4 (s). $\nu_{(CN\ co\text{-}ordinated)}$ 2329, 2302; $\nu_{(CN\ free)}$ 2251 cm^{-1}.

8.3.2. Attempted Syntheses of [Rh_2(dppe)$_2$(μ-Cl)$_3Cl_2$](BF_4) (6)

The product from Section 8.2.1 (0.20g) was stirred as a slurry in methanol (50cm^3), and then $AgBF_4$ (0.5 mole equivalents, calculated assuming the molecular formula of [Rh(dppe)(MeOH)Cl_3]) was added and a white precipitate formed. The reaction mixture was filtered to leave a clear orange solution. The methanol was removed under reduced pressure, and the product dried *in vacuo*. The phosphorus NMR of the reaction mixture indicated the desired product, **(6)** was present to the extent of 25% (by integration). The product was isolated by fractional crystallisation from dichloromethane-hexane and shown to be identical with the authentic material.

Figure 5. The Crystal Structure of [Rh(dppe)(MeCN)Cl_3] (5)

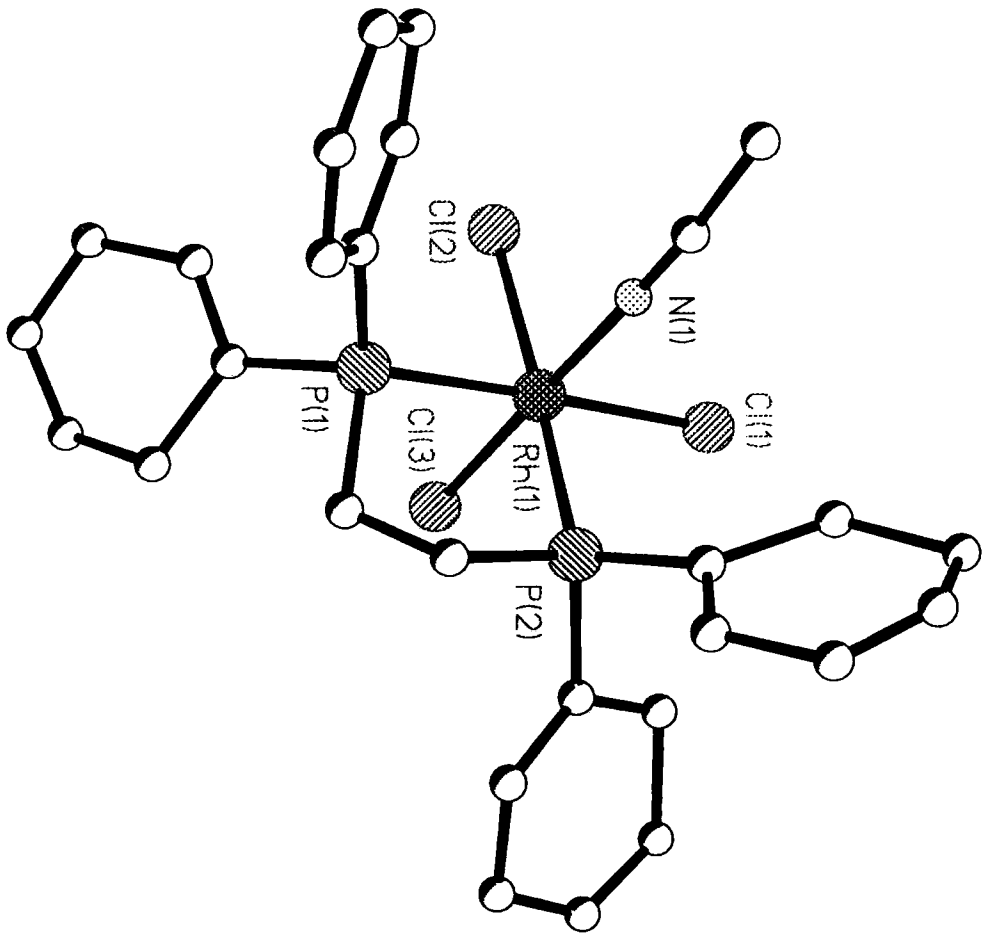

Using [Rh(dppe)(MeCN)Cl_3] (5) and $AgBF_4$

$AgBF_4$ (0.03g) was added as a solid to a solution of complex **(5)** (0.11g, 0.17mmols) in dichloromethane ($20cm^3$). The slurry was then stirred in the dark for one hour, and then was filtered to produce a yellow solution. The volume of the solution was reduced, under reduced pressure to ~ $5cm^3$, and the phosphorus NMR obtained. Comparison of the phosphorus NMR with that of an authentic sample of complex **(6)** (previously prepared) indicated that it was only 50% pure. The other components could not be identified.

8.3.3. Synthesis of [Rh(dppe)(CO)Cl_3] (7)

From [Rh_2(dppe)$_2Cl_5$](BF$_4$) (6)

Complex **(6)** (~50mg) dissolved in CD_3NO_2 ($0.5cm^3$), was freeze/thaw degassed twice and CO gas was introduced to one atmosphere. The complex reacted over a period of days and pale yellow crystals of [Rh(dppe)(CO)Cl_3] formed. The crystals, suitable for X-ray crystallography were analysed by C. W. Lehmann. (see Figure 6, page 179).[2] Found C, 47.43; H, 3.57; . $C_{27}H_{24}Cl_3OP_2Rh$ requires C, 47.92; H, 3.58%. $\nu_{(CO)}$ (s) $2100cm^{-1}$. $^{31}P\{^1H\}$ NMR (CD_3NO_2): δ 56.4 (d, $J_{Rh\text{-}P}$ 99Hz) ppm.

Attempted Synthesis from [Rh(dppe)(MeCN)Cl_3] (5)

Carbon monoxide was bubbled through a nitromethane ($20cm^3$) solution of the acetonitrile complex **(5)** (0.2g). After one day, the addition of CO was stopped and the solvent reduced to ~$3cm^3$, causing a yellow precipitate to form. Examination of the IR spectrum of the precipitate showed there were no stretches in the carbonyl region and the acetonitrile stretches were still present, indicating that no reaction had occurred.

Figure 6. The Crystal Structure of [Rh(dppe)(CO)Cl_3] (7)

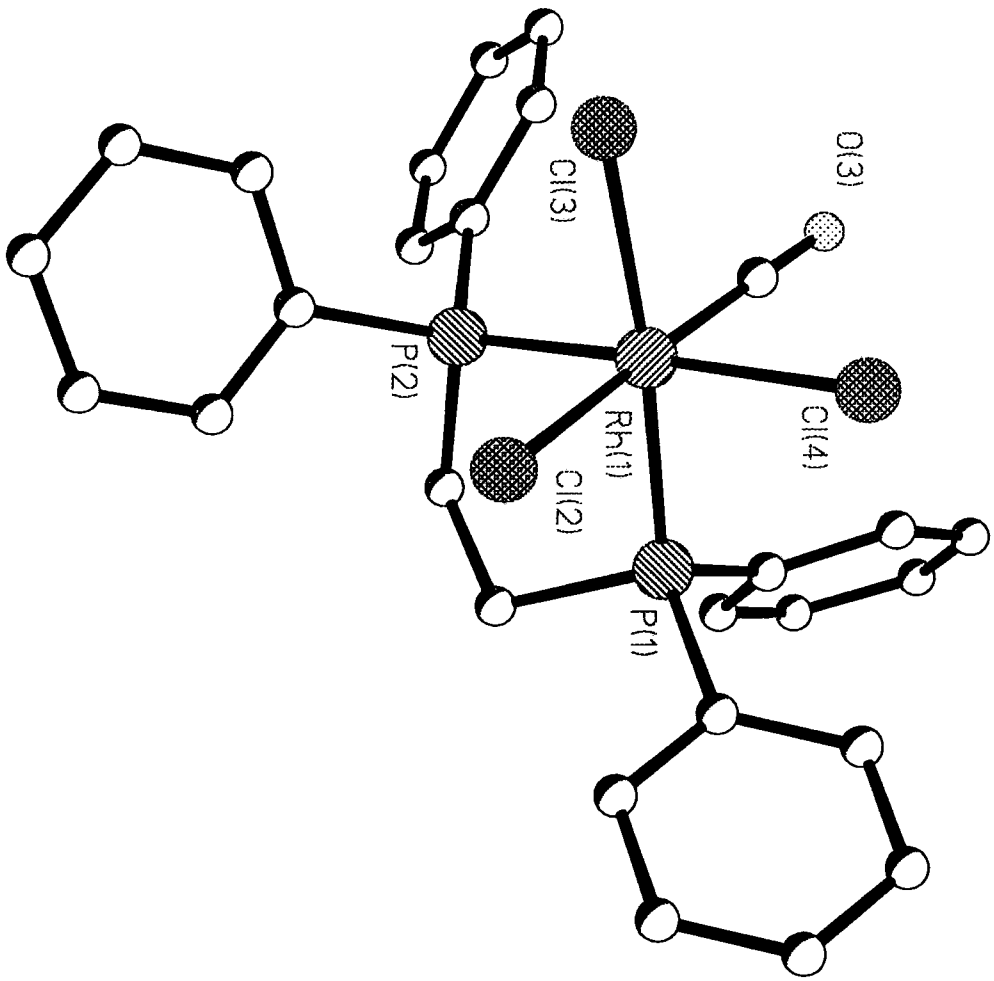

8.3.4. Synthesis of $[Rh_2(dppp)_2Cl_2(\mu\text{-}OH)(\mu\text{-}OMe)_2](Cl)$ (8)

Complex **(2)** (0.2g) was stirred in air, with a solution of excess CsF (1.04g) in methanol ($50cm^3$) for two days. At the end of this time the solution had turned from orange-yellow to pale green in colour. The solvent was removed under reduced pressure and the product recrystallised from dichloromethane-hexane (80% yield by phosphorus NMR). After recrystallisation there was only a single product. Crystals of the title compound suitable for X-ray diffraction, were grown by the slow evaporation of a concentrated solution of complex **(8)** in an NMR tube in air, and the structure elucidated by C.W. Lehmann (see Figure 8, page 181).[2] The crystals were found to be solvated, containing dichloromethane. Found C, 51.30; H, 4.74. $C_{57.5}H_{62}Cl_6O_3P_4Rh_2$ requires C, 51.40; H, 4.65%. $^{31}P\{^1H\}$ NMR (CD_2Cl_2): δ 17.3 (d, $^1J_{Rh\text{-}P}$ 109Hz) ppm. ^1H NMR (CD_2Cl_2): δ 7.68, 7.55, 7.30, 6.90 (**20H**, m, $PC_6\underline{H}_5$), 5.30 (s, $C\underline{H}_2Cl_2$), 2.99 (**2H**, tm, $PCH_2C\underline{H}_2$), 2.04 (**4H**, m, $PC\underline{H}_2$) ppm.

8.4. Discussion

8.4.1. The reactions of Chelating Phosphines with Rhodium(III) Chloride in Methanol

In contrast to rhodium(III) complexes containing mono-phosphines, there are relatively few examples reported of the reaction between bidentate-phosphines and rhodium(III)chloride. Cotton[3] found dppm reacted quantitatively with rhodium trichloride to produce a single species $[Rh(dppm)(MeOH)Cl_3]$ **(9)**, a complex soluble in methanol. The behaviour of this complex contrasts with the results obtained here, which indicate that the nature of the product depends greatly on the phosphine employed. All the phosphines used (dppe, dBpe, dcpe) produced quantities of an insoluble material. The solid state phosphorus NMR of these materials indicates the presence of several phosphorus environments. This could mean there are several isomers of the same species present.

Figure 8. The Crystal Structure of $[Rh_2(dppp)_2Cl_2(\mu\text{-}OH)(\mu\text{-}OMe)_2](Cl).CH_2Cl_2$ (8)

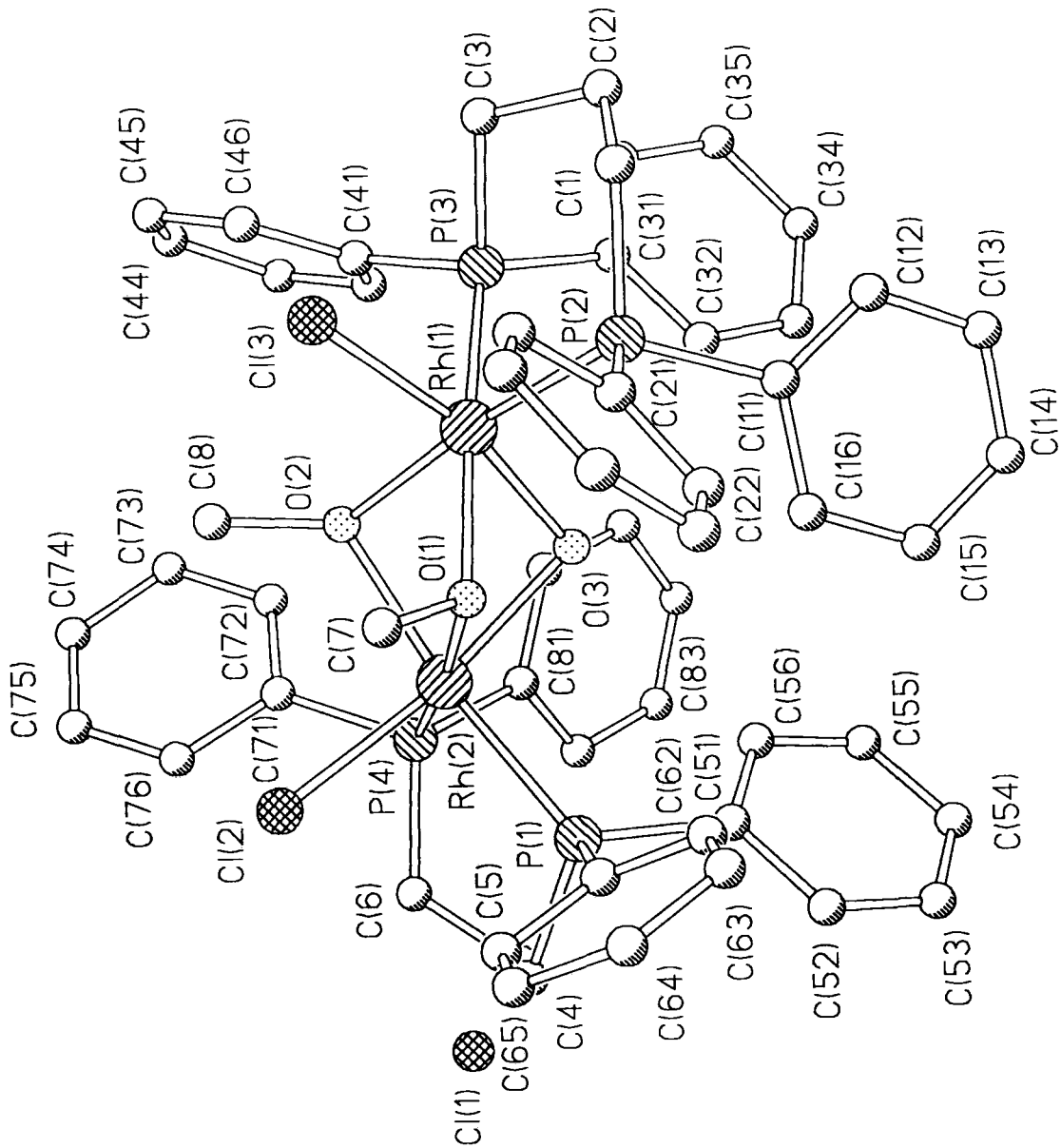

For example, if the complexes were of a similar nature to the dppm species observed by Cotton,[3] the solvent molecule could be located in *cis* or *trans* positions relative to the phosphines. Alternatively, the solid could contain no solvent molecules. The vacant co-ordination site in the [Rh(diphos)Cl_3] unit could then be used for halide bridges to other rhodium atoms resulting in a dimeric, oligomeric or polymeric material. The chemical shifts in the solid state phosphorus NMR spectra are quite large implying that most of the phosphines are chelating.[4] Also, the presence of very low frequency signals observed for dcpe and dppe may be due to species with nonchelating phosphines, for example two rhodium atoms linked by the same bridging phosphine either as a discrete molecule or as a polymer.

Further evidence for a structure of the type [$RhL_2L'X_3$] comes from the reaction of the acetonitrile to produce a crystalline, but soluble complex [Rh(dppe)(MeCN)Cl_3] **(5)**. This is isostructural with the dppm derivative observed by Cotton,[3] where the solvent molecule is perpendicular to the rhodium-phosphine plane.

Use of an alkyl chelating phosphine (dcpe) instead of an aryl phosphine (dppe) increases the number of isolable products. This may be due to the increased solubility of the complexes formed with dcpe.† Products that were insoluble for dppe become soluble when the phosphine is replaced with dcpe, permitting extraction, isolation and characterisation. Alternatively, if the insoluble product(s) are polymeric (utilising halide bridges), it is unlikely they form as polymers in solution. Instead the polymeric materials may precipitate with loss of the co-ordinated solvent molecules, or dimerise and oligomerise prior to precipitation. By increasing the solubility of these complexes having a low degree of aggregation, it is possible to extract and isolate them. When dcpe is utilised in this reaction, there are three fractions, which can be separated

† No quantitative data, known to the author exists concerning the relative solubility of a complex containing a chelating phosphine when the phosphine is changed. However, qualitatively for the complexes [Rh(diphos)(C_7H_8)](BF_4) reported in chapter 2, the solubility order in all solvents tried (e.g. MeOH, CH_2Cl_2, THF, diethylether, $CHCl_3$, CH_3NO_2) is: dBpp > dcpp > dBpe > dcpe ~ dcpp > dppe.

according to their solubilities. In addition to the insoluble products discussed above, there are two soluble fractions.

The product isolated from the supernatant liquor has been shown by X-ray crystal structural analysis to be $[Rh_2(dcpe)_2(\mu\text{-}Cl)_3Cl_2][Rh(dcpe)Cl_4]$ **(4)**. The cation is isostructural with the dppe analogue $[Rh_2(dppe)_2(\mu\text{-}Cl)_3Cl_2](BF_4)$ **(6)** (observed earlier from the reaction of excess methylchloroformate with $[Rh(dppe)(S)_2]^+$),and in complex **(6)** two phosphorus environments are observed.

Since there are three phosphorus environments in complex **(4)** we would expect to see two doublets of doublets and one doublet in a 1:1:1 ratio in the phosphorus NMR spectrum (from couplings to the rhodium and to the other phosphorus atom in the chelate ring). However this is not the case. In $CDCl_3$ solution, complex **(4)** exhibits considerable fluxionality, and at r.t. the phosphorus NMR signals are broad. Variable temperature phosphorus NMR spectroscopy (see Table 1, Figure 4, page 175) indicates there are two phosphine containing complexes (one giving signals **A** and **B**, and the other **D**) present at -50°C. One of the products giving signal **D**, contains a symmetrical phosphorus environment (a single doublet, signal **D**), and one complex giving signals **A/B** contains unsymmetrical phosphorus environments (two doublets of doublets in a 1:1 ratio, signals **A** and **B**). The coupling constants of signals **A** and **B** are similar to those observed for complex **(6)** in solution ($^1J_{Rh\text{-}P}$ 120, 116Hz **A** and **B**, $^1J_{Rh\text{-}P}$ 126Hz **(6)**). Thus the complex giving signals **A/B** is probably very similar to the solid state structure of the cation of complex **(6)**, $[Rh_2(dppe)_2(\mu\text{-}Cl)_3Cl_2]^+$. Signal **D** has a similar rhodium-phosphorus coupling constant ($J_{Rh\text{-}P}$ 121Hz, **D**) to signals **A** and **B**, which is much larger than previously reported data[5] for complexes similar to the anion of complex **(4)** ($^1J_{Rh\text{-}P}$ 93Hz,[5] $[Rh(dppe)Cl_4]^-$). However, the relative intensity of signal **D** is just a third of that of signals **A** and **B**.

Clearly, these data indicate that the solution structure is more complicated than in the solid state. As mentioned in Chapter 7, the related complex $(NH_3OH)[Rh(dppe)Cl_4]$

was not stable in solution, and dissociation of the chloride ligands occurred. A similar effect is observed for complex **(4)**; in solution an equilibrium is established involving displacement of a chloride ion by the solvent (S) to produce a neutral species.

$$S + [Rh(dcpe)Cl_4]^- \rightleftharpoons [Rh(dcpe)(S)Cl_3] + Cl^-$$

In a non co-ordinating solvent the resulting monomeric neutral unit is not very stable and dimerisation occurs, with the subsequent loss of a chloride ligand to form a more stable cationic complex:

$$2\,[Rh(dcpe)(S)Cl_3] \rightleftharpoons [Rh_2(dcpe)_2Cl_5]^+ + Cl^-$$

The activation energy for these equilibrium processes is small, hence the broad peaks in the phosphorus NMR spectrum at r.t., and in solution the equilibra lie in favour of the cationic complex $[Rh_2(dcpe)_2Cl_5]^+$. This leads to an enhancement of the phosphorus NMR signals of the cation (**A/B**) relative to the anion. Even at -50°C the exchange between the anion of complex **(4)**, $[Rh(dcpe)Cl_4]^-$ and the neutral solvate species $[Rh(dcpe)(S)Cl_3]$ is too fast for both signals to be resolved and consequently we observe an average chemical shift and coupling constant for these two species, (signal **D**).

Washing the precipitate from the methanol reaction with dichloromethane yields the third product. This contains a single rhodium-phosphine species, complex **(3)**, identified by phosphorus NMR spectroscopy. The phosphorus NMR signal of complex **(3)** in dichloromethane is a sharp doublet at r.t., δ 78.8ppm, $^1J_{Rh\text{-}P}$ 118Hz. This is in a similar position with a similar value of $^1J_{Rh\text{-}P}$ to signals **A/B** (see Table 1) and in solution, has a similar value of $^1J_{Rh\text{-}P}$ to the structurally characterised complex $[Rh_2(dppp)_2(\mu\text{-}Cl)_3Cl_2](Cl)$ **(2)**. This could suggest a degree of isostructurality. However, the signals are sharp, implying if equilibria exist, in a similar manner to those observed for complex **(4)** in chloroform, then exchange is very fast on the NMR timescale. Dichloromethane is less polar than chloroform, hence CH_2Cl_2 is less likely

to stabilise highly charged species relative to $CHCl_3$. Consequently the uncharged species $[Rh_2(dcpe)_2Cl_6]$ is favoured in a less polar medium than the ionic complex **(4)**.

In summary, the complex $[Rh_2(dcpe)_2(\mu\text{-}Cl)_3Cl_2][Rh(dcpe)Cl_4]$ **(4)** is unstable in solution. In polar solvents dissociation of chloride ions occurs and the cation $[Rh_2(dcpe)_2(\mu\text{-}Cl)_3Cl_2]^+$ is the predominant species, whilst in less polar solvents a neutral species $[Rh_2(dcpe)_2Cl_6]$ is observed.

Thermal Equilibration

Heating the solid products "[Rh(diphos)(MeOH)Cl_3]" obtained from the reaction of rhodium(III)chloride in methanol and aryl substituted chelating phosphines (dppe, dppp), causes the formation of new products. The nature of these species is dependent on the phosphine employed. Analysis of the reaction mixtures by phosphorus NMR indicates several species are formed for the phosphine dppe, but only one for the phosphine dppp. Furthermore, the products from the dppe and dppp reactions do not contain the same bridging unit, and are not structurally analogous (see Table below).

Phosphine	$^{31}P\{^1H\}$ NMR		
	δ (ppm)	J (Hz)	Rel.[1] Intensity(%)
dppe	37.1	84	69
dppp	24.8	116	100

The NMR spectrum of the dppe product is very similar to that of $[Rh(dppe)_2Cl_2](BF_4)$ (δ 37.2ppm, $J_{Rh\text{-}P}$ 84Hz), obtained in low yield by refluxing a mixture of dppe, $RhCl_3.3H_2O$, in aqueous methanol in the presence of HCl and excess halide ions, followed by ion-exchange with $NaBF_4$.[6]

The product from the reaction with dppp, complex **(2)** was structurally characterised by X-ray crystallography and identified as the novel complex $[Rh_2(dppp)_2(\mu\text{-}Cl)_3Cl_2](Cl)$. This has a similar core structure to the other dimeric

[1] Percentage of the total integral of all of the phosphorus signals observed in the phosphorus NMR spectrum.

rhodium species prepared in this study, with a triply bridged dimer unit and inequivalent phosphines, in the solid state. However, the solution $^{31}P\{^{1}H\}$ NMR spectrum indicates that the phosphorus atoms are equivalent (a single doublet due to rhodium phosphorus coupling) and this could be due to rapid exchange with the halide counter ion, breaking one of the chloride bridges; at r.t. the average structure of $[Rh_2(dppp)_2(\mu\text{-}Cl)_2Cl_4]$ is observed in solution. Fluxional behaviour in solution, on the phosphorus NMR timescale has been observed for the related mono-phosphine complex $[Rh_2(PEt_2Ph)_4Cl_5](BPh_4)$. At r.t. this is a broad doublet, but on cooling to -50°C a $^{31}P\{^{1}H\}$ NMR spectrum similar to that of $[Rh_2(dppe)_2(\mu\text{-}Cl)_3Cl_2](BF_4)$ is observed. However, this has been attributed to an *intra* rather than *inter* molecular process.[6]

8.4.2. Reaction Chemistry of Rhodium(III) Diphosphine Adducts

Attempted Synthesis of $[Rh_2(dppe)_2(\mu\text{-}Cl)_3Cl_2](BF_4)$ (6)

This novel complex was previously prepared in a four step synthesis from rhodium(III)chloride.[7] To aid in the exploration of the chemistry of complex **(6)**, alternative routes to this complex were investigated. Silver ions have been previously used successfully to remove halide ions from rhodium complexes[8] (driven by the insolubility of the silver chloride formed), and this was the strategy employed:

$$RhCl_3.3H_2O + dppe + Solvent \rightarrow [Rh(dppe)(Solvent)Cl_3] + AgBF_4 \rightarrow \mathbf{(6)} + AgCl\downarrow$$

Initially this was tried using the virtually insoluble $[Rh(dppe)Cl_3]_n$ in methanol. However, analysis of the reaction products by phosphorus NMR indicated the desired product was only present in 25% yield. The desired product was purified by three partial recrystallisations from CH_2Cl_2-hexane mixtures.

In order to increase the yield, the experiment was repeated using the more soluble and structurally characterised MeCN adduct, complex **(5)**. This reaction was more

successful and the yield improved to 50% (by integration of the phosphorus NMR spectra). The most efficient route to compound **(6)** remains the hydrogenation of [Rh(dppe)(NBD)](BF_4) in excess methylchloroformate. The low yields of the dehalogenation reactions is due to the limited solubility of the starting materials. Consequently when the very soluble **(6)** does form, the opportunity arises for further reaction with Ag^+ to form other halide bridged species.

The Synthesis of [Rh(dppe)(CO)Cl_3] (7)

Complex **(6)** reacts slowly with carbon monoxide in nitromethane solution to form the novel complex **(7)** which is relatively insoluble in nitromethane, and over the course of the reaction yields crystals suitable for X-ray diffraction. The complex is isostructural with the previously prepared acetonitrile complex, **(5)**. The carbon monoxide ligand is located *cis* to both phosphorus atoms.

Similar Rh(III) phosphine carbonyl complexes have been prepared from mono-phosphines.[9] However, for the mono phosphine analogues the phosphines sit in mutually *trans* positions.[10] The mono-phosphine analogues of complex **(7)** can be prepared in two ways, either (i) by substitution of an L type ligand of a Rh(III) analogue or (ii) by the oxidation of the Rh(I) complex with a suitable oxidising agent. *viz.*

$$\text{(i) } [Rh(PR_3)_3Cl_3] + CO \rightarrow [Rh(PR_3)_2(CO)Cl_3]^{10}$$

$$\text{(ii) } [Rh(PR_3)_2(CO)Cl] + Cl_2{}^{11} \text{ or } CCl_4{}^{11} \rightarrow [Rh(PR_3)_2(CO)Cl_3]$$

However, in the first method, reduction can occur to form the analogous Rh(I) complex, and the oxidation state of the product formed is dependent on the nature of the phosphine.[10] Previous attempts to synthesise complex **(7)** and other chelating phosphine analogues of complex **(7)** by the oxidation of [Rh(diphos)(CO)Cl] with Cl_2 have been unsuccessful.[12] Instead dimeric and polymeric species are formed, with bridging phosphine ligands.

The carbon monoxide IR stretching frequency is high (2100cm^{-1}) and this reflects the high oxidation state of the metal, and the bonding properties of the phosphine (see Table 2). Increasing the oxidation state of the metal from (+1) to (+3), increases the carbonyl stretching frequency by ~90cm^{-1}, which corresponds to a decrease of electron density on the metal and consequently a decrease in the electron density available for back-donation to the ligands. Increasing the σ donor properties of the phosphine (replacing aryl with alkyl groups on the phosphine) pushes electron density onto the metal and this is reflected in a decrease in the CO stretching frequency due to increased metal to ligand back donation.

Table 2. Carbonyl Stretching Frequencies

Complex	ν(CO) cm^{-1}
[Rh(dppe)(CO)Cl][13]	2010
[Rh(dppe)(CO)Cl_3] **(7)**	2100
[Rh(PPh_3)$_2$(CO)Cl_3][13]	2106
[Rh(PPh_2Et)$_2$(CO)Cl_3][10]	2107
[Rh($PPhEt_2$)$_2$(CO)Cl_3][10]	2089
[Rh(PEt_3)$_2$(CO)Cl_3][10]	2060

Attempts to prepare complex **(7)** by substitution of the acetonitrile ligand in complex **(5)** were unsuccessful. This is due to the high kinetic stability of complex **(5)**; which is a relatively unstrained co-ordinatively saturated 18-electron compound. Consequently, it is probable that the reaction is prevented by a large activation barrier due to the necessity of creating a vacant co-ordination site for the carbon monoxide. Low spin d^6-complexes such as complex **(5)** are noted for their kinetic stability.[14] This phenomenon is due to the large crystal field stabilisation energy, and generally substitution reactions are most favourable when moving to a ligand higher up the spectrochemical series (larger CSE). For example, nitrile ligands are higher in the series than methanol or chloro ligands.

The Synthesis of $[Rh_2(dppp)_2(\mu\text{-}OH)(\mu\text{-}OMe)_2Cl_2](Cl)$ (8)

Complex **(2)** reacts in the presence of fluoride ions in methanol, over a period of days to produce complex **(8)** in good yield. Crystals suitable for X-ray crystallography were grown and the structure was identified as the triply bridged complex shown in Figure 7. This complex adopts an alternative structural isomer to that observed for the related complex **(6)**, with the phosphines in crystallographically equivalent positions.[2] The hydroxyl group occupies the cavity created by the phenyl groups, and the methoxy groups are pointing away from the phenyl groups on the phosphines. For the related Rh(I) trimeric species $[Rh_3(diphos)_3(OR)_2](BF_4)$[15] the alkoxy groups sit above and below the plane created by the three rhodium atoms, in a cavity created by the substitutents on the phosphines. The stability of these complexes is dependent on the steric bulk of the alkoxy group in the order OH > OMe > OPr^i.[16] Consequently the forces controlling the stereochemistry in the rhodium dimer are probably steric rather than electronic in origin. In the isomer observed for complex **(8)** the dimer has isomerised to push the bulkiest groups furthest from the phenyl rings of the phosphines. However, this is only possible due to the relatively small size of the hydroxyl group.

8.5. Summary

A series of complexes of the type $[Rh_2(diphos)_2(\mu\text{-}Cl)_3Cl_2](X)$ (diphos = dppe, dcpe, dppp X = BF_4^-; $[Rh(dcpe)Cl_4]$, Cl^- respectively) have been synthesised in one or two steps from the diphosphine and rhodium(III)chloride and characterised by X-ray crystallography. In contrast to the dppe complex, the dppp and dcpe complexes are fluxional in solution at r.t. The reaction chemistry of these complexes has been explored. The dppe derivative reacts with CO to form the Rh(III) carbonyl complex $[Rh(dppe)(CO)Cl_3]$, whilst in the presence of CsF, in methanol the dppp derivative forms the hydroxy, methoxy bridged complex $[Rh_2(diphos)_2(\mu\text{-}OH)(\mu\text{-}OMe)_3Cl_2](Cl)$. Both of these complexes have been characterised by X-ray crystallography.

8.6. References

[1] Solid state phosphorus NMR using cross polarisation and magic angle spinning. The signals were broader than the Rh-P coupling constants and consequently, $^{1}J_{Rh\text{-}P}$ have not been recorded.
[2] See Chapter 9 for the crystal structure and discussion there of.
[3] F.A. Cotton, K.R. Dunbar, C.T. Eagle, L.R. Falvello, S.J. Kang, A.C. Price, M.G. Verbruggen, *Inorg. Chim. Acta*, **184**, (1991), 35-42.
[4] P.E. Garrou *Chem. Rev.*, **81**, (1981), 229-266.
[5] R.A. Cipriano, L.R. Hauton, W. Levason, D. Pletcher, N.A. Powell, M. Webster, *J. Chem. Soc. Dalton Trans.*, (1988), 2483-2490.
[6] E.B. McAslan, T.A. Stephenson, *Inorg. Chim. Acta*, **96**, (1985), L49-L51.
[7] See Chapter 7.
[8] R.R. Schrock, J.A. Osborn, *J. Am. Chem. Soc.*, **93**, (1971), 3089-3090.
[9] G.M. Intille, *Inorg. Chem.* , **11**, (1972), 695-702.
[10] J. Chatt, B.L. Shaw, *J. Chem. Soc. A*, (1966), 1437.
[11] R.F. Heck, *J. Am. Chem. Soc.*, **86**, (1964), 2796.
[12] A.R. Sanger, *J. Chem. Soc. Dalton Trans.*, (1977), 120-129.
[13] B.F.G. Johnson, J. Lewis, P.W. Robinson, *J. Chem. Soc. A*, (1970), 1100-1103.
[14] A.G. Sykes, "Kinetics of Inorganic Reactions", Pergamon Press, Oxford, 1966.
[15] J. Halpern, D.P. Riley, A.S.C. Chan, J.J. Pluth, *J. Am. Chem. Soc.*, **99**, (1977), 8055-8057.
[16] T. Yamagata, K. Tani, Y. Tatsuno, T. Saito, *J. Chem. Soc. Chem. Commun.*, (1988), 466-468.

Chapter 9

Structural Studies On Rhodium(III)-Chelating Phosphine Species

9.1 Introduction

This chapter is concerned with the crystallographic data collected for the complexes reported in Chapters 7 and 8 (see Table 1). Selected crystallographic data can be found in Appendix 7.

The complexes discussed here can be divided into three groups due to their structural characteristics. [{Rh(diphos)}(μ-X)$_3$X$_2$](X) **(A)**, (Cat.)[Rh(diphos)X$_4$] **(B)**, and [Rh(diphos)LX$_3$] **(C)**; where X is a one electron ligand such as Cl^-; Cat. is a singly charged cation, for example NH_3OH^+, and L is a two electron ligand.

Table 1. Complexes Discussed In this Chapter

Complex	Original Chapter	Figure in this Chapter (Page)
[Rh$_2$(dppp)$_2$(μ-Cl)$_3$Cl$_2$](Cl).(MeOH) **(1)**	8	1 (193)
[Rh$_2$(dppe)$_2$(μ-Cl)$_3$Cl$_2$](BF$_4$) **(2)**	7	2 (194)
[Rh$_2$(dcpe)$_2$(μ-Cl)$_3$Cl$_2$][Rh(dcpe)Cl$_4$] **(3)**	8	3,5 (195, 204)
[Rh$_2$(dppp)$_2$(μ-OH)(μ-OMe)Cl$_2$](Cl) **(4)**	8	4 (196)
[Rh(dppe)Cl$_4$](NH$_3$OH) **(5)**	7	6 (204)
[Rh(dppe)(CO)Cl$_3$] **(6)**	8	7 (207)

9.2 Discussion

9.2.1 Type (A) complexes, [{Rh(diphos)}$_2$(μ-X)$_3$X$_2$](X)

Type **(A)** complexes **(1)**, **(2)**, $[Rh_2(dcpe)_2(\mu\text{-}Cl)_3Cl_2]^+$ **(3a)**, and **(4)** (see Table 1) consist of two rhodium(III) diphosphine units bound together by three bridging anionic ligands. The dimers all possess a single positive charge, and there is a terminal chlorine ligand on each rhodium atom. However, there are reported examples with other ligands in the terminal positions (see Table 2). There are two structural configurations possible for type **(A)** complexes, **(A1)** and **(A2)** based on two facially bridging octahedra. The most predominant isomer, **(A1)** is observed in the complexes **(1)**, **(2)**, and **(3a)** (see Figures 1-3 respectively), whilst the less frequently observed isomer **(A2)** is observed in complex **(4)** (see Figure 4). Isomer **(A2)** has a higher degree of symmetry than **(A1)**. In the **(A2)** isomer, the four phosphorus atoms in the dimer are equivalent and related by a C_2 axis of rotation and a mirror plane perpendicular to the rhodium phosphine plane. This is not the case for **(A1)**, where there are two phosphorus environments, the phosphorus atoms either being *trans* to a chlorine, which is itself *trans* to a chlorine, or *trans* to a chlorine that is *trans* to a different phosphorus atom. In all cases the terminal ligands are *trans* to a bridging Cl or OH, and not a phosphine ligand. Similar structures have been reported in the literature for both rhodium and other transition metals (See Table 2).

Table 2. Reported Examples of Complexes with an [$M_2P_4(\mu\text{-}X)_3X'_2$] Core.

Complex	Complex No.	Structure Type
$[Rh_2(PMe_2Ph)_4(Cl)_3(COMe)_2](PF_6)$,[1]	**(7)**	**A1**
$[Rh_2(dBpf)(\mu\text{-}H)_3(H)_2](ClO_4)$[2]	**(8)**	**A1**
$[Rh_2(dBppf)(\mu\text{-}H)_3(H)_5](ClO_4)$[2]	**(9)**	**A1**
$[Rh_2(dppe)(\mu\text{-}Cl)_2(\mu\text{-}CH_2)(Cl)_2]$[3]	**(10)**	**A2**
$(AsPh_4)[Rh_2(O{=}PPh_2)_2(HOPPh_2)_2(\mu\text{-}Cl)_3(Cl)_2]$[4]	**(11)**	**A1**
$[Ir_2(PPh_2Me)_4(\mu\text{-}I)_3(I)_2](I_3)$[5]	**(12)**	**A2**
$(C_{14}H_{16}N_2)[Ru_2(dppb)_2(\mu\text{-}Cl)_3(Cl)_2]$[6]	**(13)**	**A1**
$[Ru_2(PBu^n{}_3)_4(\mu\text{-}Cl)_3(Cl)_2]$[7]	**(14)**	**A1**
$[Ru_2(PMe_2Ph)_4(\mu\text{-}Cl)_3(Cl)_2]$[8]	**(15)**	**A1**
$[Ru_2(PMe_3)_4(\mu\text{-}Cl)_3(Cl)_2]$[8]	**(16)**	**A2**
$[Ru_2(Chiraphos)_2(\mu\text{-}Cl)_3(Cl)_2]$[9]	**(17)**	**A1**

Figure 1. The Crystal Structure of the Type (A1) Cation in $[\{Rh(dppp)\}_2(\mu\text{-}Cl)_3Cl_2](Cl)$ (1)

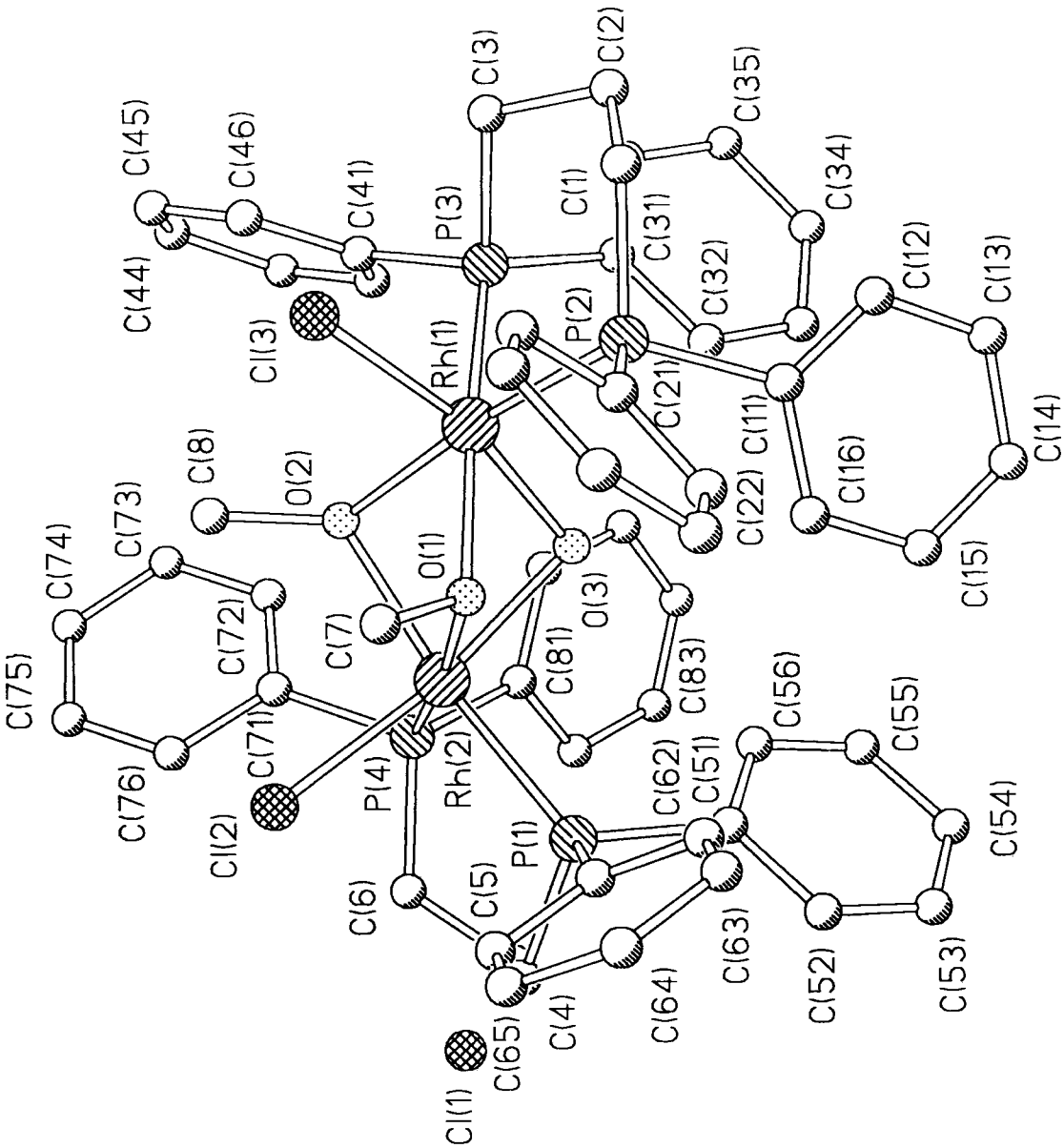

Figure 2. The Crystal Structure of the Type (A1) Cation

$[\{Rh(dppe)\}_2(\mu\text{-}Cl)_3Cl_2](BF_4)$ (2)

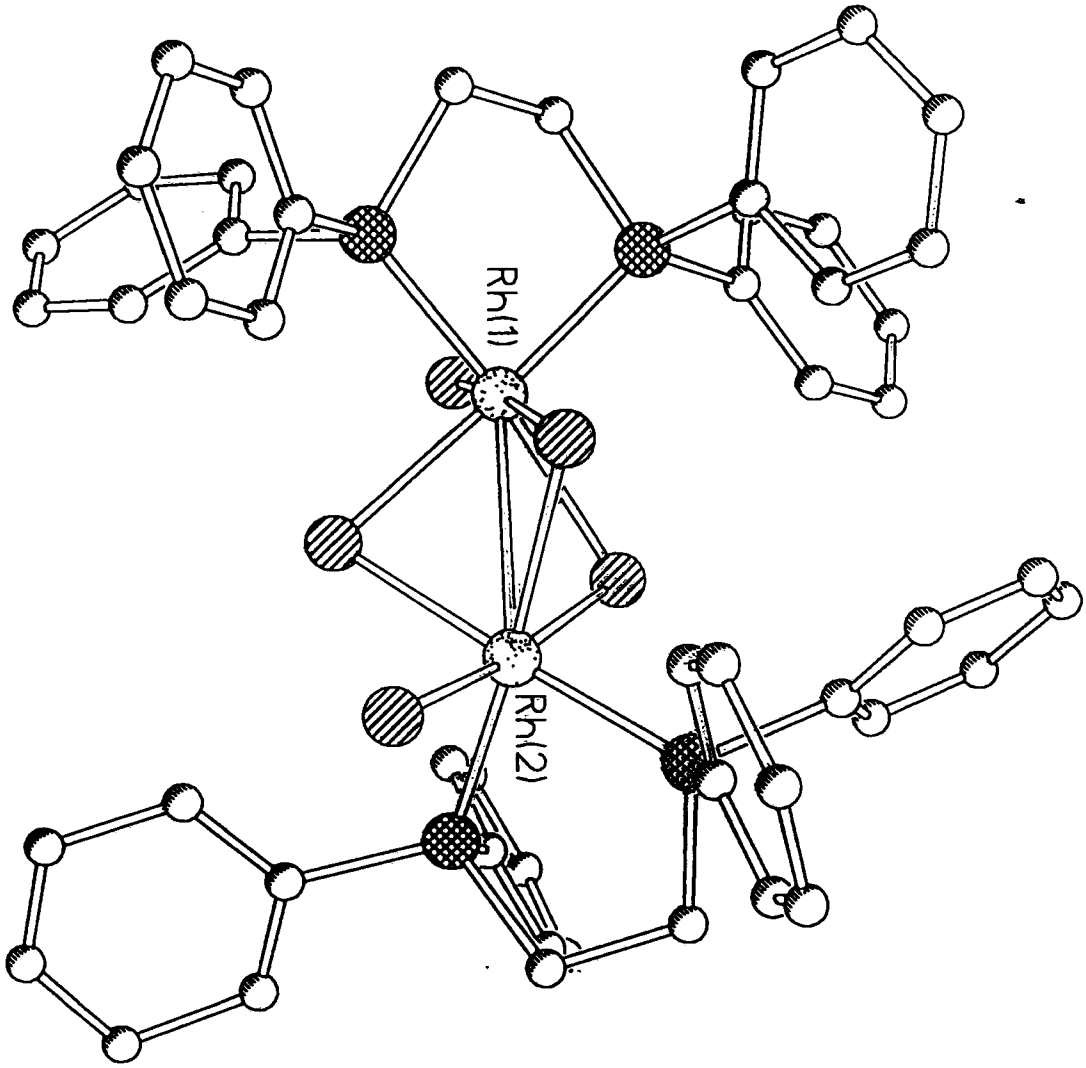

Figure 3. The Crystal Structure of the Type (A1) Cation in $[\{Rh(dcpe)\}_2(\mu\text{-}Cl)_3Cl_2][Rh(dcpe)Cl_4]$ (3)

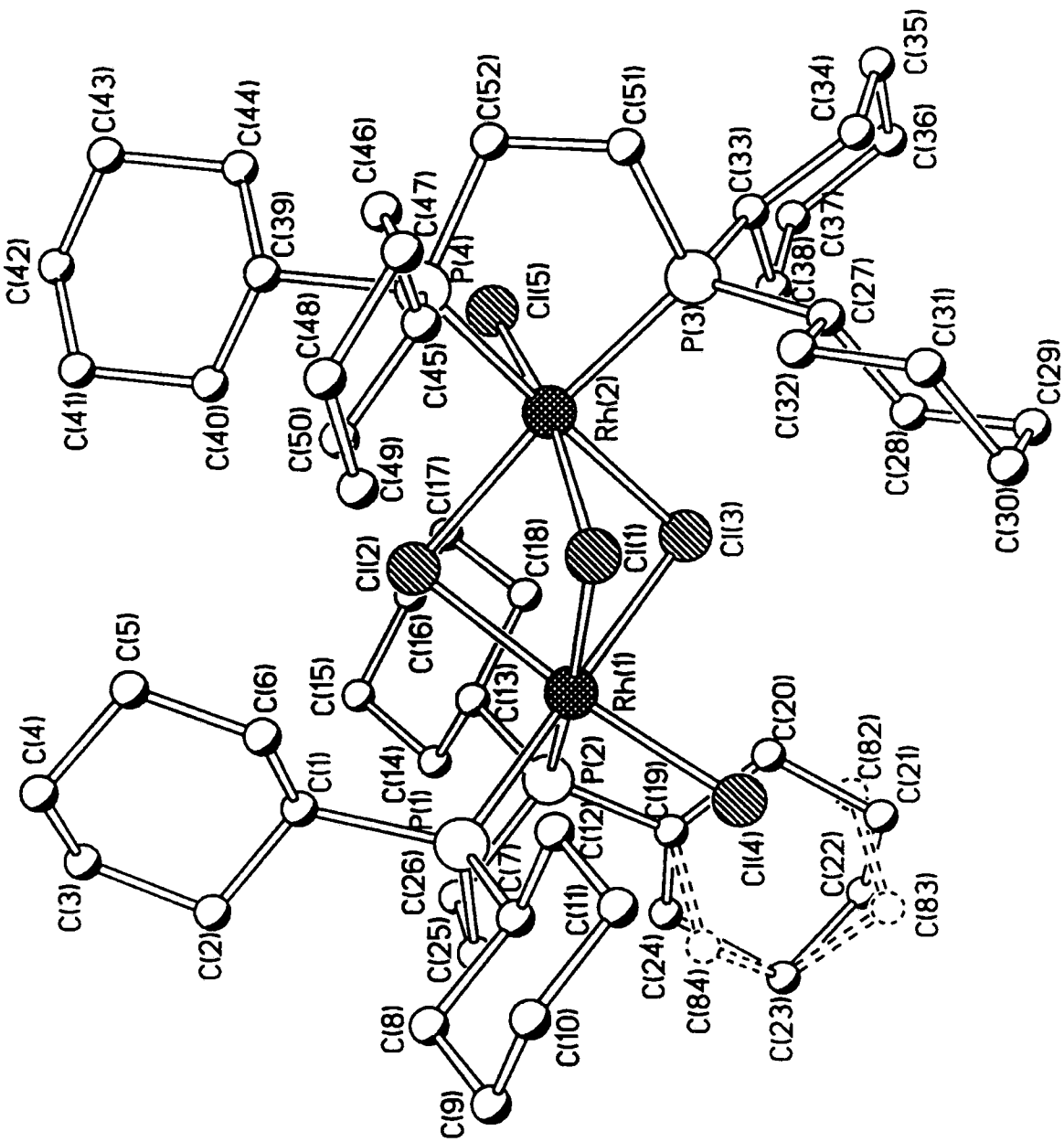

Figure 4. The Crystal Structure of the Type (A2) Cation in $[\{Rh(dppp)\}_2(\mu\text{-}OH)(\mu\text{-}OMe)_2Cl_2](Cl)$ (4)

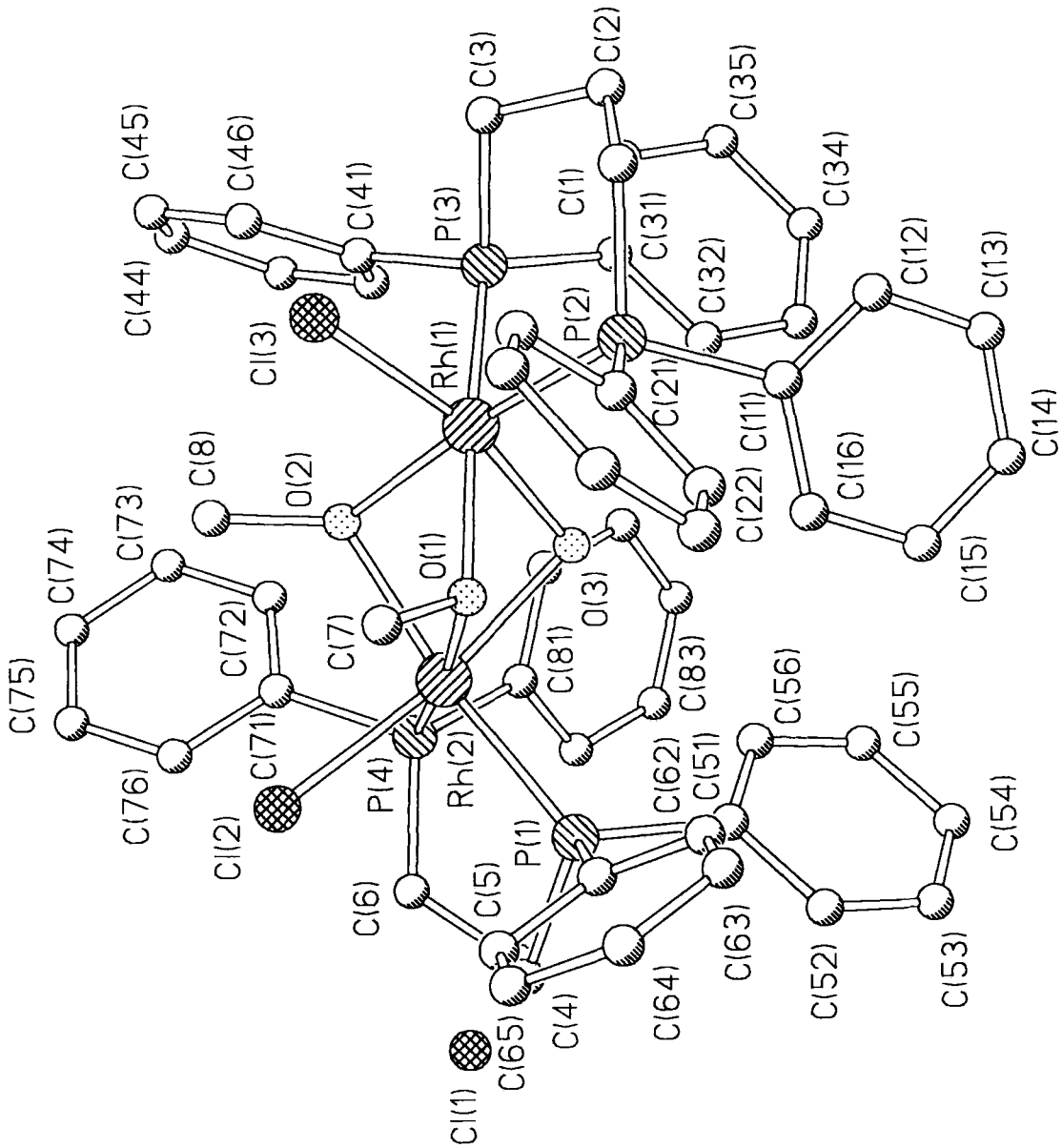

The previously reported type **(A)** complexes of Rh and Ir (complexes **(7-12)**) have the metal in the (+3) oxidation state (see Table 2). The structurally related Ru complexes **(13-17)** have been reported. Complex **(13)** is isoelectronic with the rhodium complexes **(1-4)**, and contains two Ru(II) atoms, whilst complexes **(14-17)** have Ru in mixed oxidation states, containing both Ru(II) and Ru(III). All of these complexes except for **(12)** and **(16)** contain the type **(A1)** core configuration. In the Ir complex **(12)**, all of the bonds are much longer than those observed in the rhodium analogues and the PPh_2Me ligand can rotate about the Ir-P bond. Both of these factors help to minimise steric interactions between the Ph groups and the iodine ligands; consequently this complex can adopt an **(A2)** type structure. The structural differences in the Ru complexes **(15)** and **(16)** have been attributed to the minimisation of steric interactions. Replacing a methyl with a phenyl group in complex **(15)** increases the steric bulk of the phosphine and a change in structure is observed.[9] A similar argument can be employed to explain the structural differences between complexes **(1-4)**. In complex **(4)** a cavity is created by the Ph groups. Unlike the methoxy or chlorine ligands, the hydroxyl group can fit into this cavity with minimal steric interactions with the surrounding phenyl groups. A similar situation is observed for the Rh(I) complexes $[\{Rh(diphos)\}_3(Y)_2](X)$. The stability of these complexes is dependent on the steric bulk of the Y group in the order OH ~ F > OMe > OPr^i. The most stable complexes are formed when the bridging ligand is OH, and the complex $[\{Rh(Binap)\}_3(OD)_2](ClO_4)$ has been structurally characterised.[10]

In all of these complexes the bridging ligands are not symmetrically postioned in the central unit, and this is due to the varying *trans* influences of the other ligands in the molecule. Tables 3 contains selected bond angles and lengths for complexes **(1-4)** and related species.

Table 3. Selected Mean Rh-P bond lengths (Å) and PRhP Angles (°) for Type (A) $[Rh(diphos)_2Cl_5]^+$ and Related Complexes

Complex (phosphine)*	**PRhP Angle**	**P *trans* to Cl *trans* to P**	**P *trans* to Cl *trans* to Cl**	**Rh-$Cl_{(terminal)}$**	**Rh-$Cl_{(bridging)}$ (RhClRh)**		
					***Trans* to Cl**	***Trans* to P**	***Trans* to 2P**
(1) (dppp)	92.4	2.284	2.284	2.338	2.364	2.502 (83.9)	2.474 (82.3)
(4) (dppp)	91.5	2.273	-	2.332	-	-	-
(3a) (dcpe)	85.8	2.297	2.269	2.321	2.368	2.499 (84.6)	2.484 (82.5)
(2) (dppe)	86.2	2.278	2.258	2.318	2.369	2.482 (81.8)	2.465 (80.4)
(10) (dppe)	84.7	2.249	-	2.507	-	-	2.462
(18) $[Rh_2(triphos)_2(\mu\text{-}Cl)_3](CF_3SO_3)_3$ [11]	-	2.320	-	-	-	-	2.474 (87.3)
(7) (PMe_2Ph)	99.2	2.990	2.272	-	2.458	-	2.474 (84.6)
(9) (dBppf) †	103.4	2.364	2.292	-	-	-	-
(11) (Ph_2PO/Ph_2POH)	92.3	2.271	2.274	2.314	2.352	2.547 (83.5)	2.498 (81.7)
(19) $[Rh_2(PBu^n_3)_4(\mu\text{-}Cl)_2Cl_4]$ [12]	97.6	-	2.257	2.322	2.394	2.523	-
(20) $[Rh_2(PEt_3)_4(\mu\text{-}Cl)_2Cl_4]$ [13]	97.2	-	2.278	2.322	2.372	2.522 (99.8)	-
(21) $[Rh(PPh_3)_4(\mu\text{-}OH)_2]$ [14]	97.3	2.197	-	-	-	-	-
(22) $[Rh(PPh_3)_4(\mu\text{-}Cl)_2]$ [15]	96.3	2.207	-	-			2.409 (98.9)
(23) $[Rh(PPr^i_3)_4(\mu\text{-}Cl)_2]$ [16]	104.8	2.254	-		-	-	2.435 (103.1)
(24) $[Rh_2(dfepe)_2(\mu\text{-}Cl)_2]$ [17]	84.9	2.153	-	-	-	-	2.397 (84.3)
(25)$[Rh_2(dBpm)_2(\mu\text{-}Cl)_2]$ [18]	75.7	2.190	-	-	-	-	2.423 (84.8)

* For ease of comparison, the diphosphine used in the complex is included in brackets for previously mentioned species.

† P *trans* to H *trans* to P; P *trans* to H *trans* to H.

From examining the data in Table 3 several trends can be observed relating to the structural characteristics of these compounds.

In general, those P-Rh bonds which are *trans* to a chlorine which is itself *trans* to a phosphorus are longer than those *trans* to a chlorine which is itself *trans* to a chlorine ligand. A similar observation can be made for the hydride system **(9)**, where the Rh-P bonds are longer than in the penta-chloro systems, due to the higher *trans* influence of a hydride ligand. For a given phosphine the P-Rh bonds in the **(A2)** isomers are shorter than those in the **(A1)** isomers with the same phosphine. Changing the phosphine from dppe to the more electron rich dcpe might be expected to shorten the Rh-P bonds due to the greater availability of the phosphorus lone pair. However, the opposite effect is observed and the Rh-P bonds are shorter in the dppe than the dcpe complex. The high oxidation state of the metal and the cationic charge lead to a depletion in electron density in the d orbitals on the metal which are responsible for backbonding to the ligand. Consequently the effect is probably due to the increased steric bulk in the dcpe complex and not backbonding in the dppe complex.

Increasing the size of the chelate ring from 5 to 6 increases the Rh-P bond distances, especially the Rh-P bonds *trans* to a chlorine which is *trans* to a chlorine. Again this can be explained using a steric argument. Increasing the size of the chelate ring, pushes the Ph groups on the phosphorus around the sides of the metal resulting in increased repulsion with the chlorine ligands and consequently, a lengthening of the Rh-P bonds. Replacing the adjacent terminal chlorine ligand with another phosphine dramatically increases the overall Rh-P bond lengths due to the increased steric interactions in the system, for example in the complex $[Rh_2(triphos)_2(\mu\text{-}Cl)_3]^{3+}$ **(18)**.[11] The bite angles observed in the chelating phosphine complexes are smaller than those observed in the mono-phosphine complexes **(19)** and **(20)**. The exception to this trend is complex **(11)** where the PRhP angle is reduced due to P=O····H-O-P hydrogen bonding. The Rh-P bonds in the Rh(III) complexes are longer than those in the Rh(I) complexes **(21)** to **(25)**. This can be attributed to rhodium-phosphorus backbonding in

the Rh(I) aryl-phosphine complexes, and reduced steric interactions in the Rh(I) alkyl-phosphine complexes (since Rh(I) is larger than Rh(III), and Rh(I) being four co-ordinate, has a lower number of ligands to accomodate).

Comparison of the Rh(I) complexes **(21)** and **(22)** and the Rh(III) complexes **(1)** and **(4)**, reveals that for both the Rh(I) and Rh(III) systems the Rh-P bonds which are *trans* to a chlorine are longer by ~0.01Å than those *trans* to a hydroxyl group. This may be due to the larger steric bulk of the chlorine ligand.

The $Rh\text{-}Cl_{(terminal)}$ bond length is dependent on the size of the chelate ring and the ligand *trans* to the terminal chlorine. The longest bonds are observed in complex **(10)** where the terminal chlorines are *trans* to a CH_2 group. This bond lengthening of ~0.2Å can be attributed to the higher *trans* influence of the CH_2 group compared with chlorine.[19] Increasing the size of the chelate ring slightly increases $Rh\text{-}Cl_{(terminal)}$ bond length (~0.01Å). Interestingly, replacing phenyl with cyclohexyl groups on the phosphine causes only very minor changes in the $Rh\text{-}Cl_{(terminal)}$ bond (~0.003Å) which could be accommodated in the experimental error, and the bond distances are similar to those observed in the mono-phosphine complexes **(19)** and **(20)**.

The $Rh\text{-}Cl_{(bridging)}$ bonds are longer than the $Rh\text{-}Cl_{(terminal)}$ bonds. In addition, $Rh\text{-}Cl_{(bridging)}$ *trans* to a chlorine are longer than $Rh\text{-}Cl_{(bridging)}$ *trans* to a phosphine. However, those bonds *trans* to two phosphines are shorter than those bonds *trans* to one phosphine. This is the opposite dependence to that observed with the Rh-P bond lengths. Consequently, if the Rh-P bond is long then the $Rh\text{-}Cl_{(bridging)}$ bond *trans* to it will be shorter, and *vice versa.* The longest Rh-Cl bonds are observed in the phosphite system **(11)**, and this may be due to an electronic rather than a steric influence. If some of the negative charge in this complex is localised on the metal then this would fill the d orbitals and weaken the bonding to the chlorine ligands. The RhClRh bond angles in any triply bridged complex are always larger for PRhClRhCl[‡]

[‡] Rhodium-chlorine-rhodium angle of a bridging chlorine *trans* to a phosphine and a terminal chlorine

than for PRhClRhP systems,[§] although at 82-85° these are smaller than might be expected if the bridging action is *via* donation of a lone pair from a chlorine p or sp hybrid orbital to the metal. This small reduction is due to a compromise in the complexes between the formation of strong bonds and the minimisation of steric interactions. The bridging angles[‡§] in the dichloro-bridged mono-phosphine Rh(I) and Rh(III) complexes are much larger than 90°, whilst those in the Rh(I) diphosphine complexes are smaller. This trend mirrors the trend observed in the PRhP angle, and possibly the two are related. In the Rh(I) complexes the Rh-$Cl_{(bridging)}$ bond distances are shorter than those observed in the Rh(III) complexes. Also, for the Rh(I) complexes, the Rh-Cl bonds in the aryl-phosphine systems are shorter than in the alkyl-phosphine systems. This is due to a mixture of electronic and steric effects.

Complex **(4)** has bridging OMe and OH in place of Cl ligands. Table 4 contains selected Rh-OR (R=Me or OH) bond lengths and Rh(OR)Rh bond angles for OH, and OMe bridged complexes. The Rh-OR values obtained for complex **(4)** are typical of those observed in this type of complex (see Table 4), and the shortest Rh-OH bonds are observed for the most highly charged species.

Table 4. Selected Mean Rh-OR bond lengths (Å) and RhO(R)Rh Angles (°)

Complex (phosphine)	**Rh(OR)-Å**	**Rh(OR)Rh-°**
(4) (dppp)	2.117	87.8 (OMe)
	2.079	89.8 (OH)
$[\{Rh(TACN^{**})(H_2O)\}_2(\mu\text{-}OH)_2](ClO_4)_4$[20]	2.041	100.5(OH)
$[\{RhCp^*\}_2(\mu\text{-}OH)_3](OH)$[21]	2.105	89.8 (OH)
$[\{Rh(Binap)\}_3(\mu^3\text{-}OD)_2](ClO_4)$	2.150	92.0 (OD)
$[\{Rh(DMP^{**})Cp^*\}_2(\mu\text{-}OH)_2](BF_4)_2$[22]	2.178	101.0 (OH)
$[Rh_2(PPh_3)_4(\mu\text{-}OH)_2]$	2.066	105.0 (OH)
$[Rh_2(\mu\text{-dppm})_2(CO)_2(OH)](PF_6)$[23]	2.072	98.5 (OH)

[§] Rhodium-chlorine-rhodium angle of a bridging chlorine *trans* to two phosphine ligands

[**] TACN = Triazacyclononane; DMP = 3,5 Dimethylpyrazole; Cp* = Pentamethylcyclopentadienyl

In the unit cell of the crystal structure of complex **(2)** there are two cationic rhodium dimers, several disordered $CHCl_3$ solvent molecules, one BF_4^- and one $B_2F_7^-$ counter-ion. This is only the second recorded structure of the $B_2F_7^-$ ion, and the results obtained here are in good agreement with the literature[24] (Mean values B-$F_{terminal}$ 1.39Å, B-F_{bridge} 1.54Å BFB 122°. Lit.[23] B-$F_{terminal}$ 1.37Å, B-F_{bridge} 1.51Å, BFB 128.1°). This ion has been synthesised previously from the reaction of BF_3 with BF_4^- in the presence of bulky cations. All of these requirements could be met during the synthesis of complex **(2)** and the BF_3 could come from the decomposition of silver tetrafluoroborate impurities in the [Rh(dppe)(NBD)](BF_4) starting material.

9.2.2 Type (B) Complexes, $[Rh(diphos)X_4]^-$

The type **(B)** complexes $[Rh(dcpe)Cl_4]^-$ **(3b)** and $[Rh(dppe)Cl_4]^-$ **(5)** are monomeric and have a single negative charge. They are octahedral with four chlorine ligands and a chelating phosphine (see Figures 5 and 6). Complex **(3b)** is stabilised by the very bulky cation $[\{Rh(dcpe)\}_2(\mu\text{-}Cl)_3Cl_2]^+$ (see Section 9.2.1.) whilst complex **(5)** is stabilised by hydrogen bonding interactions with the relatively small hydroxylammonium ion, $(H_3NOH)^+$. Previous examples of class **(B)** compounds reported in the literature have been stabilised by bulky cations. For example, $[Rh(btpe)Cl_4]^-$ crystallises as a salt with the dimeric rhodium complex $[\{Rh(btpe)Cl\}_2]^{2+}$.[25] The Ir complex $[Ir(dppe)I_4]^-$ crystallises in the presence of $AsPh_4^+$,[26] whilst the related complex *trans*-$[Rh(PEt_3)_2Cl_4]^-$ forms crystals with the bulky cation PPh_4^+.[27] Table 5 contains selected data for the above and related complexes.

Table 5. Mean Values of Rh-P Bond Lengths(Å) and Angles (°)

Complex (phosphine)	PRhP Angle (°)	P-Rh (Å)	Rh-Cl *trans* to P	Rh-Cl *trans* to Cl
$[Rh(dcpe)Cl_4]^-$ **(3)**	88.6	2.282	2.439	2.355
$[Rh(dppe)Cl_4]^-$ **(5)**	87.3	2.276	2.459	2.355
$[Rh(btpe)Cl_4]^-$ **(26)**	85.9	2.20	2.42	2.35
trans$[Rh(PEt_3)_2Cl_4]^-$ **(27)**	-	2.355	-	2.358
$[Rh_2(\mu\text{-}dppm)_2(\mu\text{-}Cl)_2Cl_2]$[28]	-	2.385	-	2.310

Figure 5. The Crystal Structure of the Type (B) Anion in $[Rh_2(dcpe)_2(\mu\text{-}Cl)_3Cl_2][Rh(dcpe)Cl_4]^-$ (3)

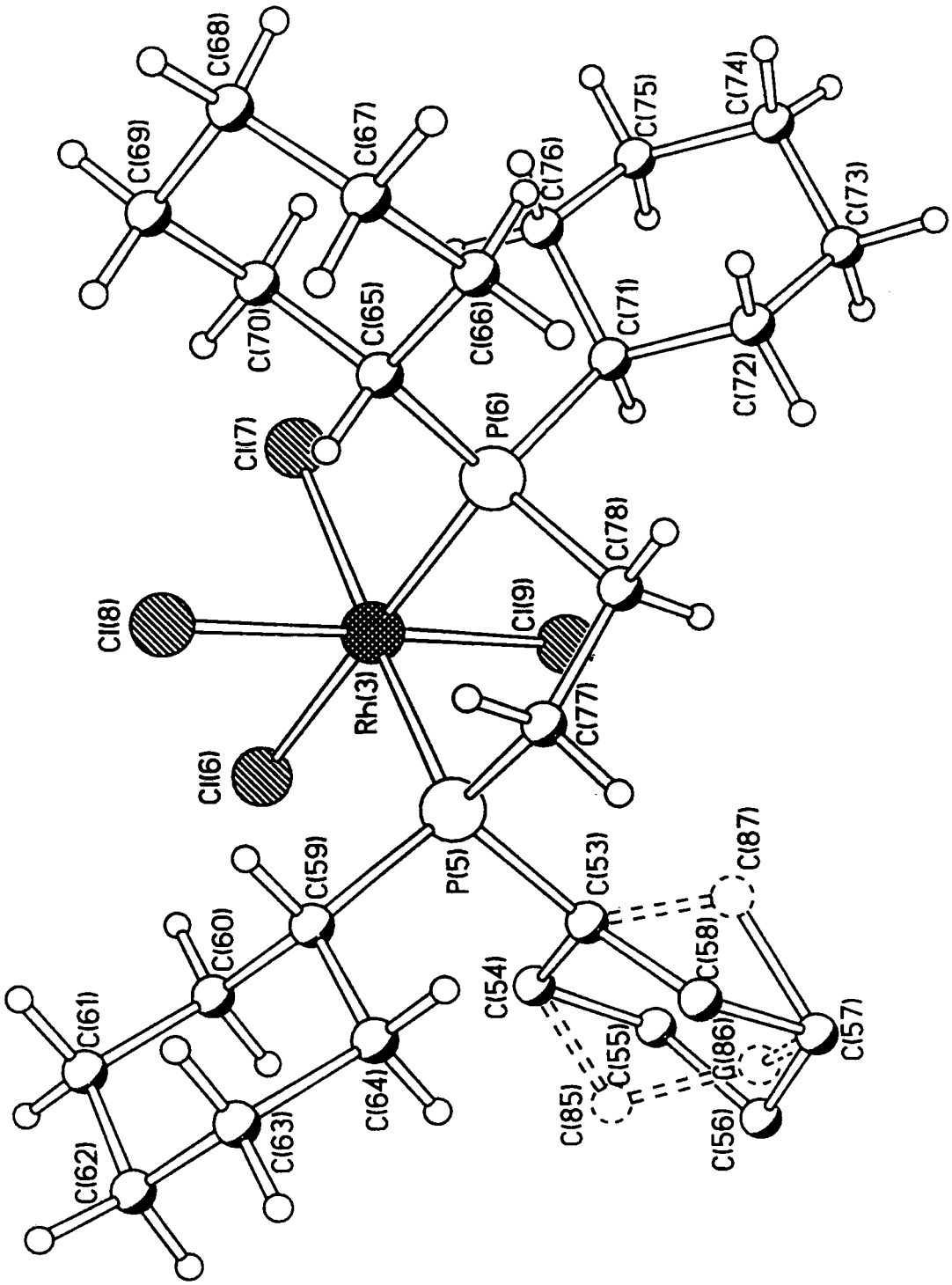

Figure 6. The Crystal Structure of the Type (B) Complex $(NH_3OH)[Rh(dppe)Cl_4]$ (5)

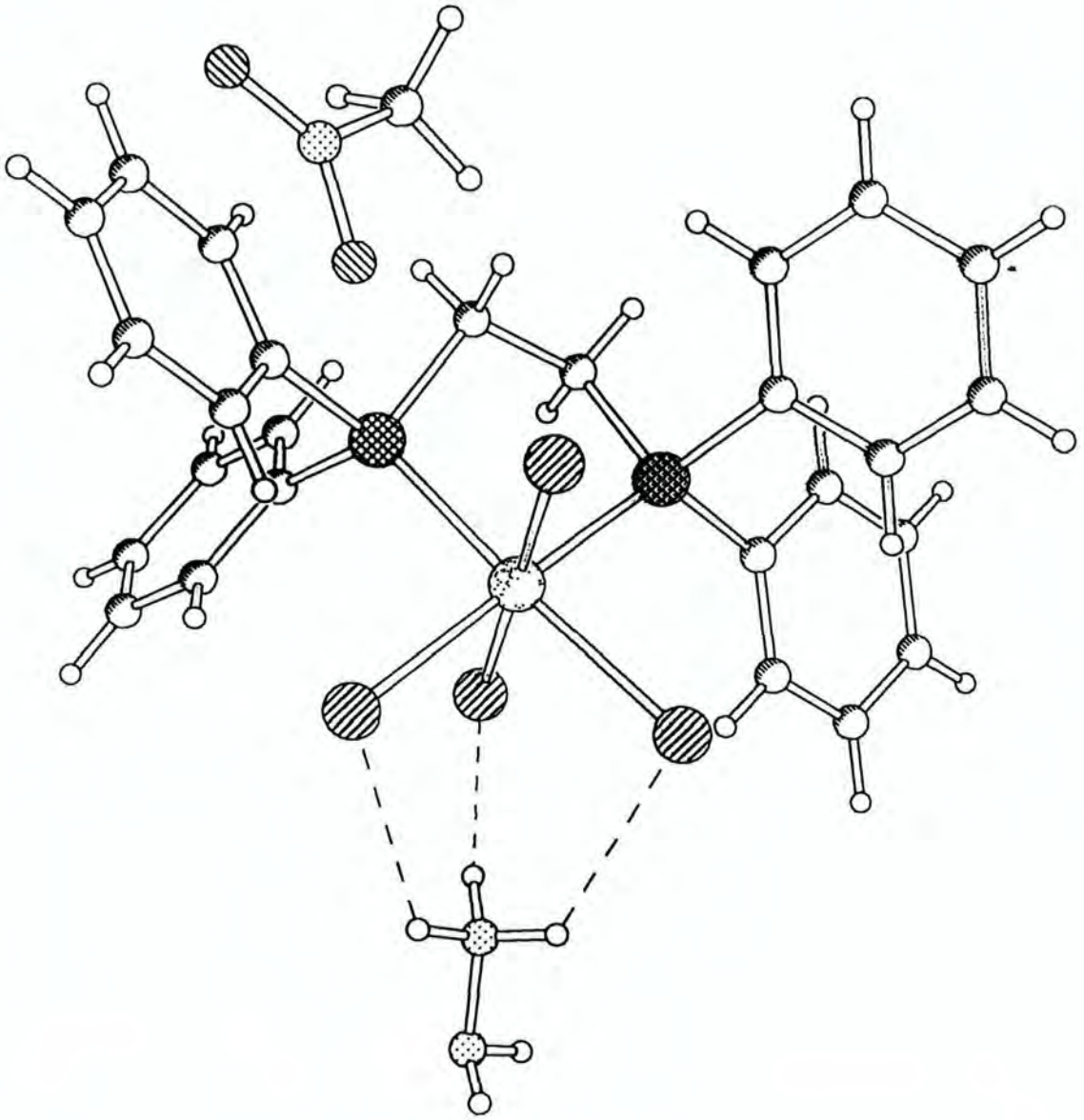

Similar to the type **(A)** complexes discussed above, the Rh-Cl bonds *trans* to a phosphorus are longer than those *trans* to a chlorine. The Rh-Cl bonds *trans* to chlorine show remarkable consistency at ~2.36Å, and these are very similar in length to the bridging Rh-Cl bonds observed for the complexes in Table 3. The only exception to this is dppm $[Rh_2(\mu\text{-dppm})_2(\mu\text{-Cl})_2Cl_2]$, where the terminal chlorine is *trans* to a bridging chlorine and is marginally shorter.

The $Rh\text{-}Cl_{(trans\ to\ Cl)}$ are longer than in the type **(A)** complexes, whilst $Rh\text{-}Cl_{(trans\ to\ P)}$ are shorter. This is probably because $Rh\text{-}Cl_{(trans\ to\ P)}$ is not involved in bridging two metal atoms. The lengthening of the Rh-Cl bonds is due to the negative charge on the complex, some of which will be localised on the metal. Similar to the type **(A)** complexes, the dcpe complex **(3)** again has longer Rh-P bonds than the dppe complex **(5)** for the reasons outlined in Section 9.2.1. However, the bite angles for both the dppe and dcpe complexes are larger in these anionic species than the dinuclear complexes. In contrast to the type **(A)** complexes, the longest Rh-Cl bonds are observed for the dppe complex **(5)**. However, this lengthening may be due to the intermolecular hydrogen-bonding present. In the unit cell of complex **(5)** there are four anionic rhodium complexes, and these are arranged in a square (see Chapter 7, Figure 2, page 154). Each chlorine ligand is involved in hydrogen bonding with the protons on the hydroxylammonium cation. In effect they are bridging, and in the complexes of type **(A)** above, bridging interactions lead to a bond lengthening. The data for the hydroxylammonium ion compare well with the previously reported example.[29] (Mean N-O distance 1.395Å, lit.[28] 1.415Å).

9.2.3 Type (C), [Rh(diphos)LX_3]

Complex **(6)**, $[Rh(dppe)(CO)Cl_3]$, is the only example of a type **(C)** complex characterised by X-ray crystallography in this work. Type **(C)** complexes are very similar to the Type **(A)** and type **(B)** mentioned above; a type **(C)** complex is a type **(B)** complex with a neutral in place of an anionic ligand. Complex **(6)** is also unusual

because it is a Rh(III) carbonyl species. Carbonyl ligands are weak σ-donors, but strong π-acceptors.[19] Consequently carbonyl ligands in Rh(III) complexes are destabilised, where the capacity for back-donation is reduced. Table 6 contains selected data for complex **(6)** and related species.

Table 6. Selected Bond lengths (Å). For Complex (6) and Related Species

Complex (phosphine)	**P-Rh**	**Rh-C (C-O)**	**Rh-Cl *trans* to CO**	**Rh-Cl *trans* to P**
(6) (dppe)	2.3051	1.885 (1.124)	2.3521	2.4277
(28) $[Rh(dppm)(MeCN)Cl_3]$[30]	2.258	-	2.301***	2.437
(29) $[Rh_2(PPh_2O)_2(PPh_2OH)-(CO)_2(\mu\text{-}Cl)_2Cl_2]$[31]	2.256	1.846 (1.138)	2.336	2.484
(30) *trans*$[Rh(PMe_3)_2(CO)(CCl_3)-(Cl)Br]$[32]	2.384	1.876 (1.128)	2.366	-
(31) *trans*$[Rh(PEt_3)_2(CO)Cl(I)-(CH_2I)]$[33]	2.377	1.838 (1.119)	2.389	-
trans$[Rh(PMePh_2)_2(CO)Cl]$[34]	2.315	1.795 (1.142)	2.362	-
trans$[Rh(PMe_2Ph)_2(CO)Cl]$[35]	2.316	1.800 (1.154)	2.356	-
trans$[Rh(PMe_3)_2(CO)Cl]$[36]	2.309	1.770 (1.146)	2.354	-
trans$[Rh(PBu^t_3)_2(CO)Cl]$[37]	2.427	1.784 (1.151)	2.389	-

*** *Trans* to MeCN

The PRhP angle for complex **(6)** is 86.78°. This is slightly smaller than that observed in $[Rh(dppe)Cl_4]^-$, although larger than in the bridged dppe complexes of type **(A)**. However, the Rh-P bond distances in this complex are longer in complex **(6)** than in $[Rh(dppe)Cl_4]^-$ and $[Rh(dppe)_2Cl_5]^+$, by up to 0.4Å. The reason for this is unclear, although there may be some residual Rh-P backbonding in the type **(A)** and **(B)** complexes, which the phosphine cannot compete for in the presence of CO. However, the Rh-Cl bond lengths are shorter in this complex than in the type **(A)** and **(B)** species.

Figure 7. The Crystal Structure of the Type (C) Complex [Rh(dppe)(CO)Cl_3] (6)

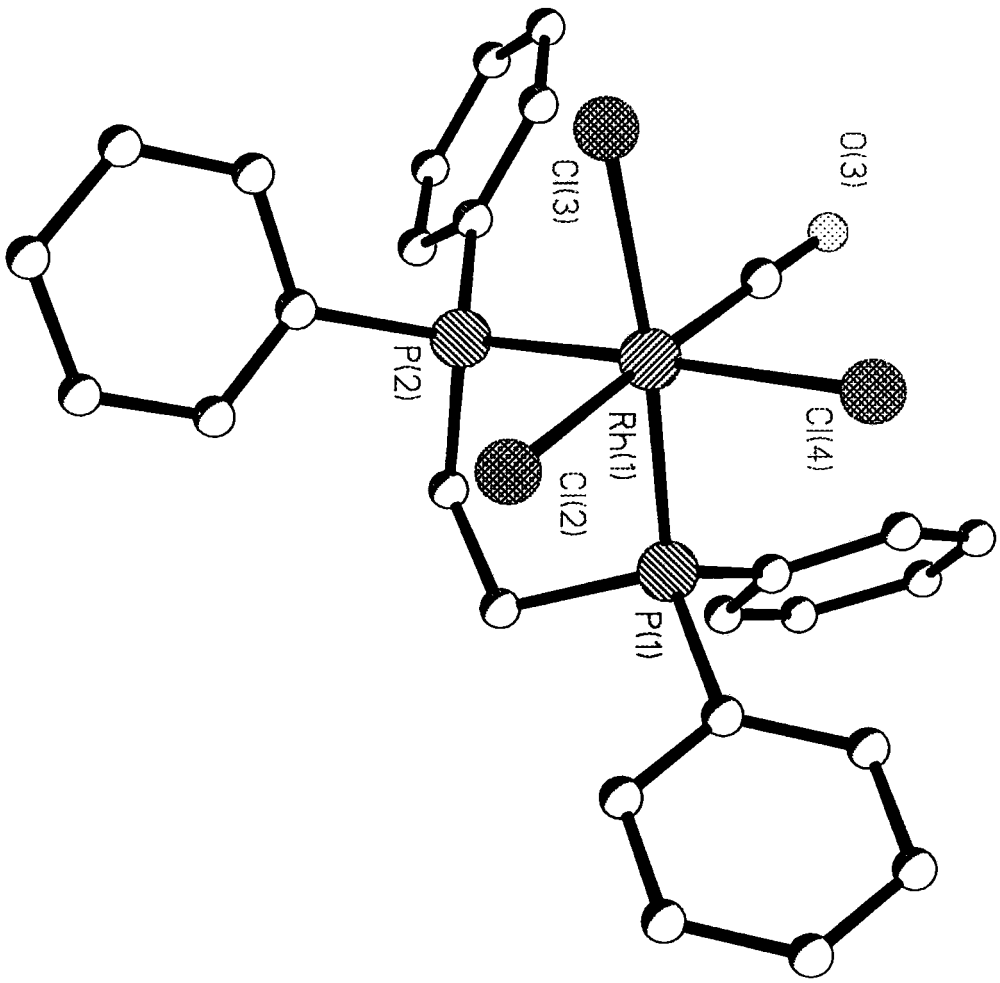

In the related dppm complex **(28)**, where the CO has been replaced by MeCN, the Rh-Cl bond *trans* to the MeCN is shorter than in complex **(6)** where it is *trans* to CO. This is because of the higher *trans* influence of the CO (a strong π-acceptor) than the MeCN.[19] Several other similar species have been observed and structurally characterised.[29]

Interestingly, when the acetonitrile ligand in complex **(28)** is replaced by PBu^n_3,[30] the phosphine is located *trans* to the dppm and not trans to a chlorine. This disposition of the ligands can be attributed to steric interactions between the ligands. However, in the related complex *fac*-$[Rh(PBu^n_3)_2\{P(OMe)_3\}Cl_3]$ the phosphite is *cis* to the two phosphines.[38]

In general for metal-carbonyl complexes, metal ligand back-donation occurs from the filled d orbitals of the metal to the π*-orbitals of the CO. Consequently the M-C and C-O bond distances can give an indication of the level of backbonding to this ligand. Increasing the back-donation from the metal to the CO, should shorten the Rh-C bond distance and lengthen the C-O bond distance. This is exactly what is observed for complexes **(6)**, **(29)**, and **(30)**, although not for complex **(31)**, with the weakest backbonding to the carbonyl ligand observed in the dppe complex reported here, **(6)**. However, the M-C and C-O bonds in complexes **(6)**, **(29)**, and **(30)**, are longer and shorter respectively than in the related Rh(I) complexes in Table 6 and this is consistent with decreased backbonding in the Rh(III) complexes due to depopulation of the d-orbitals.

9.3. Summary

A series of Rh(III)-diphosphine complexes has been structurally characterised by X-ray crystallography. The complexes can be classed into three groups according to their structural characteristics. Class **(A)** complexes are cationic and based on two facially

bridged octahedra. These can be further subdivided into the isomers **(A1)** and **(A2)** according to the positions of the terminal ligands with respect to the three bridging atoms. The **(A1)** complexes characterised here were $[Rh_2(dppp)_2(\mu\text{-}Cl)_3Cl_2]^+$, $[Rh_2(dppe)_2(\mu\text{-}Cl)_3Cl_2]^+$, and $[Rh_2(dcpe)_2(\mu\text{-}Cl)_3Cl_2]^+$. The only example of an **(A2)** type structure described here was the complex $[Rh_2(dppp)_2(\mu\text{-}OH)(\mu\text{-}OMe)Cl_2]^+$. Comparison of the literature data for these and related complexes, reveals that the major influence directing which stereoisomer is observed is steric in origin. Class **(B)** complexes are anionic, monomeric and octahedral in structure, $[Rh(dcpe)Cl_4]^-$ and $[Rh(dppe)Cl_4]^-$,being reported here. Normally these complexes only crystallise with large cations and $[Rh(dppe)Cl_4]^-$ is the first example of a class **(B)** structure with a small cation. This is because of hydrogen bonding interactions with the cation $(H_3NOH)^+$. Class **(C)** type complexes are neutral and octahedral and the structure of $[Rh(dppe)(CO)Cl_3]$ is reported here. Comparison of this complex with literature data for other rhodium carbonyls reveals there is very little back donation to the carbonyl ligand in this complex. Comparison of the bond angles and bond lengths about the metal reveal systematic differences occur as the diphosphine is varied. The shortest Rh-Cl and Rh-P bond lengths for the complexes observed here occur with the phosphine dppe. Increasing the chelate bite angle or replacing the phenyl for cyclohexyl groups on the phosphine increases the steric bulk about the phosphine and this leads to an overall lengthening of the Rh-P bonds about the rhodium atom.

9.4. References

[1] M.A. Bennet, J.C. Jeffery, G.B. Robertson, *Inorg. Chem.*, **20**, (1981), 330
[2] I.R. Butler, W.R. Cullen, T.J. Kim, F.W.B. Einstein, T. Jones, *J. Chem. Soc. Chem. Commun.*, (1984), 719; F.W.B. Einstein, T. Jones, *Acta Cryst. C (Cr. Str. Comm.)*, **41**, (1985), 365.
[3] M.D. Fryzuk, *Organometallics*, **10**, (1991), 3767-3769.
[4] J.A.S. Duncan, T.A. Stephenson, M.D. Walkinshaw, D. Hedden, D.M. Roundhill, *J. Chem. Soc. Dalton. Trans.*, (1984), 801-807.
[5] M.J. Nolte, E. Singleton, E. Van der Stok, *Acta Cryst. Sect. B*, **34**, (1978), 1684.
[6] S.N. Gamaga, R.H. Morris, S.J. Rettig, D.C. Thackray, I.S. Thorburn, B.R. James, *J. Chem. Soc. Chem. Commun.*, (1987), 894.
[7] G. Chioccola, J.J. Daly, *J. Chem. Soc. A*, (1968), 1981.
[8] F.A. Cotton, R.C. Torralba, *Inorg. Chem.*, **30**, (1991), 2196.
[9] I.S. Thorburn, S.J. Rettig, B.R. James, *Inorg. Chem.* **25**, (1986), 234.
[10] T. Yamagata, K. Tani, Y. Tatsuno, T. Saito, *J. Chem. Soc. Chem. Commun.*, (1988), 466.
[11] F. Bachechi, *Acta Cryst. C(Cr. Str. Comm.)*, **50**, (1994), 1069.

[12] J.A. Muir, M.M. Muir, A.J. Rivera, *Acta Cryst. Sect. B*, **30**, (1974), 2062.
[13] F.A. Cotton, S.J. Kang, S.K. Mandel, *Inorg. Chim. Acta*, **206**, (1993), 29
[14] H.A. Brune, R.Hemmer, J. Unsin, K. Holl, U. Thewalt, *Z. Naturforsch Teil B*, **43**, (1988), 487.
[15] M.D. Curtis, W.M. Butler, J. Greene, *Inorg. Chem.*, **17**, (1978), 2928.
[16] P. Binger, J. Haas, G. Glaser, R. Goddard, C. Kruger, *Chem. Ber.*, **127**, (1994), 1927.
[17] R.C. Schnabel, D.M. Roddick, *Inorg. Chem.*, **32**, (1993), 1513.
[18] P. Hoffman, C.Meier, W. Hiller, M. Heckel, J. Reide, M.U. Schmidt, *J. Organomet. Chem.*, **490**, (1995), 51.
[19] R.H. Crabtree, "The Organometallic Chemistry of the Transition Elements" Wiley-Interscience, Chichester, 1988.
[20] K. Wieghardt, W.Schmidt, B. Nuber, B. Prikner, J. Weiss, *Chem. Ber.*, **113**, (1980), 36.
[21] A. Nutton, P.M. Bailey, P.M. Maitlis, *J. Chem. Soc. Dalton. Trans.*, (1981), 1997.
[22] L.A. Oro, D. Camona, M.P. Lamata, M.C. Apreda, C. Foces-Foces, F.H. Cano, P.M. Maitlis, *J. Chem. Soc. Dalton Trans.*, (1984), 1823.
[23] C.A. Tucker, C. Woods, J.L.E. Burn, *Inorg. Chim. Acta*, **126**, (1987), 141.
[24] P. Braustein, L. Douce, J. Fischer, N.C. Craig, G. Goetz-Grandmont, D. Matt, *Inorg. Chim. Acta*, **194**, (1992), 151-156.
[25]M.F.M. Mohammad, F.M. Al-Dulaymni, P.B. Hitchcock, R.L. Richards, *J. Organomet. Chem.*, **338**, (1988), C31-C34; M.F.M. Mohammad, F.M. Al-Dulaymni, P.B. Hitchcock, D.L. Huges, R.L. Richards, *J. Chem. Soc. Dalton. Trans.*, (1992), 241.
[26] Y.N.G. Cheong, C.D. Meyer, J.A. Osborn, *J. Chem. Soc. Chem. Commun.*, (1990), 869.
[27] F.A. Cotton, S.J. Kang, *Inorg. Chem.*, **32**, (1993), 2336-2342.
[28] F.A. Cotton, K.R. Dunbar, C.T. Eagle, L.R. Falvello, A.C. Price, *Inorg. Chem.*, **28**, (1989), 1754.
[29] K.N. Trueblood, C.B. Knobbler, D.S. Lawrence, R.V. Stevens, *Acta Cryst. Sect. A*, **37**, (1981), C90: *J. Am. Chem. Soc.*, **104**, (1982), 1355.
[30]F.A. Cotton, K.R. Dunbar, C.T. Eagle, L.R. Falvello, S.J. Kang, A.C. Price, M.G. Verbruggen, *Inorg. Chem.* **184**, (1991), 35-42.
[31] L.A. Glinskaya, E.N. Yurchenko, S.F. Solodovnikov, L.S. Gracheva, R.F. Klevtsova, *Zh. Strukt. Khim.*, **23**, (1982), 79-3.
[32] C.J. Cable, H. Adams, N.A. Bailey, J. Crosby, C. White, *J. Chem. Soc. Chem. Commun.*, (1991) 165.
[33] R.C. Gash, D.J. Cole-Hamilton, R. Whyman, J.C. Barnes, M.C. Simpson, *J. Chem. Soc. Dalton. Trans.*, (1994), 1963.
[34] F. Dahan, R. Choukroun, *Acta Cryst., C(Cr. Str. Comm.)*, **41**, (1985), 704.
[35] H. Schumann, S. Jurgis, M. Eisen, J. Blum, *Inorg. Chim. Acta*, **172**, (1990), 191.
[36] S.E. Boyd, L.D. Field, T.M. Hambley, M.G. Partridge, *Organometallics*, **12**, (1993), 1720.
[37] R.L. Harlow, S.A. Westcott, D.L. Thorn, R.T. Baker, *Inorg. Chem.*, **31**, (1992), 323.
[38] F.H. Allen, G. Chany, T.F. Lai, L.M. Lee, A. Pidcock, *J. Chem. Soc. D*, (1970), 1297.

Chapter 10

Conclusions

Rhodium-chelating diphosphine complexes are active catalysts for a range of reactions (see Chapter 1). With this in mind, a series of complexes of the type $[Rh(diphos)(C_7H_8)](BF_4)$ **(1)** (diphos = dBpe, dBpp, dcpp, Boxylyl, dppe, dppp, dppb, dcpe) has been synthesised and two of these (diphos = dBpe, dcpcp) have been structurally characterised by X-ray crystallography. During the synthesis of these compounds, two silver by-products $[Ag_2(\mu\text{-dBpp})_2](BF_4)_2$ and $[Ag_2(\mu\text{-dBpe})(H_2O)_2](BF_4)_2$ have been isolated and characterised by X-ray crystallography; the former has been independently synthesised from $AgBF_4$ and dBpp.

The influence of the steric and electronic properties of the phosphine on the chelate chemical shift $(\Delta r)^{1,*}$ of the chelating phosphine, observed in the phosphorus NMR, and other spectroscopic parameters have been investigated for the type **(1)** and $[Rh(diphos)(CO)_2](BF_4)$ **(2)** complexes. In these complexes, Δr (and the phosphorus chemical shift) increases as the electron donating ability of the substituents on the phosphine and decreases in the order $Bu^t > Cy > Ph$. However, if there is a high degree of steric congestion in the molecule this order can be interrupted. Increasing the size of the chelate ring from 5 to 6 changes the order to $Cy > Bu^t > Ph$ for type **(1)** complexes, but not in the less sterically congested type **(2)** complexes which retain the original order. An inverse relationship between $^1J_{Rh\text{-}P}$ coupling constants and Rh-P bond distances has been observed before in complexes of the type $[Rh(PR_3)Cl_3]$.[2] A similar trend can be seen in the type **(1)** complexes; increasing the steric properties and basicity of the diphosphine leads to an increase in the Rh-P bond distance, a decrease

* The chelate chemical shift is the difference in the phosphorus chemical shifts between a chelating complex and a non-chelating analogue; see chapter 2 for a full description of the chelate chemical shift.

in $^{1}J_{Rh-P}$ and a decrease in the chemical shift for the carbon-carbon double bond $\delta_{C=C}$ in the co-ordinated diene. The decrease in $\delta_{C=C}$ is mirrored by an increase in the carbon-carbon bond distance and a decrease in the Rh-C bond distance, corresponding to an activation of the diene due to the increased metal-ligand back donation.

Complexes of the type **(1)** are found to be active hydroformylation catalysts (120°C, 450psi 1:2 $CO:H_2$). However, they are inactive for the related process of hydroesterification. This is due to the formation of type **(2)** complexes, which are very stable under the conditions used. The rate of hydroformylation of 1-hexene and the selectivity towards linear aldehyde products, using type **(1)** complexes are dependent on the phosphines employed. The greatest rates and selectivities were achieved with the phosphine dppb. Replacing the Ph groups on the phosphine with Bu^{t} or Cy groups causes a change in mechanism and contrary to other studies,[3] increasing the chelate ring size or sterically hindering the phosphine backbone, decreases the selectivity towards the linear products.

In an effort to study the individual steps in an idealised catalytic carbonylation cycle the reaction of the type **(1)** complexes with hydrogen, CO and ethene were investigated. Throughout these studies the behaviour of the phosphine Boxylyl was found to be unusual and normally differs from the other phosphines studied.

The products from the hydrogenation of complexes of the type $[Rh(diphos)(C_7H_8)](BF_4)$ **(1)** (diphos = dBpe, dBpp, dcpe, dcpp, dcpcp, Boxylyl) are dependent on the solvent and the phosphine, and were studied by VT NMR as a consequence of the fluxional nature of the products formed. In methanol the square-planer Rh(I) di-solvate species of the type $[Rh(diphos)(MeOH)_2](BF_4)$ **(3)** were formed. However, the phosphine Boxylyl complex, **(3)**, exhibits temperature dependent, reversible thermochroism due to square planer-tetrahedral isomerism. In THF, hydrides and complex **(3)** (diphos = dBpe) are both observed, and in the non co-ordinating solvent CD_2Cl_2, the same hydrides are also detected. Generally under an

atmosphere of hydrogen, several hydride species can be observed in rapid equilibrium with each other. Three major hydride species can be identified $[Rh_2(diphos)_2H_6]$, $[Rh_2(diphos)_2H_4]$, $[Rh(diphos)H_2]^+$, often present in several isomeric forms. The distribution of these species is dependent on the phosphine employed; increasing the steric bulk of the phosphine favours the formation of the dimeric tetra-hydride. The Boxylyl ligand produces exceptional results, and the hydrides formed are green rather than red in colour; the predominant species in solution are Rh(I) and not Rh(III) complexes. Hydrogenation of type **(1)** complexes in $CDCl_3$ leads to the formation of complexes of the type $[Rh(diphos)(\mu\text{-}Cl)_2H_2]^+$ **(4)** as the major species, due to the partial chlorination of the hydrides by the chloroform solvent. When the Boxylyl system was investigated under the same conditions, a range of other products was observed in the NMR spectra and attempts are made to identify them. An alternative synthesis of complex **(4)** was achieved from the reaction of HCl with either the hydrides derived from **(1)** in CD_2Cl_2, or complexes of the type **(3)**.

Addition of ethene to the hydrides formed in from type **(1)** (diphos = dBpp) in CD_2Cl_2, leads to the formation of several rhodium species, containing alkene, alkyl and hydride ligands. Addition of CO to the hydride or alkyl systems, leads to the formation of type **(2)** complexes which are reaction "sinks" in these circumstances.

Due to the variety of products formed from the direct reaction of H_2, CO, and ethene with complexes of the type **(1)**, alternative routes to the formation of catalytic intermediates, especially acyls and alkyls were explored, and included the oxidative addition of organohalides (RX) to Rh(I) complexes.

The reactions of $[Rh(dppe)Cl]_2$ with RX (RX = EtCl, EtCOCl, $Br(CH_2)_2CO_2Me$, $ClCO_2Me$) have been investigated. Reaction with EtCOCl leads to the formation of a Rh(III) acyl species $[Rh(dppe)(COEt)Cl_2]$. However, attempts to create vacant co-ordination positions by dehalogenation with $AgBF_4$ led to the formation of several products *via* decarbonylation and β-hydride elimination. Similarly, the intended

products from the reaction with $Br(CH_2)_2CO_2Me$ were not obtained because of subsequent de-insertion reactions. Addition of CO to these reaction mixtures resulted in the formation of $[Rh(dppe)(CO)_2]^+$, which again, is the sink for reactions involving CO. The reaction with EtCl did not proceed until $AgBF_4$ was added, at which point the solution turned colourless. However, further identification of the product in C_6D_6 by NMR methods was hampered due to the presence of the (novel) impurity $[Ag(C_6D_6)_3](BF_4)$ which was characterised by X-ray crystallography. The reaction of $[Rh(dppe)Cl]_2$ with methylchloroformate in CD_3NO_2 was rapid and a Rh(III) halide complex $(NH_3OH)[Rh(dppe)Cl_4]$ **(5)** was formed; the hydroxylammonium ion arising from reaction of $ClCO_2Me$ with the solvent, whilst the reaction of $ClCO_2Me$ with $[Rh(dppe)(MeOH)_2]^+$ produced the halide bridged dimeric species $[Rh_2(dppe)_2(\mu\text{-}Cl)_3Cl_2](BF_4)$ **(6)**.

With a view to finding alternative synthetic routes to $[Rh_2(diphos)_2Cl_5]^+$ type complexes, the reaction of $RhCl_3.3H_2O$ with diphosphines was investigated. The products are dependent on both the phosphine and the conditions employed. At r.t. in methanol, several products are observed which are insoluble. However, for dcpe, soluble products are formed, which are in equilibrium in solution, but crystallise to form the ionic complex $[Rh_2(dcpe)_2(\mu\text{-}Cl)_3Cl_2[Rh(dcpe)Cl_4]$ **(7)**. If the dppp system is heated in refluxing methanol similar products can be formed and $[Rh_2(dppp)_2(\mu\text{-}Cl)_3Cl_2](Cl)$ **(8)** has been isolated. Complexes **(7)** and **(8)** are both fluxional in solution. In the presence of CsF in methanol, complex **(8)** reacts to form $[Rh_2(diphos)(\mu\text{-}OH)(\mu\text{-}OMe)_2Cl_2](Cl)$ **(9)**, which has a related core structure to complex **(8)**, consisting of two rhodium diphosphine units and three bridging ligands with oxygen ligands replacing the three bridging chloro-ligands of complex **(8)**. This difference arises due to the steric interactions of the phosphine with the bridging ligands. Alternative routes to $[Rh_2(dppe)_2(\mu\text{-}Cl)_3Cl_2](BF_4)$ **(6)** have been discovered, although these only proceed in low overall yield due to the insolubility of the starting materials, $[Rh(dppe)(MeCN)Cl_3]$ and the products from the reaction of $RhCl_3.3H_2O$ with dppe. Complex **(6)** reacts with carbon monoxide to form the novel Rh(III)

carbonyl complex [Rh(dppe)(CO)Cl_3] **(10)**. However, attempts to synthesise **(10)** from [Rh(dppe)(MeCN)Cl_3] were unsuccessful due to the kinetic stability of this compound. Inspection of the structural data for complexes **(5)** to **(10)** and data in the literature, shows that as the steric bulk of the diphosphine system increases, all of the metal-ligand bond distances also increase due to the interaction of the phosphine with the bridging ligands. This contrasts with the results obtained for the type **(1)** complexes, where increasing the steric bulk of the phosphine causes an increase in the Rh-P bond distances, but a decrease in the Rh-C bond distances.

Summary

Type **(1)** complexes are active catalyst precursors for hydroformylation, but not hydroesterification, this being attributed to the high stability of the type **(2)** complexes which provide a sink for the rhodium complexes under hydroesterification conditions.

Routes to potential catalytic intermediates have been investigated: from the reaction of type **(1)** complexes with hydrogen, CO, and ethene and from the oxidative addition of RX to Rh(I) complexes. This has led to the formation of several new rhodium(III) halide species and their chemistry has been investigated.

References

[1] P.E. Garrou *Chem. Rev.*, **81**, (1981), 229-266.
[2] G.G. Mather, A. Pidcock, *J. Chem. Soc. Dalton Trans.*, (1973), 2095-2099.
[3] C.P. Casey, G.T. Whiteker, M.G. Melville, L.M. Petrovich, J.A. Gavney Jr., D.R. Powell, *J. Am. Chem. Soc.*, **114**, (1992), 5535-5543.

Appendix 1

Experimental Parameters

Unless otherwise stated, all reactions were carried out under a dry, oxygen free nitrogen atmosphere, using standard vacuum line techniques, and the solvents were dried and freshly distilled prior to use. $RhCl_3.3H_2O$, and the diphosphines dBpp, DBpe, dcpe, dcpp, and Boxylyl were supplied by ICI Acrylics, all other reagents were purchased commercially.

The NMR spectra were recorded on a Bruker AC250 spectrometer at ambient temperature and the following frequencies: phosphorus 101MHz, carbon 70MHz, proton 250MHz. The variable temperature NMR studies were carried out on a Varian NMR spectrometer at the following frequencies: phosphorus 161MHz, proton 400MHz. The proton and carbon NMR spectra are referenced to the ^{1}H and ^{13}C chemical shifts of the solvent as an internal standard, and reported with respect to $SiMe_4$. The ^{31}P spectra are referenced to an external frequency lock, and reported with respect to 85% H_3PO_4 at 0ppm. Unless otherwise stated, the infra-red spectra were recorded as KBr discs at $2cm^{-1}$ resolution on a Perkin-Elmer 1600 series FT-IR spectrometer.

The mass-spectra were recorded on a VG analytical 707E spectometer. Fast atom bombardment using xenon was used on the complexes in a nitrobenzylalcohol matrix or methanol-glycerol matrix. The carbon, hydrogen and nitrogen elemental analyses were measured on a CE 440 elemental analyser.

Appendix 2

Supplementary Data for Chapter 2

Table 1. Crystal Structure Data and Refinement for [Rh(dBpe)(C_7H_8)][BF_4]

Empirical formula	C25 H48 B F4 P2 Rh
Formula Weight	600.29
Temperature	423(2) K
Wavelength	0.71073 Å
Crystal System	
Space Group	
Unit Cell Dimensions	a = 11.491(2) Å; alpha 90°. b = 18.401(3) Å; beta 91.807(5)°. c = 13.207(2) Å; gamma 90°.
Volume	2791.1(7) $Å^3$
Z	4
Density (Calculated)	1.429 Mg/m^3
F(000)	0.765mm^{-1}
Crystal Size	
Theta Range for data Collection	1.90 to 25.86°.
Index Ranges	$-12 \leq h \leq 13$, $-21 \leq k \leq 22$, $-13 \leq l \leq 15$
Reflections Collected	11842
Independant Reflections	4821 [R(int) = 0.0339]
Refinement Method	Full Matrix least squares on F^2
data/restraints/parameters	4821/0/310
Goodness of fit on F^2	1.079
Final R indices [I>2sigma(I)]	R1 = 0.0304, wR2 = 0.0572
R indices (all data)	R1 = 0.0329, wR2 = 0.0774
Largest diff. peak and hole	0.888 and -0.605 $Å^{-3}$

Table 2. Crystal Structure Data and Refinement for [Rh(dcpcp)(C_7H_8)][BF_4]

Empirical formula	C39 H66 B F4 O P2 Rh
Formula weight	802.58
Temperature	150(2) K
Wavelength	0.71073 Å
Crystal system	Triclinic
Space group	P-1
Unit cell dimensions	a = 9.762(1) Å; alpha = 100.38(1)° . b = 9.795(1)Å; beta = 98.07(1)°. c = 20.108(1) Å; gamma = 90.08(1)°.
Volume	1871.8(3) A^3
Z	2
Density (calculated)	1.424 Mg/m^3
Absorption coefficient	0.592 mm^{-1}
F(000)	868
Crystal size	0.5 x 0.3 x 0.05 mm
Theta range for data collection	2.08 to 25.55°.
Index ranges	-11 ≤ h ≤ 11 -6<=k<=11 -24≤ l ≤ 22
Reflections collected	8477
Independent reflections	6047 [R(int) = 0.0367]
Absorption correction	Semi-empirical on Laue equivalents
Max. and min. transmission	1.0000 and 0.7886
Refinement method	Full-matrix least-squares on F^2
Data / restraints / parameters	6023 / 33 / 449
Goodness-of-fit on F^2	1.104
Final R indices [I>2sigma(I)]	R1 = 0.0566 wR2 = 0.1444
R indices (all data)	R1 = 0.0654 wR2 = 0.1610
Largest diff. peak and hole	1.410 and -0.986 $e.A^{-3}$

Appendix 3
Supplementary Data For Chapter 3

3.1 Crystal Structure Data and Refinement for $[Ag_2(\mu\text{-}Bu^t_2P(CH_2)_3PBu^t_2)_2]\ (BF_4)_2.2CH_2Cl_2$

Empirical formula	C40 H88 Ag2 Cl4 B2 F8 P4
Formula Weight	1224.14
Temperature	150(2) K
Wavelength	0.71073 Å
Crystal System	Triclinic
Space Group	P-1
Unit Cell Dimensions	a = 11.476(3) Å; alpha 67.49 (2)°. b = 11.559(3) Å; beta 82.37 (2)°. c = 12.485(3) Å; gamma 65.71 (2)°.
Volume	1393.9 (6) $Å^3$
Z	1
Density (Calculated)	1.458 Mg/m^3
Absorption Coefficient	1.063 mm^{-1}
F(000)	632
Crystal Size	0.3 x 0.3 x 0.1 mm
Theta Range for data Collection	2.59 to 25.00 deg.
Index Ranges	$-13 \leq h \leq 12$, $-13 \leq k \leq 0$, $-14 \leq l \leq 13$
Reflections Collected	5169
Independent Reflections	4902 [R(int) = 0.0225]
Refinement Method	Full Matrix least squares on F^2
data/restraints/parameters	4902/0/310
Goodness of fit on F^2	1.013
Final R indices [I>2sigma(I)]	R1 = 0.0439, wR2 = 0.0890
R indices (all data)	R1 = 0.0691, wR2 = 0.0948
Largest diff. peak and hole	1.143 and -0.829 $Å^{-3}$

Table 2. B-F Bond Lengths (Å) and Bond Angles (°) for $[Ag(Bu^t_2P(CH_2)_3PBu^t_2)]_2(BF_4)_2.2CH_2Cl_2$

F(4)-B-F(2)	109.3(5)	F(1)-B-F(3)	108.1(4)
F(4)-B-F(1)	110.7(5)	B-F(4)	1.360(6)
F(2)-B-F(1)	109.2(5)	B-F(2)	1.373(7)
F(4)-B-F(3)	110.2(5)	B-F(1)	1.376(7)
F(2)-B-F(3)	109.3(5)	B-F(3)	1.402(7)

Table 3. Crystal Structure Data and Refinement for for $[Ag_2(\mu\text{-}Bu^t_2P(CH_2)_2PBu^t_2)(H_2O)_2]_2(BF_4)_2$.

Empirical formula	C18 H44 Ag2 B2 F8 O2 P2
Formula weight	743.83
Temperature	150(2) K
Wavelength	0.71073 Å
Crystal system	Monoclinic
Space group	P2(1)/n
Unit cell dimensions	a = 7.8285(10) Å; alpha = 90°. b = 16.134(2) Å; beta = 103.951(8)°. c = 12.035(2) Å; gamma = 90°.
Volume	1475.3(5) A^3
Z	2
Density (calculated)	1.675 Mg/m^3
Absorption coefficient	1.500 mm^{-1}
F(000)	748
Crystal size	0.40 x 0.40 x 0.07 mm
Theta range for data collection	2.15 to 25.74 deg.
Index ranges	$-9 \leq h \leq 7$, $-12 \leq l \leq 14$, $-19 \leq k \leq 18$
Reflections collected	6107
Independent reflections	2513 [R(int) = 0.0407]
Absorption correction	Integration
Max. and min. transmission	0.9007 and 0.5154
Refinement method	Full-matrix least-squares on F^2
Data / restraints / parameters	2513 / 0 / 242
Goodness-of-fit on F^2	1.099
Final R indices [I>2sigma(I)]	R1 = 0.0327 wR2 = 0.0834
R indices (all data)	R1 = 0.0362 wR2 = 0.0860
Largest diff. peak and hole	0.380 and -0.727 $Å.^{-3}$

Table 4. B-F Bond Lengths (Å) and Bond Angles (°) for $[Ag_2(\mu\text{-}Bu^t{}_2P(CH_2)_2PBu^t{}_2)(H_2O)_2]_2(BF_4)_2$.

B-F(4)	1.370(5)	F(4)-B-F(1)	112.4(4)
B-F(1)	1.375(5)	F(4)-B-F(2)	108.4(3)
B-F(2)	1.394(5)	F(1)-B-F(2)	109.3(4)
B-F(3)	1.397(5)	F(4)-B-F(3)	109.7(4)
		F(1)-B-F(3)	109.0(3)
		F(2)-B-F(3)	108.0(4)

Appendix 4

Supplementary Data For Chapter 5

4.1. Peak Positions for all Phosphorus and Proton NMR Signals for the Hydrogenation of [Rh(dBpe)(C_7H_8)](BF_4) in CD_2Cl_2

Peak	δ - ppm (J -Hz)				
	30°C	**0°C**	**-30°C**	**-60°C**	**-90°C**
$^{31}P\{^1H\}$ NMR *(C8)*	128.0 (br d)	126.6 (d, 131)	126.7 (d, 100)	(d m,132)	slightly broader
(C9)				(br d, 130)	Sharper 129.3 (d, 139)
(A3)	139.0 (d, 122)	No Change	No Change	No Change	No Change
	118.8 (d, 102)	sharper (d, 167.9)	116.2 (d, 169)	No Change	No Change
(B2)	115.6 (d, 140)	115.2 (dd, $J_1$139, J_2 10)	broader 114.6 (d, 130)	No Change	113.9 (d, 139)
	114.3 (d m, 174)	113.7 (d, 94)	No Change	No Change	112.2 (br d, 84)
					111.0 (br d,103)
(D)	102.2 (d, 147)	No Change	No Change	broader	101.0 (br s)
^1H NMR *(C1)*				-9.35 (br d, 128.8)	-9.30 (br dt, 115)
(C2)		-10.66 (br s)	larger	No Change	-10.30 (br tm)
(A1)	-10.85 (tm, J_1 74.4, J_2 7.2)	No Change	No Change	No Change	No Change
(A2)	m -18.71 (m, J_1 18.0, J_2 18.8)	No Change	No Change	No Change	No Change
(C3)		-20.40 (br s)	larger	No Change	-20.57 (br q, 22.4)
(C4)			-21.60 (br s, small)	sharper	-21.40 (br s)
(B1)	-22.7 (m, J_1 25.2, J_2 23.6)	No Change	No Change	No Change	-22.77 (br s)

4.2 Peak Positions for all Phosphorus and Proton Signals for the Hydrogenation of [Rh(dBpp)(C_7H_8)](BF_4) in CD_2Cl_2

	δ - ppm (J -Hz)		
Peak	**30°C**	**-30°C**	**-90°C**
$^{31}P\{^1H\}$ NMR A		75.4 (br d,105)	74.4 (d, 94, **105P**)
B		67.7 (br d, 86)	66.9 (d, 102, **116P**)
C	64.6 (br dd, 142)	63.4 (Sh dd, J_1 34, J_2 15)	62.3 (Shdd J_1 134, J_2 12, **126P**)
D	59.2 (Sh dd, J_1 462, J_2 35)	No Change	No Change
^1H NMR A		-8.14 (br d)	-8.28 (dm, J_1 112.4, J_2 6.9, **1H**)
B		-9.87 (br m)	-9.95 (tm, J_1 72.4, **2H**)
C	-21.94 (dt, J_1 25.2)	No Change	No Change (**2H**)
D		-23.96 (br t)	-23.94 (t, J_1 20.2, **1H**)

4.3 Peak Positions for all Phosphorus and Proton NMR Signals for the Hydrogenation of [Rh(dcpe)(C_7H_8)](BF_4) in CD_2Cl_2.

	δ - ppm (J - Hz)				
Peak	**RT**	**0°C**	**-30°C**	**-60°C**	**-90°C**
$^{31}P\{^1H\}$ NMR A	105.3 (d, 136, **17P**)	No Change	No Change	No Change	106.6 (d,136)
B	97.0 (d, 118, **15P**)	(splits) 100.9 (dm, 135)	100.3 (br dm, 135)	No Change	Broad doublet with C (101)
C		97.4 (dm, 121)	97.9 (br dd, 118)	No Change	
D	91.3 (d, 144)	91.0 (d, 143)	Broad Hump	Disappears	Disappears
1H NMR A	-9.12 (**22H**, tm)	No Change	No Change	No Change	Broader
B	-18.70 (**7.4H** dt)	No Change	No Change	No Change	Broader
C				broad hump -22.0	Broader

4.4. Peak Positions for all Phosphorus and Proton NMR Signals for the Hydrogenation of [Rh(dcpp)(C_7H_8)](BF_4) CD_2Cl_2

Peak	δ - ppm (J - Hz) RT	0°C	-30°C	-60°C	-90°C
$^{31}P\{^1H\}$ NMR *(A3)*	58.8 (dt, J_1 126 J_2 13)	Broader	Sharper	59.2 (d, 133)	59.1 (br s)
(C?)	54.0 (dm, 135)	Broader	No Change	No Change	No Change
(D)	97.1 (dm, 116)	Broader	Sharper 48.9 (d,120)	48.8 (br s)	50.0 (br s)
(C?)				65.5 (br s)	No Change
^1H NMR *(A1)*	-11.02 (tm, 79.6)	No Change	No Change	-9.35 (br d, 128.8)	Broader
(A2)	-17.99 br dt, ~20)	No Change	No Change	No Change	Broader
	-18.82 (sh d, 20.0)	-18.8 (br s)	Sharper -18.82	multiplet	Broader
	-21.47 (br d)	-20.97 (br s)	No Change	Broader -20.32	Splitting
				-19.42 (br s)	Broader

4.5. Peak Positions for all Phosphorus and Proton NMR Signals for the Hydrogenation of [Rh(Boxylyl)(C_7H_8)](BF_4) in CD_2Cl_2

Peak	δ - ppm (J - Hz) RT	0°C	-30°C	-60°C	-90°C
$^{31}P\{^1H\}$ NMR *(E1)*	73.6 (d, 229)	No Change	No Change	73.0	No Change
	65.1 (br d, 123)	64.4 (d, 138)	Broader	Broad Hump	Multiplets 62.2-65.3
			Broad Hump 80.0	Broad Hump	Broad Hump
^1H NMR *(E2)*	-21.7 (br s)	-21.6 (br s)	-21.4 (br s)	-21.0 (br s)	No Change
		-23.2 (br s)	-23.19 (br s)	-23.18 (br s)	No Change
				-24.9 (br s)	-23.87 (br d, 115.6)
				-25.4 (br s)	No Change
(E4)			Merged with (E3)	Demerging	-10.25 (br s)
(E3)			-9.6 (br s)	-9.3 (br s)	-9.12 (br d, 122.8)

4.6. Peak Positions for all Phosphorus and Proton NMR Signals for the Reaction of the Hydrides from the Hydrogenation of [Rh(dBpp)(C_7H_8)](BF_4) and Ethene in CD_2Cl_2

Peak	δ - ppm (J -Hz)				
	20°C	**0°C**	**-20°C**	**-60°C**	**-80°C**
$^{31}P\{^1H\}$ NMR *(F1)*	83.9 (d, 182)	84.0 (d, 185)	No Change	No Change	84.3 (d, 193)
(F3)	78.8 (d, 18)	78.2 (d, 49)	No Change	No Change	76.7 (d, 59)
(F4)	78.2 (d, 58)	77.4 (dd, 67)	No Change	No Change	76.1 (dd, 152)
(F6)	75.3 (dd, 123, 13)	No Change	75.3 (d, 124)	75.5 (dd, 125, 13)	75.7 (dd, 136, 13)
(G1)	73 (br s)	No Change	75.1 (br s)	(br d)	73.6 (br d, 210)
(G2)	Merged with *(G1)*	No Change	71.5 (dd)	70.2 (dm, 210)	70.0 (ddd, 212, 15)
(G3)	69 (br s)	69 (br d)	69 (br d)	broad (dm)	67.1 (dm, 98)
(F2)	56.5 (d, 199)	No Change	No Change	55.3 (d, 198)	54.8 (d, 198)
^1H NMR *(G4)*	-8.7 (br s)	-8.4 (br s)	-8.36 (br dd)	-8.37 (dt J_1 112Hz)	-8.38 (**19.5H**, dt J_1 122.8)
(G5)	Merged with G4	Merged with G4	-9.92 (br s)	-10.02 (br tm)	-10.03 (**11.5H**, m)
(F5)	-20.95 (pq)	No Change	No Change	-20.66 (pq, J_1 22, J_2 17.6)	-20.59 (**6.7H**, pq, J_1 20.4)
(G6)	-24.12 (br s)	No Change	-24.11 (br m)	-24.05 (br t)	-24.07 (**25.2H**, pq, J_1 19.6)
(G7)	-24.83 (br s)	No Change	-24.83 (s)	-25.11 (m)	-25.15 (**13.4H**, m)

Appendix 5

Supplementary Data For Chapter 6

5.1. Peak Positions for all Phosphorus and Proton NMR Signals from the Hydrogenation of [Rh(dBpe)(C_7H_8)](BF_4) in $CDCl_3$.

Peak	δp in ppm (Coupling constant J in Hz) 10°C	-10°C	-30°C	-50°C
$^{31}P\{^1H\}$ NMR				
A	113.2 (d,134)	very broad	113.3 (**3P**, dd, J_1 136 J_2 18) 111.4 (**1P**, brd J 137)	113.3 (dd, J_1 136 J_2 18) 111.4 (brd J 137)
Z1	111.1 (d, 118)	110.8 (d, 118)	110.5 (d, 118)	110.2 (d, 118)
Z2	102.7 (d, 145)	102.3 (d, 150)	101.9 (d, 150)	101.6 (br d)
Z3	102.4 (d, 145)	102.1 (d,149)	101.9 (d, 150)	101.5 (d, 150)
Z4	89.1 (d, 150)	89.0 (d, 151)	88.9 (d,152)	88.8 (br d)
^1H NMR				
B	-18.72 (br s)	Broader singlet	-18.48 (**3H**, pq) -19.06 (**1H**, br s)	-18.50 (pq, J_1 15.2, J_2 22.2, **B1**) -19.05 (pq, J_1 17.6, **B2**)

5.2. Peak Positions for all Phosphorus and Proton NMR Signals from the Hydrogenation of [Rh(dcpe)(C_7H_8)](BF_4) in $CDCl_3$.

Peak	δp in ppm (Coupling constant J in Hz) 10°C	-10°C	-30°C	-50°C
$^{31}P\{^1H\}$ NMR				
A	100 (br m)	101.0 (br d,126) 99.5 (br d, 138)	100.2 (dd, J_1 135, J_2 17, **A1**) 99.6 (br d, 137, **A2**)	101.3 (dd, J_1 136, J_2 18, **A1**) 99.1 (br m)
Z1	88.8 (d, 116)	No Change	No Change	89.1 (d, 114)
Z8		89.6 (br d, 114)	89.5 (d, 120)	No Change
Z8	-	77.5 (d, 111)	78.4 (d, 116)	78.2 (d, 116)
Z5	80.4 (d, 123)	80.0 (d, 123)	79.7 (d, 123)	79.0 (br d)
Z6	77.6 (d, 117)	78.5 (br d, 119)	77.6 broad singlet	77.0 (br s)
Z7	69.0 (123)	68.7 (d, 129)	No Change	68.6 (d, 128)

^{1}H NMR				
B	-18.49 (m)	broad doublet	-18.35 -20.4 (br s)	-18.30 (pq, J_1 18.4, J_2 19.6, **B1**) -18.65 (m, **B2**)

5.3. Peak Positions for all Phosphorus and Proton NMR Signals from the Hydrogenation of [Rh(Boxylyl)(C_7H_8)](BF_4) in $CDCl_3$.

Peak	**20°C**	**0°C**	**-30°C**	**-50°C**
$^{31}P\{^1H\}$ NMR				
D1	90 (br hump)	94.1 (br d, 136)	93.2 (br hump)	93.1 (br d 128)
D2	80 (br hump)	Broad feature 93-60	77.1 (br Hump)	77.0 (br d,127)
D3	62 (br d)	Broad feature 93-60	64.8 (br Hump)	63.8 (br d, 125)
D4	58 (br hump)	56.0 (br d)	55.3 (dd, 132)	54.9 (sh dd, 133, 22)
^{1}H NMR				
C1	-12.22 (br s)	-12.26 (br s)	-12.2 (br s)	-12.1 (br s)
C2	-17.00 (m)	-16.93 (s)	-16.83 (s)	-16.74 (br s)
	-19.39 (m)	-19.34 (s)	-19.24 (s)	-19.30 (br s)
C3	-17.30 (s)	-17.28 (s)	-17.20 (s)	-19.30 (br s)
C5	-21.18 (br s)	-18.20	-18.16	-18.13
		-21.63	-21.66	-21.70
C4	-25.9(br dd)	No Change	-25.60 (dd)	-24.37 (dd, 187)

Appendix 6

Supplementary Data for Chapter Seven

6.1. $[Ag(C_6D_6)_3](BF_4)$

This complex was formed as a by-product of the reaction of EtCl with $[Rh_2(dppe)_2Cl_2]$ in deutero-benzene. It was necessary to add the silver complex to cause reaction to occur. This molecule consists of a silver atom surrounded by three benzene rings and interacting with a single flourine atom from the tetrafluoroborate counterion, which is diordered over two positions in the crystal. One of the benzene rings has two carbon atoms interacting with the silver in an η^2-bonding manner. However, the other two benzene rings appear only to be bound *via* a single carbon atom.

Table 1. Crystal data and structure refinement Data for $[Ag(C_6D_6)_3](BF_4)$

Empirical formula	C18D18AgBF4
Formula weight	447.1
Temperature	150(2) K
Wavelength	0.71073 A
Crystal system	Orthorhombic
Space group	Pca2(1) (No. 29)
Unit cell dimensions	a = 16.549(1) Å; alpha = 90°, b = 8.373(1) Å; beta = 90°, c = 12.498(1) Å; gamma = 90°
Volume	1731.8(3) $Å^3$
Z	4
Density (calculated)	1.714 g/cm^3
Absorption coefficient	1.199 mm^{-1}
F(000)	856
Crystal size	0.2 x 0.1 x 0.1 mm
Theta range for data collection	2.43 to 25.68°.
Index ranges	$-17 \le h \le 19$, $-9 \le k \le 10$, $-14 \le l \le 9$
Reflections collected	7155
Independent reflections	2248 [R(int) = 0.0774]
Absorption correction	None
Refinement method	Full-matrix least-squares on F^2

Data / restraints / parameters	2206 / 31 / 243
Goodness-of-fit on F^2	1.139
Final R indices [I>2sigma(I)]	R1 = 0.0493 wR2 = 0.1104
R indices (all data)	R1 = 0.0814 wR2 = 0.1701
Absolute structure parameter	-0.01(13)
Largest diff. peak and hole	0.415 and -0.709 e.Å^{-3}

Table 2. Bond Lengths (Å), and Bond Angles (°) for [Ag(C$_6$D$_6$)$_3$](BF$_4$)

Ag-C(11)	2.480(14)	Ag-C(31)	2.487(13)
Ag-F(1)	2.488(8)	Ag-C(22)	2.525(12)
Ag-C(21)	2.536(12)	C(11)-C(16)	1.32(3)
C(11)-C(12)	1.37(3)	C(12)-C(13)	1.37(2)
C(13)-C(14)	1.36(2)	C(14)-C(15)	1.36(3)
C(15)-C(16)	1.37(2)	C(21)-C(26)	1.36(2)
C(21)-C(22)	1.39(2)	C(22)-C(23)	1.38(2)
C(23)-C(24)	1.36(2)	C(24)-C(25)	1.38(2)
C(25)-C(26)	1.38(2)	C(31)-C(36)	1.34(2)
C(31)-C(32)	1.36(3)	C(32)-C(33)	1.37(2)
C(33)-C(34)	1.37(2)	C(34)-C(35)	1.35(2)
C(35)-C(36)	1.37(2)	F(1)-B(1B)	1.42(3)
F(1)-B(1A)	1.44(3)	B(1A)-F(2A)	1.38(2)
B(1A)-F(3A)	1.38(2)	B(1A)-F(4A)	1.38(2)
B(1B)-F(3B)	1.36(2)	B(1B)-F(2B)	1.36(2)
B(1B)-F(4B)	1.38(2)		
C(11)-Ag-C(31)	100.4(6)	C(11)-Ag-F(1)	99.4(6)
C(31)-Ag-F(1)	97.6(5)	C(11)-Ag-X	126.5(4)
C(31)-Ag-X	122.0(4)	F(1)-Ag-X	105.0(4)
C(16)-C(11)-C(12)	120(1)	C(16)-C(11)-Ag	94(1)
C(12)-C(11)-Ag	94(1)	C(13)-C(12)-C(11)	119(2)
C(14)-C(13)-C(12)	121(2)	C(15)-C(14)-C(13)	120(1)
C(14)-C(15)-C(16)	118(2)	C(11)-C(16)-C(15)	123(2)
C(26)-C(21)-C(22)	120(1)	C(26)-C(21)-Ag	104.2(8)
C(22)-C(21)-Ag	73.6(7)	C(23)-C(22)-C(21)	119(1)
C(23)-C(22)-Ag	103.4(8)	C(21)-C(22)-Ag	74.5(7)
C(24)-C(23)-C(22)	121(1)	C(23)-C(24)-C(25)	119.5(13)
C(24)-C(25)-C(26)	120(1)	C(21)-C(26)-C(25)	121(1)
C(36)-C(31)-C(32)	121(2)	C(36)-C(31)-Ag	96.4(9)
C(32)-C(31)-Ag	92.3(11)	C(31)-C(32)-C(33)	120(2)
C(32)-C(33)-C(34)	119(2)	C(35)-C(34)-C(33)	119(1)
C(34)-C(35)-C(36)	122(2)	C(31)-C(36)-C(35)	119(2)
B(1B)-F(1)-Ag	132(1)	B(1A)-F(1)-Ag	114.5(9)
F(2A)-B(1A)-F(3A)	113(2)	F(2A)-B(1A)-F(4A)	112(2)
F(3A)-B(1A)-F(4A)	112(3)	F(2A)-B(1A)-F(1)	108(2)
F(3A)-B(1A)-F(1)	107(2)	F(4A)-B(1A)-F(1)	105(2)
F(3B)-B(1B)-F(2B)	112(2)	F(3B)-B(1B)-F(4B)	111(3)
F(2B)-B(1B)-F(4B)	108(2)	F(3B)-B(1B)-F(1)	109(2)
F(2B)-B(1B)-F(1)	108(2)	F(4B)-B(1B)-F(1)	108(2)

Figure 1. The Crystal Structure of $[Ag(C_6D_6)_3](BF_4)$

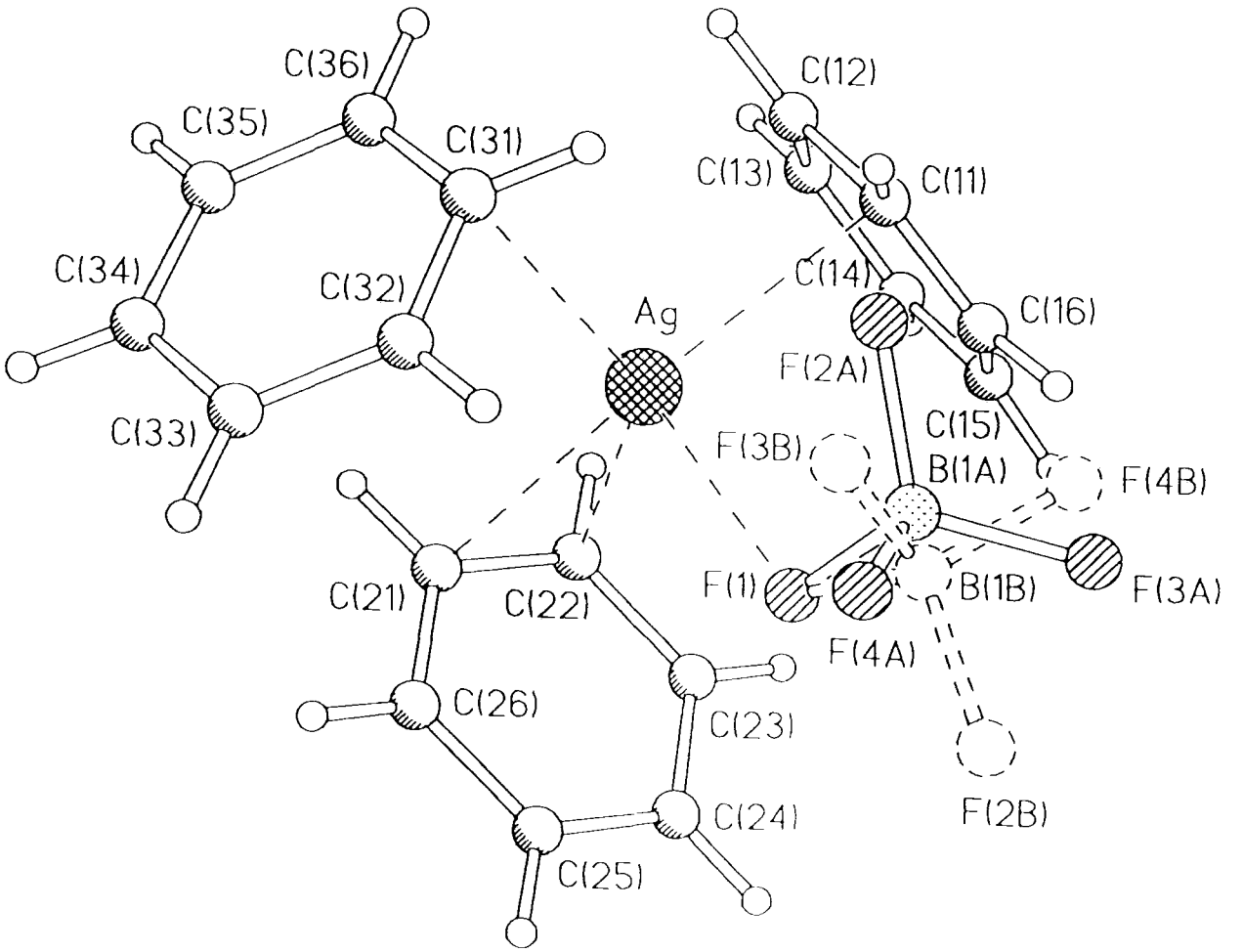

Appendix 7

Supplementary Crystallographic Data for Chapter 9

7.1. $[Rh_2(dppp)_2(\mu\text{-}Cl)_3Cl_2](Cl).4(CH_3OH).3H_2O$ (1)

Table 1. Crystal Structure Data and Refinement for Complex (1)

Empirical formula	$(C54\ H52\ Cl5\ P4\ Rh2)^+Cl^-.4CH_3OH.3H_2O$
Formula weight	1425.57
Temperature	153(2) K
Wavelength	0.71073 Å
Crystal system	Monoclinic
Space group	P2(1)/c
Unit cell dimensions	a = 10.577(1) Å; alpha = 90° b = 19.775(1) Å; beta = 99.21(1)°. c = 31.720(1) Å; gamma = 90°.
Volume	6549.0(7) A^3
Z	4
Density (calculated)	1.446 g/cm^3
Absorption coefficient	0.893 mm^{-1}
F(000)	2920
Theta range for data collection	1.66 to 25.89°
Index ranges	$-9 \le h \le 12$, $-23 \le k \le 24$, $-36 \le l \le 38$
Reflections collected	28915
Independent reflections	11352 [R(int) = 0.0394]
Absorption correction	Semi-empirical from Laue equivalents
Max. and min. transmission	0.8947 and 0.8326
Refinement method	Full-matrix least-squares on F^2
Data / restraints / parameters	11288 / 0 / 694
Goodness-of-fit on F^2	1.093
Final R indices [I>2sigma(I)]	R1 = 0.0512 wR2 = 0.1222
R indices (all data)	R1 = 0.0689 wR2 = 0.1444
Largest diff. peak and hole	0.933 and -1.028 $e.Å^{-3}$

Table 2. Selected Bond Lengths (Å) And Angles (°) for Complex (1) Containing Rh,P, or Cl

Rh(1)-P(2)	2.281(1)	Rh(1)-P(1)	2.284(1)
Rh(1)-Cl(1)	2.335(1)	Rh(1)-Cl(2)	2.367(1)
Rh(1)-Cl(3)	2.467(1)	Rh(1)-Cl(4)	2.517(1)
Rh(2)-P(3)	2.283(1)	Rh(2)-P(4)	2.286(1)
Rh(2)-Cl(5)	2.341(1)	Rh(2)-Cl(4)	2.360(1)
Rh(2)-Cl(3)	2.480(1)	Rh(2)-Cl(2)	2.486(1)
P(1)-C(11)	1.807(6)	P(1)-C(21)	1.823(6)
P(1)-C(1)	1.834(6)	P(2)-C(31)	1.829(6)
P(2)-C(3)	1.830(6)	P(2)-C(41)	1.834(5)
P(3)-C(61)	1.819(6)	P(3)-C(4)	1.831(6)
P(3)-C(51)	1.833(5)	P(4)-C(6)	1.823(5)
P(4)-C(71)	1.824(5)	P(4)-C(81)	1.831(5)
O(4)-C(04)	1.51(2)	O(5)-C(05)	1.352(14)
O(6)-C(06)	1.410(11)	O(7)-C(07)	1.433(13)
P(2)-Rh(1)-P(1)	91.52(5)	P(2)-Rh(1)-Cl(1)	89.04(5)
P(1)-Rh(1)-Cl(1)	87.82(5)	P(2)-Rh(1)-Cl(2)	100.55(5)
P(1)-Rh(1)-Cl(2)	95.85(5)	Cl(1)-Rh(1)-Cl(2)	169.61(5)
P(2)-Rh(1)-Cl(3)	94.49(5)	P(1)-Rh(1)-Cl(3)	173.93(5)
Cl(1)-Rh(1)-Cl(3)	93.18(5)	Cl(2)-Rh(1)-Cl(3)	82.17(4)
P(2)-Rh(1)-Cl(4)	173.90(5)	P(1)-Rh(1)-Cl(4)	94.53(5)
Cl(1)-Rh(1)-Cl(4)	90.32(5)	Cl(2)-Rh(1)-Cl(4)	79.72(4)
Cl(3)-Rh(1)-Cl(4)	79.49(4)	P(3)-Rh(2)-P(4)	93.18(5)
P(3)-Rh(2)-Cl(5)	85.69(5)	P(4)-Rh(2)-Cl(5)	89.59(5)
P(3)-Rh(2)-Cl(4)	95.57(5)	P(4)-Rh(2)-Cl(4)	100.72(5)
Cl(5)-Rh(2)-Cl(4)	169.51(5)	P(3)-Rh(2)-Cl(3)	175.19(5)
P(4)-Rh(2)-Cl(3)	91.45(5)	Cl(5)-Rh(2)-Cl(3)	95.61(5)
Cl(4)-Rh(2)-Cl(3)	82.32(4)	P(3)-Rh(2)-Cl(2)	95.85(5)
P(4)-Rh(2)-Cl(2)	170.73(5)	Cl(5)-Rh(2)-Cl(2)	89.04(5)
Cl(4)-Rh(2)-Cl(2)	80.48(4)	Cl(3)-Rh(2)-Cl(2)	79.56(4)
Rh(1)-Cl(2)-Rh(2)	84.16(4)	Rh(1)-Cl(3)-Rh(2)	82.26(4)
Rh(2)-Cl(4)-Rh(1)	83.63(4)	C(11)-P(1)-C(21)	104.5(3)
C(11)-P(1)-C(1)	106.9(3)	C(21)-P(1)-C(1)	101.4(3)
C(11)-P(1)-Rh(1)	108.3(2)	C(21)-P(1)-Rh(1)	120.8(2)
C(1)-P(1)-Rh(1)	113.7(2)	C(31)-P(2)-C(3)	108.5(3)
C(31)-P(2)-C(41)	102.6(3)	C(3)-P(2)-C(41)	99.7(3)
C(31)-P(2)-Rh(1)	113.5(2)	C(3)-P(2)-Rh(1)	113.7(2)
C(41)-P(2)-Rh(1)	117.3(2)	C(61)-P(3)-C(4)	107.2(3)
C(61)-P(3)-C(51)	104.8(2)	C(4)-P(3)-C(51)	102.8(3)
C(61)-P(3)-Rh(2)	109.2(2)	C(4)-P(3)-Rh(2)	113.5(2)
C(51)-P(3)-Rh(2)	118.5(2)	C(6)-P(4)-C(71)	106.8(3)
C(6)-P(4)-C(81)	103.4(2)	C(71)-P(4)-C(81)	103.6(2)
C(6)-P(4)-Rh(2)	113.0(2)	C(71)-P(4)-Rh(2)	116.1(2)
C(81)-P(4)-Rh(2)	112.8(2)	C(2)-C(1)-P(1)	111.9(4)

C(2)-C(3)-P(2)	120.3(4)	C(5)-C(4)-P(3)	113.6(4)
C(5)-C(6)-P(4)	117.5(4)	C(86)-C(81)-P(4)	120.3(4)
C(12)-C(11)-P(1)	121.1(4)	C(16)-C(11)-P(1)	118.9(4)
C(22)-C(21)-P(1)	124.3(4)	C(26)-C(21)-P(1)	116.8(5)
C(32)-C(31)-P(2)	122.1(4)	C(36)-C(31)-P(2)	118.2(4)
C(46)-C(41)-P(2)	117.3(4)	C(42)-C(41)-P(2)	123.4(4)
C(56)-C(51)-P(3)	121.1(4)	C(52)-C(51)-P(3)	119.8(4)
C(62)-C(61)-P(3)	118.6(4)	C(66)-C(61)-P(3)	121.6(4)
C(76)-C(71)-P(4)	119.5(4)	C(72)-C(71)-P(4)	121.4(4)
C(82)-C(81)-P(4)	121.6(4)		

Table 3. Selected Bond Lengths (Å) And Angles (°) for Complex (1) Not Containing Rh, Cl or P.

C(1)-C(2)	1.536(8)	C(2)-C(3)	1.533(8)
C(4)-C(5)	1.533(8)	C(5)-C(6)	1.540(7)
C(11)-C(12)	1.388(8)	C(11)-C(16)	1.402(8)
C(12)-C(13)	1.399(8)	C(13)-C(14)	1.389(10)
C(14)-C(15)	1.378(9)	C(15)-C(16)	1.395(8)
C(21)-C(22)	1.396(8)	C(21)-C(26)	1.419(8)
C(22)-C(23)	1.396(8)	C(23)-C(24)	1.387(9)
C(24)-C(25)	1.379(10)	C(25)-C(26)	1.392(9)
C(31)-C(32)	1.392(8)	C(31)-C(36)	1.396(8)
C(32)-C(33)	1.393(8)	C(33)-C(34)	1.377(9)
C(34)-C(35)	1.386(9)	C(35)-C(36)	1.389(8)
C(41)-C(46)	1.401(8)	C(41)-C(42)	1.401(8)
C(42)-C(43)	1.381(8)	C(43)-C(44)	1.377(9)
C(44)-C(45)	1.381(9)	C(45)-C(46)	1.396(8)
C(51)-C(56)	1.383(8)	C(51)-C(52)	1.401(7)
C(52)-C(53)	1.389(8)	C(53)-C(54)	1.386(9)
C(54)-C(55)	1.387(9)	C(55)-C(56)	1.397(8)
C(61)-C(62)	1.395(8)	C(61)-C(66)	1.402(8)
C(62)-C(63)	1.393(8)	C(63)-C(64)	1.388(9)
C(64)-C(65)	1.389(9)	C(65)-C(66)	1.391(9)
C(71)-C(76)	1.396(8)	C(71)-C(72)	1.409(7)
C(72)-C(73)	1.400(8)	C(73)-C(74)	1.367(9)
C(74)-C(75)	1.384(9)	C(75)-C(76)	1.398(8)
C(81)-C(82)	1.399(7)	C(81)-C(86)	1.404(8)
C(82)-C(83)	1.390(8)	C(83)-C(84)	1.377(8)
C(84)-C(85)	1.389(8)	C(85)-C(86)	1.390(8)
C(4)-C(5)-C(6)	114.0(5)	C(12)-C(11)-C(16)	119.9(5)
C(11)-C(12)-C(13)	119.9(6)	C(14)-C(13)-C(12)	119.8(6)
C(15)-C(14)-C(13)	120.6(6)	C(14)-C(15)-C(16)	120.0(6)
C(15)-C(16)-C(11)	119.8(6)	C(22)-C(21)-C(26)	118.7(5)
C(23)-C(22)-C(21)	120.4(6)	C(24)-C(23)-C(22)	119.9(6)
C(25)-C(24)-C(23)	120.8(6)	C(24)-C(25)-C(26)	120.0(6)

C(25)-C(26)-C(21)	120.1(6)	C(32)-C(31)-C(36)	119.7(5)
C(31)-C(32)-C(33)	119.7(6)	C(34)-C(33)-C(32)	120.2(6)
C(33)-C(34)-C(35)	120.6(6)	C(34)-C(35)-C(36)	119.6(6)
C(35)-C(36)-C(31)	120.2(6)	C(46)-C(41)-C(42)	118.5(5)
C(43)-C(42)-C(41)	120.3(6)	C(44)-C(43)-C(42)	120.8(6)
C(43)-C(44)-C(45)	120.1(6)	C(44)-C(45)-C(46)	119.9(6)
C(45)-C(46)-C(41)	120.4(6)	C(56)-C(51)-C(52)	118.7(5)
C(53)-C(52)-C(51)	120.2(6)	C(54)-C(53)-C(52)	120.8(6)
C(53)-C(54)-C(55)	119.4(5)	C(54)-C(55)-C(56)	119.9(6)
C(51)-C(56)-C(55)	121.1(5)	C(62)-C(61)-C(66)	119.6(5)
C(63)-C(62)-C(61)	119.9(6)	C(64)-C(63)-C(62)	120.5(6)
C(63)-C(64)-C(65)	119.8(6)	C(64)-C(65)-C(66)	120.3(6)
C(65)-C(66)-C(61)	119.9(6)	C(76)-C(71)-C(72)	119.0(5)
C(73)-C(72)-C(71)	119.5(5)	C(74)-C(73)-C(72)	120.4(5)
C(73)-C(74)-C(75)	121.1(6)	C(74)-C(75)-C(76)	119.4(6)
C(71)-C(76)-C(75)	120.5(5)	C(82)-C(81)-C(86)	118.1(5)
C(83)-C(82)-C(81)	120.5(5)	C(84)-C(83)-C(82)	120.8(5)
C(83)-C(84)-C(85)	119.6(5)	C(84)-C(85)-C(86)	120.1(6)
C(85)-C(86)-C(81)	120.8(5)	C(3)-C(2)-C(1)	114.1(5)

7.2. 2[$Rh_2(dppe)_2(\mu\text{-}Cl)_3Cl_2$]($BF_4$)($B_2F_7$) (2)

Table 4. Crystal Structure and Refinement Data for Complex (2)

Empirical formula	C113 H114 B3 Cl28 F11 P8 Rh4
Formula weight	3365.47
Temperature	150(2) K
Wavelength	0.71073 Å
Crystal system	Monoclinic
Space group	P2(1)/c
Unit cell dimensions	a = 22.161(6) Å; alpha = 90°. b = 20.516(6) Å; beta = 99.40(2)°. c = 30.701(8) Å; gamma = 90°.
Volume	13771(6) $Å^3$
Z	4
Density (calculated)	1.623 g/cm^3
Absorption coefficient	1.167 mm^{-1}
F(000)	6728
Crystal size	0.54 x 0.21 x 0.13 mm
Theta range for data collection	2.56 to 23.10°.
Index ranges	$0 \le h \le 18$, $0 \le k \le 19$, $-29 \le l \le 29$
Reflections collected	11508
Independent reflections	11070 [R(int) = 0.0828]
Absorption correction	Integration
Max. and min. transmission	0.87 and 0.66

Refinement method	Full-matrix least-squares on F^2
Data / restraints / parameters	11070 / 170 / 817
Goodness-of-fit on F^2	1.086
Final R indices [I>2sigma(I)]	R1 = 0.0995 wR2 = 0.2081
R indices (all data)	R1 = 0.2029 wR2 = 0.2349
Largest diff. peak and hole	1.028 and -0.944 e.Å^{-3}

Table 5. Bond Lengths (Å) and Angles (°) For Complex (2), Including Rh, P, Cl, and B.

Rh(1A)-P(1A)	2.260(6)	Rh(1A)-P(2A)	2.280(6)
Rh(1A)-Cl(4A)	2.325(6)	Rh(1A)-Cl(3A)	2.361(6)
Rh(1A)-Cl(2A)	2.460(5)	Rh(1A)-Cl(1A)	2.463(6)
Rh(1A)-Rh(2A)	3.181(3)	Rh(2A)-P(3A)	2.256(6)
Rh(2A)-P(4A)	2.275(6)	Rh(2A)-Cl(5A)	2.314(6)
Rh(2A)-Cl(1A)	2.376(6)	Rh(2A)-Cl(2A)	2.469(6)
Rh(2A)-Cl(3A)	2.501(6)	P(1A)-C(11A)	1.805(12)
P(1A)-C(21A)	1.838(13)	P(1A)-C(1A)	1.88(2)
P(2A)-C(31A)	1.821(12)	P(2A)-C(41A)	1.843(12)
P(2A)-C(2A)	1.85(2)	P(3A)-C(51A)	1.795(12)
P(3A)-C(61A)	1.82(2)	P(3A)-C(3A)	1.82(2)
P(4A)-C(71A)	1.804(11)	P(4A)-C(81A)	1.818(13)
P(4A)-C(4A)	1.83(2)	Rh(1B)-P(1B)	2.265(6)
Rh(1B)-P(2B)	2.265(6)	Rh(1B)-Cl(4B)	2.322(6)
Rh(1B)-Cl(3B)	2.368(6)	Rh(1B)-Cl(2B)	2.450(6)
Rh(1B)-Cl(1B)	2.481(6)	Rh(1B)-Rh(2B)	3.176(3)
Rh(2B)-P(3B)	2.245(6)	Rh(2B)-P(4B)	2.272(6)
Rh(2B)-Cl(5B)	2.317(6)	Rh(2B)-Cl(1B)	2.370(6)
Rh(2B)-Cl(2B)	2.475(6)	Rh(2B)-Cl(3B)	2.489(6)
P(1B)-C(11B)	1.802(12)	P(1B)-C(1B)	1.80(2)
P(1B)-C(21B)	1.820(12)	P(2B)-C(2B)	1.81(2)
P(2B)-C(31B)	1.822(12)	P(2B)-C(41B)	1.849(12)
P(3B)-C(51B)	1.802(12)	P(3B)-C(3B)	1.82(2)
P(3B)-C(61B)	1.86(2)	P(4B)-C(4B)	1.82(2)
P(4B)-C(71B)	1.830(12)	P(4B)-C(81B)	1.834(12)
Cl(1)-C(1S)	1.81(5)	Cl(2)-C(1S)	1.81(5)
Cl(1')-C(1S')	1.78(4)	Cl(2')-C(1S')	1.77(4)
Cl(3)-C(2S)	1.73(2)	Cl(4)-C(2S)	1.76(2)
Cl(4')-C(2S)	1.70(2)	Cl(5)-C(3S)	1.61(2)
Cl(6)-C(3S)	1.73(3)	Cl(6')-C(3S)	1.56(3)
Cl(7)-C(4S)	1.62(3)	Cl(8)-C(4S)	1.67(3)
Cl(9)-C(5S)	1.58(3)	Cl(10)-C(5S)	1.71(3)
Cl(11)-C(6S)	1.69(3)	Cl(12)-C(6S)	1.72(3)
Cl(13)-C(7S)	1.71(3)	Cl(14)-C(7S)	1.68(3)
Cl(15)-C(8S)	1.58(4)	Cl(16)-C(8S)	1.73(4)
Cl(17)-C(9S)	1.63(5)	Cl(18)-C(9S)	1.58(6)

Cl(19)-C(10S)	1.63(5)	Cl(20)-C(10S)	1.69(5)
B(1)-F(2)	1.36(3)	B(1)-F(1)	1.35(3)
B(1)-F(3)	1.37(3)	B(1)-F(4)	1.41(4)
B(2)-F(6)	1.29(4)	B(2)-F(5)	1.43(4)
B(2)-F(7)	1.45(4)	B(2)-F(8)	1.50(4)
B(3)-F(10)	1.35(2)	B(3)-F(9)	1.37(2)
B(3)-F(10')	1.37(3)	B(3)-F(11')	1.39(3)
B(3)-F(11)	1.41(2)	B(3)-F(9')	1.45(3)
B(3)-F(8)	1.58(5)	P(1A)-Rh(1A)-Cl(4A)	90.0(2)
P(1A)-Rh(1A)-P(2A)	85.8(2)	P(1A)-Rh(1A)-Cl(3A)	98.3(2)
P(2A)-Rh(1A)-Cl(4A)	85.5(2)	Cl(4A)-Rh(1A)-Cl(3A)	171.4(2)
P(2A)-Rh(1A)-Cl(3A)	97.3(2)	P(2A)-Rh(1A)-Cl(2A)	176.7(2)
P(1A)-Rh(1A)-Cl(2A)	91.2(2)	Cl(3A)-Rh(1A)-Cl(2A)	84.5(2)
Cl(4A)-Rh(1A)-Cl(2A)	93.1(2)	P(2A)-Rh(1A)-Cl(1A)	101.4(2)
P(1A)-Rh(1A)-Cl(1A)	172.8(2)	Cl(3A)-Rh(1A)-Cl(1A)	81.5(2)
Cl(4A)-Rh(1A)-Cl(1A)	90.0(2)	P(1A)-Rh(1A)-Rh(2A)	127.0(2)
Cl(2A)-Rh(1A)-Cl(1A)	81.6(2)	Cl(4A)-Rh(1A)-Rh(2A)	121.5(2)
P(2A)-Rh(1A)-Rh(2A)	133.3(2)	Cl(2A)-Rh(1A)-Rh(2A)	49.94(13)
Cl(3A)-Rh(1A)-Rh(2A)	51.09(14)	P(3A)-Rh(2A)-P(4A)	86.5(2)
Cl(1A)-Rh(1A)-Rh(2A)	47.73(13)	P(4A)-Rh(2A)-Cl(5A)	90.8(2)
P(3A)-Rh(2A)-Cl(5A)	85.9(2)	P(4A)-Rh(2A)-Cl(1A)	92.8(2)
P(3A)-Rh(2A)-Cl(1A)	100.0(2)	P(3A)-Rh(2A)-Cl(2A)	94.2(2)
Cl(5A)-Rh(2A)-Cl(1A)	173.3(2)	Cl(5A)-Rh(2A)-Cl(2A)	93.2(2)
P(4A)-Rh(2A)-Cl(2A)	176.0(2)	P(3A)-Rh(2A)-Cl(3A)	175.5(2)
Cl(1A)-Rh(2A)-Cl(2A)	83.2(2)	Cl(5A)-Rh(2A)-Cl(3A)	93.5(2)
P(4A)-Rh(2A)-Cl(3A)	98.0(2)	Cl(2A)-Rh(2A)-Cl(3A)	81.4(2)
Cl(1A)-Rh(2A)-Cl(3A)	80.4(2)	P(4A)-Rh(2A)-Rh(1A)	127.3(2)
P(3A)-Rh(2A)-Rh(1A)	129.9(2)	Cl(1A)-Rh(2A)-Rh(1A)	50.11(14)
Cl(5A)-Rh(2A)-Rh(1A)	123.4(2)	Cl(3A)-Rh(2A)-Rh(1A)	47.26(13)
Cl(2A)-Rh(2A)-Rh(1A)	49.68(13)	Rh(1A)-Cl(2A)-Rh(2A)	80.4(2)
Rh(2A)-Cl(1A)-Rh(1A)	82.2(2)	C(11A)-P(1A)-C(21A)	102.6(7)
Rh(1A)-Cl(3A)-Rh(2A)	81.7(2)	C(21A)-P(1A)-C(1A)	107.6(9)
C(11A)-P(1A)-C(1A)	107.3(8)	C(21A)-P(1A)-Rh(1A)	113.8(6)
C(11A)-P(1A)-Rh(1A)	118.0(5)	C(31A)-P(2A)-C(41A)	103.0(7)
C(1A)-P(1A)-Rh(1A)	106.9(7)	C(41A)-P(2A)-C(2A)	106.3(8)
C(31A)-P(2A)-C(2A)	106.6(9)	C(41A)-P(2A)-Rh(1A)	117.6(5)
C(31A)-P(2A)-Rh(1A)	117.6(6)	C(51A)-P(3A)-C(61A)	104.6(8)
C(2A)-P(2A)-Rh(1A)	104.9(7)	C(61A)-P(3A)-C(3A)	107.8(10)
C(51A)-P(3A)-C(3A)	107.0(9)	C(61A)-P(3A)-Rh(2A)	118.3(7)
C(51A)-P(3A)-Rh(2A)	112.9(5)	C(71A)-P(4A)-C(81A)	106.3(7)
C(3A)-P(3A)-Rh(2A)	105.7(7)	C(81A)-P(4A)-C(4A)	104.1(9)
C(71A)-P(4A)-C(4A)	108.3(9)	C(81A)-P(4A)-Rh(2A)	114.5(6)
C(71A)-P(4A)-Rh(2A)	115.3(5)	C(2A)-C(1A)-P(1A)	112(2)
C(4A)-P(4A)-Rh(2A)	107.7(7)	C(4A)-C(3A)-P(3A)	109(2)
C(1A)-C(2A)-P(2A)	108(2)	C(16A)-C(11A)-P(1A)	116.0(9)
C(3A)-C(4A)-P(4A)	108(2)	C(26A)-C(21A)-P(1A)	120.5(10)

C(12A)-C(11A)-P(1A)	123.6(9)	C(36A)-C(31A)-P(2A)	120.9(9)
C(22A)-C(21A)-P(1A)	119.5(10)	C(42A)-C(41A)-P(2A)	120.9(8)
C(32A)-C(31A)-P(2A)	119.1(9)	C(52A)-C(51A)-P(3A)	119.5(8)
C(46A)-C(41A)-P(2A)	119.0(8)	C(66D)-C(61A)-P(3A)	125.3(14)
C(56A)-C(51A)-P(3A)	120.4(8)	C(66A)-C(61A)-P(3A)	123.4(14)
C(62A)-C(61A)-P(3A)	117.8(14)	C(76A)-C(71A)-P(4A)	121.3(8)
C(62D)-C(61A)-P(3A)	115.0(14)	C(82A)-C(81A)-P(4A)	118.6(9)
C(72A)-C(71A)-P(4A)	118.4(8)	P(1B)-Rh(1B)-P(2B)	86.1(2)
C(86A)-C(81A)-P(4A)	121.4(9)	P(2B)-Rh(1B)-Cl(4B)	86.3(2)
P(1B)-Rh(1B)-Cl(4B)	90.1(2)	P(2B)-Rh(1B)-Cl(3B)	96.9(2)
P(1B)-Rh(1B)-Cl(3B)	97.0(2)	P(1B)-Rh(1B)-Cl(2B)	92.1(2)
Cl(4B)-Rh(1B)-Cl(3B)	172.4(2)	Cl(4B)-Rh(1B)-Cl(2B)	93.1(2)
P(2B)-Rh(1B)-Cl(2B)	178.1(2)	P(1B)-Rh(1B)-Cl(1B)	173.6(2)
Cl(3B)-Rh(1B)-Cl(2B)	83.9(2)	Cl(4B)-Rh(1B)-Cl(1B)	90.8(2)
P(2B)-Rh(1B)-Cl(1B)	100.2(2)	Cl(2B)-Rh(1B)-Cl(1B)	81.6(2)
Cl(3B)-Rh(1B)-Cl(1B)	81.8(2)	P(2B)-Rh(1B)-Rh(2B)	131.6(2)
P(1B)-Rh(1B)-Rh(2B)	127.2(2)	Cl(3B)-Rh(1B)-Rh(2B)	50.83(14)
Cl(4B)-Rh(1B)-Rh(2B)	122.2(2)	Cl(1B)-Rh(1B)-Rh(2B)	47.61(13)
Cl(2B)-Rh(1B)-Rh(2B)	50.17(13)	P(3B)-Rh(2B)-Cl(5B)	86.0(2)
P(3B)-Rh(2B)-P(4B)	86.4(2)	P(3B)-Rh(2B)-Cl(1B)	99.1(2)
P(4B)-Rh(2B)-Cl(5B)	90.1(2)	Cl(5B)-Rh(2B)-Cl(1B)	173.9(2)
P(4B)-Rh(2B)-Cl(1B)	93.5(2)	P(4B)-Rh(2B)-Cl(2B)	176.7(2)
P(3B)-Rh(2B)-Cl(2B)	93.2(2)	Cl(1B)-Rh(2B)-Cl(2B)	83.3(2)
Cl(5B)-Rh(2B)-Cl(2B)	93.1(2)	P(4B)-Rh(2B)-Cl(3B)	99.5(2)
P(3B)-Rh(2B)-Cl(3B)	174.0(2)	Cl(1B)-Rh(2B)-Cl(3B)	81.6(2)
Cl(5B)-Rh(2B)-Cl(3B)	93.0(2)	P(3B)-Rh(2B)-Rh(1B)	128.9(2)
Cl(2B)-Rh(2B)-Cl(3B)	81.0(2)	Cl(5B)-Rh(2B)-Rh(1B)	123.4(2)
P(4B)-Rh(2B)-Rh(1B)	128.7(2)	Cl(2B)-Rh(2B)-Rh(1B)	49.51(14)
Cl(1B)-Rh(2B)-Rh(1B)	50.62(14)	Rh(2B)-Cl(1B)-Rh(1B)	81.8(2)
Cl(3B)-Rh(2B)-Rh(1B)	47.52(13)	Rh(1B)-Cl(3B)-Rh(2B)	81.6(2)
Rh(1B)-Cl(2B)-Rh(2B)	80.3(2)	C(11B)-P(1B)-C(21B)	101.9(7)
C(11B)-P(1B)-C(1B)	105.0(8)	C(11B)-P(1B)-Rh(1B)	119.2(5)
C(1B)-P(1B)-C(21B)	110.2(9)	C(21B)-P(1B)-Rh(1B)	112.7(5)
C(1B)-P(1B)-Rh(1B)	107.3(7)	C(2B)-P(2B)-C(41B)	107.2(8)
C(2B)-P(2B)-C(31B)	107.0(9)	C(2B)-P(2B)-Rh(1B)	106.2(8)
C(31B)-P(2B)-C(41B)	104.8(7)	C(41B)-P(2B)-Rh(1B)	115.1(5)
C(31B)-P(2B)-Rh(1B)	116.0(5)	C(51B)-P(3B)-C(61B)	102.0(8)
C(51B)-P(3B)-C(3B)	106.8(8)	C(51B)-P(3B)-Rh(2B)	115.4(5)
C(3B)-P(3B)-C(61B)	107.7(9)	C(61B)-P(3B)-Rh(2B)	118.5(6)
C(3B)-P(3B)-Rh(2B)	105.7(7)	C(4B)-P(4B)-C(81B)	105.1(8)
C(4B)-P(4B)-C(71B)	108.9(9)	C(4B)-P(4B)-Rh(2B)	105.8(7)
C(71B)-P(4B)-C(81B)	104.6(7)	C(81B)-P(4B)-Rh(2B)	117.7(5)
C(71B)-P(4B)-Rh(2B)	114.3(5)	C(1B)-C(2B)-P(2B)	106.9(14)
C(2B)-C(1B)-P(1B)	111.1(14)	C(3B)-C(4B)-P(4B)	110.9(14)
C(4B)-C(3B)-P(3B)	108.1(14)	C(12B)-C(11B)-P(1B)	114.6(8)
C(16B)-C(11B)-P(1B)	125.0(8)	C(26B)-C(21B)-P(1B)	121.1(9)

C(22B)-C(21B)-P(1B)	118.8(9)	C(36B)-C(31B)-P(2B)	120.8(8)
C(32B)-C(31B)-P(2B)	119.1(8)	C(46B)-C(41B)-P(2B)	120.3(8)
C(42B)-C(41B)-P(2B)	119.6(8)	C(56B)-C(51B)-P(3B)	121.0(9)
C(52B)-C(51B)-P(3B)	118.8(9)	C(62B)-C(61B)-P(3B)	119.9(13)
C(66E)-C(61B)-P(3B)	120.7(13)	C(66B)-C(61B)-P(3B)	120.3(13)
C(62E)-C(61B)-P(3B)	118.5(13)	C(72B)-C(71B)-P(4B)	120.2(9)
C(76B)-C(71B)-P(4B)	119.7(9)	C(82B)-C(81B)-P(4B)	119.1(8)
C(86B)-C(81B)-P(4B)	120.8(8)	Cl(2')-C(1S')-Cl(1')	109(3)
Cl(1)-C(1S)-Cl(2)	104(4)	Cl(4')-C(2S)-Cl(4)	92(2)
Cl(4')-C(2S)-Cl(3)	108(2)	Cl(6')-C(3S)-Cl(5)	150(3)
Cl(3)-C(2S)-Cl(4)	113(2)	Cl(7)-C(4S)-Cl(8)	121(2)
Cl(5)-C(3S)-Cl(6)	104(3)	Cl(11)-C(6S)-Cl(12)	116(2)
Cl(9)-C(5S)-Cl(10)	123(2)	Cl(15)-C(8S)-Cl(16)	118(2)
Cl(14)-C(7S)-Cl(13)	115(2)	Cl(19)-C(10S)-Cl(20)	114(3)
Cl(18)-C(9S)-Cl(17)	116(4)	F(2)-B(1)-F(3)	112(3)
F(2)-B(1)-F(1)	114(3)	F(2)-B(1)-F(4)	104(3)
F(1)-B(1)-F(3)	114(3)	F(3)-B(1)-F(4)	107(3)
F(1)-B(1)-F(4)	104(3)	F(6)-B(2)-F(7)	114(3)
F(6)-B(2)-F(5)	116(3)	F(6)-B(2)-F(8)	117(3)
F(5)-B(2)-F(7)	103(3)	F(7)-B(2)-F(8)	100(3)
F(5)-B(2)-F(8)	106(3)	F(10')-B(3)-F(11')	112(3)
F(10)-B(3)-F(9)	116(3)	F(9)-B(3)-F(11)	110(2)
F(10)-B(3)-F(11)	110(2)	F(11')-B(3)-F(9')	105(3)
F(10')-B(3)-F(9')	106(3)	F(9)-B(3)-F(8)	104(3)
F(10)-B(3)-F(8)	109(3)	F(11')-B(3)-F(8)	123(3)
F(10')-B(3)-F(8)	115(3)	F(9')-B(3)-F(8)	91(3)
F(11)-B(3)-F(8)	108(3)	B(2)-F(8)-B(3)	122(2)

Table 6. Bond Lengths (Å) and Angles (°) For Complex (2) Except those Containing Rh, P, B, and Cl.

C(1A)-C(2A)	1.46(3)	C(61A)-C(66D)	1.38(2)
C(3A)-C(4A)	1.55(3)	C(61A)-C(66A)	1.39(2)
C(61A)-C(62A)	1.38(2)	C(62A)-C(63A)	1.40(2)
C(61A)-C(62D)	1.40(2)	C(64A)-C(65A)	1.37(2)
C(63A)-C(64A)	1.41(2)	C(64A)-C(63D)	1.39(2)
C(64A)-C(65D)	1.38(2)	C(62D)-C(63D)	1.39(2)
C(65A)-C(66A)	1.39(2)	C(3B)-C(4B)	1.48(3)
C(65D)-C(66D)	1.38(2)	C(61B)-C(62B)	1.37(2)
C(1B)-C(2B)	1.55(3)	C(61B)-C(66B)	1.38(2)
C(61B)-C(66E)	1.35(2)	C(63B)-C(64B)	1.39(2)
C(61B)-C(62E)	1.37(2)	C(64B)-C(65E)	1.37(2)
C(62B)-C(63B)	1.37(2)	C(65B)-C(66B)	1.38(2)
C(64B)-C(65B)	1.33(2)	C(65E)-C(66E)	1.38(2)
C(64B)-C(63E)	1.39(2)	C(61A)-C(62A)-C(63A)	120.9(13)
C(62E)-C(63E)	1.38(2)	C(65D)-C(64A)-C(63D)	118.4(12)

C(62A)-C(61A)-C(66A)	118.5(12)	C(64A)-C(65A)-C(66A)	119.4(12)
C(66D)-C(61A)-C(62D)	119.6(12)	C(63D)-C(62D)-C(61A)	119.5(13)
C(62A)-C(63A)-C(64A)	118.1(12)	C(64A)-C(65D)-C(66D)	119.9(13)
C(65A)-C(64A)-C(63A)	119.8(12)	C(62B)-C(61B)-C(66B)	119.5(12)
C(61A)-C(66A)-C(65A)	120.7(13)	C(62B)-C(63B)-C(64B)	118.1(12)
C(62D)-C(63D)-C(64A)	120.0(12)	C(65B)-C(64B)-C(63B)	121.0(12)
C(61A)-C(66D)-C(65D)	120.0(14)	C(65B)-C(66B)-C(61B)	119.6(13)
C(66E)-C(61B)-C(62E)	119.8(12)	C(62E)-C(63E)-C(64B)	118.3(13)
C(61B)-C(62B)-C(63B)	120.5(13)	C(61B)-C(66E)-C(65E)	120.0(13)
C(65E)-C(64B)-C(63E)	117.8(13)	C(61B)-C(62E)-C(63E)	119.8(13)
C(64B)-C(65B)-C(66B)	120.1(13)	C(64B)-C(65E)-C(66E)	119.0(13)

7.3. $[Rh_2(dcpe)_2(\mu\text{-}Cl)_3Cl_2][Rh(dcpe)Cl_4].2CH_2Cl_2$ (3)

Table 7. Crystal Structure Data and Refinement for Complex (3)

Empirical formula	C80 H148 Cl13 P6 Rh3
Formula weight	2065.38
Temperature	150(2) K
Wavelength	0.71073Å
Crystal system	Orthorhombic
Space group	Pna2 (1)
Unit cell dimensions	a = 29.970(3) Å; alpha 90°. b = 12.7052(12) Å; beta 90° c = 24.774(2) Å; gamma 90°
Volume	9433(2) $Å^3$
Z	4
Density (calculated)	1.454 g/cm^3
F(000)	4296
Crystal Size	0.36 x 0.24 x 0.24 mm
Theta range for data collection	1.64 to 26.37°.
Index ranges	$-36 \le h \le 36$, $-13 \le k \le 15$, $-30 \le l \le 20$
Reflections collected	40340
Independent reflections	14676 [R(int) = 0.0668]
Absorption correction	None
Refinement method	Full Matrix least squares on F^2
Data / restraints / parameters	14668/29/975
Goodness-of-fit on F^2	1.165
Final R indices [I>2sigma(I)]	R1 = 0.0499, wR2 = 0.1047
R indices (all data)	R1 = 0.0567, wR2 = 0.1124
Largest diff. peak and hole	0.675 and -0.978 $eÅ^{-3}$

Table 8. Selected Bond Lengths (Å) And Angles (°) for Complex (3) Containing Rh, P or Cl

Rh(1)-P(2)	2.263(2)	P(6) -C(78)	1.827 (8)
Rh(1)-P(1)	2.308(2)	P(6)-C(65)	1.848(8)
Rh(1)-Cl(4)	2.323(2)	P(6)-C(71)	1.869(8)
Rh(1)-Cl(2)	2.353(2)	P(3)-Rh(2)-C1(3)	93.19(7)
Rh(1)-Cl(3)	2.477(2)	P(4)-Rh(2)-C1(3)	177.59(7)
Rh(1)-Cl(1)	2.499(2)	Cl(5)-Rh(2)-Cl(3)	96.39(7)
Rh(2)-P(3)	2.275(2)	Cl(l)-Rh(2)-Cl(3)	79.76(6)
Rh(2)-P(4)	2.286(2)	P(3)-Rh(2)-Cl(2)	173.83(7)
Rh(2)-Cl(5)	2.318(2)	P(4)-Rh(2)-Cl(2)	101.34(7)
Rh(2)-Cl(1)	2.382(2)	Cl(5)-Rh(2)-C1(2)	90.19(6)
Rh(2)-Cl(3)	2.491(2)	Cl(l)-Rh(2)-C1(2)	79.19(6)
Rh(2)-Cl(2)	2.499(2)	Cl(3)-Rh(2)-C1(2)	80.67(6)
P(1)-C(25)	1.801(7)	C(25)-P(1)-C(7)	104.0(4)
P(1)-C(7)	1.821(8)	C(25)-P(l)-C(1)	106.7(4)
P(1)-C(1)	1.843(8)	C(7)-P(l)-C(1)	110.7(4)
P(2)-C(26)	1.817(7)	C(25)-P(l)-Rh(l)	104.8(2)
P(2)-C(13)	1.822(8)	C(7)-P(l)-Rh(l)	117.3(3)
P(2)-C(19)	1.823(9)	C(l)-P(l)-Rh(l)	112.2(3)
P(3)-C(27)	1.824(8)	C(26)-P(2)-C(13)	103.1(3)
P(3)-C(51)	1.839(7)	C(26)-P(2)-C(19)	106.4(4)
P(3)-C(33)	1.855(8)	C(13)-P(2)-C(19)	108.7(4)
P(4)-C(52)	1.813(7)	C(26)-P(2)-Rh(l)	107.1(2)
P(4)-C(45)	1.837(8)	C(13)-P(2)-Rh(l)	113.4(3)
P(4)-C(39)	1.854(8)	C(l9)-P(2)-Rh(l)	116.8(3)
Rh(3) -P(6)	2.274 (2)	C(27)-P(3)-C(51)	103.1(3)
Rh(3) - P(5)	2.289 (2)	C(27)-P(3)-C(33)	106.9(4)
Rh(3) -Cl (8)	2.346 (2)	C(S1)-P(3)-C(33)	102.5(4)
Rh(3) -Cl (9)	2.363 (2)	C(27)-P(3)-Rh(2)	119.5(3)
Rh(3) -Cl (6)	2.438 (2)	C(51)-P(3)-Rh(2)	109.0(2)
Rh(3) -Cl (7)	2.440 (2)	C(33)-P(3)-Rh(2)	113.8(2)
P(5) -C (77)	1.822 (8)	C(52)-P(4)-C(45)	105.9(3)
P(5)-C(53)	1.848(9)	C(52)-P(4)-C(39)	106.3(3)
P-(5) -C(59)	1.854 (8)	C(45)-P(4)-C(39)	105.8(4)
P(2)-Rh(l)-P(1)	85.84(7)	C(24)-C(l9)-P(2)	122.6(9)
P(2)-Rh(l)-C1(4)	93.27(7)	C(84)-C(l9)-P(2)	119.1(7)
P(l)-Rh(l)-Cl(4)	86.66(7)	C(20)-C(l9)-P(2)	117.1(6)
P(2)-Rh(l)-C1(2)	93.54(7)	C(26)-C(25)-P(1)	108.2 (5)
P(l)-Rh(l)-C1(2)	96.76(7)	C(25) -C (26) -P(2)	110.4 (5)
Cl(4)-Rh(l)-C1(2)	172.58(7)	C(28)-C(27)-P(3)	114.8(5)
P(2)-Rh(l)-Cl(3)	95.30(7)	C(32)-C(27)-P(3)	114.5(6)
P(l)-Rh(l)-C1(3)	178.65(7)	C(38)-C(33)-P(3)	119.1(5)
Cl(4)-Rh(l)-Cl(3)	92.56(7)	C (34) -C(33)-P(3)	113.5 (5)
Cl(2)-Rh(l)-C1(3)	83.90(6)	P(5)-Rh(3)-Cl(7)	175.76(7)

P(2)-Rh(l)-Cl(l)	170.77(7)	Cl(8)-Rh(3)-Cl(7)	90.24(7)
P(l)-Rh(l)-Cl(l)	101.13(7)	Cl(9)-Rh(3)-C1(7)	89.76(7)
Cl(4)-Rh(l)-Cl(l)	93.17(7)	Cl(6)-Rh(3)-Cl(7)	89.71(6)
Cl(2)-Rh(l)-Cl(l)	79.73(6)	C(77)-P(5)-C(53)	106.2(4)
Cl(3)-Rh(l)-Cl(l)	77.81(6)	C(77)-P(5)-C(59)	101.2(4)
P(3)-Rh(2)-P(4)	84.78(7)	C(53)-P(5)-C(59)	108.0(4)
P(3)-Rh(2)-Cl(5)	91.16(7)	C(77)-P(5)-Rh(3)	104.4(3)
P(4)-Rh(2)-Cl(5)	84.96(7)	C(53)-P(5)-Rh(3)	117.3(3)
P(3)-Rh(2)-Cl(l)	99.16(7)	C(S9)-P(5)-Rh(3)	117.7(2)
P(4)-Rh(2)-Cl(l)	99.26(7)	C(78)-P(6)-C(65)	105.1(4)
Cl(5)-Rh(2)-Cl(l)	169.14(7)	C(78)-P(6)-C(71)	103.5(4)
C(39)-P(4)-Rh(2)	122.1(3)	C(65)-P(6)-C(71)	110.0(4)
Rh(2)-Cl(l)-Rh(l)	84.30(6)	C(78)-P(6)-Rh(3)	103.5(3)
Rh(l)-Cl(2)-Rh(2)	84.88(6)	C(65)-P(6)-Rh(3)	115.8(3)
Rh(l)-C1(3)-Rh(2)	82.52(5)	C(71)-P(6)-Rh(3)	117.2(3)
C(12) -C(7) -P(1)	116.0 (6)	C(87)-C(53)-P(5)	125.6(10)
C (8) -C (7) -P(1)	113.9 (5)	C(58)-C(53)-P(S)	120.1(7)
C(14) -C(13) -P(2)	114.7 (6)	C(54)-C(53)-P(S)	113.8(5)
C(18)-C(13)-P(2)	117.4(5)	C(72)-C(71)-P(6)	115.0(6)
C(40) -C(39) -P(4)	114.3 (6)	C(76)-C(71)-P(6)	115.3(6)
C (44) -C(39)- P(4)	114.1 (6)	C(78)-C(77) -P(5)	110.7 (6)
C(46)-C(45)-P(4)	115.4(6)	C(77)-C(78) -P(6)	110.3 (5)
C(50)-C(45)-P(4)	111.7 (5)	P(6)-Rh(3)-C1(6)	176.30(7)
C(52)-C(51)-P(3)	110.0(5)	P(5)-Rh(3)-Cl(6)	94-07(7)
C(51)-C(52)-P(4)	108.5(5)	Cl(8)-Rh(3)-Cl(6)	89.04(7)
P(6)-Rh(3)-P(5)	88.56(7)	Cl(9)-Rh(3)-Cl(6)	89.14(7)
P(6)-Rh(3)-Cl(8)	93.66(7)	P(6)-Rh(3)-Cl(7)	87.76(7)
P(5)-Rh(3)-Cl(8)	87.91(8)	C(70)-C(65)-P(6)	115.2(5)
P(6)-Rh(3)-Cl(9)	88.15(7)	Cl(8)-Rh(3)-Cl(9)	178.19(7)
P(5)-Rh(3)-Cl(9)	92.21(8)		

Table 9. Selected Bond Lengths (Å) And Angles (°) for Complex (3) Not Containing Rh, P or Cl

C(1)-C(6)	1.504(11)	C(5)-C(6)	1.523(11)
C(1)-C(2)	1.552(11)	C(7)-C(12)	1.539(10)
C(2)-C(3)	1.540(12)	C(7)-C(8)	1.547(10)
C(3)-C(4)	1.516(13)	C(8)-C(9)	1.531(11)
C(4)-C(5)	1.518(12)	C(9)-C(10)	1.518(12)
C(30)-C(31)	1.508(13)	C(10)-C(11)	1.523(12)
C(31)-C(32)	1.514(11)	C(11)-C(12)	1.508(11)
C(33)-C(38)	1.526(10)	C(13)-Cl14)	1.529(10)
C(33)-C(34)	1.529(10)	C(13)-C(18)	1.549(11)
C (34)-C(35)	1.522 (12)	C(14)-C(15)	1.546(12)
C (35)-C(36)	1.524 (13)	C(15)-C(16)	1.542(13)
C(36)-C(37)	1.516(12)	C(16)-C(17)	1.471(12)

C(37)-C(38)	1.537(11)	C(17)-C(18)	1.527(11)
C (39)-C(40)	1.506 (11)	C(19)-C(24)	1.46(2)
C(39)-C(44)	1.523(12)	C(19)-C(84)	1.48(2)
C(40)-C(41)	1.534(12)	C(19)-C(20)	1.535(10)
C(41)-C(42)	1.492 (14)	C(20)-C(82)	1.56(2)
C(42)-C(43)	1.519(12)	C(20)-C(21)	1.58(2)
C(43)-C(44)	1.550 (12)	C(21)-C(22)	1.54(2)
C(45)-C(46)	1.524 (11)	C(22)-C(23)	1.57(2)
C(45)-C(50)	1.529 (10)	C(82)-C(83)	1.53(2)
C(46)-C(47)	1.532 (11)	C(83)-C(23)	1.56(2)
C(47)-C(48)	1.514(12)	C(23)-C(84)	1.611(14)
C(48) -C(49)	1.530 (11)	C(23)-C(24)	1.64(2)
C(49) -C(50)	1.534 (11)	C(25)-C(26)	1.519(10)
C(51) -C(52)	1.535 (10)	C(27)-C(28)	1.541(11)
C(68)-C(69)	1.506(12)	C(27)-C(32)	1.548(11)
C(69) -C(70)	1.523(12)	C(28)-C(29)	1.524(11)
C (71) -C (72)	1.513(12)	C(29)-C(30)	1.540(14)
C (71) -C (76)	1.531(11)	C(1') -C(79)	1.724 (10)
C(72) -C(73)	1.522(13)	C(2') -C(79)	1.749 (11)
C(73)-C(74)	1.502(13)	C(3') -C(80)	1.75 (2)
C(74)-C(75)	1.508(13)	C(3') -C(81)	1.77 (3)
C(75)-C(76)	1.537(11)	C(4')-C(80)	1.75(2)
C(77)-C(78)	1.512(11)	C(4')-C(81)	1.77 (3)
C(6)-C(1)-C(2)	111.1(6)	C(53) -C(87)	1.42 (2)
C(3)-C(2)-C(1)	108.0(7)	C(53)-C(58)	1.507(13)
C(4)-C(3)-C(2)	113.5(7)	C(53)-C(54)	1.530(11)
C(3)-C(4)-C(5)	109.4(7)	C(54)-C(55)	1.54(2)
C (4)-C (5)-C(6)	110.5 (7)	C(54)-C(85)	1.56(2)
C(1)-C(6)-C(5)	113.1(7)	C(55) -C(56)	1.52 (2)
C (12)-C(7)-C(8)	111.3 (6)	C(56)-C(57)	1.54(2)
C(9)-C(8)-C(7)	111.2 (7)	C (85) -C(86)	1.54 (3)
C(10)-C(9)-C(8)	111.1(7)	C(86)-C(57)	1.59(3)
C (9)-C(10)-C(11)	111.2 (7)	C(57)-C(87)	1.58(2)
C(12)-C(11) -C(10)	112.9 (7)	C(57)-C(58)	1.62(2)
C(11)-C(12)-C(7)	110.5(7)	C(59) -C(60)	1.503 (11)
C(14)-C(13)-C(18)	109.6(7)	C(59) -C(64)	1.541 (10)
C(13)-C(14)-C(15)	109.9(7)	C(60) -C(61)	1.513 (12)
C(16)-C(15)-C(14)	110.7(8)	C(61) -C(62)	1.543 (12)
C (17)-C(16)-C(15)	110.6 (7)	C(62)-C(63)	1.508(12)
C(16)-C(17) -C(18)	112.2 (8)	C(63)-C(64)	1.554(12)
C(17)-C(18)-C(13)	110.7(7)	C(65)-C(70)	1.535(11)
C(24)-C(l9)-C(20)	114.6(10)	C(65) -C (66)	1.550 (10)
C(84)-C(l9)-C(20)	114.8(9)	C(66)-C(67)	1.526(12)
C(33)-C(38)-C(37)	110.0(7)	C(67)-C(68)	1.535(14)
C(40)-C(39)-C(44)	112.7(7)	C(l9)-C(20)-C(82)	113.0(9)
C(40) -C(39) -P(4)	114.3 (6)	C(l9) -C(20) -C(21)	112.2 (12)

C(39)-C(40)-C(41)	112.3 (7)	C (22)-C(21)-C(20)	110 (2)
C(42)-C(41)-C(40)	111.5(8)	C(21)-C(22)-C(23)	104(2)
C(41)-C(42)-C(43)	113.1 (8)	C(83)-C(82)-C(20)	110.1(12)
C(42)-C(43)-C(44)	111.6(8)	C(82)-C(83)-C(23)	107.2 (14)
C(39)-C(44)-(43)	109.3 (7)	C(83)-C(23)-C(84)	107.3 (10)
C(46)-C(45)-C(50)	110.1(6)	C(22) -C(23)-C(24)	104.0 (13)
C(45)-C(46)-C(47)	107.9(7)	C(19)-C(24)-C(23)	108.2 (12)
C(48)-C(47)-C(46)	113.7(7)	C(19)-C(84)-C(23)	109.0(9)
C(47)-C(48)-C(49)	112.0(7)	C(28)-C(27)-C(32)	111.1(7)
C(48)-C(49)-C(50)	110.1(7)	C (29)-C(28)-C(27)	110.3 (7)
C(45)-C(50)-C(49)	111.0(6)	C(28)-C(29)-C (30)	109.5 (8)
C(56)-C(57)-C(58)	114(2)	C(31)-C(30)-C(29)	110.2(8)
C(53)-C(58)-C(57)	104.0(10)	C(30)-C(31)-C(32)	111.9 (7)
C(53)-C(87)-C(57)	110.5(13)	C(31)-C(32)-C(27)	109.7 (7)
C(60)-C(59)-C(64)	110.2(7)	C(38)-C(33)-C(34)	109.4(6)
C(59)-C(60)-C(61)	111.2(7)	C (35)-C(34)-C(33)	111.3 (7)
C(60)-C(61)-C(62)	111.9(8)	C (34)-C(35)-C(36)	111.6 (8)
C(63)-C(62)-C(61)	109.5(7)	C(37)-C(36)-C(35)	111.4(7)
C(62)-C(63)-C(64)	111.5(8)	C(36)-C(37)-C(38)	111.4(7)
C(59)-C(64)-C(63)	110.0(7)	C(80)-C(3')-C(81)	4(4)
C(70)-C(65)-C(66)	109.1(7)	C(80)-C(4')-C(81)	4(4)
C(66)-C(67)-C(68)	111.6(8)	C(87)-C(53)-C(54)	111.3(10)
C(67)-C(66)-C(65)	110.2(7)	C(58)-C(53)-C(54)	118.6(9)
C(69)-C(68)-C(67)	110.8(8)	C(53)-C(54)-C(55)	107.7(9)
C(72)-C(71)-C(76)	109.2 (7)	C(53)-C(54)-C(85)	118.6(10)
C(71)-C(72)-C(73)	111.7(8)	C(56)-C(55)-C(54)	118(2)
C(74)-C(73)-C(72)	112.8(8)	C(55)-C(56)-C(57)	101(2)
C(73)-C (74)-C(75)	110.9 (8)	C(86)-C(85)-C(54)	104(2)
C(74)-C(75) -C(76)	111.2 (7)	C(85)-C(86)-C(57)	114(2)
C(71)-C(76) -C(75)	110.6 (8)	C(87)-C(57)-C(86)	100(2)
C(68)-C(69)-C(70)	111.4(8)	C(69)-C(70)-C(65)	110.7 (7)

7.4. $[Rh(dppe)Cl_4](NH_3OH).1.25CD_3NO_2$ (4)

Table 10. Crystal Structure Data and Refinement for Complex (4)

Empirical formula	C27.25 H28 D3.75 Cl4 N2.25 O3.50 P2 Rh
Formula weight	753.45
Temperature	150(2) K
Wavelength	0.71073 Å
Crystal system	Triclinic
Space group	P-1
Unit cell dimensions	a = 11.641(1) Å; alpha = 89.37(1)°. b = 15.009(1) Å; beta = 81.89(1)°.

	c = 36.565(3) Å; gamma = 83.70(1)°
Volume	6286.5(14) $Å^3$
Z	8
Density (calculated)	1.592 Mg/m^3
Absorption coefficient	1.020 mm^{-1}
F(000)	3056
Crystal size	0.30 x 0.20 x 0.03 mm
Theta range for data collection	1.48 to 25.78°.
Index ranges	$-13 \leq h \leq 13$, $-18 \leq k \leq 16$, $-40 \leq l \leq 44$
Reflections collected	26160
Independent reflections	19312 [R(int) = 0.0427]
Absorption correction	None
Refinement method	Full-matrix-block least-squares on F^2
Data / restraints / parameters	18455 / 12 / 1450
Goodness-of-fit on F^2	1.062
Final R indices [I>2sigma(I)]	R1 = 0.0596 wR2 = 0.1102
R indices (all data)	R1 = 0.0938 wR2 = 0.1316
Largest diff. peak and hole	0.833 and -0.764 $e.Å^{-3}$

Table 11. Selected Bond Lengths (Å) And Angles (°) for Complex (4) Containing Rh, P, Cl, N or O

Rh(1A)-P(1A)	2.269(2)	Rh(1A)-P(2A)	2.275(2)
Rh(1A)-Cl(3A)	2.347(2)	Rh(1A)-Cl(4A)	2.360(2)
Rh(1A)-Cl(1A)	2.452(2)	Rh(1A)-Cl(2A)	2.458(2)
P(1A)-C(11A)	1.817(7)	P(1A)-C(21A)	1.820(7)
P(1A)-C(1A)	1.823(7)	P(2A)-C(41A)	1.823(7)
P(2A)-C(2A)	1.829(7)	P(2A)-C(31A)	1.835(7)
N(1A)-O(1A)	1.412(7)	Rh(1B)-P(1B)	2.273(2)
Rh(1B)-P(2B)	2.277(2)	Rh(1B)-Cl(3B)	2.354(2)
Rh(1B)-Cl(4B)	2.365(2)	Rh(1B)-Cl(1B)	2.461(2)
Rh(1B)-Cl(2B)	2.467(2)	P(1B)-C(1B)	1.815(7)
P(1B)-C(21B)	1.820(8)	P(1B)-C(11B)	1.841(7)
P(2B)-C(2B)	1.818(8)	P(2B)-C(41B)	1.824(7)
P(2B)-C(31B)	1.827(8)	N(1B)-O(1B)	1.385(7)
Rh(1C)-P(1C)	2.277(2)	Rh(1C)-P(2C)	2.280(2)
Rh(1C)-Cl(4C)	2.336(2)	Rh(1C)-Cl(3C)	2.366(2)
Rh(1C)-Cl(1C)	2.449(2)	Rh(1C)-Cl(2C)	2.486(2)
P(1C)-C(1C)	1.816(7)	P(1C)-C(11C)	1.824(7)
P(1C)-C(21C)	1.829(7)	P(2C)-C(31C)	1.820(7)
P(2C)-C(2C)	1.823(7)	P(2C)-C(41C)	1.826(7)
N(1C)-O(1C)	1.371(8)	Rh(1D)-P(1D)	2.276(2)
Rh(1D)-P(2D)	2.281(2)	Rh(1D)-Cl(3D)	2.355(2)
Rh(1D)-Cl(4D)	2.357(2)	Rh(1D)-Cl(2D)	2.444(2)
Rh(1D)-Cl(1D)	2.456(2)	P(1D)-C(1D)	1.828(7)

P(1D)-C(21D)	1.832(7)	P(1D)-C(11D)	1.835(8)
P(2D)-C(2D)	1.816(7)	P(2D)-C(31D)	1.823(7)
P(2D)-C(41D)	1.838(8)	N(1D)-O(1D)	1.410(7)
O(2A)-N(0A)	1.153(11)	O(3A)-N(0A)	1.236(11)
N(0A)-C(0A)	1.490(12)	O(2B)-N(0B)	1.213(9)
O(3B)-N(0B)	1.217(9)	N(0B)-C(0B)	1.476(10)
O(2C)-N(0C)	1.222(8)	O(3C)-N(0C)	1.211(8)
N(0C)-C(0C)	1.482(10)	O(2D)-N(0D)	1.198(9)
O(3D)-N(0D)	1.196(9)	N(0D)-C(0D)	1.481(11)
O(2E)-N(0E)	1.199(9)	O(3E)-N(0E)	1.228(9)
N(0E)-C(0E)	1.482(10)	O(2E')-N(0E')	1.194(9)
O(3E')-N(0E')	1.165(9)	N(0E')-C(0E')	1.486(10)
P(1A)-Rh(1A)-P(2A)	87.55(7)	P(1A)-Rh(1A)-Cl(3A)	91.02(7)
P(2A)-Rh(1A)-Cl(3A)	88.39(7)	P(1A)-Rh(1A)-Cl(4A)	89.34(7)
P(2A)-Rh(1A)-Cl(4A)	91.28(7)	Cl(3A)-Rh(1A)-Cl(4A)	179.49(7)
P(1A)-Rh(1A)-Cl(1A)	178.19(7)	P(2A)-Rh(1A)-Cl(1A)	93.14(6)
Cl(3A)-Rh(1A)-Cl(1A)	90.67(6)	Cl(4A)-Rh(1A)-Cl(1A)	88.97(6)
P(1A)-Rh(1A)-Cl(2A)	90.18(6)	P(2A)-Rh(1A)-Cl(2A)	175.88(7)
Cl(3A)-Rh(1A)-Cl(2A)	88.21(6)	Cl(4A)-Rh(1A)-Cl(2A)	92.13(6)
Cl(1A)-Rh(1A)-Cl(2A)	89.23(6)	C(11A)-P(1A)-C(21A)	100.6(3)
C(11A)-P(1A)-C(1A)	107.0(4)	C(21A)-P(1A)-C(1A)	105.2(3)
C(11A)-P(1A)-Rh(1A)	116.1(2)	C(21A)-P(1A)-Rh(1A)	120.4(2)
C(1A)-P(1A)-Rh(1A)	106.4(2)	C(41A)-P(2A)-C(2A)	106.8(4)
C(41A)-P(2A)-C(31A)	104.0(3)	C(2A)-P(2A)-C(31A)	104.3(3)
C(41A)-P(2A)-Rh(1A)	115.8(2)	C(2A)-P(2A)-Rh(1A)	105.1(2)
C(31A)-P(2A)-Rh(1A)	119.7(2)	C(2A)-C(1A)-P(1A)	109.1(5)
C(1A)-C(2A)-P(2A)	110.7(5)	C(16A)-C(11A)-P(1A)	118.0(5)
C(12A)-C(11A)-P(1A)	123.7(6)	C(26A)-C(21A)-P(1A)	124.0(5)
C(22A)-C(21A)-P(1A)	117.5(5)	C(32A)-C(31A)-P(2A)	123.7(5)
C(36A)-C(31A)-P(2A)	117.5(5)	C(46A)-C(41A)-P(2A)	118.6(6)
C(42A)-C(41A)-P(2A)	122.2(6)	P(1B)-Rh(1B)-P(2B)	87.59(7)
P(1B)-Rh(1B)-Cl(3B)	90.92(7)	P(2B)-Rh(1B)-Cl(3B)	88.85(7)
P(1B)-Rh(1B)-Cl(4B)	91.32(7)	P(2B)-Rh(1B)-Cl(4B)	93.13(7)
Cl(3B)-Rh(1B)-Cl(4B)	177.07(7)	P(1B)-Rh(1B)-Cl(1B)	177.43(7)
P(2B)-Rh(1B)-Cl(1B)	89.86(7)	Cl(3B)-Rh(1B)-Cl(1B)	88.74(6)
Cl(4B)-Rh(1B)-Cl(1B)	89.10(6)	P(1B)-Rh(1B)-Cl(2B)	90.06(7)
P(2B)-Rh(1B)-Cl(2B)	177.40(7)	Cl(3B)-Rh(1B)-Cl(2B)	90.09(6)
Cl(4B)-Rh(1B)-Cl(2B)	88.01(7)	Cl(1B)-Rh(1B)-Cl(2B)	92.50(6)
C(1B)-P(1B)-C(21B)	107.9(4)	C(1B)-P(1B)-C(11B)	103.9(3)
C(21B)-P(1B)-C(11B)	102.3(3)	C(1B)-P(1B)-Rh(1B)	105.3(3)
C(21B)-P(1B)-Rh(1B)	114.6(2)	C(11B)-P(1B)-Rh(1B)	121.9(3)
C(2B)-P(2B)-C(41B)	103.8(4)	C(2B)-P(2B)-C(31B)	107.2(4)
C(41B)-P(2B)-C(31B)	101.7(3)	C(2B)-P(2B)-Rh(1B)	106.4(2)
C(41B)-P(2B)-Rh(1B)	121.2(3)	C(31B)-P(2B)-Rh(1B)	115.4(2)
C(2B)-C(1B)-P(1B)	110.7(5)	C(1B)-C(2B)-P(2B)	110.0(5)
C(26B)-C(21B)-P(1B)	118.0(6)	C(22B)-C(21B)-P(1B)	123.2(6)

C(36B)-C(31B)-P(2B)	117.2(6)	C(32B)-C(31B)-P(2B)	121.7(7)
C(42B)-C(41B)-P(2B)	127.3(6)	C(46B)-C(41B)-P(2B)	114.0(6)
P(1C)-Rh(1C)-P(2C)	86.90(7)	P(1C)-Rh(1C)-Cl(4C)	93.49(7)
P(2C)-Rh(1C)-Cl(4C)	87.33(7)	P(1C)-Rh(1C)-Cl(3C)	85.10(7)
P(2C)-Rh(1C)-Cl(3C)	95.65(7)	Cl(4C)-Rh(1C)-Cl(3C)	176.62(7)
P(1C)-Rh(1C)-Cl(1C)	173.95(7)	P(2C)-Rh(1C)-Cl(1C)	88.63(6)
Cl(4C)-Rh(1C)-Cl(1C)	90.37(7)	Cl(3C)-Rh(1C)-Cl(1C)	91.29(7)
P(1C)-Rh(1C)-Cl(2C)	94.94(7)	P(2C)-Rh(1C)-Cl(2C)	173.76(7)
Cl(4C)-Rh(1C)-Cl(2C)	86.60(7)	Cl(3C)-Rh(1C)-Cl(2C)	90.46(7)
Cl(1C)-Rh(1C)-Cl(2C)	89.93(6)	C(1C)-P(1C)-C(11C)	107.9(3)
C(1C)-P(1C)-C(21C)	104.9(3)	C(11C)-P(1C)-C(21C)	103.2(3)
C(1C)-P(1C)-Rh(1C)	104.8(2)	C(11C)-P(1C)-Rh(1C)	116.5(2)
C(21C)-P(1C)-Rh(1C)	118.7(2)	C(31C)-P(2C)-C(2C)	105.7(3)
C(31C)-P(2C)-C(41C)	101.9(3)	C(2C)-P(2C)-C(41C)	106.2(3)
C(31C)-P(2C)-Rh(1C)	115.0(2)	C(2C)-P(2C)-Rh(1C)	107.1(2)
C(41C)-P(2C)-Rh(1C)	120.0(2)	C(2C)-C(1C)-P(1C)	110.3(5)
C(1C)-C(2C)-P(2C)	109.6(5)	C(12C)-C(11C)-P(1C)	123.2(6)
C(16C)-C(11C)-P(1C)	117.4(6)	C(22C)-C(21C)-P(1C)	121.8(6)
C(26C)-C(21C)-P(1C)	119.7(6)	C(36C)-C(31C)-P(2C)	119.6(5)
C(32C)-C(31C)-P(2C)	122.7(6)	C(46C)-C(41C)-P(2C)	124.5(6)
C(42C)-C(41C)-P(2C)	116.5(5)	P(1D)-Rh(1D)-P(2D)	87.21(7)
P(1D)-Rh(1D)-Cl(3D)	91.44(7)	P(2D)-Rh(1D)-Cl(3D)	92.37(7)
P(1D)-Rh(1D)-Cl(4D)	89.94(7)	P(2D)-Rh(1D)-Cl(4D)	89.07(7)
Cl(3D)-Rh(1D)-Cl(4D)	178.06(7)	P(1D)-Rh(1D)-Cl(2D)	90.67(7)
P(2D)-Rh(1D)-Cl(2D)	176.06(7)	Cl(3D)-Rh(1D)-Cl(2D)	91.01(7)
Cl(4D)-Rh(1D)-Cl(2D)	87.61(7)	P(1D)-Rh(1D)-Cl(1D)	178.28(7)
P(2D)-Rh(1D)-Cl(1D)	92.49(7)	Cl(3D)-Rh(1D)-Cl(1D)	86.89(7)
Cl(4D)-Rh(1D)-Cl(1D)	91.75(7)	Cl(2D)-Rh(1D)-Cl(1D)	89.73(6)
C(1D)-P(1D)-C(21D)	106.1(3)	C(1D)-P(1D)-C(11D)	104.4(3)
C(21D)-P(1D)-C(11D)	101.8(3)	C(1D)-P(1D)-Rh(1D)	105.7(2)
C(21D)-P(1D)-Rh(1D)	116.6(2)	C(11D)-P(1D)-Rh(1D)	120.9(2)
C(2D)-P(2D)-C(31D)	106.6(3)	C(2D)-P(2D)-C(41D)	104.8(3)
C(31D)-P(2D)-C(41D)	100.6(3)	C(2D)-P(2D)-Rh(1D)	104.8(2)
C(31D)-P(2D)-Rh(1D)	118.3(2)	C(41D)-P(2D)-Rh(1D)	120.5(2)
C(2D)-C(1D)-P(1D)	108.6(5)	C(1D)-C(2D)-P(2D)	109.3(5)
C(12D)-C(11D)-P(1D)	123.6(6)	C(16D)-C(11D)-P(1D)	116.4(6)
C(26D)-C(21D)-P(1D)	117.8(6)	C(22D)-C(21D)-P(1D)	122.9(6)
C(36D)-C(31D)-P(2D)	122.4(6)	C(32D)-C(31D)-P(2D)	117.5(6)
C(42D)-C(41D)-P(2D)	124.3(6)	C(46D)-C(41D)-P(2D)	115.9(6)
O(2A)-N(0A)-O(3A)	127.1(11)	O(2A)-N(0A)-C(0A)	120.6(11)
O(3A)-N(0A)-C(0A)	112.2(10)	O(2B)-N(0B)-O(3B)	125.4(9)
O(2B)-N(0B)-C(0B)	118.0(8)	O(3B)-N(0B)-C(0B)	116.5(8)
O(3C)-N(0C)-O(2C)	123.7(7)	O(3C)-N(0C)-C(0C)	118.3(7)
O(2C)-N(0C)-C(0C)	118.0(7)	O(3D)-N(0D)-O(2D)	124.8(9)
O(3D)-N(0D)-C(0D)	120.4(8)	O(2D)-N(0D)-C(0D)	114.8(9)
O(2E)-N(0E)-O(3E)	131(2)	O(2E)-N(0E)-C(0E)	111.8(13)

O(3E)-N(0E)-C(0E)	116.1(14)	O(3E')-N(0E')-O(2E')	124(2)
O(3E')-N(0E')-C(0E')	116.8(14)	O(2E')-N(0E')-C(0E')	118.6(14)

Table 12. Selected Bond Lengths (Å) And Angles (°) for Complex (4) Not Containing Rh, Cl, P, N, or O

C(1A)-C(2A)	1.526(9)	C(11A)-C(16A)	1.393(10)
C(11A)-C(12A)	1.394(10)	C(12A)-C(13A)	1.397(11)
C(13A)-C(14A)	1.387(12)	C(14A)-C(15A)	1.380(11)
C(15A)-C(16A)	1.386(10)	C(21A)-C(26A)	1.395(9)
C(21A)-C(22A)	1.406(9)	C(22A)-C(23A)	1.389(10)
C(23A)-C(24A)	1.384(10)	C(24A)-C(25A)	1.388(9)
C(25A)-C(26A)	1.379(9)	C(31A)-C(32A)	1.385(9)
C(31A)-C(36A)	1.394(10)	C(32A)-C(33A)	1.397(10)
C(33A)-C(34A)	1.373(10)	C(34A)-C(35A)	1.365(10)
C(35A)-C(36A)	1.389(10)	C(41A)-C(46A)	1.374(10)
C(41A)-C(42A)	1.392(10)	C(42A)-C(43A)	1.388(12)
C(43A)-C(44A)	1.401(12)	C(44A)-C(45A)	1.365(11)
C(45A)-C(46A)	1.407(10)	C(1B)-C(2B)	1.536(10)
C(11B)-C(12B)	1.372(10)	C(11B)-C(16B)	1.387(11)
C(12B)-C(13B)	1.384(10)	C(13B)-C(14B)	1.378(12)
C(14B)-C(15B)	1.379(13)	C(15B)-C(16B)	1.405(11)
C(21B)-C(26B)	1.383(10)	C(21B)-C(22B)	1.386(10)
C(22B)-C(23B)	1.404(12)	C(23B)-C(24B)	1.367(13)
C(24B)-C(25B)	1.375(13)	C(25B)-C(26B)	1.378(11)
C(31B)-C(36B)	1.377(11)	C(31B)-C(32B)	1.391(11)
C(32B)-C(33B)	1.370(13)	C(33B)-C(34B)	1.34(2)
C(34B)-C(35B)	1.39(2)	C(35B)-C(36B)	1.419(12)
C(41B)-C(42B)	1.347(11)	C(41B)-C(46B)	1.390(11)
C(42B)-C(43B)	1.403(11)	C(43B)-C(44B)	1.326(13)
C(44B)-C(45B)	1.356(13)	C(45B)-C(46B)	1.411(12)
C(1C)-C(2C)	1.528(10)	C(11C)-C(12C)	1.376(10)
C(11C)-C(16C)	1.396(10)	C(12C)-C(13C)	1.383(11)
C(13C)-C(14C)	1.363(11)	C(14C)-C(15C)	1.350(11)
C(15C)-C(16C)	1.408(10)	C(21C)-C(22C)	1.356(11)
C(21C)-C(26C)	1.368(10)	C(22C)-C(23C)	1.385(12)
C(23C)-C(24C)	1.378(12)	C(24C)-C(25C)	1.360(12)
C(25C)-C(26C)	1.387(12)	C(31C)-C(36C)	1.378(10)
C(31C)-C(32C)	1.396(10)	C(32C)-C(33C)	1.397(11)
C(33C)-C(34C)	1.372(12)	C(34C)-C(35C)	1.389(11)
C(35C)-C(36C)	1.395(10)	C(41C)-C(46C)	1.369(9)
C(41C)-C(42C)	1.392(9)	C(42C)-C(43C)	1.388(10)
C(43C)-C(44C)	1.374(11)	C(44C)-C(45C)	1.401(11)
C(45C)-C(46C)	1.401(10)	C(1D)-C(2D)	1.530(10)
C(11D)-C(12D)	1.382(10)	C(11D)-C(16D)	1.393(10)
C(12D)-C(13D)	1.401(10)	C(13D)-C(14D)	1.382(11)

C(14D)-C(15D)	1.369(11)	C(15D)-C(16D)	1.394(11)
C(21D)-C(26D)	1.381(11)	C(21D)-C(22D)	1.384(10)
C(22D)-C(23D)	1.384(11)	C(23D)-C(24D)	1.387(13)
C(24D)-C(25D)	1.386(13)	C(25D)-C(26D)	1.384(11)
C(31D)-C(36D)	1.390(10)	C(31D)-C(32D)	1.397(10)
C(32D)-C(33D)	1.391(10)	C(33D)-C(34D)	1.380(11)
C(34D)-C(35D)	1.397(11)	C(35D)-C(36D)	1.392(10)
C(41D)-C(42D)	1.389(10)	C(41D)-C(46D)	1.394(10)
C(42D)-C(43D)	1.397(10)	C(43D)-C(44D)	1.387(11)
C(44D)-C(45D)	1.374(11)	C(45D)-C(46D)	1.387(11)
C(16A)-C(11A)-C(12A)	118.2(7)	C(11A)-C(12A)-C(13A)	120.9(8)
C(14A)-C(13A)-C(12A)	119.6(8)	C(15A)-C(14A)-C(13A)	120.0(8)
C(14A)-C(15A)-C(16A)	120.2(8)	C(15A)-C(16A)-C(11A)	121.1(7)
C(26A)-C(21A)-C(22A)	118.3(6)	C(23A)-C(22A)-C(21A)	120.7(7)
C(24A)-C(23A)-C(22A)	119.8(7)	C(23A)-C(24A)-C(25A)	120.0(7)
C(26A)-C(25A)-C(24A)	120.4(7)	C(25A)-C(26A)-C(21A)	120.8(6)
C(32A)-C(31A)-C(36A)	118.8(7)	C(31A)-C(32A)-C(33A)	119.9(7)
C(34A)-C(33A)-C(32A)	120.8(7)	C(35A)-C(34A)-C(33A)	119.4(7)
C(34A)-C(35A)-C(36A)	120.9(7)	C(35A)-C(36A)-C(31A)	120.1(7)
C(46A)-C(41A)-C(42A)	119.2(7)	C(46A)-C(41A)-P(2A)	118.6(6)
C(42A)-C(41A)-P(2A)	122.2(6)	C(43A)-C(42A)-C(41A)	120.5(9)
C(42A)-C(43A)-C(44A)	119.6(8)	C(45A)-C(44A)-C(43A)	120.2(8)
C(44A)-C(45A)-C(46A)	119.7(8)	C(41A)-C(46A)-C(45A)	120.8(7)
C(12B)-C(11B)-C(16B)	120.4(7)	C(11B)-C(12B)-C(13B)	120.0(8)
C(14B)-C(13B)-C(12B)	120.3(9)	C(13B)-C(14B)-C(15B)	120.3(8)
C(14B)-C(15B)-C(16B)	119.5(9)	C(11B)-C(16B)-C(15B)	119.4(9)
C(26B)-C(21B)-C(22B)	118.8(8)	C(21B)-C(22B)-C(23B)	119.4(8)
C(24B)-C(23B)-C(22B)	120.2(9)	C(23B)-C(24B)-C(25B)	120.8(9)
C(24B)-C(25B)-C(26B)	119.0(9)	C(25B)-C(26B)-C(21B)	121.8(8)
C(36B)-C(31B)-C(32B)	121.0(8)	C(33B)-C(32B)-C(31B)	119.3(10)
C(34B)-C(33B)-C(32B)	121.3(11)	C(33B)-C(34B)-C(35B)	120.9(11)
C(34B)-C(35B)-C(36B)	118.9(10)	C(31B)-C(36B)-C(35B)	118.6(10)
C(42B)-C(41B)-C(46B)	118.7(7)	C(41B)-C(42B)-C(43B)	120.3(9)
C(44B)-C(43B)-C(42B)	120.8(9)	C(43B)-C(44B)-C(45B)	121.4(9)
C(44B)-C(45B)-C(46B)	118.4(10)	C(41B)-C(46B)-C(45B)	120.4(9)
C(12C)-C(11C)-C(16C)	119.3(7)	C(11C)-C(12C)-C(13C)	119.8(8)
C(14C)-C(13C)-C(12C)	121.5(8)	C(15C)-C(14C)-C(13C)	119.3(8)
C(14C)-C(15C)-C(16C)	121.3(8)	C(11C)-C(16C)-C(15C)	118.7(7)
C(22C)-C(21C)-C(26C)	118.3(7)	C(21C)-C(22C)-C(23C)	120.5(9)
C(24C)-C(23C)-C(22C)	120.9(9)	C(25C)-C(24C)-C(23C)	118.8(8)
C(24C)-C(25C)-C(26C)	119.6(8)	C(21C)-C(26C)-C(25C)	121.9(9)
C(36C)-C(31C)-C(32C)	117.6(7)	C(33C)-C(32C)-C(31C)	121.0(8)
C(34C)-C(33C)-C(32C)	120.0(8)	C(33C)-C(34C)-C(35C)	120.2(8)
C(34C)-C(35C)-C(36C)	118.9(8)	C(31C)-C(36C)-C(35C)	122.2(7)
C(46C)-C(41C)-C(42C)	119.0(7)	C(46C)-C(41C)-P(2C)	124.5(6)
C(42C)-C(41C)-P(2C)	116.5(5)	C(43C)-C(42C)-C(41C)	121.4(7)

C(44C)-C(43C)-C(42C)	119.4(7)	C(43C)-C(44C)-C(45C)	120.2(7)
C(46C)-C(45C)-C(44C)	119.4(7)	C(41C)-C(46C)-C(45C)	120.7(7)
C(12D)-C(11D)-C(16D)	120.0(7)	C(11D)-C(12D)-C(13D)	119.6(7)
C(14D)-C(13D)-C(12D)	119.8(8)	C(15D)-C(14D)-C(13D)	120.7(8)
C(14D)-C(15D)-C(16D)	119.9(7)	C(11D)-C(16D)-C(15D)	119.9(7)
C(26D)-C(21D)-C(22D)	119.3(7)	C(21D)-C(22D)-C(23D)	120.3(8)
C(22D)-C(23D)-C(24D)	120.4(9)	C(23D)-C(24D)-C(25D)	119.3(8)
C(26D)-C(25D)-C(24D)	120.1(9)	C(34D)-C(33D)-C(32D)	120.3(8)
C(33D)-C(34D)-C(35D)	120.0(7)	C(36D)-C(35D)-C(34D)	119.9(8)
C(31D)-C(36D)-C(35D)	120.1(7)	C(42D)-C(41D)-C(46D)	119.7(7)
C(41D)-C(42D)-C(43D)	119.7(7)	C(44D)-C(43D)-C(42D)	119.7(8)
C(45D)-C(44D)-C(43D)	120.8(8)	C(44D)-C(45D)-C(46D)	119.8(8)
C(45D)-C(46D)-C(41D)	120.2(8)		

7.5. [Rh(dppe)(CO)Cl_3] (5)

Table 13. Crystal Structure Data and Refinement for Complex (5)

Empirical formula	C27H24Cl3OP2Rh
Formula weight	564.76
Temperature	150(2) K
Wavelength	0.71073 Å
Crystal system	Monoclinic
Space group	P2(1)/n
Unit cell dimensions	a = 11.797(4) Å; alpha = 90°
	b = 13.621(5) Å; beta = 92.159(6)°
	c = 16.241(5) Å; gamma = 90°
Volume	Z 2607.8(14) A^3 4
Density (calculated)	1.438 Mg/m^3
Absorption coefficient	0.897 mm^{-1}
F(000)	1144
Crystal size	0.40 x 0.30 x 0.15 mm
Theta range for data collection	1.95 to 23.27°
Limiting indices	$-12 \leq h \leq 13$ $-15 \leq k \leq 10$ $-15 \leq l \leq 18$
Reflections collected	9917
Independent reflections	3707 [R(int) = 0.0321]
Absorption correction	Semi-empirical from psi-scans
Max. and min. transmission	0.94 and 0.65
Refinement method	Full-matrix least-squares on F^2
Data/restraints/parameters	3707/ 0 / 307
Goodness-of-fit on F^2	1.049
Final R indices [I>2sigma(I)]	R1 = 0.0225 wR2 = 0.0565
R indices (all data)	R1 = 0.0241 wR2 = 0.0577
Largest diff. peak and hole	0.411 and -0.380 $e.Å^{-3}$

Table 14. Selected Bond Lengths (Å) And Angles (°) for (5) Containing Rh, P, O, and Cl

Rh(1)-C(3)	1.885(3)	P(1)-C(21)	1.819(3)
Rh(1)-P(2)	2.3051(8)	P(1)-C(11)	1.820(3)
Rh(1)-P(1)	2.3051(8)	P(2)-C(41)	1.806(3)
Rh(1)-Cl(2)	2.3521(9)	P(2)-C(31)	1.823(3)
Rh(1)-Cl(3)	2.4189(8)	P(2)-C(2)	1.835(2)
Rh(1)-Cl(4)	2.4364(8)	O(3)-C(3)	1.124(3)
P(1)-C(1)	1.818(2)		
C(3)-Rh(1)-P(2)	93.93(8)	P(2)-Rh(1)-Cl(3)	90.31(3)
C(3)-Rh(1)-P(1)	96.46(8)	P(1)-Rh(1)-Cl(3)	173.99(2)
P(2)-Rh(1)-P(1)	86.78(3)	Cl(2)-Rh(1)-Cl(3)	91.37(3)
C(3)-Rh(1)-Cl(2)	177.49(8)	C(3)-Rh(1)-Cl(4)	85.06(8)
P(2)-Rh(1)-Cl(2)	88.56(3)	P(2)-Rh(1)-Cl(4)	177.28(2)
P(1)-Rh(1)-Cl(2)	83.30(3)	P(1)-Rh(1)-Cl(4)	90.82(3)
C(3)-Rh(1)-Cl(3)	88.98(8)	Cl(2)-Rh(1)-Cl(4)	92.44(3)
C(31)-P(2)-Rh(1)	115.91(9)	Cl(3)-Rh(1)-Cl(4)	92.20(3)
C(2)-P(2)-Rh(1)	106.09(8)	C(1)-P(1)-C(21)	106.91(12)
C(2)-C(1)-P(1)	109.6(2)	C(1)-P(1)-C(11)	107.19(12)
P(1)-C(1)-H(1A)	109.75(8)	C(21)-P(1)-C(11)	106.53(12)
P(1)-C(1)-H(1B)	109.75(9)	C(1)-P(1)-Rh(1)	104.40(8)
C(1)-C(2)-P(2)	111.6(2)	C(21)-P(1)-Rh(1)	118.18(9)
P(2)-C(2)-H(2A)	109.31(8)	C(11)-P(1)-Rh(1)	113.00(8)
P(2)-C(2)-H(2B)	109.31(8)	C(41)-P(2)-C(31)	105.98(11)
O(3)-C(3)-Rh(1)	176.4(2)	C(41)-P(2)-C(2)	107.61(12)
C(16)-C(11)-P(1)	121.3(2)	C(31)-P(2)-C(2)	104.53(12)
C(12)-C(11)-P(1)	119.2(2)	C(41)-P(2)-Rh(1)	115.89(8)
C(22)-C(21)-P(1)	119.8(2)	C(32)-C(31)-P(2)	118.8(2)
C(26)-C(21)-P(1)	121.5(2)	C(46)-C(41)-P(2)	120.6(2)
C(36)-C(31)-P(2)	121.9(2)	C(42)-C(41)-P(2)	119.9(2)

Table 15. Selected Bond Lengths (Å) And Angles (°) for (5) Not Containing Rh, P, Cl, or O

C(1)-C(2)	1.527(3)	C(32)-C(33)	1.385(4)
C(1)-H(1A)	0.99	C(32)-H(32)	0.95
C(1)-H(1B)	0.99	C(33)-C(34)	1.387(4)
C(2)-H(2A)	0.99	C(33)-H(33)	0.95
C(2)-H(2B)	0.99	C(34)-C(35)	1.376(4)
C(11)-C(16)	1.390(4)	C(34)-H(34)	0.95
C(11)-C(12)	1.394(4)	C(35)-C(36)	1.395(4)
C(12)-C(13)	1.382(4)	C(35)-H(35)	0.95
C(12)-H(12)	0.95	C(36)-H(36)	0.95
C(13)-C(14)	1.385(5)	C(41)-C(46)	1.393(4)
C(13)-H(13)	0.95	C(41)-C(42)	1.395(4)

C(14)-C(15)	1.380(5)	C(42)-C(43)	1.390(4)
C(14)-H(14)	0.95	C(42)-H(42)	0.95
C(15)-C(16)	1.388(4)	C(43)-C(44)	1.377(4)
C(15)-H(15)	0.95	C(43)-H(43)	0.95
C(16)-H(16)	0.95	C(44)-C(45)	1.379(4)
C(21)-C(22)	1.387(4)	C(44)-H(44)	0.95
C(21)-C(26)	1.394(4)	C(45)-C(46)	1.387(4)
C(22)-C(23)	1.389(4)	C(45)-H(45)	0.95
C(22)-H(22)	0.95	C(46)-H(46)	0.95
C(23)-C(24)	1.374(5)	C(25)-H(25)	0.95
C(23)-H(23)	0.95	C(26)-H(26)	0.95
C(24)-C(25)	1.369(5)	C(31)-C(36)	1.389(4)
C(24)-H(24)	0.95	C(31)-C(32)	1.402(4)
C(25)-C(26)	1.389(4)	C(2)-C(1)-H(1B)	109.75(14)
C(2)-C(1)-H(1A)	109.75(13)	C(1)-C(2)-H(2A)	109.31(13)
H(1A)-C(1)-H(1B)	108.2	H(2A)-C(2)-H(2B)	108.0
C(1)-C(2)-H(2B)	109.31(14)	C(13)-C(12)-C(11)	119.9(3)
C(16)-C(11)-C(12)	119.5(3)	C(11)-C(12)-H(12)	120.1(2)
C(13)-C(12)-H(12)	120.1(2)	C(12)-C(13)-H(13)	119.7(2)
C(12)-C(13)-C(14)	120.7(3)	C(15)-C(14)-C(13)	119.3(3)
C(14)-C(13)-H(13)	119.7(2)	C(13)-C(14)-H(14)	120.3(2)
C(15)-C(14)-H(14)	120.3(2)	C(14)-C(15)-H(15)	119.6(2)
C(14)-C(15)-C(16)	120.8(3)	C(15)-C(16)-C(11)	119.8(3)
C(16)-C(15)-H(15)	119.6(2)	C(11)-C(16)-H(16)	120.1(2)
C(15)-C(16)-H(16)	120.1(2)	C(21)-C(22)-C(23)	120.7(3)
C(22)-C(21)-C(26)	118.8(2)	C(23)-C(22)-H(22)	119.7(2)
C(21)-C(22)-H(22)	119.7(2)	C(24)-C(23)-H(23)	120.0(2)
C(24)-C(23)-C(22)	119.9(3)	C(25)-C(24)-C(23)	120.2(3)
C(22)-C(23)-H(23)	120.0(2)	C(23)-C(24)-H(24)	119.9(2)
C(25)-C(24)-H(24)	119.9(2)	C(24)-C(25)-H(25)	119.7(2)
C(24)-C(25)-C(26)	120.5(3)	C(25)-C(26)-C(21)	120.0(3)
C(26)-C(25)-H(25)	119.7(2)	C(21)-C(26)-H(26)	120.0(2)
C(25)-C(26)-H(26)	120.0(2)	C(33)-C(32)-C(31)	119.9(3)
C(36)-C(31)-C(32)	119.3(2)	C(31)-C(32)-H(32)	120.0(2)
C(33)-C(32)-H(32)	120.0(2)	C(32)-C(33)-H(33)	119.8(2)
C(32)-C(33)-C(34)	120.4(3)	C(35)-C(34)-C(33)	120.0(3)
C(34)-C(33)-H(33)	119.8(2)	C(33)-C(34)-H(34)	120.0(2)
C(35)-C(34)-H(34)	120.0(2)	C(34)-C(35)-H(35)	119.9(2)
C(34)-C(35)-C(36)	120.3(3)	C(31)-C(36)-C(35)	120.1(2)
C(36)-C(35)-H(35)	119.9(2)	C(35)-C(36)-H(36)	119.9(2)
C(31)-C(36)-H(36)	119.9(2)	C(43)-C(42)-C(41)	119.6(3)
C(46)-C(41)-C(42)	119.5(2)	C(41)-C(42)-H(42)	120.2(2)
C(43)-C(42)-H(42)	120.2(2)	C(42)-C(43)-H(43)	119.7(2)
C(44)-C(43)-C(42)	120.6(3)	C(43)-C(44)-H(44)	120.1(2)
C(43)-C(44)-C(45)	119.9(3)	C(44)-C(45)-C(46)	120.5(3)
C(45)-C(44)-H(44)	120.1(2)	C(46)-C(45)-H(45)	119.8(2)

C(44)-C(45)-H(45)	119.8(2)	C(45)-C(46)-H(46)	120.1(2)
C(45)-C(46)-C(41)	119.9(3)		
C(41)-C(46)-H(46)	120.1(2)		

7.6. $[Rh_2(dppp)_2Cl_2(OMe)_2(OH)](Cl).\ 4CH_2Cl_2$ (6)

Table 16. Crystal Structure Data and Refinement for Complex (6)

Empirical formula	C60 H67 Cl11 O3 P4 Rh2
Formula weight	1555.79
Temperature	153(2) K
Wavelength	0.71073 A
Crystal system	Monoclinic
Space group	Cc
Unit cell dimensions	a = 10.364(1) Å; alpha = 90°. b = 26.281(2) Å; beta = 100.74(1)°. c = 24.621(2) Å; gamma = 90°.
Volume	6589(1) $Å^3$
Z	4
Density (calculated)	1.568 g/cm^3
Absorption coefficient	1.087 mm^{-1}
F(000)	3152
Crystal size	0.56 x 0.35 x 0.08 mm
Theta range for data collection	1.55 to 25.73°.
Index ranges	$-11 \le h \le 12$ $-30 \le k \le 32$ $-28 \le l \le 18$
Reflections collected	15720
Independent reflections	8222 [R(int) = 0.0343]
Absorption correction	Semi-empirical from psi-scans
Max. and min. transmission	0.9901 and 0.7658
Refinement method	Full-matrix least-squares on F^2
Data / restraints / parameters	8209 / 11 / 721
Goodness-of-fit on F^2	1.045
Final R indices [I>2sigma(I)]	R1 = 0.0403 wR2 = 0.1092
R indices (all data)	R1 = 0.0430 wR2 = 0.1169
Absolute structure parameter	-0.01(3)
Largest diff. peak and hole	1.066 and -0.799 $e.A^{-3}$

Table 17. Selected Bond Lengths (Å) and Angles (°) for Complex (6) Including Rh, P, Cl and O

Rh(1)-O(3)	2.087(5)	Rh(1)-O(1)	2.097(6)
Rh(1)-O(2)	2.129(5)	Rh(1)-P(3)	2.269(2)
Rh(1)-P(2)	2.279(2)	Rh(1)-Cl(3)	2.329(2)
Rh(1)..Rh(2)	2.936(1)	Rh(2)-O(3)	2.070(5)
Rh(2)-O(2)	2.103(5)	Rh(2)-O(1)	2.139(5)
Rh(2)-P(1)	2.272(2)	Rh(2)-P(4)	2.279(2)
Rh(2)-Cl(2)	2.334(2)	P(1)-C(51)	1.825(7)
P(1)-C(4)	1.827(8)	P(1)-C(61)	1.828(8)
P(2)-C(1)	1.816(9)	P(2)-C(11)	1.816(7)
P(2)-C(21)	1.830(9)	P(3)-C(41)	1.821(8)
P(3)-C(31)	1.831(7)	P(3)-C(3)	1.838(9)
P(4)-C(6)	1.823(9)	P(4)-C(81)	1.825(8)
P(4)-C(71)	1.835(7)	O(1)-C(7)	1.423(8)
O(2)-C(8)	1.429(8)	Cl(4)-C(10)	1.729(10)
Cl(5)-C(10)	1.737(11)	Cl(6)-C(20)	1.742(12)
Cl(7A)-C(20)	1.698(12)	Cl(7B)-C(20)	1.761(10)
Cl(8A)-C(30A)	1.76(2)	Cl(9A)-C(30A)	1.75(2)
Cl(8B)-C(30B)	1.74(2)	Cl(9B)-C(30B)	1.81(2)
Cl(10)-C(40A)	1.69(2)	Cl(11)-C(40A)	1.83(2)
Cl(12)-C(40B)	1.77(2)	Cl(13)-C(40B)	1.74(2)
O(3)-Rh(1)-O(1)	75.4(2)	O(3)-Rh(1)-O(2)	73.7(2)
O(1)-Rh(1)-O(2)	80.8(2)	O(3)-Rh(1)-P(3)	97.1(2)
O(1)-Rh(1)-P(3)	172.4(1)	O(2)-Rh(1)-P(3)	95.7(2)
O(3)-Rh(1)-P(2)	103.5(1)	O(1)-Rh(1)-P(2)	92.7(1)
O(2)-Rh(1)-P(2)	173.3(2)	P(3)-Rh(1)-P(2)	90.63(8)
O(3)-Rh(1)-Cl(3)	167.4(2)	O(1)-Rh(1)-Cl(3)	97.2(1)
O(2)-Rh(1)-Cl(3)	95.2(1)	P(3)-Rh(1)-Cl(3)	89.78(7)
P(2)-Rh(1)-Cl(3)	86.91(7)	O(3)-Rh(2)-O(2)	74.6(2)
O(3)-Rh(2)-O(1)	74.9(2)	O(2)-Rh(2)-O(1)	80.4(2)
O(3)-Rh(2)-P(1)	98.8(2)	O(2)-Rh(2)-P(1)	172.4(1)
O(1)-Rh(2)-P(1)	94.4(2)	O(3)-Rh(2)-P(4)	101.3(1)
O(2)-Rh(2)-P(4)	92.6(1)	O(1)-Rh(2)-P(4)	172.7(2)
P(1)-Rh(2)-P(4)	92.31(7)	O(3)-Rh(2)-Cl(2)	169.0(1)
O(2)-Rh(2)-Cl(2)	97.7(1)	O(1)-Rh(2)-Cl(2)	96.3(1)
P(1)-Rh(2)-Cl(2)	88.40(7)	P(4)-Rh(2)-Cl(2)	86.67(7)
C(51)-P(1)-C(4)	101.5(3)	C(51)-P(1)-C(61)	104.8(3)
C(4)-P(1)-C(61)	105.4(4)	C(51)-P(1)-Rh(2)	117.8(3)
C(4)-P(1)-Rh(2)	114.2(3)	C(61)-P(1)-Rh(2)	111.8(3)
C(1)-P(2)-C(11)	106.6(4)	C(1)-P(2)-C(21)	101.8(4)
C(11)-P(2)-C(21)	105.4(4)	C(1)-P(2)-Rh(1)	116.3(3)
C(11)-P(2)-Rh(1)	111.7(2)	C(21)-P(2)-Rh(1)	114.0(3)
C(41)-P(3)-C(31)	104.5(4)	C(41)-P(3)-C(3)	103.3(4)
C(31)-P(3)-C(3)	101.9(4)	C(41)-P(3)-Rh(1)	113.5(3)

C(31)-P(3)-Rh(1)	119.1(3)	C(3)-P(3)-Rh(1)	112.7(3)
C(6)-P(4)-C(81)	106.2(4)	C(6)-P(4)-C(71)	102.9(4)
C(81)-P(4)-C(71)	103.8(3)	C(6)-P(4)-Rh(2)	115.2(2)
C(81)-P(4)-Rh(2)	113.9(3)	C(71)-P(4)-Rh(2)	113.7(2)
C(7)-O(1)-Rh(1)	123.7(5)	C(7)-O(1)-Rh(2)	122.3(4)
Rh(1)-O(1)-Rh(2)	87.7(2)	C(8)-O(2)-Rh(2)	121.0(5)
C(8)-O(2)-Rh(1)	122.5(4)	Rh(2)-O(2)-Rh(1)	87.8(2)
Rh(2)-O(3)-Rh(1)	89.8(2)	C(2)-C(1)-P(2)	119.8(6)
C(2)-C(3)-P(3)	112.9(6)	C(16)-C(11)-P(2)	116.9(6)
C(5)-C(4)-P(1)	112.4(6)	C(26)-C(21)-P(2)	119.2(8)
C(5)-C(6)-P(4)	115.8(5)	C(32)-C(31)-P(3)	122.2(7)
C(12)-C(11)-P(2)	123.9(7)	C(46)-C(41)-P(3)	119.2(6)
C(22)-C(21)-P(2)	123.2(6)	C(52)-C(51)-P(1)	118.9(6)
C(36)-C(31)-P(3)	117.9(7)	C(66)-C(61)-P(1)	117.6(6)
C(42)-C(41)-P(3)	122.0(6)	C(76)-C(71)-P(4)	118.4(7)
C(56)-C(51)-P(1)	122.1(5)	C(82)-C(81)-P(4)	121.6(7)
C(62)-C(61)-P(1)	122.2(7)	C(84)-C(83)-C(82)	121.8(8)
C(72)-C(71)-P(4)	122.1(6)	C(86)-C(85)-C(84)	118.5(10)
C(86)-C(81)-P(4)	118.6(5)	Cl(4)-C(10)-Cl(5)	112.9(6)
C(81)-C(82)-C(83)	118.8(9)	Cl(6)-C(20)-Cl(7B)	107.6(9)
C(83)-C(84)-C(85)	120.1(8)	Cl(8B)-C(30B)-Cl(9B)	110.0(12)
C(81)-C(86)-C(85)	120.9(8)	Cl(12)-C(40B)-Cl(13)	107(2)
Cl(7A)-C(20)-Cl(6)	112.7(7)	Cl(10)-C(40A)-Cl(11)	113.1(11)
Cl(9A)-C(30A)-Cl(8A)	113.3(13)		

Table 18. Selected Bond Lengths (Å) and Angles (°) for Complex (6) Excluding Rh, P, Cl, and O

C(1)-C(2)	1.526(13)	C(4)-C(5)	1.525(10)
C(2)-C(3)	1.537(11)	C(11)-C(12)	1.380(12)
C(5)-C(6)	1.524(10)	C(12)-C(13)	1.405(12)
C(11)-C(16)	1.445(12)	C(14)-C(15)	1.371(13)
C(13)-C(14)	1.39(2)	C(21)-C(22)	1.379(14)
C(15)-C(16)	1.373(11)	C(22)-C(23)	1.403(13)
C(21)-C(26)	1.419(12)	C(24)-C(25)	1.35(2)
C(23)-C(24)	1.38(2)	C(31)-C(36)	1.368(14)
C(25)-C(26)	1.372(13)	C(32)-C(33)	1.396(11)
C(31)-C(32)	1.399(12)	C(34)-C(35)	1.38(2)
C(33)-C(34)	1.374(14)	C(41)-C(42)	1.379(11)
C(35)-C(36)	1.394(13)	C(42)-C(43)	1.390(13)
C(41)-C(46)	1.403(11)	C(44)-C(45)	1.358(13)
C(43)-C(44)	1.418(14)	C(51)-C(56)	1.402(11)
C(45)-C(46)	1.396(11)	C(52)-C(53)	1.374(11)
C(51)-C(52)	1.428(10)	C(54)-C(55)	1.381(12)
C(53)-C(54)	1.376(12)	C(61)-C(62)	1.375(11)
C(55)-C(56)	1.373(10)	C(62)-C(63)	1.396(12)

C(61)-C(66)	1.405(12)	C(64)-C(65)	1.39(2)
C(63)-C(64)	1.38(2)	C(71)-C(72)	1.372(13)
C(65)-C(66)	1.378(11)	C(72)-C(73)	1.422(12)
C(71)-C(76)	1.421(12)	C(74)-C(75)	1.38(2)
C(73)-C(74)	1.40(2)	C(81)-C(86)	1.391(13)
C(75)-C(76)	1.400(12)	C(82)-C(83)	1.410(13)
C(81)-C(82)	1.387(11)	C(84)-C(85)	1.414(14)
C(83)-C(84)	1.34(2)	C(6)-C(5)-C(4)	115.2(6)
C(85)-C(86)	1.398(11)	C(14)-C(13)-C(12)	119.2(9)
C(1)-C(2)-C(3)	113.4(8)	C(16)-C(15)-C(14)	121.7(9)
C(12)-C(11)-C(16)	119.0(7)	C(22)-C(21)-C(26)	117.6(8)
C(11)-C(12)-C(13)	120.7(9)	C(24)-C(23)-C(22)	119.5(12)
C(15)-C(14)-C(13)	120.6(8)	C(24)-C(25)-C(26)	121.2(10)
C(15)-C(16)-C(11)	118.8(8)	C(36)-C(31)-C(32)	119.7(8)
C(21)-C(22)-C(23)	120.9(9)	C(34)-C(33)-C(32)	119.8(9)
C(25)-C(24)-C(23)	120.3(10)	C(34)-C(35)-C(36)	119.2(11)
C(25)-C(26)-C(21)	120.5(10)	C(42)-C(41)-C(46)	118.8(7)
C(33)-C(32)-C(31)	119.5(9)	C(42)-C(43)-C(44)	119.3(9)
C(33)-C(34)-C(35)	120.9(9)	C(44)-C(45)-C(46)	121.7(8)
C(31)-C(36)-C(35)	120.8(10)	C(56)-C(51)-C(52)	118.6(6)
C(41)-C(42)-C(43)	121.4(8)	C(52)-C(53)-C(54)	122.1(7)
C(45)-C(44)-C(43)	119.1(8)	C(56)-C(55)-C(54)	120.6(7)
C(45)-C(46)-C(41)	119.6(7)	C(62)-C(61)-C(66)	120.2(7)
C(53)-C(52)-C(51)	118.6(8)	C(64)-C(63)-C(62)	120.2(9)
C(53)-C(54)-C(55)	119.5(7)	C(66)-C(65)-C(64)	121.4(9)
C(55)-C(56)-C(51)	120.6(7)	C(72)-C(71)-C(76)	119.5(7)
C(61)-C(62)-C(63)	120.2(9)	C(74)-C(73)-C(72)	117.3(10)
C(63)-C(64)-C(65)	119.2(9)	C(74)-C(75)-C(76)	120.4(10)
C(65)-C(66)-C(61)	118.8(8)	C(86)-C(81)-C(82)	119.7(8)
C(71)-C(72)-C(73)	121.9(9)	C(75)-C(76)-C(71)	119.2(10)
C(75)-C(74)-C(73)	121.6(8)		

Appendix 8

Colloquia, Lectures and Seminars Attended.

8.1. Lectures and Colloquia At Durham

1993

October 20 Dr. P. Quayle†, University of Manchester
Aspects of Aqueous ROMP Chemistry

October 21 Prof. R. Adams†, University of South Carolina, USA
Chemistry of Metal Carbonyl Cluster Complexes : Development of Cluster Based Alkyne Hydrogenation Catalysts

November 24 Dr. P.G. Bruce†, University of St. Andrews
Structure and Properties of Inorganic Solids and Polymers

December 1 Prof. M.A. McKervey†, Queen's University, Belfast
Synthesis and Applications of Chemically Modified Calixarenes

1994

January 26 Prof. J. Evans†, University of Southampton
Shining Light on Catalysts

February 9 Prof. D. Young†, University of Sussex
Chemical and Biological Studies on the Coenzyme Tetrahydrofolic Acid

February 16 Prof. K.H. Theopold, University of Delaware, USA
Paramagnetic Chromium Alkyls : Synthesis and Reactivity

March 25 Dr. J. Dilworth, University of Essex
Technetium and Rhenium Compounds with Applications as Imaging Agents

April 28 Prof. R. J. Gillespie, McMaster University, Canada

The Molecular Structure of some Metal Fluorides and Oxofluorides: Apparent Exceptions to the VSEPR Model.

October 19 Prof. N. Bartlett, University of California
Some Aspects of Ag(II) and Ag(III) Chemistry

November 2 Dr P. G. Edwards, University of Wales, Cardiff
The Manipulation of Electronic and Structural Diversity in Metal Complexes - New Ligands

November 3 Prof. B. F. G. Johnson, Edinburgh University
Arene-metal Clusters

November 9 Dr G. Hogarth, University College, London
New Vistas in Metal-imido Chemistry

November 10 Dr M. Block, Zeneca Pharmaceuticals, Macclesfield
Large-scale Manufacture of ZD 1542, a Thromboxane Antagonist Synthase Inhibitor

November 16 Prof. M. Page, University of Huddersfield
Four-membered Rings and β-Lactamase

November 23 Dr J. M. J. Williams, University of Loughborough
New Approaches to Asymmetric Catalysis

December 7 Prof. D. Briggs, ICI and University of Durham
Surface Mass Spectrometry

1995

January 11 Prof. P. Parsons, University of Reading
Applications of Tandem Reactions in Organic Synthesis

January 18 Dr G. Rumbles, Imperial College, London
Real or Imaginary Third Order Non-linear Optical Materials

January 25 Dr D. A. Roberts, Zeneca Pharmaceuticals
The Design and Synthesis of Inhibitors of the Renin-angiotensin System

February 1 Dr T. Cosgrove, Bristol University
Polymers do it at Interfaces

February 8 Dr D. O'Hare, Oxford University

	Synthesis and Solid-state Properties of Poly-, Oligo- and Multidecker Metallocenes
March 1	Dr M. Rosseinsky, Oxford University Fullerene Intercalation Chemistry
March 22	Dr M. Taylor, University of Auckland, New Zealand Structural Methods in Main-group Chemistry
May 4	Prof. A. J. Kresge, University of Toronto *The Ingold Lecture* Reactive Intermediates : Carboxylic-acid Enols and Other Unstable Species
May 27	Prof. J.M. Lehn, Louis Pasteur University Perspectives in Suparmolecular Chemistry From Molecular Recognition Towards Self Organisation
May 29	Dr D. Milstein *(ICI Wilton)* Effects of Phosphine Structure on Pd Catalysed C-C bond Formation and Breaking.
June 6	Dr R. Snaith, Cambridge University Ionic Molecules Formed By S Block Molecules, Synthesis and Strutures and Uses.
June 9	Dr N.G. Connelly, University of Bristol Studies on Redox Active Organometallic and Co-ordination Compounds
June 14	Prof. J.R. Dilworth, University of Essex New Applications of Co-ordination Compounds
June 16	Dr S. Strauss Co-ordinative Unsaturation, a New Look at an old Idea
June 20	Dr K.J Cavell, University of Tasmania Fundamental Studies on the Insertion Processes and the Development of Catalysts for CO and Olefin Conversions
October 13	Prof. R. Schmutzler, Univ Braunschweig, FRG.

Calixarene-Phosphorus Chemistry: A New Dimension in Phosphorus Chemistry

November 1 Prof. W. Motherwell, UCL London
New Reactions for Organic Synthesis

November 15 Dr Andrea Sella, UCL, London
Chemistry of Lanthanides with Polypyrazoylborate Ligands

November 29 Prof. Dennis Tuck, University of Windsor, Ontario, Canada
New Indium Coordination Chemistry

1996

January 10 Dr Bill Henderson, Waikato University, NZ
Electrospray Mass Spectrometry - a new sporting technique

February 21 Dr C R Pulham , Univ. Edinburgh
Heavy Metal Hydrides - an exploration of the chemistry of stannanes and plumbanes

March 6 Dr Richard Whitby, Univ of Southampton
Tandem Reactions on a Zirconium Template

March 13 Prof. Dave Garner, Manchester University
Mushrooming in Chemistry

† Invited specially for the graduate training programme.

8.2. External Colloquia and Events Attended

1. 3rd ICI-Katalco Symposium on Catalytic Chemistry, Darlington May 1994 (Poster Contribution)
2. 4th ICI-Katalco Symposium on Catalytic Chemistry, Darlington May 1995 (Poster Contribution)
3. 5th ICI-Katalco Symposium on Catalytic Chemistry, Darlington May 1996 (Oral Contribution: Towards Alkoxycarbonylation Using Rhodium Catalysts)

4. The 5th Firth Symposium, Sheffield, September 1993.

5. The RSC Autumn Symposium 1995, Sheffield, (Poster Contribution)